

Design and Operation of a 20 kW_{th} Fluidised Bed Combustor for Biomass Oxy-fuel Combustion

A Thesis Submitted to

The Univesity of Nottingham

By

Farooq Sher

BSc, MSc Chemical Engineering
AMIChemE, MAIChE, PMPEC, MPIChE, MIEAust

For the degree of

Doctor of Philosophy

Project Supervisors

Professor Hao Liu, Dr. Chenggong Sun, Professor Colin E. Snape

School of Chemical and Environmental Engineering
The Univeristy of Nottingham
United Kingdom

SEPTEMBER 2016

Abstract

Due to growing concerns about climate change, the heat and power sector is continuously facing challenges to reduce CO_2 emissions. Carbon capture and storage (CCS) is one of the short-medium term measures that can mitigate CO_2 emissions emitted from fossil fuels utilisation. Oxy-fuel combustion is a promising technology for CSS that can be integrated into the new and the current fleet of power plants. Biomass is a carbon neutral renewable source of energy that can replace fossil fuels. If the biomass is utilised as a fuel in oxy-fuel combustion it could lead even to negative CO_2 emissions. Although the sintering and agglomeration problems associated with the combustion of non-woody biomasses in the fluidised beds are still major issues, fluidised beds have emerged as one of the best among the other proven biomass combustion technologies, mainly due to their fuel flexibility, low SOx and NOx emissions. However, oxy-fuel combustion technology in fluidised beds is in the early stages of development and still needs a lot of research for improvement before its application on full-scale power plants.

In this work basic combustion fundamentals of different biomass fuels in terms of energy production were studied using thermogravimetric analysis (TGA) under air, N_2, CO_2 and selected oxy-fuel ($30\%O_2/70\%CO_2$) reaction environments. Then a 20 kW_{th} bubbling fluidised bed combustor (BFBC) was designed, manufactured and successfully tested for a range of biomass fuels under air and oxy-fuel combustion environments. The agglomeration and sintering behaviour of these biomass fuels during combustion under air was also investigated using different analytical techniques such as SEM-EDX,

XRD and XRF. The biomass fuels investigated in this study include domestic wood, industrial wood, miscanthus, wheat straw and peanut shell pellets. The BFBC testing of these biomass fuels focused on the influence of operating conditions, the effect of excess air level and fuel feed rate on the hydrodynamics, temperature profiles and emissions, NOx, CO_2 and CO within the BFBC. Air staging can be very effective in reducing NOx emissions of non-woody biomass fuels especially when the secondary air was injected at the higher level with an overall low excess air level. A maximum NOx reduction percentage of 30% was achieved for the non-woody biomasses during air staging combustion.

The non-isothermal TGA analyses under N_2 and CO_2 showed almost identical weight loss (R), reactivity (R_M) and activation energy (Ea) profiles in devolatilisation zones. However, when devolatilisation occurred under CO_2 conditions at temperatures higher than 700 ^oC, an additional weight loss was observed for all biomass fuels, being indicative of the contribution of CO_2-char gasification reactions. Under air and oxy-fuel ($30\%O_2/70\%CO_2$) results showed almost similar profiles for R, R_M and Ea. In oxy-fuel atmospheres, by replacing N_2 with CO_2 a slight increase in the maximum rate of weight loss (R_{Max}) was observed in both reaction zones for all studied biomasses.

The unstaged and staged air combustion experiments in the 20 kW_{th} BFBC showed that higher excess air always led to higher NOx emissions for any of the biomass fuels tested because less CO and char were available in the reactor to promote NOx reductions. Due to the consequence of the high volatile matter content of the biomass fuels, the maximum temperatures were achieved at the top of the dense bed and/or beginning of

the freeboard, which suggests that the main combustion reaction takes place in this part of the combustor. Air staging leads to higher temperatures in the freeboard, especially at low excess air levels, as a result of additional combustion in the freeboard under staged air conditions. Air staging can be very effective in reducing NOx emissions of non-woody biomass fuels especially when the secondary air was injected at the higher level with an overall low excess air level. A higher percentage of carbon in ash was obtained while working under air staging conditions than that of without air staging combustion.

The results of oxy-fuel combustion tests in the 20 kW_{th} BFBC showed that oxy-fuel combustion was different from air combustion in several ways, including reduced gas temperatures, delayed flame ignition, increased CO emissions under 21%O_2/79%CO_2 and 25%O_2/75%CO_2 oxy-mixtures. Many of these parameters were associated with differences in properties of the main diluting gases CO_2 and N_2 in oxy-fuel and air combustion respectively. In order to match the biomass oxy-fuel combustion gas temperatures to those of air combustion, the oxygen concentration in the mixture of O_2/CO_2 has to be increased to 30% or higher. Moreover, the oxy-fuel combustion with 30%O_2/70%CO_2 has shown higher efficiencies than air, which indicates biomass fuels can be successfully combusted in the BFBC under oxy-fuel combustion conditions.

The agglomeration and sintering behaviour was observed under continuous air combustion conditions in the 20 kW_{th} BFBC. The analysis using SEM-EDX, XRD and XRF concluded that the potassium present in wheat straw was mainly responsible for agglomeration, which was detected in the form of KCl and K_2O in the bed material and cyclone ash samples.

Acknowledgements

I am thankful to Allah almighty, the most generous and beneficent for the kindness, wisdom and knowledge He has bestowed upon me throughout my life up to this stage.

I would like to express my sincere gratitude and thanks to my supervisors; Professor Hao Liu, Dr. Chenggong Sun and Professor Colin E. Snape for their guidance, help, encouragement and advice during the course of this research. I would also like to acknowledge the support of my friends, students and staff at the University of Nottingham, particularly, Dr. Miguel A. Pans, Dr. Wenbin Zhang, Dr. Anup Patel, Dianne Vincent, Adrian Quinn and Michael Winfield who have all provided me with their time, support, and advice towards the successful completion of this research work.

This research work would not have been possible without the technical help from the technicians, I would like to say special thanks to Jonathan Moss and Dave Taylor at the Department of Architecture and Built Environment, the University of Nottingham for their technical help and support during construction of the experimental setup.

Finally, I would like to express my utmost appreciation to my beloved family; my father Muhammad Zafar Dahar, my wonderful mother in this world Zareena, my sisters; Roquyya, Kalsoom, Ayesha, Fatima and my brothers Bilal, Azam, Usman for their infinite prayer, support, love and great words of encouragement during the completion this research work all through the years.

Dedication

I dedicate this thesis to my father Professor (R) Muhammad Zafar Dahar who has dedicated his life to educating the others.

Table of Contents

Abstract ..... **i**
Acknowledgements ..... **iv**
Table of Contents ..... **vi**
Table of Figures ..... **xi**
List of Tables ..... **xviii**
Nomenclatures ..... **xx**
Chapter 1 Introduction **1**
1.2 Background 1
1.3 The World Energy Consumption 2
1.4 Emission Trends 4
1.4.1 CO_2 Emissions by Sector 5
1.5 UK Renewable Energy Future Plan 6
1.6 Biomass as a Source of Energy 8
1.6.1 Biomass Global Energy Potential 9
1.7 Carbon Capture and Storage (CCS) 9
1.7.1 Carbon Capture Technologies 10
1.8 Difference in Air and Oxy-fuel Combustion 13
1.9 Motivation Objectives and Novelty of the Research 13
1.10 Thesis Layout 15
Chapter 2 Literature Review **18**
2.1 Biomass 18
2.1.1 Types of Biomass 19
2.1.2 Composition of Biomass 20
2.1.3 Energy Content of Biomass 23
2.1.4 Physical Properties of Biomass 25
2.1.5 Effect of Biomass Elements on Combustion 26
2.2 Biomass Conversion Technologies 27
2.2.1 Thermochemical Conversion of Biomass 29
2.3 Biomass Combustion Mechanism 30
2.4 Fluidised Bed Combustion 32

2.4.1 Bubbling Fluidised Bed 33
2.4.2 Circulating Fluidised Bed 34
2.4.3 Hybrid Type BFB and CFB 36
2.5 Design and Operation Variables 36
2.5.1 Design variants 36
2.5.2 Fuel Preparation 37
2.5.3 The Combustor 37
2.5.4 Particle Circulation and Collection 39
2.6 Gaseous Pollutant Emissions 40
2.6.1 CO Emissions 40
2.6.2 NO_X Emission 43
2.7 Research Challenges of Biomass Oxy-fuel Combustion 51
Chapter 3 Design and Construction of Experimental Setup 54
3.1 Introduction 54
3.2 Pre-Design Requisites 57
3.3 Hydrodynamics and Combustion Design Parameters 58
3.3.1 Fluidisation Velocities 58
3.3.2 Fluidising Gases 63
3.3.3 Gas Distributor 64
3.3.4 Biomass Combustion Stoichiometry 67
3.3.5 Main Reactor and Free Board 68
3.3.6 Gas-Solid Separation Cyclone 69
3.3.7 Gas Distribution Plate 71
3.3.8 Biomass Feeding System 73
3.3.9 Water Cooled Heat Extraction Probe 77
3.3.10 Flue Gas Sampling Probe 78
3.3.11 Supporting Frame 79
3.3.12 Air and Oxy-fuel Gases supply Piping and Sizing 80
3.4 Instrumentation and Process Control 84
3.4.1 Temperature Measurements 85
3.4.2 Pressure Measurements 87

3.4.3 Flue Gas Measurements 87
Chapter 4 Materials and Experimental Methods 89
4.1 Introduction 89
4.2 Material Selection and Characterisation 92
4.2.1 Bed Material 92
4.2.2 Biomass Fuels 93
4.2.3 Proximate and Ultimate Analysis 94
4.3 Thermogravimetric Analysis 98
4.4 Cold Rig Testing 100
4.4.1 Minimum Fluidisation Velocity Measurements 100
4.4.2 Visual Observations during Plexiglas Cold Rig Testing 104
4.4.3 Biomass Feeding System Calibration 105
4.5 Operational Procedure of BFBC 106
4.5.1 Pre Start-up Checks 106
4.5.2 Start-up Procedure 107
4.5.3 Unstaged and Staged Air Combustion Procedure 109
4.5.4 Oxy-fuel Combustion Procedure 113
4.5.5 Shutdown Procedure 115
4.6 Bed Material and Ash Characterisation 115
4.6.1 Bed Material Sampling 115
4.6.2 Cyclone Reject Sampling 116
4.6.3 SEM-EDX 117
4.6.4 XRD 119
4.6.5 XRF 121
Chapter 5 Thermal Analysis of Biomass Fuels 124
5.1 Introduction 124
5.2 Biomass Fuels and Sample Preparation 126
5.3 Chemical Analysis 126
5.4 Experimental Techniques and Kinetic Analysis 127
5.5 Results and Discussion 131
5.5.1 Location of Biomass Fuels in Van Krevelen Diagram 131

5.5.2 Thermal Degradation under N_2 Atmosphere 133
5.5.3 Thermal Degradation under Air Atmosphere 138
5.5.4 Thermal Degradation under CO_2 Atmosphere 141
5.5.5 Thermal Degradation under Oxy-fuel Atmosphere 146
5.6 Reactivity and Kinetic Analysis 150
5.7 Summary 156
Chapter 6 Unstaged and Staged Air Combustion of Biomass Fuels 159
6.1 Introduction 159
6.2 Biomass Fuels Characteristics 163
6.3 Experimental Procedure and Conditions 163
6.3.1 Combustion Efficiency Calculations 164
6.4 Results and Discussion 167
6.4.1 Effect of Unstaged Excess Air on NOx and CO Emissions 167
6.4.2 Effect of Biomass Composition on NOx Emissions 169
6.4.3 Effect of Air Staging on Temperature Profiles 171
6.4.4 Effect of Air Staging on NOx Emissions 175
6.4.5 Effect of Air Staging on CO Emissions 177
6.4.6 Combustion Efficiency 180
6.4.7 Effect of Air Staging on the Efficiency loss due to Unburned Carbon content in Fly Ash 185
6.5 Agglomeration and Sintering Effect 187
6.6 Summary 188
Chapter 7 Oxy-fuel Combustion of Biomass Fuels 190
7.1 Introduction 190
7.2 Biomass Fuels Characteristics 192
7.3 Experimental Procedure and Conditions 192
7.4 Results and Discussion 194
7.4.1 Effect on Combustion Fundamentals 194
7.4.2 Effect of Environment on Fuel Combustion and Temperatures Profiles 195
7.4.3 Effect of Combustion Environment on CO_2 Emissions 200
7.4.4 Effect of Combustion Environment on NOx Emissions 201

7.4.5 Effect of Combustion Environment on CO Emissions 206
7.5 Effect of Combustion Environment on Sintering and Agglomeration Behaviour 210
7.6 Summary 211
Chapter 8 Bed Material and Ash Characterisation 214
8.1 Introduction 214
8.2 Sample Preparation and Methodology 216
8.3 Results and Discussion 217
8.3.1 Visual Observations 217
8.3.2 Agglomeration during Air Combustion 219
8.3.3 Bed Material Analysis 220
8.3.4 Cyclone Ash Analysis 225
8.3.5 Surface Morphology and Spot Analysis 228
8.3.6 Control of Agglomeration 233
8.4 Summary 233
Chapter 9 Conclusions and Future Work 235
9.1 Combustion Fundamentals 237
9.2 Un-staged and Air-staged Combustion 237
9.3 Oxy-fuel Combustion 238
9.4 Agglomeration and Sintering Behaviour 240
9.5 Suggestions for Future Work 241
References 243
Appendix A 272
Appendix B 282
Appendix C 292
Appendix D 302
Appendix E 307
Appendix F 309

Table of Figures

Figure 1.1: The world energy consumption by fuel type history and projection [4]. 3

Figure 1.2: Total global energy consumption by source [8]. 4

Figure 1.3: Global carbon emissions from fossil fuels over years [11]. 5

Figure 1.4: World CO_2 emissions by sector[13]. 6

Figure 1.5: Main processes for carbon capture [38]. 11

Figure 2.1: The closed carbon cycle showing that CO_2 used during photosynthesis process released back to the atmosphere after biomass combustion [51]..... 19

Figure 2.2: Lignocellulose biomass composition and structure: cellulose, hemicellulose, and lignin [56]..... 21

Figure 2.3: The Van Krevlen showing compositional differences among coals and biomass [60]..... 24

Figure 2.4: An overview of biomass to power and heat conversion technologies [74]. 28

Figure 2.5: Schematic representation of the main stages of biomass combustion process [78]..... 30

Figure 2.6: Representation of; a) bubbling fluidised bed boiler (BFB), b) circulating fluidised bed (CFB) boiler [103]. 35

Figure 3.1: Bubbling fluidised bed combustor (BFBC) process flow diagram. 56

Figure 3.2: BFBC during construction; (a) main reactor section, (b) freeboard section. 68

Figure 3.3: Altered high-efficiency cyclone for BFBC; (a) before insulation, (b) after insulation..... 70

Figure 3.4: Sintered distribution plate; a) before fixing, b) after fixing into the flange. 72

Figure 3.5: Full view of the biomass BFBC feeding system. 73

Figure 3.6: Shaft bearing assembly with auger position used in biomass BFBC feeding system. 74

Figure 3.7: Conveyor section of the biomass BFBC feeding system. 75

Figure 3.8: Top view of the BFB combustor feeder hopper equipped with safety features. 76

Figure 3.9: Water cooled heat extraction probe arrangements into the BFBC. 77

Figure 3.10: Water cooled flue gas sampling probe for BFBC. 78

Figure 3.11: The blower fan for BFBC (back and front view the fan sitting on the anti-vibrating mounts). 81

Figure 3.12: The variable area volumetric flowmeter for air supply to the BFBC. 82

Figure 3.13: Oxy-fuel gas system showing separate gas supplies with solenoid safety valve. 83

Figure 3.14: Thermocouples locations on the BFBC. 86

Figure 3.15: Gas sampling unit including analysers and computer with dataTaker software. 88

Figure 4.1: TGA Q-500 from TA instruments. 94

Figure 4.2: Leco CHNS 628 elemental analysers. 95

Figure 4.3: Pressure drop measurements using sintered distribution plate without sand. 101

Figure 4.4: Pressure drop measurements using sintered distribution plate without and sand. 101

Figure 4.5: The cold rig testing; (a) before fluidisation, (b) after fluidisation. 104

Figure 4.6: Feeding system calibration using five different biomass fuel pellets; domestic wood (DW), industrial wood (ID), miscanthus (MIS), peanut shell pellets (PS) and wheat straw (WS). 106

Figure 4.7: Full experimental setup including bubbling fluidised bed combustor (BFBC) with auxiliaries. 108

Figure 4.8: FEI Quanta 600 scanning electron microscope. 118

Figure 4.9: Siemens D500 X-ray powder diffraction system. 120

Figure 4.10: Bruker S8 Tiger high-end wavelength dispersive XRF. 123

Figure 5.1: Van Krevelen plot for studied biomass fuels; BS, MIS, WW, WS, SRC and DW in comparison with other fuels including biomass (cotton stalk, shea meal, sugar cane bagasse) from Munir et al. [24], RDF = refuse derived fuels. 132

Figure 5.2: TGA profiles of the different biomass fuels under; (a) N_2, (b) air. 134

Figure 5.3: (a) DTG profiles of the biomass fuels under N_2, (b) Arrhenius plots for devolatilisation zone. 135

Figure 5.4: Typical DTG profile for biomass, weight loss under the first shoulder (shaded blue) in the first DTG peak corresponds to hemicellulose contents and the weight loss under the main DTG peak (shaded red) corresponds to cellulose contents. 136

Figure 5.5: (a) DTG profiles of the biomass fuels under air, (b) Arrhenius plots for devolatilisation zone and (c) Arrhenius plots for char combustion zone. 140

Figure 5.6: TGA profiles of the different biomass fuels under; (a) CO_2, (b) oxy-fuel. 142

Figure 5.7: (a) DTG profiles of the biomass fuels under CO_2, (b) Arrhenius plots for devolatilisation zone and (c) Arrhenius plots for Char-CO_2 reaction zone. 144

Figure 5.8: (a) DTG profiles of different biomass fuels under oxy-fuel fuel, (b) Arrhenius plots for devolatilisation zone and (c) Arrhenius plots for char combustion zone. 147

Figure 6.1: Temperature profiles at the different heights of the main reactor and freeboard, the pressure drop across the dense bed and the gas composition (CO_2, O_2, NOx and CO) at the outlet of the BFBC during a typical experiment for miscanthus pellet combustion without air staging (WAS). The NOx and CO are corrected @ 6% O_2 on dry basis. 168

Figure 6.2: (a) Effect of excess air on NOx emissions for different biomass fuels tested without air staging. (b) The nitrogen content of the different biomass fuels. The NOx emissions are corrected @6% O_2 on dry basis. 170

Figure 6.3: Temperature profiles for peanut, straw, miscanthus, industrial wood and domestic wood pellets at different excess air levels without air staging (WAS) and with air staging combustion at injection level one (AS1) and injection level two (AS2). ... 172

Figure 6.4: Effect of excess air on NOx emissions for peanut, straw, miscatnhus, industrial wood and domestic wood pellets without air staging (WAS) and with staging air combustion at injection level one (AS1) and injection level two (AS2). The NOx are corrected @6% on dry basis. 174

Figure 6.5: Effect of the overall excess air level on the reduction percentage of NOx emissions, in comparison to the NOx emissions under without air staging (WAS) and staging air with the secondary air injected at two locations AS1 and AS2. 177

Figure 6.6: Effect of excess air on CO emissions for peanut, straw, miscanthus, industrial wood and domestic wood under conditions of without air staging (WAS) and

with air staging combustion at injection level one (AS1) and injection level two (AS2). The CO is corrected @6% on dry basis. 178

Figure 6.7: Combustion efficiency without considering carbon in fly ash for peanut, straw, miscanthus, industrial wood and domestic wood pellets without air staging (WAS) and with air staging at injection level one (AS1) and injection level two (AS2). 181

Figure 6.8: Effect of excess air on efficiency loss due to incomplete combustion (IC) for peanut, straw, miscanthus, industrial wood and domestic wood pellets under conditions of without using air staging (WAS) and with air staging at injection level one (AS1) and at injection level two (AS2). 183

Figure 6.9: (a) Unburnt carbon (UBC) content in the fly ash for different biomass fuels, (b) Efficiency loss due to UBC content in the fly ash. 186

Figure 7.1: The temperature profiles, measured at different heights of the reactor and freeboard with the gas compositions at the outlet of the BFBC during miscanthus pellets combustion under air and oxy-fuel. 194

Figure 7.2: Temperature profiles under air and different oxy-fuel environments; (a) domestic wood pellets, (b) miscanthus pellets and (c) straw pellets. 196

Figure 7.3: NOx emissions from different types of biomass fuels under air and different oxy-fuel combustion environment. 202

Figure 7.4: Effect of bed temperatures on NOx emissions for all type of biomass fuels under air and different oxy-fuel combustion environments. 204

Figure 7.5: CO emissions from different types of biomass fuels under air and different oxy-fuel combustion environment. 207

Figure 7.6: Effect of CO on NOx emissions for all types of biomass fuels under air and oxy-fuel combustion environments. 208

Figure 7.7: Effect of bed temperatures on CO emissions for all type of biomass fuels under air and different oxy-fuel combustion environments..... 209

Figure 8.1: The bed samples collected from different biomass fuels; (a) fresh sand, (b) domestic wood, (c) industrial wood, (d) miscanthus, (e) wheat straw and (f) peanut shell. 218

Figure 8.2: The bed material along with agglomerates from wheat straw pellets combustion in BFBC. 219

Figure 8.3: The XRF elemental composition in the bed material obtained from different biomass fuels under air combustion. All results are C and O free basis..... 221

Figure 8.4: The XRF elemental oxides composition in the bed material obtained from different biomass fuels under air combustion. 221

Figure 8.5: The XRD spectrum of wheat straw pellets cyclone ash. 224

Figure 8.6: The XRF elemental composition in the cyclone ash obtained from different biomass fuels under air combustion, the results presented are without Si. 226

Figure 8.7: The XRF elemental oxides composition in the cyclone ash obtained from different biomass fuels under air combustion, the results presented are without Si..... 226

Figure 8.8: SEM micrographs from different bed material at 7.0 ×7.5 cm scale; (a) fresh sand, (b) domestic wood, (c) industrial wood, (d) miscanthus (e) wheat straw and (f) peanut shell. 230

Figure 8.9: SEM micrograph images showing the internal structure of agglomerated bed material at different magnifications; (a) agglomerated bed materials particles, (b) typical agglomerated particle magnified showing the spot analysis point. 231

Figure 8.10: EDX elemental spot analysis with elemental spectrum at point 1in agglomerated bed material mentioned in Figure 8.5. 232

List of Tables

Table 2.1: Structural analyses of various types of biomasses [57]. 22

Table 2.2: The design parameters BFB and CFB [105, 110-112]. 37

Table 4.1: An overview of the complete experimental research plan. 91

Table 4.2: Physical analysis of Garside 14/25 sand [219]. 92

Table 4.3: Chemical analysis of Garside 14/25 sand [219]. 93

Table 4.4: Ultimate analysis, proximate analysis and calorific values of biomass fuels. 97

Table 4.5: Experimental matrix for the tests performed under without air staging and with air staging combustion. 111

Table 4.6: Experimental matrix of the tests performed under oxy-fuel combustion. ... 114

Table 5.1: Ultimate analysis, proximate analysis and calorific values of biomass fuel samples. 129

Table 5.2: Compositions of the biomass fuels. 137

Table 5.3: Thermogravimetric parameters of biomass fuels under N_2 and air environment. 145

Table 5.4: Thermogravimetric parameters of biomass fuels under CO_2 and oxy-fuel environment. 148

Table 5.5: Reactivity parameters of biomass fuels under N_2, air, CO_2 and oxy-fuel environments. 152

Table 5.6: Kinetic parameters of biomass fuels under N_2, air, CO_2 and oxy-fuel environments. 154

Table 6.1: Operating conditions for without and with air staging combustion. 164

Table 7.1: Operating conditions for the oxy-fuel combustion. 193

Nomenclatures

Symbol	Description	SI Units
A	Pre-exponent factor	[s-1]
C	Constant, concentration	[-], [kg/m^3]
C_{O2}	O_2 concentration	[kmol/m^3]
C_{mix}	Mixture rate constant	[-]
C_p	Specific heat capacity	[J/kgK]
D	Diameter of cylinder	[m]
Q_1	Bed-to-particle heat transfer rate	[W]
Q_2	Rate of heat conduction through char layer	[W]
q	Specific burning rate of char based on external surface	[kg (C)/m^{2}s]
d	Particle diameter	[m]
Mc	Molecular weight of carbon	[kg/kmol]
ΔH_v	Heat of volatilization	[J/kg]
k	Overall rate coefficient	[m/s]
k_c	Chemical reaction rate coefficient	[m/s]
k_e	Effective thermal conductivity	[m/s]
t	Time	[s]
t_c	Time for char combustion	[s]
T_{bed}	Bed temperature	[K]
T_{s0}	Surface temperature of solid	[K]
D_{ig}	Diffusion coefficient of gaseous species i	[m^2/s]
ρ_s	Density of solid	[kg/m^3]
ρ_{sc}	Density of char layer	[kg/m^3]
d_p	Particle diameter	[m]
E	Activation energy	[J/mol]
H_{evp}	Evaporation heat of solid material	[J/kg]
H	Enthalpy	[J/kg]

k	Rate constant	[1/s]
k_a	Radiation absorption coefficient	[1/m]
k_s	Radiation scattering coefficient	[1/m]
k_d	Rate constant of char burning due to diffusion	[kg/atm.m^{2}s]
k_r	Rate constant of char burning due to chemical kinetic	[kg/atm.m^{2}s]
P	Mean pressure	[Pa]
p	Pressure	[Pa]
q_r	Radiative heat flux	[W/m^2]
$Q_{c,r}$	Heat absorbed by solid	[W/m^2]
Q_{sh}	Thermal source term of solid phase	[W/m^2]
R	Universal gas constant, process rate	[J/molK],[kg/m^{3}s]
S	Source term, stoichiometric coefficient in reactions	[-]
S_a	Particle surface	[m^2]
T	Temperature	[K]
t	Time	[s]
V	Volume	[m^3]
v	Velocity	[m/s]
z	Distance	[m]

Greek Symbols

Symbol	Description	SI Units
σ	Width of distribution in activation energies	[-]
σ_s	Radiation scattering coefficient	[1/m]
ε	Emissivity	[-]
λ	Thermal dispersion coefficient	[W/mK]
ϕ	Void fraction in bed, equivalence ratio	[-], [W/mK]
ρ	Density	[kg/m^3]
Φ	Parameter to be solved	[-]

ω	Volume fraction	[-]
μ	Viscosity	[Pa]
κ	Permeability	[m^2]

Abbreviations

BS	Barley straw
SRC	Willow SRC
WW	Waste wood
D.WOOD	Domestic wood
I.WOOD	Industrial wood
MIS	Miscanthus
WS	Wheat straw
PS	Peanut shell
FB	Fluidised bed
BFB	Bubbling fluidised bed
CFB	Circulating fluidised bed
BFBC	Bubbling fluidised bed combustor
SEM-EDX	Scanning electron microscopy- Energy-dispersive X-ray spectroscopy
XRD	X-Ray diffraction
XRF	X-ray fluorescence
GC-MS	Gas chromatography-mass spectrometry
RDF	Refuse derived fuel
NOx	Oxides of nitrogen
LLV	Low heating value
HHV	High heating value
FC	Fix carbon
VM	Volatile matter
EU	European Union
RE	Renewable energy

UNFCCC	United Nations framework convention on climate change
GEF	Global environmental facility
UNEP	United Nations environment programme
GHG	Greenhouse gases
CCS	Carbon capture and storage

Chapter 1

Introduction

1.2 Background

Climate change is most probably the greatest threat to mankind and environmental challenge of our generation. Global warming is observed and projected as an increase in the earth's atmospheric and oceanic average temperatures. The widely predicted reason for global warming is due to an increased level of greenhouse gases (GHGs) concentration in the atmosphere, most importantly carbon dioxide (CO_2). The main source of CO_2 emission is through human activities like the expenditure of fossil fuels such as coal, oil and natural gas for energy production with potentially devastating effects. The use of fossil fuels has increased the CO_2 concentration in our atmosphere and as a result, the earth's surface temperature has gone up. Over the past hundred years the global average temperature has increased about 0.6 ^{o}C [1] and is predicted to continuously rise at a rapid rate.

The CO_2 emissions are expected to increase further as the energy demands are to increase worldwide especially in the emerging economies (e.g. India, China, and Latin America) of the developing world. It has been far and widely recognised that high levels of CO_2 in the atmosphere also brings major costs to the economy and damage to the environment. According to World Health Organisation [2], as a direct result of air pollution around 18, 000 people die each day, as well as 6.5 million deaths associated to air pollution each year, which is much greater than the number from HIV, tuberculosis and road injuries combined. One of the most important sources of CO_2 emission is power generation. Reducing fossil fuel consumption for energy production and promoting alternative renewable energy technologies may provide the ultimate solution.

1.3 The World Energy Consumption

Energy is expected to play a dynamic role in the economic and social progress of the world over the entire 21st century [3]. Figure 1.1 represents the past and future projection of the world energy consumption [4]. The substantial growth of bio-energy, predominantly for the modern energy carriers such as biofuels (produced from renewable resources) and electricity has been observed over the past decade. Heat production by biomass has increased by about 2% per year, bioelectricity has increased each year by about 9% and the production of biofuels has increased approximately eight fold, which exceeds 20% growth per year in the same span of time. In the EU, energy supply by biomass alone accounts for two thirds of the total renewable energy production; this is 4% of the total EU energy [5, 6].

In 2035, the world primary energy consumption is estimated to be at the peak and energy consumption could rise up to 15,914 million metric tonnes of oil equivalent. Primary energy consumption of the world is predicted to fall by the year of 2050; energy consumption could fall to 14,906 million metric tonnes of oil equivalent [7]. Figure 1.2 represents the further energy contribution by sector for 2013. Today's world depends on fossil fuels for more than 80% for its energy usage. It will take time to change the picture dramatically for alternative fuels. We need to find ways to reduce CO_2 emission from industrial sources especially power plants until renewable energy sources and sustainable technologies can be widely deployed.

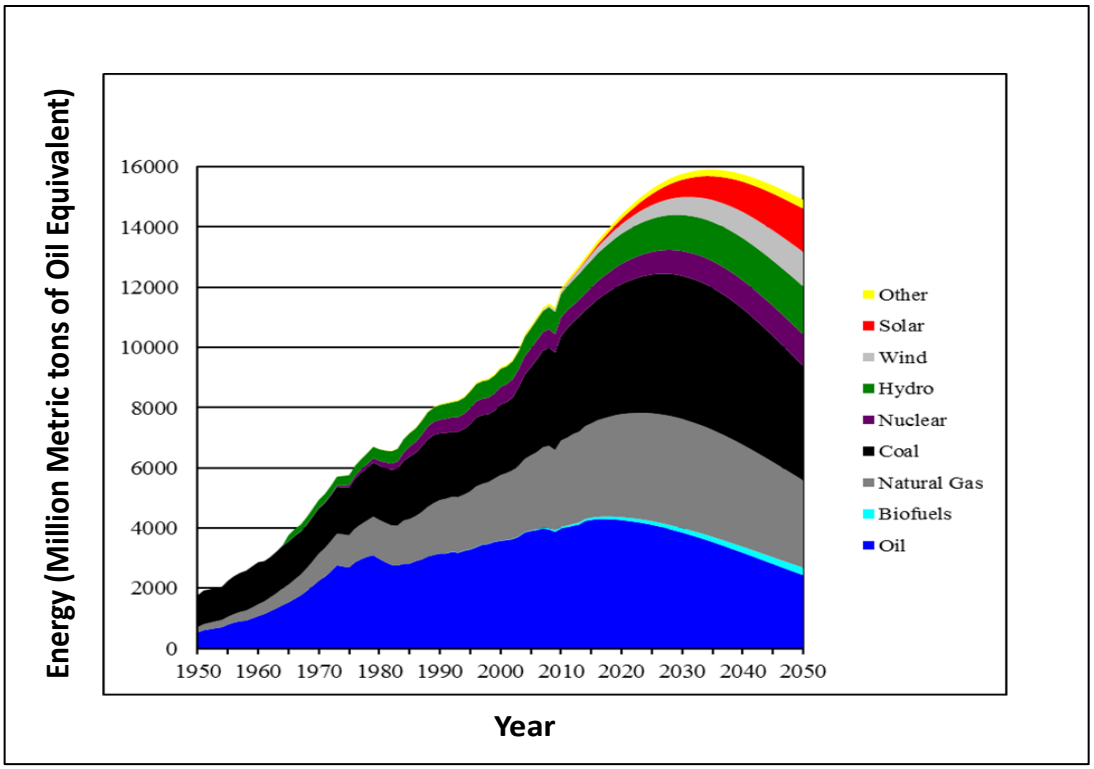


Figure 1.1: The world energy consumption by fuel type history and projection [4].

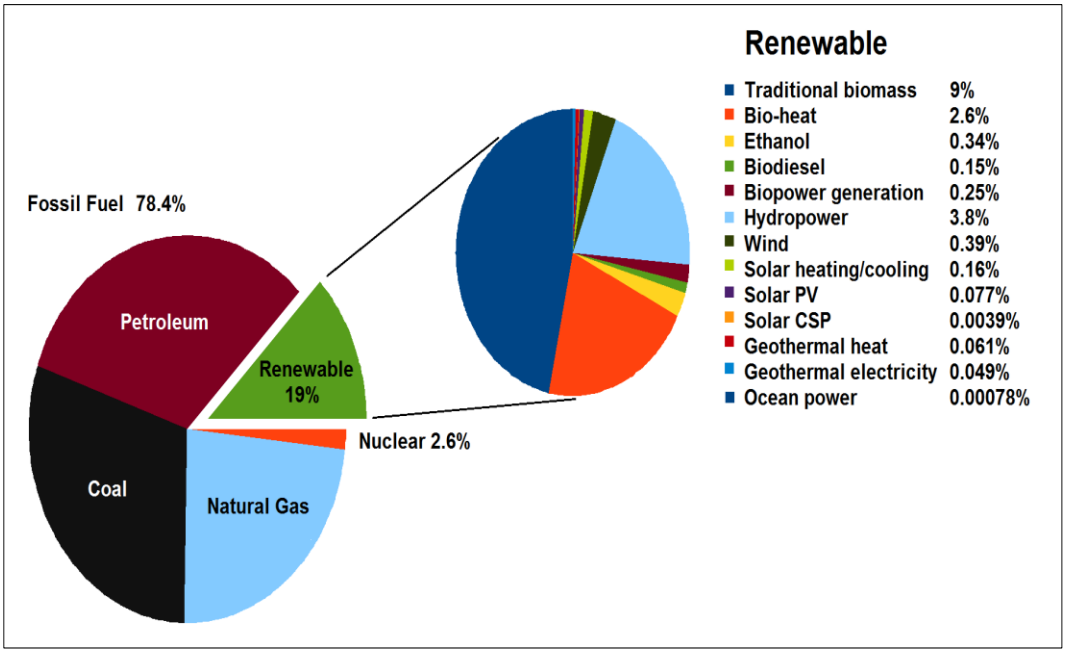


Figure 1.2: Total global energy consumption by source [8].

1.4 Emission Trends

The atmospheric concentrations of GHGs; methane, nitrous oxide and carbon dioxide have increased by about, 151%, 17% and 31% respectively between 1750 and 2000 [9]. With a global radiative forcing of 1.74 Wm^{-2}, the CO_2 is the supreme contributor among well mixed long-lived GHGs in the atmosphere [10]. The CO_2 emissions due to industrial processes and burning of fossil fuels have been accelerated on a global scale. The CO_2 growth rate has increased by more than 3% per year from 2000 to 2004, as opposed to 1.1% per year from 1990 to 1999 [11], also shown in Figure 1.3. Moreover, CO_2 emissions are highest with the solid fuels about 4,000 million metric tonnes per year. Since, 2000 the emissions growth rate of most of the fossil fuels has increased exponentially according to Intergovernmental Panel on Climate Change (IPCC) emissions scenario which was established in the late 1990s [11, 12].

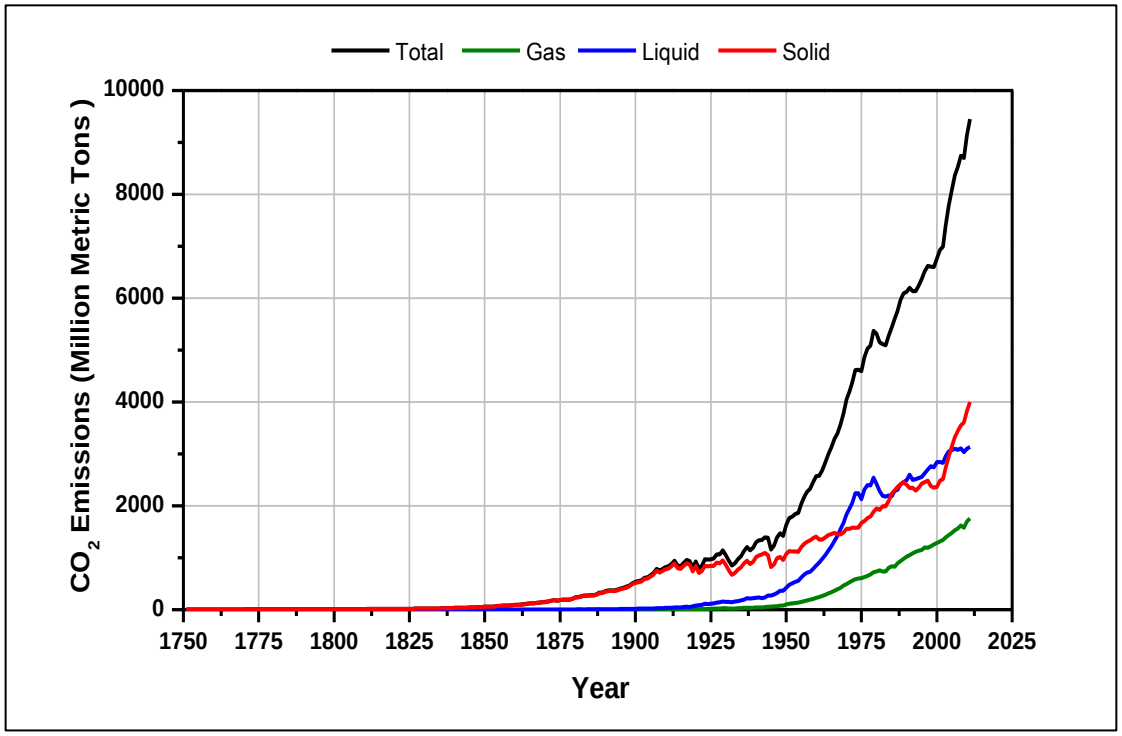


Figure 1.3: Global carbon emissions from fossil fuels over years [11].

1.4.1 CO_2 Emissions by Sector

The increase in the release of the amount of CO_2 is primarily due to the combustion of fossil fuels for energy purposes. The majority of worldwide CO_2 emissions (about 85%) are from transport, industry, heat and power generation. The electricity and heat generation account for about 42% of total CO_2 emissions as shown in Figure 1.4. The sector of electricity and heat generation is completely dominated by the use of coal, which produces twice the level of CO_2 emissions produced by natural gas for the same energy output. However, coal is favoured for its low cost and widespread availability [13]. Recently, constant increasing tendencies in the carbon intensity of energy have been observed in both developing and developed regions of the world [14]. The emissions growth rate is strongest in the rapidly developing economies of the world. So far no region of the world has managed to decrease carbon in its energy supply.

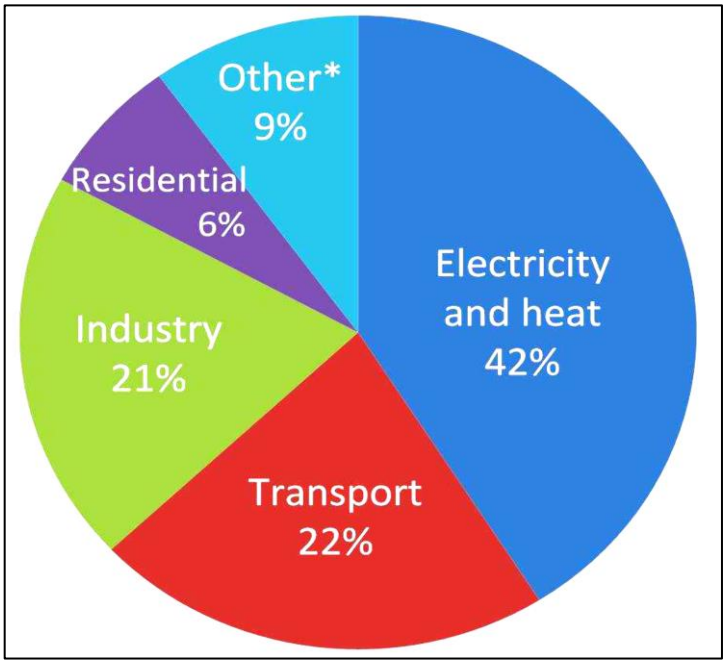


Figure 1.4: World CO_2 emissions by sector*[13].

1.5 UK Renewable Energy Future Plan

The UK Government believes that an urgent action at home and abroad is required to deal with the severest threat of climate change. A wide range of control measures are required to decarbonise the economy. Both the UK energy policy (2008) and the Energy Act (2015) clearly focus on reducing CO_2 emissions rather than supply security or energy cost [15]. The development of renewable energy sources, together with nuclear power and carbon capture and storage (CCS) will also enable the UK to play its full part in international efforts to reduce the harmful GHGs production [16]. Today only about 5.5% of the UK energy demands are met by renewables, but the target is to deliver 15% of its total energy consumption from renewable sources by 2020 [17]. There are

* Includes energy industries other than electricity and heat generation for example agriculture, fishing and other emissions not specified elsewhere.

increasing number of studies, reports, and roadmaps which all share the vision that the UK will meet the target by 2020 [17-19].

In the offshore wind, the UK leads the world with more than 11 GW of capacity in planning and more than 700 wind turbines have already been installed. The biggest onshore wind projects in Europe are already under construction in Wales and Scotland [17]. The UK has 15 nuclear reactors altogether generating 10 GW, equivalent to 21% of the UK electricity generation capacity, however during the early 2020s, half of the nuclear capacity is to be retiring as many of the UK's nuclear power stations are expected to close. If they are not replaced, there might not be enough electricity supply to meet demand [20]. The review of current energy policy by UK government in 2006, has given green signal to build new generation nuclear power plants [16]. To support the new build, planning and design certification laws were streamlined; any new nuclear reactors will be built without direct subsidy from the government and solely financed by the private sectors [21]. Currently, there is 4.3 GW electricity capacity in the pipeline from biomass including energy from waste. It is anticipated that the biomass energy potential pipeline is higher than this because many projects from fossil fuel to biomass conversion are not currently taken into account within the recent statistics.

The conversion of three 645 MW units at the Drax coal-fired power plant to burn biomass is one manifestation of the focus on renewables [22]. Each Drax unit is burning about 4 million tonnes of biomass, mostly imported wood pellets, per year. Drax reported that the average carbon saving resulting from burning of biomass instead of coal was above 80% over the full life cycle [23]. In August 2015, Drax was considered

to be the biggest sole loser from the removal of Climate Change Levy exemption for renewables [24]. Co-firing biomass with coal is one of the most effective means of producing renewable electricity and it was providing more than 400 MW of UK's capacity in 2012. Moreover, the UK government has the plan to ramp up the use and supply of biomass for transport, heat and power while ensuring sustainability and protecting the environment [18, 25].

1.6 Biomass as a Source of Energy

Biomass appears to be an attractive energy option that could be used to generate heat, electricity or different forms of power due to following three main reasons [26].

- It is largest and most important renewable resource that could be developed sustainably in the future.
- It appears to have formidable optimistic environmental properties to reduced GHGs emissions such as SOx and NOx.
- It appears to have the significant economic potential for the future if fossil fuel prices increase.

Moreover, versatility is amongst many other vital features of biomass as an alternative source of energy. In comparison with fossil energy resources (coal, oil, natural gas), biomass resources are more common and widespread throughout the globe.

1.6.1 Biomass Global Energy Potential

Biomass global energy potential is widely recognised because it is the 4th largest source after oil, coal and natural gas. Recently, biomass has drawn worldwide attention as an energy source which is renewable, highly productive, carbon neutral and easy to transport and store. Globally, biomass annual primary production is equal to 4,500 EJ of solar energy captured each year. 225 EJ, which is about 5% of this energy, could cover about 50% of the total primary energy demand of the world [27]. However, the energy potential of the biomass depends in part on the land availability. Presently, devoted growing land for energy crop biomass is only 0.19% of the world's total dry land area, which is only 0.5–1.7% agricultural land across the globe [27]. As a result, in modern society, biomass along with the other renewable energy resources is capable of providing all the required energy demands both locally and in most parts of the world.

1.7 Carbon Capture and Storage (CCS)

In the past two decades, many countries and organisations have taken initiatives in mitigating and adapting to global climate change; such as the United Nations Framework Convention on Climate Change (UNFCCC) [28], the United Nations Environment Programme (UNEP) [29] and the Intergovernmental Panel on Climate Change (IPCC) [30]. The most important initiative was the use of non-polluting and renewable sources of energy. Other mitigation actions include carbon sequestration clean development mechanism and joint implementation [31]. It is not easy to achieve the large CO_2 emission reductions just by consuming less energy or by substituting fossil fuels with alternative renewable energy sources that release less or no CO_2.

Today's world relies on fossil fuels for more than 80% of its energy usage [32], changing the pictures vividly will take time. Hence, CCS offers a way to achieve reductions in large sources of CO_2 emissions from industry and power plants until sustainable and cleaner energy technologies can be extensively deployed.

1.7.1 Carbon Capture Technologies

The main objective of carbon capturing is to produce a concentrated stream of pure CO_2 which can be transported and sequestered to a suitable place such as underground or in deep oceans. CO_2 capture technologies are usually classified into four categories [33, 34] post-combustion, pre-combustion, oxy-fuel combustion, and emerging technologies. Three major carbon capture technologies [35] are shown in Figure 1.5. The consideration of one technology over another is dependent on various criteria such as the fuel type, retrofit capabilities, costs, power plant size or desirable by-products as well as on the product purity. There are advantages and disadvantages associated with each capture process.

1.7.1.1 Post-combustion Capture

This process captures CO_2 from the stream of flue gases produced by the combustion of fossil fuels or other carbonaceous materials. Mainly the flue gas is composed of N_2 (≈ 75%), CO_2 (≈3–15%), other minor components are O_2, H_2O and impurities like SOx and NOx. The flue gas exits the process at near atmospheric pressure. Typically, separation is achieved via chemical absorption with mono-ethanolamine (MEA) and other amines such as sterically hindered amine (KS-1) in an absorber where the flue gas is scrubbed with an amine solution, normally capturing 85 to 90% of the CO_2 [36].

Commonly stated advantages with post-combustion capture are flexibility for retrofitting to existing power plants and the possibility to temporarily shut down the CO_2 capture process whilst maintaining power production [37].

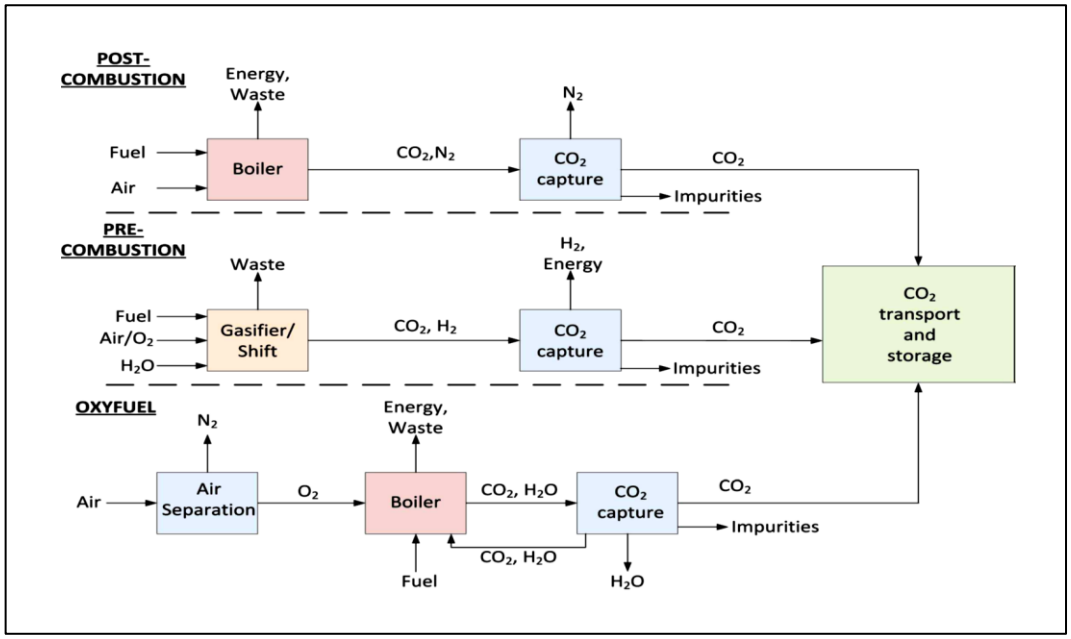


Figure 1.5: Main processes for carbon capture [38].

1.7.1.2 Pre-combustion Capture

This process removes CO_2 from the fuel prior to its combustion. It usually involves the removal of CO_2 after gasification and the water gas shift reaction. The synthesis gas or syngas, a mixture composed of CO and H_2, is produced from hydrocarbons contained in fossil fuels or biomass by gasification. The fuel reacts with oxygen and steam to produce CO and H_2. After the water gas shift reaction between H_2O and CO, additional H_2 is formed along with CO_2. The syngas from the gasifier is at high pressure (2–7 MPa) and the CO_2 concentration is higher than for post-combustion capture at about

15–60% [39]. Once CO_2 is removed from the syngas, the remaining H_2 can be combusted in a gas turbine to generate clean power [37].

1.7.1.3 Oxy-fuel Combustion Capture

This process uses pure oxygen for combustion which removes the large part of nitrogen in the flue gas replacing it by CO_2. The flue gas consists of a stream of CO_2 with water vapours and smaller amounts of pollutants such as SOx. After water is condensed and additional air pollutants removal, the flue gas is left with a near pure stream of CO_2 that can be sent straight away for storage. The major attraction of oxy-fuel combustion is that it avoids costly auxiliaries for post-combustion CO_2 capture system. However, an air separation unit (ASU) is required to produce the comparatively pure oxygen required for combustion. An ASU adds significant cost to the technology.

Theoretically, oxy-fuel systems can capture all of the CO_2 produced, although in most current designs the capture efficiency is about 90% as a result of the additional gas treatment systems required to remove impurities. However, according to several techno-economic evaluation studies, oxy-fuel combustion is considered as one of the most energy and cost efficient carbon capture technology among the others [40, 41].

1.7.1.4 Emerging Technologies

These technologies involve a combination of processes and products that have either been demonstrated in the laboratory or in the field but substantial improvements in efficiency and cost over the state of the art technologies are still needed and under research. These technologies include chemical looping combustion, membrane

separation, enzyme-based systems, mineralisation, carbonation-calcination cycles and ionic liquids, etc. The option to significantly reduce the electricity cost and the energy penalty cost with CCS from power plants is under consideration [42-45].

1.8 Difference in Air and Oxy-fuel Combustion

Oxy-fuel combustion differs from conventional air combustion in several ways such as delayed flame ignition, reduced flame temperature, reduced SOx and NOx emissions. Several of these effects can be described by the differences in the properties of main diluting gases N_2 and CO_2 in the air and oxy-fuel combustion respectively. The density of the flue gas is higher in oxy-fuel combustion because the molecular weight of CO_2 is 44 as compared to 28 for N_2. The heat capacity of CO_2 is higher than N_2.

The diffusion rate of oxygen in CO_2 is smaller than that in N_2, only 0.8 times that in N_2. The flue gases have high emittance power because of the high level of CO_2 and H_2O during oxy-fuel combustion [46]. Therefore, in oxy-fuel conditions heat transfer and reaction kinetics are influenced by the differences in the properties of CO_2 from N_2.

1.9 Motivation Objectives and Novelty of the Research

The aim of this research is to design, construct, commission and experimentally evaluate the pilot scale bubbling fluidised bed (BFB) combustor for air and oxy-fuel combustion of different biomass fuels (woody and non-woody).

More specific objectives of this research are:

- To study the different biomass fuels characteristics such as devolatilisation, thermal degradation, reactivity, the energy of activation etc. under N_2, Air, CO_2 and oxy-fuel using thermogravimetric analysis (TGA).
- To investigate the combustion behaviour of different biomass fuels during air combustion using a different level of excess air with the BFB combustor.
- To study the effectiveness of the air staging combustion for NOx reduction with the BFB combustor.
- To study the emission characteristics such as NOx, CO and CO_2 of different biomass fuels under air and oxy-fuel combustion.
- To investigate the oxy-fuel combustion behaviour of biomass fuels using various O_2/CO_2 mixture ratios such as; $21\%O_2/79\%CO_2$, $25\%O_2/75\%CO_2$ and $30\%O_2/70\%CO_2$.
- To investigate the biomass fuels' bed material and ash characteristics using SEM/EDX, XRD and XRF analysis under air combustion conditions.

According to the literature review this research has following novel features:

- A range of woody (domestic wood, industrial wood) and non-woody (miscanthus, wheat straw, peanut shell) biomasses are systematically investigated in a 20 kW_{th} BFBC.

- The air staging combustion is investigated for a range of biomasses in the 20 kW_{th} BFBC by injecting secondary air from two different heights named as AS1 and AS2, there is no such literature available which show 100% biomass air staging combustion from two different locations and different heights.
- The oxy-fuel combustion using 100% biomass fuels is investigated in the 20 kW_{th} BFBC under different oxy-fuel environments as $21\%O_2/79\%CO_2$, $25\%O_2/75\%CO_2$ and $30\%O_2/70\%CO_2$. There are several studies available on biomass co-combustion with coal but no such investigations have been made using 100% pure biomass firing under this wide range of oxidant mixtures on a pilot scale fluidised beds.
- After hundreds of hour's operation, there were no de-fluidisation or technical issues with the 20 kW_{th} BFBC during a range of biomass fuels combustion under air, air staging and oxy-fuel combustion conditions.

1.10 Thesis Layout

This thesis is laid out in subsequent chapters as follows:

Chapter 2: Literature Review

A review of biomass, its properties and conversion of biomass fuels into sustainable energy is described. An overview of fluidised bed combustion (FBC) with its types and fuels flexibilities is presented. Furthermore, different parameters and challenges affecting biomass FBC are investigated and summarised. Finally, a review of emissions during solid fuels combustion and emission control technologies is presented.

Chapter 3: Design and Manufacturing of Experimental Setup

A full description of the design of 20 kW_{th} bubbling fluidised bed (BFB) combustor is presented together with the important design calculations. The drawings and pictures of different parts of the BFB combustion system are also presented in this chapter.

Chapter 4: Experimental Methodology

A description is given on the experimental procedures used in Chapter 5, 6, 7 and 8 for the characterisation, thermal behaviour, air combustion, air staging combustion and oxy-fuel combustion of different biomass fuels.

Chapter 5: Thermal Analysis and Characterisation

The biomass combustion fundamentals including; thermal degradation, reactivity, the energy of activation and their relationship with different primary fuel properties under a range of reactant gas environments are presented. As well as some identified reaction zones of interest, in terms of their devolatilisation, gasification and combustion behaviours are also described.

Chapter 6: Un-staged and Air-staged Combustion

The effects of excess air, without staging air and with staging air on the gas emissions and temperature profiles were thoroughly investigated. In order to study the effects of the secondary air injection location on the gas emissions, the staging air was injected at two different heights of the combustor.

Chapter 7: Oxy-fuel Combustion

The oxy-fuel combustion of biomass fuels is studied under different conditions. The various reaction environments investigated include 21%O_2/79%CO_2, 25%O_2/75%CO_2 and 30%O_2/70%CO_2.

Chapter 8: Bed Material and Ash Characterisation

The characteristics of bed material and cyclone ash under air combustion are studied by means of SEM/EDX, XRD and XRF.

Chapter 9: Conclusions and Future Work

Conclusions from each chapter are summarised and recommendations are made for future work.

Chapter 2

Literature Review

2.1 Biomass

Biomass is a biological origin organic material that comes from different sources typically plants and animals. Biomass is a renewable source of energy, it contains stored energy from the sun during the process of photosynthesis [47]. As far as environmentally concerned, the use of biomass offers considerable benefits. Biomass absorbs the same amount of carbon dioxide during growth from the atmosphere as it releases during its utilisation in combustion applications. Therefore, biomass does not contribute to the greenhouse effect, rather it helps in recycling the atmospheric CO_2 as shown in Figure 2.1. Biomass can be directly burned to get chemical energy in the form of heat. Moreover, biomass can also be transformed to biogas or liquid biofuels that can be burned as fuels [48]. Hence, the energy obtained from biomass or biofuels is termed as bioenergy [49]. About 14% of the worldwide energy consumption is from biomass

from which a significant portion, about 35% is consumed in developing countries while a minor portion, about 3% is consumed in developed and industrialised countries [50].

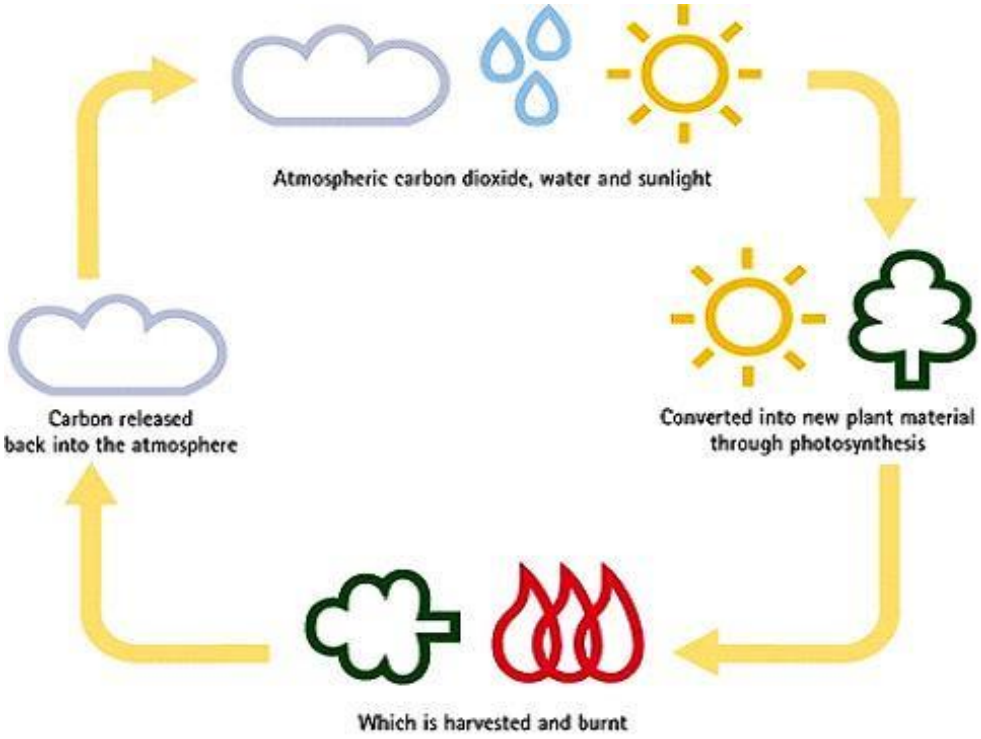


Figure 2.1: The closed carbon cycle showing that CO_2 used during photosynthesis process released back to the atmosphere after biomass combustion [51].

2.1.1 Types of Biomass

Different researchers characterise biomass in different methods, but one simple way, based on the properties of biomass [26, 52], defines main types as;

- Wood and woody: Including soft wood, hard wood, demolition wood etc.
- Non-woody or herbaceous: Including grasses, stalks, straw, etc.
- Energy crops: Including specially cultivated for energy purposes such as maize.
- Aquatic: Including algae, seaweeds, kelp, reed and rushes, etc.

- Derivatives: Including waste from food, saw, and paper industries, etc.
- Wastes: Including sewage sludge, manures, refuse derived fuel (RDF), etc.

In these categories, the properties of biomass vary in a wide range due to its diverse nature. For example, the moisture contents can simply vary by a factor of two in all types of biomasses except energy crops.

2.1.2 Composition of Biomass

The most important stage during the study and application of a fuel is the identification and characterisation of its chemical composition and physical properties. These basic characteristics are the unique code that determines the quality, properties, potential applications and environmental impacts of the fuel. The composition of each biomass differs dependent on the species and the geographic location where it has been grown. In general, biomass comprises of cellulose, hemicellulose, lignin and some other extracts. Cellulose is a linear glucose polymer comprising a linear chain of 1,4-D-glucopyranose components linked as 1-4 in the b-configuration having an average molecular weight of about 100,000 [53]. Hemicellulose is a combination of polysaccharides with variable composition mostly sugars, for example glucose, mannose, xylose and arabinose and methyl-glucuronic and galacturonic acids, having an average molecular weight around 30,000 [52, 53].

Lignin is an irregular group of amorphous, chemically related compounds with high molecular weight. The lignin structure consists of three carbon chain attached with a ring of six carbon atoms know as phenyl-propane. These could have zero (I), one (II) or

two (III) metoxyl groups attached to the rings. The source of the polymer defines the proportions of each structure, grasses for example have structure-I, the wood of conifers show structure-II and deciduous wood comes up with structure-III [54, 55]. Biomasses are highly oxygenated compared with those conventional fossil fuels due to their carbohydrate structure. As an example, the molecular structures for cellulose, hemicellulose, and lignin is presented in Figure 2.2.

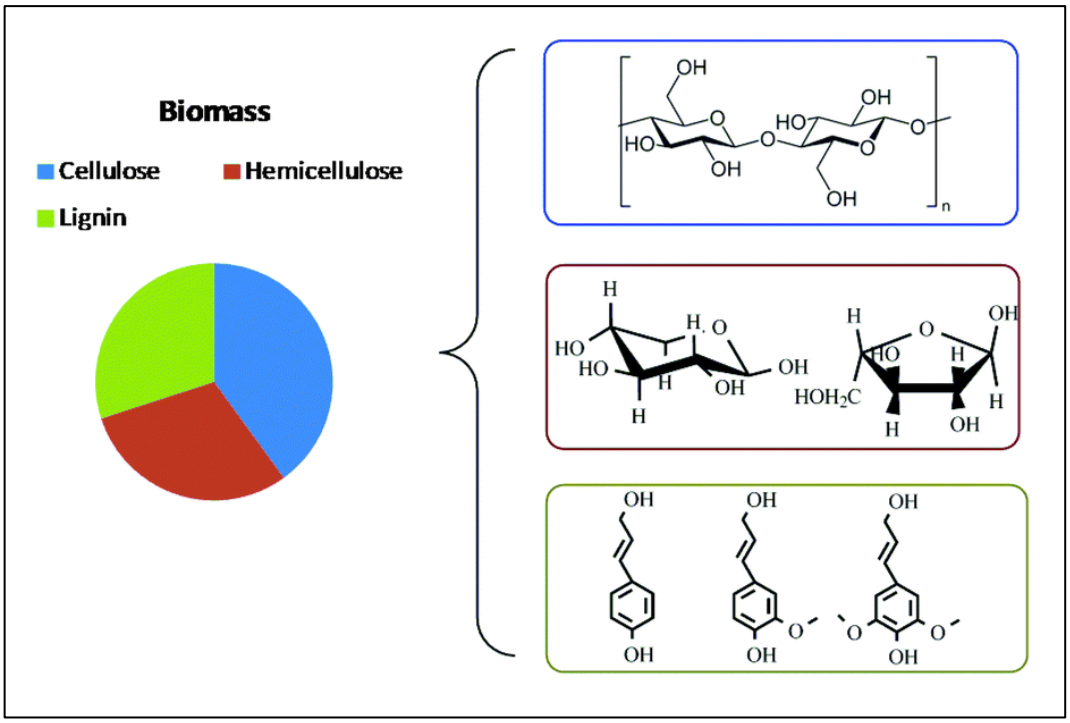


Figure 2.2: Lignocellulose biomass composition and structure: cellulose, hemicellulose, and lignin [56].

The content of these main components in biomass varies. According to Ayhan Demirbas [57], cellulose is normally the biggest fraction, constituting, about 40 to 50% by weight, the hemicellulose represents 20 to 40% by weight and lignin contents are about 30 to 40% in woody biomass. Typically, extractives value is 5 to 10% in herbaceous plants [48, 52]. A comparative structural analysis of different biomasses is

given in Table 2.1. An extensive variation in the distribution of ash content and inorganic species can be observed in both non-woody and wood types. The ash content of biomass fluctuates over a wide range from less than 1% by weight such as in clean wood to more than 20% in rice husks [58]. Silica and potassium are the two major ash forming species for all of the agricultural residues, excluding rape straw [53].

The irrigation and fertiliser usage in the growth of herbaceous plants lead to higher inorganic species contents in comparison to wood and woody biomass [59]. In particular, the alkali content is much higher in the herbaceous fuels in comparison to the woody and coal fuels [53]. The mix of inorganic species within each material affects both the combustion properties of the fuel and additionally the design and operation of the combustion system.

Table 2.1: Structural analyses of various types of biomasses [57].

Biomasses	**Composition (wt%)**			
	Hemicelluloses	Cellulose	Lignin	Extractives
Hazelnut shell	30.4	26.8	42.9	3.3
Beech wood	31.2	45.3	21.9	1.6
Spruce wood	20.7	49.8	27	2.5
Corncob	31	50.5	15	3.5
Tea waste	19.9	30.2	40	9.9
Walnut shell	22.7	25.6	52.3	2.8
Almond shell	28.9	50.7	20.4	2.5
Sunflower shell	34.6	48.4	17	2.7
Wood bark	29.8	24.8	43.8	1.6

2.1.3 Energy Content of Biomass

The heating value or chemical energy content stands one of the most important parameters when considering different types of biomass species for fuel and energy applications. Typically, the higher the carbon content, the bigger the energy or heating value. It is apparent that the more hydrocarbon like the lower the degree of oxygenation and the higher the heating value [26]. Carbon is usually a dominant element in biomass consisting of 30 to 60% on dry basis but having a higher concentration in woody biomasses as compared with herbaceous biomasses. The polysaccharide content of biomass makes it much more oxygen rich about 30 to 40% than coal with an oxygen content of about 10% in terms of energy production [49, 60]. Therefore, biomass materials with a lower O:C ratio and higher lignin content correspond to a higher calorific value.

Additionally, biomasses have a higher moisture content, lower density, less nitrogen and sulphur, more chlorine, potassium and silica, less aluminium and iron and have a lower heating value, in comparison to coal [53]. The moisture content varies depending on the kind of biomass, for example newly cut wood contains 30 to 60% moisture on as received basis [61]. The compounds that are formed and released during biomass pyrolysis are named as volatiles or volatile matter, while the carbon remaining in the char after pyrolysis is called fixed carbon. Generally, the percentage of biomass released during combustion as volatiles is 70 to 86% on the dry basis [62]. In coal, the share of volatiles is less, with a higher amount of fixed carbon [52]. Some of these variances are beneficial, whilst others generate technological issues and challenges. It is a fact that high moisture content reduces the thermal efficiency during combustion,

lowers the maximum flame temperature and can cause problems during ignition. The optimal moisture content in most biomass fuels is around 15%, although furnaces can usually handle a maximum of 65% moisture [60]. A scientific way of comparison of biomass with fossil fuels, is in terms of their H:C and O:C ratios, is known as Van Krevlen diagram [60], represented in Figure 2.3.

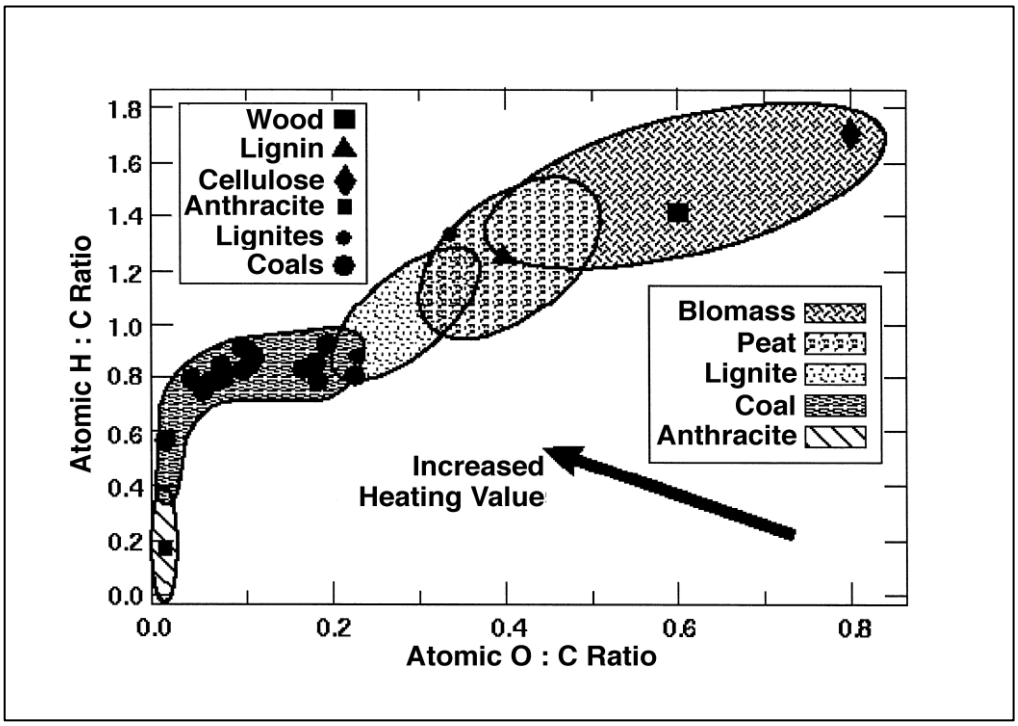


Figure 2.3: The Van Krevlen showing compositional differences among coals and biomass [60].

Comparing the biofuels with coal it is clear that the high proportion of O and H compared with C reduces the energy value of the fuel because less energy is present in C–O and C–H bonds than in C–C bonds. Moreover, the energy content of a material is high if O: C respective ratios are lower. Therefore, a distinction can also be made from the Van Krevlen diagram between different energy carriers derived from biomass fuels.

2.1.4 Physical Properties of Biomass

Physical properties related to biomass species such as porosity, density, internal surface area and variability as well as fuel preparation methods such as shape distribution, bulk density and particle size vary greatly. Depending on the choice of the combustion technology, various pre-treatment steps such as sizing (crushing, shredding, chipping, etc.) and drying methods are required to fulfil the process requirements [63].

The steps involved in storing and processing biomass, such as densification, influence the particle size, ash and moisture content in the biomass. Even the degree of contamination varies, for example during wheat straw washing, the alkali and chlorine contents reduce. Therefore, some parameter like specific gravity, particle shape and size are important for the fuel preparation, feeding and combustion processes [64]. These properties strongly affect inside the combustion chamber among others like dust emissions, combustion kinetics, entrainment and segregation problems particularly in fluidised beds (FBs).

The bulk density is most important physical property among all others due to economic and technical reasons. Most of the biomasses, especially from agricultural sources, such as rice husk and wheat straw have low bulk densities. For instance, the bulk density of rice husks and chopped wheat straw are 100–125 and 50–120 kg/m^3 respectively [65, 66]. These are very low in comparison with the density of coal, which is in the range of 800–900 and 560–600 kg/m^3 for bituminous and brown coals respectively [67]. There are various disadvantages associated with the lower bulk density of biomass; such as expensive transportation, huge storage requirement, comparatively low heating values,

feeding problems, process control complications and limitations of combustion technologies applied. However, some of these disadvantages can be overcome by applying densification process, it removes inter and intra-particle voids present in the biomass fuels. The most commonly used densification techniques are briquetting, baling and pelletisation [68].

2.1.5 Effect of Biomass Elements on Combustion

During the utilisation of biomass, certain elements deserve special attention. These elements include nitrogen (N), chlorine (Cl), potassium (K), sulphur (S) and silicon (Si). The most important element in different combustion related problems with regard to its behaviour is chlorine. The high content of Cl in some biomasses can cause severe damage to the combustion equipment. The Cl is found in high amounts in a certain type of biomass, for example, wheat straw. It could also affect the operation by inducing Cl on the super-heated tube surfaces causing high-temperature corrosion.

Moreover, Cl helps the movement of many inorganic compounds, specifically potassium chloride (KCl), which is amongst the utmost stable high temperature containing gas phase alkali species. Very often Cl concentration dictates the quantity of alkali (K) vapourised during the combustion process, as powerfully as it dictates the transportation of alkali from the biomass fuel to the surface, where alkali every so often forms sulphates. In the absence of Cl, alkali hydroxides such as KOH are the main stable gas phase species in oxidising moisture environment conditions [7, 60]. The Si and K percentages are usually higher in herbaceous biomasses. These high proportions of S together with K and Cl also play its part in causing severe ash deposition

complications at moderate or high temperatures during combustion. The reactions of alkali-silica to form alkali silicates are the basic sources of these problems which soften or melt the silicates at lower temperatures (even less than 700 ^{o}C), the reaction of alkali with S forms alkali sulphates on the heat transfer surfaces of the combustor [57, 60, 69, 70]. The compounds containing alkali play a leading role in both of the above processes; K is the dominant alkali sources in most of the biomasses [57, 60, 70, 71]. The S content is typically low in biomass, but S present in coal may cause severe problems during the co-firing combustion process. The high fractions of Si, Cl and K also cause severe issues of agglomeration in FBs.

The pyrolysis based pre-treatment process followed by char washing could be used to remove K from wheat straw. The K element is retained in char through the pyrolysis process of straw at moderate temperatures. Whereas residual Cl and K are removed from the residual char through water [57, 72]. Then pyrolysis gases and char might be used in a conventional boiler without complications. To evaluate these pre-treatment processes, research knowledge about the char wash procedure is required. Chlorine and sulphur along with nitrogen are also accountable for gas emissions such as HCl, SOx and NOx and to some extent dioxins and furans [7, 57, 72, 73].

2.2 Biomass Conversion Technologies

To make use of the energy available in biomass, it is essential to utilise a technology to either release the energy directly by burning of materials for heat or to convert it into other forms such as solid or liquid fuel. Biomass can be transformed into valuable forms

of energy through a number of different routes. Currently, there are two main conversion pathways, each appropriate for the specific type of biomass and specific form of energy products; thermochemical and biochemical as represented in Figure 2.4 [74, 75]. A numbers of factors influence the choice of the conversation process such as quality and type of biomass, preferred form of energy, environmental, and economic factors. In most of these cases, the form of energy required usually determines the process path, followed by the quantity and type of biomass. Thermochemical is a combined application of heat and chemical processes to produce energy from biomass. The thermochemical conversion processes mainly comprises pyrolysis, gasification and combustion.

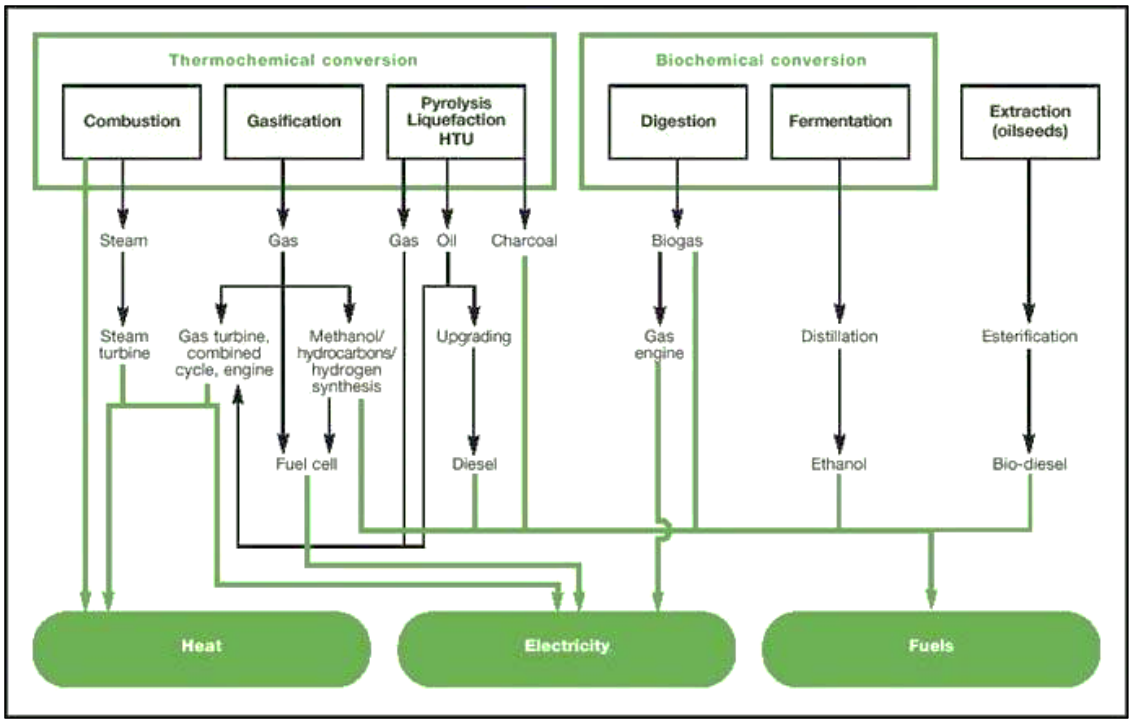


Figure 2.4: An overview of biomass to power and heat conversion technologies [74].

In the biochemical process, the enzymes such as bacteria or some other micro-organisms are used to break down the biomass molecules into a liquid form of fuels. Some of the biochemical conversion processes are fermentation and anaerobic digestion. The chemical conversion or extraction processes implicate the use of chemical agents for conversion of biomass into liquid fuels [76]. From the related technologies, combustion is the most important option and accountable for more than 97% of the world's bioenergy production [57]. Although relevant biomass conversion technologies exist and continue to be developed, some are not yet cost-effective, such as the large-scale conversion of cellulosic biomass to transportation fuels.

2.2.1 Thermochemical Conversion of Biomass

Biomass thermochemical conversion processes including combustion, gasification, and pyrolysis are under development worldwide and several of these processes are established on effective fluidisation and utilise fluidised beds as part of the equipment [77]. Around the globe, most biomasses have been utilised for energy purposes by the direct combustion that converts biomass into heat. In the combustion process biomass is exposed to a series of chemical reactions in which carbon oxidises in the form of carbon dioxide, hydrogen oxidises into water and energy is produced in the form of heat [74]. The most important facts in combustion are: (1) chemical reactions are exothermic, (2) combustion can only happen if there is sufficient heat to increase the temperature of the unburned gases, (3) most combustion reactions are gas phased due to the high temperatures, and (4) combustion is more efficient if there is just enough oxygen present for burning the fuel [50].

2.3 Biomass Combustion Mechanism

The biomass combustion process consists of series heterogeneous and homogeneous reactions. Though there are lots of different combustion systems existing in the market, the combustion principle of biomass is fundamentally the same for each. The important process steps consist of drying, pyrolysis/devolatilisation and char combustion respectively. The schematic descriptions of these main steps of combustion are shown in Figure 2.5 [78]. All types of biomasses contain moisture, which has to be removed before the actual combustion can start. This first initial heat for drying is supplied by the flames radiation and second from the stored heat inside the chamber of the combustion system.

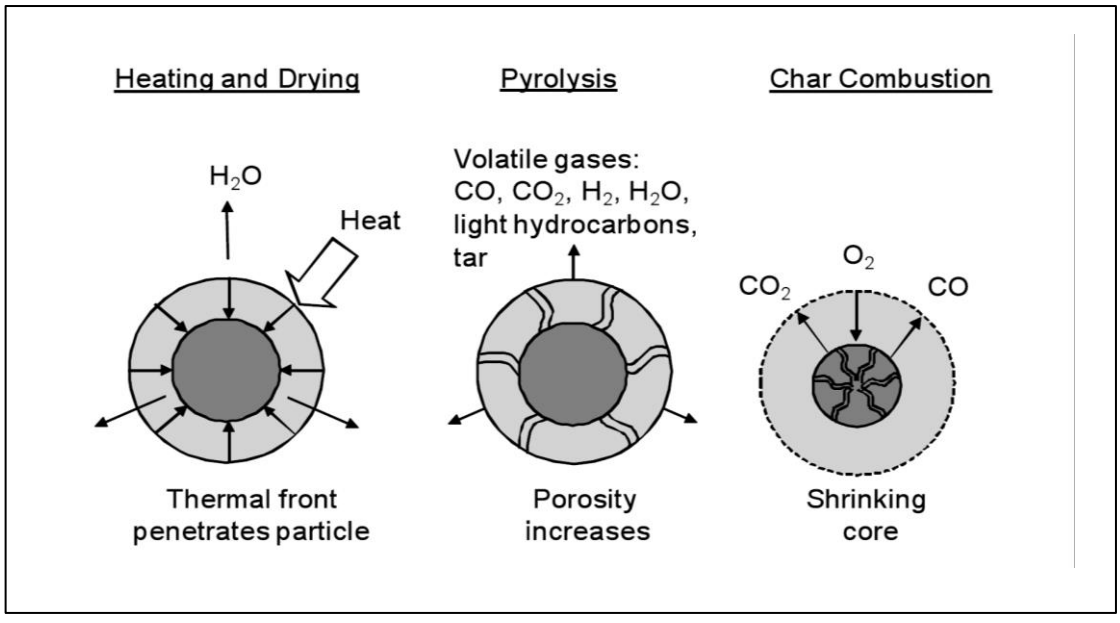


Figure 2.5: Schematic representation of the main stages of biomass combustion process [78].

The devolatilisation of biomass starts when the temperature reaches between 200–350 ^{o}C, and during this process, the volatile matter is released. The volatiles are comprise of methane (CH_4), carbon dioxide (CO_2), carbon monoxide (CO) along with other

compounds with high molecular weight such as tar that shrink into a liquid form when cooled down. This mixture of gases burnt with oxygen (O_2) from the air produces a yellow colour flame. The heat released during the burning of these gases is used to dry the fresh biomass and likewise release further volatiles hence, this process is self-sustaining. A sufficient amount of oxygen has to be provided for continuous sustaining especially this part of the combustion process. The char is the main remaining substance after burning all the volatiles in biomass [78].

The char combustion starts at a temperature about >750 ºC in the system. The oxygen is again required for the oxidation of char and for the bed of fire where it mixes with CO to form CO_2. All these stages can occur even at the same time during the combustion process [79]. It is worth bearing in mind that a sufficiently long residence time in a combustion system permits the fuel to be totally burned off. Moreover, there must be sufficient air in the combustion system for the complete combustion. The additional use of excess air largely reduces the CO formation by letting more CO react with O_2. Therefore, a good indication of complete combustion is less CO present in the flue gas.

However, excessively high excess air will lead to the loss of the released energy and lower the system efficiency as more of the gas takes away energy from the combustor [78]. To improve the economic cost and combustion system efficiency of a system, it is important to achieve complete combustion.

2.4 Fluidised Bed Combustion

The fluidised bed technology is named after the matter within the fluidised bed boilers and determines the way in which the combustion process is managed. The ultimate goal of the fluidised bed combustion (FBC) was 'getting rid of waste' when this technology was first introduced. Since its start in 1970's this technology has expanded recognition in various industrial applications [80].

Those applications can be categorised as (1) chemical reactions and catalysis practices (2) physical and mechanical practices. The FBs are equipped with excellent mixing capabilities; therefore, the physical processes such heating, cooling, mixing, drying, coating and granulations take benefit of these excellent mixing capabilities of FBs [81]. With temperature uniformity, ease of process control and good heat transfer, these parameters rise when there is good mixing of solids, and can be easily handled in an efficient way [82]. Moreover, FBs are virtuous medium to carry out the reactions involving a gas and a solid contact [83]. For synthesis reactions, FBs are preferred over fixed beds due to strict demand of temperature control in the reaction zone and therefore FB reactors give nearly isothermal conditions. In addition, the hydrocarbon reforming and cracking process is carried out in pneumatic solid circulating systems using single or multiple FBs [84].

In combustion applications, FBs have been known for their capacity to burn low-grade fuels such as biomass with low calorific value, high moisture and ash contents [85-87]. Currently operating commercial FB boilers around the world are not only burning coal

but also waste materials, refuse derived fuels and biomasses as well as co-firing [80]. Additional new application of FBs are in CCS through two practices; oxy-fuel and chemical looping combustion [88, 89]. The fuel flexibility, less emission, reuse of non-hazardous by-products and the possibility of retrofitting in existing power plants are additional benefits of FB technology [90, 91]. Nevertheless, FBs also show disadvantages such as gas bubbles causing chemical and mechanical difficulties, bypassing of solids by bubbles lowers the efficiency during the conversion of gaseous reactants, erosion due to the particle abrasion and entrainment of solids etc. [81, 92].

Many technological developments have been put forward for FBC and its derivatives, because as the technology matures, the drivers such as market, regulatory constraints and technical challanges have improved. Up to now the main developing areas are environmental compliances, scale up and fuel flexibility in design [93, 94]. Further research and development efforts on these aspects will be significant in the development of FBC in future. More efforts to increase efficiency reduce capital and operating cost as well as improvements during construction and operation are being already set. Nowadays, the fuel conversion application in FBs technology especially using biomass is one of the hot research topics. The development of oxy-fuel combustion technology in FBs is also a current state of art in the market [93-96]. Three flowing variants of FB technology were developed since this technologies evolved.

2.4.1 Bubbling Fluidised Bed

The bubbling fluidised beds (BFB) are the first generation of FBC technology. It is confirmed from concrete industrial experience over the past serval decades that BFB

technology can be well suited for the use of difficult and problematic fuels such as; fuels containing low volatiles, high moisture and ash contents, for example, anthracite, petroleum coke, municipal solid waste, sludge's and refuse-derived fuel [97]. A schematic representation of a BFB boiler is given in Figure 2.6a. Generally, BFB consists of a chamber with a distribution plate at the lowest part through which steam or air is introduced into the reactor. Biomass is feed over the distribution plate into the moving bed of fine-grained material usually sand.

The operational fluidisation velocity is always lower than that of terminal velocity of the bed material; therefore the freeboard region has only a gas flow which comprises of ash and a small amount of other particles (bed material). The bed temperature in BFBs is typically in the range of 800 to 900 °C [98]. Hence, BFBs are also well suited to smaller industrial applications including the combustion of waste materials. Dos Santos et al. and many other researchers recommend the use of a BFBs for combustion of biomass due to several striking characteristics, such as high combustion efficiency, pollutant emission control, and a high heat transmission rate between the solid bed material and the injected biomass [99]. Therefore, BFBs can achieve combustion efficiency of 96–98% and improve the heat transfer rate by 60–80 times over that of conventional pulverised fuel combustors [100].

2.4.2 Circulating Fluidised Bed

The circulating fluidised bed (CFB) was the second version derived from the BFB technology and outdoes its prototype in terms of S removal applications and combustion efficiency [101]. Applications of CFB have changed over the time such as the

installation capacity gradually increased. In addition, with time the CFB has transformed from industrial applications to utility applications [102].

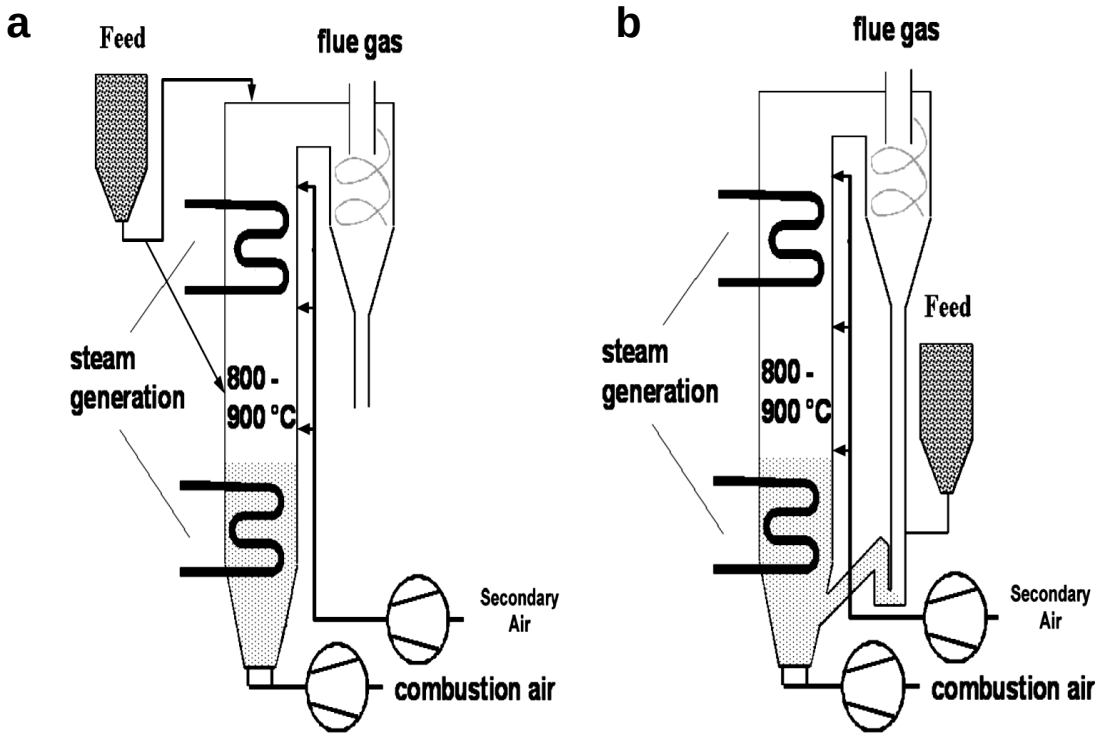


Figure 2.6: Representation of; a) bubbling fluidised bed boiler (BFB), b) circulating fluidised bed (CFB) boiler [103].

In contrast to BFBs, in CFBs the methodology for fluidisation velocity lies in the order of magnitude of their terminal velocity, meaning that the bed material is also carried out into the freeboard establishing a solid/ gas flow in the whole reactor. The bed material is circulated from the main reactor to the cyclone separator, where the fly ash is separated and the bed material along with unburned char are returned back to the reactor [104].

The CFBs can be operated at elevated pressure, hence they can be utilised directly for the end user applications such as in gas turbines where the compression of the gas is

required during the process. The CFB features a higher specific input and higher mixing efficiency as compared to BFB but has some complex disadvantages such as the greater demands on the fuel properties (e.g. specific size) and higher pressure loss which results in high process power consumption [103].

2.4.3 Hybrid Type BFB and CFB

The hybrid type BFB and CFB are the third generation of FBC technology. They were developed to get combined advantages of BFBs and CFBs for their applicability in the medium scale industrial operations with a varying range of capacities. The hybrid types of fluidised beds have a small market share in comparison with BFBs and CFBs [105, 106].

2.5 Design and Operation Variables

The main design parameter and components of different types of FBs combustors are as follows.

2.5.1 Design variants

In both of the major technologies of the BFB and CFB almost similar principle has been utilised although the design and installation parameters considerably varies. The FBC design is dependent on the type of the fuel and steam conditions required although it is also included by site conditions and emissions requirements. Some major design parameters of both technologies reported by other researchers are presented in Table 2.2 [107-109].

Table 2.2: The design parameters BFB and CFB [105, 110-112].

Design parameter	BFB	CFB
Combustion temperature (^{o}C)	760–870	800–900
Fuel particle size (mm)	0–50	0–25
Fluidisation velocities (m/s)	1–3	3–10
Solids circulation	No[1]	Yes
Lime stone[2] particle size (mm)	0.3–0.5	0.1–0.2
Average steam parameters		
Steam flow (kg/s) (range)	36 (13–139)	60 (12–360)
Steam temperature (^{o}C) (range)	466 (150–543)	506 (180–580)
Steam pressure (bar) (range)	72 (10–160)	103 (0–275)

[1]Circulation of (large) unburned particles is possible in the case of bad burnout.

[2]In the case when limestone is used for in bed sulphur removal.

2.5.2 Fuel Preparation

Some additional fuel preparations are required before feeding the fuel into the FBs for combustion. Serval techniques are available for processing the fuel from the production site to storage and finally into the combustion system [113]. The main steps of these techniques are cleaning, sizing, drying and separation of impurities such as non-combustibles from the fuel. The separation process is most important while dealing with waste biomass fuels. The size < 25 mm is generally required for CFB, whereas size <50 mm is suitable for BFB [113, 114].

2.5.3 The Combustor

The majority of the fuel particles in BFB fed into the sand bed immediately with available oxygen in the primary air flowing upward into the reactor also shown in Figure 2.6a. The lower combustion zone of the BFB combustor holds a high-density material (fuel mixture) and ash. The lined refractory protects the inner part of the

combustor from high temperatures and from corrosion/ erosion. During combustion, hot water vapours act like a heat buffer which enables higher heat transfer between the fuel particles. That is the reason the BFB combustors are less sensitive to fuel moisture content variations and are very compatible for biomass combustion [115].

The low fluidisation velocity and longer residence time in BFB combustors allow efficient combustion of the fuels having low calorific value with bigger particle sizes [116]. Moreover, the staged combustion could be applicable in the different parts of the combustor. In staged combustion, the secondary air is introduced above the main combustion zone, which increases fuel to oxidant ratio and results in better combustion [117]. The section above the main combustion zone is termed as freeboard zone or freeboard, in this section, the solid particles connection is always low. The non-oxidised fuel particles are combusted in the freeboard zone with secondary air under sub-stoichiometric conditions. The use of secondary air is very common for the fuels having higher volatile contents like biomass because they are combusted above the bed [118].

The fluidisation velocity is the main difference between BFB and CFB which is lower in BFB as compared with CFB. Due to higher fluidisation velocities and strong mixing in CFB, the flue gas heat transmission patterns are different from those of BFB. In BFB combustor the heat transfer and solid particles concentration slowly decrease alongside the height of the combustor [98]. The temperature distributions in a CFB are more homogenous than those in a BFB. The temperatures during combustion in a CFB are higher whereas a BFB operates with lower combustion temperatures due to poor fuel quality, high moisture contents and bigger fuel particle sizes [119, 120].

2.5.4 Particle Circulation and Collection

In BFB combustion the proportion of ash particles and non-combustible solids is high. If the quantity of these solids become too high it could prevent the combustor from working properly, hence it is necessary to collect these solids to make sure a stable operation of the BFB system. The solids along with fly ash can be collected from the cyclone separator or similar device installed at the end of the flue gas path as shown in Figure 2.6a. On the other hand, the unburned fuel particles during CFB operation are fed back to the reactor which improves the overall combustion efficiency of the system. In a typical power plant, the flue gas from the boiler is led to an electrostatic precipitator (ESP), bag house or another solid cyclone which collects the remaining fine particles before the hot gas is discharged from the stack.

In CFB combustors high percentage of solid partials are also found in the upper part of the reactor due to high operating fluidisation velocities. These solids mainly consist of bed material and unburnt fuel particles; in this case, these particles must be separated from the hot flue gas before it enters into the convective pass through the combustor [121]. Similarly, a cyclone or any other collection device is used to get solids out from the combustion system. Up to 100% solids can be easily separated with a high-efficiency cyclone by centrifugal force. An external fluidised bed heat exchanger is used to cool down the collected solid particles and fed into the combustor again for a new cycle [98]. In a CFB the temperature needs to be kept at operational conditions especially during combustion of low calorific value fuels and that are usually controlled by the adjustment of the solids circulation and flue gas recirculation rates [114].

2.6 Gaseous Pollutant Emissions

This section gives an overview of some major gas pollutants which are related to biomass combustion and of co-combustion with coal under air and oxy-fuel environment, with a focus on small to pilot-scale fluidised bed systems. Some common difficulties have been acknowledged, their mechanisms are described and some remedies have been investigated as well.

2.6.1 CO Emissions

During biomass combustion and co-combustion with coal, carbon monoxide (CO) emissions are often the main concern [116, 122]. CO emissions go to the classification of unburnt pollutants which are essentially produced as an outcome of incomplete or unfinished combustion of a fuel. The CO emissions of biomass combustion in FBs can be higher than those of coal combustion, especially when biomass fuels are combusted in small scale units which were designed only for coal combustion and have not been altered for biomass or co-combustion with coal. The higher CO emissions are potentially due to the high volatile matter contents in biomass fuels [123, 124].

A significant amount of CH_4 has also been detected during devolatilisation of biomass, which afterward changes into CO and CO_2, further above in the freeboard region of the FBs [124]. Shorter freeboards characterised by small residence time also cause high CO emissions in the small scale combustion units. Biomass has comparatively high volatile matter content compared with that of coal and therefore biomass fuels require extra residence time in the freeboard to burn completely [122]. The biomasses with high ash

content results in an ash layer formation around the biomass fuel particle which makes the oxygen diffusion tough [114]. The typical location of heat exchangers in the FBs freeboard zone reduces the temperature in that region and consequently prevents the transformation of CO to CO_2. Rough or improper feeding of biomass could also result in high emissions of CO during combustion [125].

Under conditions of high-temperature and high partial pressure, CO_2 can dissociate into CO and O_2 through a strongly endothermic reaction. In the flame zone during oxy-fuel firing both of these conditions are present [126]. Hence, gasification of carbon, a CO_2 dissociate reaction (see Eq. 2.1), could also contribute in increasing the CO production during oxy-fuel firing (see Eq. 2.1) [127-130]. However, there is a dissimilarity in opinion among researchers as whether it is the thermal dissociation [131] or the CO_2 gasification reaction [132], that plays the main role in the significantly increase of CO concentration in the flame zone compared to air combustion.

$$CO_2 \rightleftharpoons CO + 0.5O_2 \tag{2.1}$$

Another important way which can increase the CO concentration in the flame zone during oxy-fuel combustion is the reaction of CO_2 with H radicals. The high concentration of CO_2 in oxy-fuel combustion environment induces a possible alteration of the composition of O/H radical pool due to the competition between O_2 and CO_2 for H radicals, (see Eq. 2.2 and Eq. 2.3) [130, 133].

$$H + CO_2 \rightleftharpoons CO + OH \tag{2.2}$$

$$H + O_2 \rightleftharpoons O + OH \quad (2.3)$$

During oxy-fuel combustion, the ratio of OH to both O and H radicals is increased but the total amount of radicals is supposed to decrease compared with air combustion due to high particle pressure of CO_2. In addition, the reaction of CO_2 with CH_2 and with H radicals are similarly found to enhance the CO concentration in the flame zone [133, 134].

Wang et al. [135] performed experiments in a 3 MW_{th} horizontal furnace for both air and oxy-fuel combustion with similar flame temperatures and reported no significant change in the concentration of CO both within the exhaust and the latter part of the flame zone. Based on modelling study results, five time an increase in the level of CO emission within the flame was anticipated. The concentration of CO in the flame zone was expected to be slightly higher than for air firing under oxy-fuel conditions with the same oxidant composition as in air based on modelling results but the experiential values were lower than theoretically predicted. All of the tests yield a full CO burnout before exhaust.

Woycenko et al. [136] performed combustion experiments in the IFRF 2.5 MW_{th} furnace and showed an increased level of CO within the flame zone. Before the exit of the furnace, the CO combustion was completed and no significant emission of CO was observed. Similar results were achieved by Liu et al. [137], Scheffknecht and Co-workers [138, 139] by changing the oxygen concentration from 30 to 21% in oxy-fuel tests; an increase in the concentration of CO from 34 to 200 ppmv was observed due to

delayed ignition and lower peak temperature. The investigations of Glarborg and Co-workers [130, 140, 141] on natural gas combustion show that high levels of CO_2 in oxy-fuel combustion inhibit the complete oxidation of fuel-CO to CO_2 at high temperatures even when excess oxygen is used. Though, the consequence is most noticeable under the fuel-rich conditions. There is no such sign that high CO_2 levels affect the CO oxidation at excess oxygen and low temperatures, and therefore there must be no risk of high emissions of CO from the oxy-fuel fired plant if the mixing of oxidant and fuel is sufficient [126].

In conclusions, taking into account of the high volatile matter content of biomass which needs longer residence time in freeboards for combustion, larger freeboards are recommended in terms of design improvements of FBs for biomass combustion. With small scale FBs, the internal heat exchangers present in freeboards and splashing zones could be removed to retain these regions at higher temperatures and consequently to help the complete conversion of CO to CO_2. Another important factor for complete combustion is excess air; with a higher level of excess air complete burn out of the fuel can be attained under both air and oxy-fuel environments. Air staging and total system load can also be used as effective techniques to increase the residence time of the fuel in the hot region of FB combustors [122, 126, 142, 143].

2.6.2 NO_X Emission

The compounds of nitrogen including nitrogen oxide (NO) and nitrogen dioxide (NO_2) are frequently known as nitrogen oxides (NOx), and nitrous oxide (N_2O). NOx emissions perform a significant part in the atmospheric reactions that generate injurious

particulate matter (PM), ground level ozone and acid rain. In mixture with hydrocarbons (HC) these emissions photochemically lead to the creation of ozone, which results in eye irritation, lung and other major health problems in urban environments. NOx emissions also contribute to haze air pollution in our nationwide parks and wasteland areas [103, 144, 145].

Generally, there are three main pathways for NOx formation in combustion systems [122, 146]:

- Thermal NOx: formed at adequately high temperatures from the dissociation of the atmospheric air into O_2 and N_2.
- Fuel NOx: formed in the result of reactions relating fuel bound N contents.
- Prompt NOx: formed due to fast reactions inside the flame zone involving fuel bound HC radicals and N_2.

Thermal NOx are more significant when firing solid fuels in suspension systems with comparatively low stoichiometric ratios (SR) like 1.1 to 1.3 and typically at high temperatures, >1500 °C [147]. Specifically, in fluidised beds systems, the temperatures are generally <900 °C, hence the creation of thermal NOx is very unlikely. It is extensively reported in the literature that most of the NOx originates from fuel-N during combustion [57, 148, 149]. Nevertheless, some researchers have also specified a significant volume of prompt NOx formation in these combustion systems [146, 150]. Fuel NOx is of considerable great importance during the combustion of solid fuels because fuel NOx is formed as a result of the oxidation of the nitrogen within the fuel.

Typically FB systems are operated at 815 to 925 °C and at such temperatures the formation of NOx from the fuel-N dominates [57, 150, 151]. The formation of NOx from fuel-N proceeds by the oxidation reaction of the nitrogenous species released during devolatilisation and the oxidation of the nitrogen reserved in the char of the solid fuel, where NO is the main species with NO_2 typically less than 5% [103]. However, at low temperature in the downstream route of the flue gas, NO is readily oxidised to NO_2 hence, NO and NOx are exchangeable [152, 153].

The dispersal of the nitrogen among the volatiles and the leftover char is approximately proportional to the volatile matter content in the solid fuel. The char content in biomass fuels is small, hence during the devolatilisation process, a maximum of the nitrogen is supposed to be in the volatile form that is about 66 to 75% [103]. Therefore, NOx formation is via two different ways; (1) through the gas phase oxidation of the nitrogenous group in the volatiles, (2) through the heterogeneously catalysed oxidation of the char bound nitrogen species in the fuel [154-156]. It is believed that up to 20% of the total NOx formed during pulverised coal combustion under air is due to thermal NOx and about 80 to 100% is derived from fuel NOx, while the prompt NOx mechanism is insignificant, dependent on the amount of fuel bound N species [157, 158]. It is confirmed from the pilot and large scale combustion units that high NOx emission levels, up to 1000 mg/m^3, could be generated from biofuel combustion [114, 154, 159]. These high NOx emissions are a direct implication of the comparatively high nitrogen contents in these biofuels. There is a limited effect of operating conditions on the NOx from biomass as it is intensely dependent on fuel-N [148, 160].

The formation of fuel NOx is mainly a function of the nitrogen proportion in the fuel, the concentration of available oxygen during the primary pyrolysis, reactivity of the fuel and oxygen in the primary combustion sections of the combustor [151, 161]. In oxy-fuel combustion, the lower level of molecular nitrogen usually suppresses the formation of thermal NOx and prompt NOx and therefore possibly lowers the overall rate of NOx emission. In general, the amount of NOx emission from oxy-fuel plants could be reduced by between one-third and half of those under air combustion conditions [136, 162-165]. Moreover, by increasing oxygen concentration, higher than 21% to get adequate flame temperatures, could result in an increase of fuel NOx formation in oxy-fuel combustion environment [166].

Furthermore, some studies on biomass combustion also show a decreasing NO formation with rising fuel-N contents but not as expressively as other solid fuels like coal [149, 152, 156, 167]. That could be most likely due to the char which is present in comparatively high concentrations in the case of coal, being more effective in decreasing the overall NOx emission levels by catalysing the reduction of NO by CO [160]. However, this effect is not that important for biomass due to lower char content but is a valid reason for co-combustion systems [114]. The clarification for typically low but occasionally high NOx emission levels comes from the fact that biomass has high volatile content and low nitrogen content. It means that the leading source of NOx and N_2O is originating from biomass volatile contents[103]. Usually, NOx emission from high nitrogen contents biomass is very high, as the lower char contents in bed and hence the oxidation of NH_3 arising from the volatiles has little char available for reduction by CO. Hence, the NOx emissions are reliant on unburned carbon contents in

the fly ash, the lesser the NOx emissions, the higher the unburned carbon during combustion [168].

2.6.2.1 NOx in Oxy-fuel Combustion

Okazaki and Ando [169] performed experiments in a small-scale laboratory reactor, assessed the comparative influence on NO reduction mechanisms. And found that re-burn type reactions, i.e. reactions of recycled NOx with hydrocarbons, is the leading mechanism for the decrease in NOx emissions and it accounts for 50 to 80% of the reduction in NO experimentally observed in oxy-fuel combustion conditions. Reactions of NOx with N-volatiles were also evaluated to contribute about 10 to 50% to the NO reduction. In oxy-fuel combustion, the reduction of NO on char was established to be of negligible importance [126].

Andersson et al. [170] studied modelling on oxy-fuel combustion of lignite by means of comprehensive chemical kinetics and concluded that the formation of NO from fuel-N is similar or even slightly higher under oxy-fuel combustion compared with that of under air combustion. Moreover, the destruction mechanisms under oxy-fuel combustion conditions are enhanced compared with that of under air conditions, leading to an overall reduction in the NO emission levels. In oxy-fuel at high temperatures (>1500 ^{o}C) the near-elimination of molecular nitrogen facilities the reduction of NO by limiting the formation of NO through the Zeldovich mechanism [171].

Mendiara and Glarborg [126, 140, 141] examined the consequences of the changes on NO formation and destruction considering the oxidation of CH_4 doped with either NH_3

or NO in a laminar flow reactor. The results showed that CO_2 acts to encourage NO formation from volatile-N contents under fuel-rich conditions while it obstructs NO at both stoichiometric and fuel-lean conditions during combustion. The formation of NO is preferred by the rise in OH-concentration at lower oxygen concentration. Under oxygen excess conditions, the low formation of NO is caused by the control of the O/H radical pool particularly O. During re-burning a high concentration of CO_2 had only a minor influence on the NO reduction efficiency under reducing conditions.

Okazaki and Ando [158] showed the importance of NOx reduction on the char surfaces due to CO reaction. The CO levels rise because of the high CO_2 concentrations. The promoting effect of CO on NOx reduction on char mechanism is mostly important in fluidised bed conditions [145], i.e. at temperatures below the characteristics of pulverised fuel combustion. Hu et al. [172] performed a sequence of test runs in an entrained-flow reactor to analyse the influence of oxygen concentration, excess oxygen, and gas phase temperature to explain the significance of each parameter on formation and destruction of NOx. The studies indicate that there are two contrasting factors influencing formation and reduction of NOx in coal combustion[126]; the oxidation of fuel-N by oxygen and oxidising species, and the reduction of NOx by reducing agents such as resident char and hydrocarbons from pyrolysis.

2.6.2.2 NOx Reduction Technologies

2.6.2.2.1 Air Staging

Air staging has been comprehensively investigated in order to reduce the formation of NOx in BFB and CFB combustors. The staging enables a significant NOx reduction up

to about 30–80% [147, 173]. The primary and secondary air should be inserted in geometrically well-separated sections of the combustor. Additionally, the air flow rate should be controlled to be able to safeguard a primary air ratio of 0.6 to 0.8 in the furnace[114]. The excess oxygen quantity, assured by the secondary air, which should be as low as with the side limitation that a complete combustion, has to be reached. The air staging technology has also been effectively applied in the lower temperatures operating systems [114, 156]. However, precise process control is essential for air staging combustion, to confirm an operation at the excess air ratio desirable in the different zones of the combustion.

2.6.2.2.2 Reburning or Secondary Fuel Injection

Reburning is also a possible solution to reduce high emissions of NOx. This modified technology removes NOx from the combustion products by means of a reducing agent which is fuel during combustion. The principle is based on the reaction of hydrocarbon fragments (CH) with NOx. The returning is achieved through the injection of secondary fuel downstream of the fuel-lean primary zone of the combustor [174]. Typically the reburning zone is operated in the overall fuel-rich environment, permitting a major fraction of the primary NOx to be reduced to N_2 and other nitrogenous species.

The additional air is also introduced in the third zone to establish overall fuel-lean conditions which allow the combustion of the remaining fragments of the fuel. This type of NOx reduction mechanism has been applied to the full-scale industrial plants and seems to be striking when natural gas is utilised as the reburning fuel to extinguish NOx produced in pulverised coal firing systems [175]. Usually, NOx reduction is

primarily happening in the reburn zone of the combustor as a result of the reactions between NO and hydrocarbon fragments such as CH, CH_2 (see Eq. 2.5), these reactions usually yield HCN according to the follow chemical reaction pathway [103].

$$NO + CH_i \rightarrow HCN \rightarrow NCO \rightarrow NH \rightarrow N \rightarrow N_2 \quad (2.5)$$

The last part of this chemical reaction pathway is known as reverse Zeldovich reaction which converts N to N_2 [176]. It is also accepted as the primary mechanism route for the formation of NO and destruction of thermal NOx. The biomasses containing low nitrogen and high volatile contents are suggested to be used as reburning fuels such as wood or waste wood [177]. Wood is the biomass with low nitrogen contents as compared to that of coal, which results in lower nitrogen oxides production from fuel-N during combustion. Usually, fuel reburning consumes 10 to 20% of the total heat input of the system, hence large amounts of biomass are not essential as compared with 100% biomass firing [103].

2.6.2.2.3 Selective Catalytic Reduction

If NOx reduction by primary methods (Air staging or Fuel staging) is not efficient enough then selective catalytic reduction (SCR) could be used to meet the required limiting values [61,119,136]. In SCR ammonia or urea is injected over a catalyst at a temperature of about 250 to 450 °C and selective non-catalytic reduction (SNCR) by introducing ammonia into a separate chamber called reduction chamber at a temperature of between 850 to 950 °C [147] according to the following reaction (see Eq. 2.4). The rate of NOx conversion is essentially dependent on the molar ratio of NH_3 and NOx,

reaction temperatures, number and locations of ammonia injection nozzles. FBCs function at high temperatures found to be favourable for the maximum rate of NOx conversion [178].

$$2NO + 4NH_3 + 2O_2 + 2H_2O = 3N_2 + 8H_2O \quad (2.4)$$

Usually, to changing concentrations of NOx in the gas stream, the NH_3 injection rates are adjusted. It was observed that mole ratios of NOx and NH_3 well above the stoichiometric NH_3 to NOx equilibrium ratio encourage a high rate of NOx reduction, on the other hand, it also results in greater than before and undesired NH_3 slip [103]. The NOx emissions from biomass fuels do not contain any fuel-N remained unknown. Up to 95% NOx emissions reduction in for SCR and 90% for SNCR have been reported in the literature [178].

2.7 Research Challenges of Biomass Oxy-fuel Combustion

The oxy-fuel combustion has been recognised as a promising technology for CO_2 capture, while biomass combustion in oxy-fuel has the potential to reduce the CO_2 emission even to below zero [179-182]. The combustion characteristics under oxy-fuel conditions differ from those under air combustion in several ways; such as gas composition, gas density and flow field. The difference in gas atmospheres practised by the particles of fuel can also have an effect on the processes of combustion, including char reaction, ignition, combustion characteristics and subsequently ash and pollutants formation [183]. An overview of research activities and technology developments on oxy-fuel combustion has been recently studied [46, 184-186]. An effort was made to

summarise the focus and the main findings of these works. The integration of biomass in the oxy-fuel has not yet been studied comprehensively and there are exposed questions preceding to utilise biomass in oxy-fuel combustion environment as for example, the ignition of blends under oxy-fuel atmosphere, appropriate temperature conditions, the level of flue gas cleaning earlier to recirculation, the effect of components in biomass ash under CO_2 and high O_2 concentration conditions or ash deposition behaviour under varying oxy-gas environments. The flue gas enrichment in S and Cl due to the necessary recirculation in oxy-fuel can affect the ash and deposition formation, building additional ash melting and increasing the formation of fine ash particles [183].

Limited work has been reported on the trace elements emissions during oxy-fuel combustion of biomass. The tendency for slagging and fouling during oxy-fuel firing is equally topic to investigate. It is important to consider whether there are any special issues concerning biomass combustion compared with coal during oxy-fuel, as some issues could have a significant impact on the combustion process and associated phenomena. More importantly, special attention should be given to the volatile matter content and ash composition during biomass combustion under oxy-fuel [126, 187-191].

Challenges for oxy-fuel biomass combustion in FBs indicate difficult start-up, difficult ignition (it is ignited above the bed), matching of heat transfer characteristics in the retrofitted boilers, combustion characteristics, emission levels, necessities for gas cleaning-especially SO_2, noise, and erosion of the heat exchanger walls [192-194]. The steady burning is achievable at 800–1100 ^oC, but below 800 ^oC the burning is noisy

often with violent small bursts, and above 1100 ^{o}C the particulate may start fusing and clogging [57, 192, 193, 195-197]. A number of concerns, environmental, technical and economic, related with biomass combustion exist, but none of these represent a overwhelming difficulty for using this sustainable energy resource. Biomass oxy-fuel combustion technology in FBs is still in the emerging phase and much more essential research is still required in order to gain a deeper understanding of the combustion behaviour of biomass under oxy-fuel conditions.

Chapter 3

Design and Construction of Experimental Setup

3.1 Introduction

The pilot scale 20 kW_{th} bubbling fluidised bed combustor (BFBC) has been designed, manufactured and commissioned in Energy Technologies Building (ETB) at the University of Nottingham, UK. The process flow diagram for the BFBC is shown in Figure 3.1. The overall rig dimensions are 3 m high with a plan area of approximately 1×3 m and the arrangement incorporates the following major components; (1) bubbling fluidised bed reactor (BFBR), which is composed of three sections: plenum, main reactor and free board connected with flanges to ease fabrication, maintenance and allow for flexibility with regard to the internal geometry; (2) high-efficiency gas-solid cyclone, (3) biomass screw feeder; (4) fluidising blower fan; (5) flue gas sampling unit; (6) flue gas analysers and data logging system. Air is supplied to the system by a blower

fan through a flexible stainless steel hose connected to the air chamber at the bottom of the BFBR. An air pre-heater is also installed on the flexible stainless steel hose after the air flow rotameter to heat the air before introduction into the reactor during the start-up of the rig. The staging air is introduced from two different locations; 700 mm and 1100 mm from the distribution plate.

A small proportion of air is also fed through biomass feeding hopper to prevent backfire and to stop the hot sand particles coming into the feeding pipe. In order to minimise heat loss during operation, the outer walls of the BFBC and the gas-solid cyclone are wrapped with 38 mm of the insulating sheet (calcium magnesium silicate) and held together by aluminium tape. The biomass fuel pellets are fed to the reactor by means of a screw feeding system located just above the distributor plate. The hopper has a separate air supply line to create backpressure to prevent hot gas flow into the feed line and biomass hopper from the BFBR.

The combustor is operated at a temperature between 750 and 850 °C. A sintered type of plate is used as a distributor, which is flanged between the plenum and main reactor section of the reactor. The tests also include analysing the effect of the distributor on the process performance. Temperature and pressure indicators are used to evaluate and determine the fluidisation characteristics, gas and solids flow patterns. The temperatures inside the reactors are controlled by a water cooled heat extraction probe. The water inlet and outlet temperatures are measured to enable estimation of the heat transfer coefficient. The BFBC is designed to allow easy modification and simulation of alternative designs.

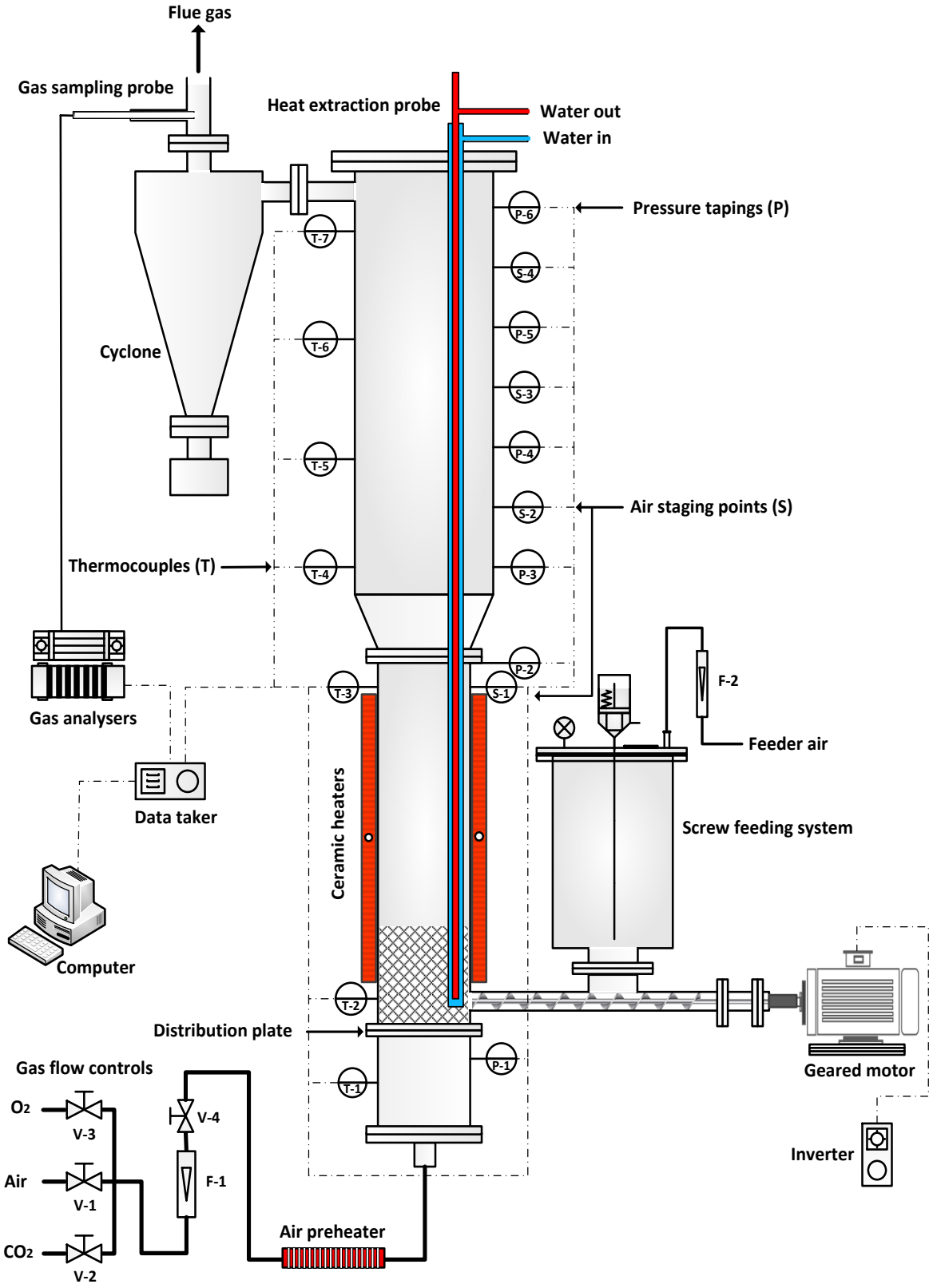


Figure 3.1: Bubbling fluidised bed combustor (BFBC) process flow diagram.

3.2 Pre-Design Requisites

The following important design decisions were made due to available space, budget, health and safety issues.

- The BFBC should be medium size (pilot scale) and cost competitive with conventional solid fuel firing systems in the market.
- The BFBC should satisfy the major research objectives, such as to study the internal hydrodynamics of the combustor, the performance of the cyclone, and to ensure optimum reaction conditions within the main reactor and reliable biomass feeding.
- The length of the BFBC shall not be more than 3 meters and it will be divided into three sections plenum or air chamber, main reactor or fluidising zone and freeboard respectively.
- The freeboard region of BFBC shall be longer and bigger than the main bed region to maximise the residence time of biomass fuel particles and to make sure complete combustion of volatile matter within the combustor.
- There is no natural gas supply in the laboratory B 27, ETB where the BFBC is going to be commissioned. Hence, electrical heaters had to be installed to heat up the reactor to 500–600°C during start-ups. The decision was made to use two Watlow semi-cylindrical ceramic fibre heaters around the main reactor section.
- The biomass pellets size range between 15–30 mm shall be used as the main fuel in BFBC, with the fuel feeding rate within 3–5 kg/h corresponding to approximately 20 kW thermal input.

- The Garside sand 14/25 shall be used as bed material unit which is also used by several UK industrial scale FBC.
- The continuous operation of BFBC shall be limited to about 10–12 hours per day rather than 24/7 due to health and safety restrictions within the University.

3.3 Hydrodynamics and Combustion Design Parameters

During fluidisation, a hydrodynamic gas-solid interaction occurs in the system causing transformation in the behaviour of the fine solid to transform in a fluid like state. This gas-solid interaction affects the environmental and operating characteristics of the BFB reactor and also serves as a differentiating factor between various types of FBs. To ensure that the gas-solid behaviour corresponds to the expectation of a bubbling fluidised system, the basic hydrodynamic parameters need to be determined and could be used as a design specification for the BFB combustor design.

3.3.1 Fluidisation Velocities

3.3.1.1 Minimum Fluidisation Velocity

The minimum fluidisation velocity is defined as the minimum superficial gas velocity where particle fluidisation is achieved. Consider a bed of particles resting on a distributor designed for a uniform upward flow of gas, for instance, a porous sintered metal plate. Fluidisation is considered to start at the gas velocity at which the solid particles weight become equal the drag on the particles from the increasing gas flow rate. The drag applied on the solid particles equals the net gravitational force applied on the particles as represented in Eq. (3.1) [198].

$$\frac{\Delta P}{L} = (\rho_s - \rho_g)(1-\varepsilon)g \tag{3.1}$$

From Ergun Equation [199];

$$\frac{\Delta P}{L} = 1.75\frac{(1-\varepsilon_m)}{\varepsilon_m{}^3}\frac{\rho_g u_o{}^2}{\varphi_s d_p} + 150\frac{(1-\varepsilon_m)^2\mu}{\varepsilon_m{}^3}\frac{u_o}{(\varphi_s d_p)^2} \tag{3.2}$$

where d_p is the surface mean particle diameter, g is the acceleration of gravity, L is the height of the fixed bed, u_o is the superficial fluid velocity through a bed of solids (measured on an empty tube basis), ε_m is the void fraction in a packed bed, μ is the viscosity of fluid, ρ_g is the fluid density, ρ_s is the density of solids, φ_s is the sphericity of a particle, and ΔP is the pressure drop.

The bed becomes fluidised at the minimum fluidising velocity where the drag force on the particles is greater than the gravitational force. In this fluidised state, the particles are suspended in the fluid and create more efficient mixing of the upward flowing fluid. Comparing Eq. (3.1) and Eq. (3.2) provides a calculation for the minimum fluidising velocity:

$$\left(\frac{d_p{}^3\rho_g(\rho_s-\rho_g)g}{\mu^2}\right) = \frac{1.75}{\varphi_s\varepsilon^3{}_{mf}}\left(\frac{d_p u_{mf}\rho_g}{\mu}\right)^2 + \frac{150(1-\varepsilon_{mf})}{\varphi_s{}^2\varepsilon^3{}_{mf}}\left(\frac{d_p u_{mf}\rho_g}{\mu}\right) \tag{3.3}$$

where u_{mf} is the superficial fluid velocity at minimum fluidising conditions and ε_{mf} is the void fraction in a bed at the minimum fluidisation.

The Reynolds number plays an important part in determining the minimum fluidisation velocity by characterising the system based on the density, fluid velocity, and viscosity of the system. Eq. (3.3) can also be rewritten as

$$\mathrm{Ar} = \frac{1.75}{\varphi_s \varepsilon^3_{mf}} \mathrm{Re}^2_{p,mf} + \frac{150(1-\varepsilon_{mf})}{\varphi_s{}^2 \varepsilon^3_{mf}} \mathrm{Re}_{p,mf} \tag{3.4}$$

where Ar is the Archimedes number, Kunii et al, [200].

$$\mathrm{Ar} = \left(\frac{d_p{}^3 \rho_g (\rho_s - \rho_g) g}{\mu^2} \right) \tag{3.5}$$

When the particles are very small Eq. (3.3) can be simplified as Eq. (3.6), Kunii et al, [200].

$$u_{mf} = \frac{d_p{}^2 (\rho_s - \rho_g) g}{150\mu} \frac{\varepsilon^3_{mf} \varphi_s{}^2}{1-\varepsilon_{mf}} \qquad , \mathrm{Re}_{p,mf} < 20 \tag{3.6}$$

For very large particles Eq. (3.3) can be simplified as Eq. (3.7), Kunii et al. [200].

$$u_{mf}{}^2 = \frac{d_p (\rho_s - \rho_g) g}{1.75\mu} \varepsilon^3_{mf} \varphi_s \qquad , \mathrm{Re}_{p,mf} > 1000 \tag{3.7}$$

When ε_{mf} and φ_s are not known, one can still estimate u_{mf} for bed of irregular particles with no seemingly longer or shorter dimension. Wen and Yu [201] suggested a simplified form of the Eq. (3.3) by assuming the following established on experimental data:

$$\frac{1}{\varphi_s \varepsilon^3_{mf}} \cong 14 \qquad \text{and} \qquad \frac{(1-\varepsilon_{mf})}{\varphi_s{}^2 \varepsilon^3_{mf}} \cong 11$$

In a simplified form, the Eq. (3.3) in expressions of Reynolds number and Archimedes number is summarised to Eq. (3.8).

$$\mathrm{Re}_{mf} = 14\sqrt{C_1^2 + C_2 \mathrm{Ar}} - C_1 \tag{3.8}$$

There are various groups of values recommended for the constants of C_1 and C_2 based on the different database used for correlation. A section of C_1 and C_2 values is shown in Table 3.1 [201-205].

Table 3.1: Different values of constants C_1 and C_2 from literature.

Reference	C_1	C_2
Wen and Yu (1966a)	33.7	0.0408
Richardson (1971)	25.7	0.0365
Saxena and Vogel (1977)	25.3	0.0571
Babu et al. (1978)	25.25	0.0651
Grace (1982)	27.2	0.0408
Chitester et al. (1984)	28.7	0.0494

According to Grace (1982) [206], a change of C_1 from 33.7 is suggested by Wen and Yu [201] to 27.2 improve the fit for fine particles. For the limiting cases for small particles where the kinetic energy term is not important, and for large particles where it is dominant, the simplified equations become [207]:

For $\mathrm{Ar} < 10^3$ and $\mathrm{Re}_{mf} = 7.5 \times 10^{-4}$

$$u_{mf} = 0.00075 \frac{d_p (\rho_s - \rho_g) g}{\mu} \tag{3.9}$$

For Ar >10^7 and $Re_{mf} = 0.202\sqrt{Ar}$

$$u_{mf} = 0.202\sqrt{\frac{d_p(\rho_s - \rho_g)g}{\rho_g}} \tag{3.10}$$

3.3.1.2 Maximum Fluidisation Velocity

If the gas velocity is amplified to an adequately high value, nevertheless, the drag on a single particle will exceed the gravitational force on the particle, and the particle will be entrained by the gas and carried out of the fluidised bed. The point at which the drag on a single particle is nearly to go above the gravitational force applied on it is called the maximum fluidisation velocity [208].

When the upward rising velocity of the gas exceeds the freefall terminal velocity of the solid particle (u_t), the particle will be supported upward with the steam of gas [208]. For the fine solid particles, the Reynolds numbers will be minor, and two relationships presented by Kunii and Levenspiel [200] are as:

$$u_t = \frac{\eta d^2_p}{18\mu} \qquad (Re < 0.4) \tag{3.11}$$

$$u_t = \left(\frac{1.78\times10^{-2}\eta^2}{\rho_g\mu}\right)^{1/3} d_p \qquad (0.4 < Re < 500) \tag{3.12}$$

where $\eta = (\rho_s - \rho_g)\, g$

Therefore, from above equations, the minimum and maximum superficial velocities are calculated at which the bed of solids can be operated [198]. The incoming superficial

velocity (u_0) must be above the minimum fluidisation velocity but below the slugging (u_{ms}) and terminal (u_t) velocities.

$$u_{mf} < u_o < u_t \text{ and } u_{mf} < u_o < u_{ms}$$

Minimum fluidisation velocity calculations are given in Appendix A.

3.3.2 Fluidising Gases

3.3.2.1 Air Volumetric Flowrate

The air volumetric flow rate at ambient conditions determines the amount of air required to be supplied in order to meet the combustion conditions requirement. The normalised air volumetric flow rate is calculated using Eq. (3.13).

$$Q = Q_{amb}\left[\frac{(T_{amb}+273)}{(T+273)}\right] \tag{3.13}$$

where Q is the volumetric air flow rate at temperature T(°C) and Q_{amb} is the volumetric air flow rate at ambient temperature T_{amb} (°C). The air volumetric flow rate (m^3/s) required for the combustion process is determined using the following Eq. (3.14).

$$Q = U\,A \tag{3.14}$$

where U is the air superficial velocity (m/s) assumed to be eight times of U_{mf} calculated earlier in section 3.3.3.1 and A is the cross-sectional area (m^2) of the BFB reactor.

3.3.2.2 Air Mass Flowrate

The air mass flow rate (kg/s) required for combustion is determined using Eq. (3.15).

$$M = \rho_{g,amb}\, Q_{amb} \tag{3.15}$$

where ρ_g density of air and Q_{amb} is the air volumetric flow rate at ambient temperature.

3.3.2.3 Excess Air Ratio

All FB combustion systems operate on excess air rather than stoichiometric conditions. The fuel feed rate has to be adjusted for these conditions. The excess air is calculated using Eq. (3.16).

$$F_{\%\ \text{Excess Air}} = \frac{F_{stoic}}{\left(1+\frac{\%\ \text{Excess Air}}{100}\right)} \tag{3.16}$$

3.3.3 Gas Distributor

The theoretical pressure drop (ΔP), which affects the uniformity and stability of fluidisation in the FB, needs to be determined. In BFB the cause of ΔP which influences the uniformity of airflow distribution through all the section of the bed has been attributed to two factors which are distributor pressure drop (ΔP_d) and solids bed pressure drop (ΔP_b) [177]. The need to know the pressure drop across the BFB is also an important parameter required for fluidised bed fan sizing as the fan needs to be able to supply higher pressure than the ΔP across the bed for fluidisation to occur.

3.3.3.1 Distributor Pressure Drop

The distributor can be directly designed from orifice theory, the distributor pressure drop is determined using Eq. (3.17) [177].

$$\Delta P_d = \frac{\rho_g}{C_D^2} \frac{U_h^2}{2} \tag{3.17}$$

where C_D is the orifice discharge coefficient described and U_h is the air superficial velocity in the orifices. The orifice discharge coefficient, C_D can be determined using equation (3.18) [80].

$$C_D = \frac{1}{\sqrt{\frac{1}{C_{D,plate}^2} + \frac{1}{C_{D,h}^2}}} \tag{3.18}$$

Where $C_{D,plat}$ is the discharge coefficient through the perforated plate and $C_{D,h}$ is discharged coefficient through the orifices (Sánchez-Prieto et al. 2014). $C_{D,plate}$ is determined using discharge coefficient equation deduced by Quereshi and Creasy as given in Eq. (3.19) [209].

$$C_{D,plate} = 0.82 \left(\frac{t_d}{d_{noz}}\right)^{0.13} \tag{3.19}$$

where d_{noz} is the nozzle diameter which accounts for the perforated plate contribution and t_d is the distributor plate thickness. $C_{D,h}$ is determined by Eq. (3.20) which is a slightly corrected version of equation (3.19) [80]as following.

$$C_{D,h} = 0.82 \left(\frac{t_d}{d_h}\right)^{0.13} \quad (3.20)$$

where d_h is the orifice diameter which accounts for the orifice contribution to the distributor pressure drop. Finally, the air superficial velocity in the orifices, U_h is determined using following Eq. (3.21) [210, 211].

$$U_h = \left(\frac{4}{\pi}\right) \left(\frac{1}{N_h\, d_h^2}\right) U \quad (3.21)$$

where N_h is the number of orifice per unit area of the distributor.

3.3.3.2 Solids Bed Pressure Drop

The pressure drop due to bed material (solids) in BFB is determined by using following Eq. (3.22) [80].

$$\Delta P_b = (1 - \varepsilon)\rho_s\, H\, g \quad (3.22)$$

where H is the expanded height of the bed, ε is the bed voidage at combustion conditions and g is gravitationally constant. The expanded bed height H is determined using flowing Eq. (3.23) [119].

$$\frac{H_o}{H} = \frac{1-\varepsilon}{1-\varepsilon_o} \quad (3.23)$$

where H_o is the static bed height and ε_o is the bed voidage at static and ambient conditions. Bed voidage ε at combustion condition is determined using Eq. (3.24) [177] and bed voidage at static condition ε_o is determined using equation (3.25) [212].

$$\varepsilon = \frac{U+1}{U+2} \tag{3.24}$$

$$\varepsilon_o = 1 - \frac{\rho_b}{\rho_s} \tag{3.25}$$

where ρ_b is the bulk density of the bed.

3.3.4 Biomass Combustion Stoichiometry

The fuel stoichiometry is very important while working with the combustion of solid fuels for energy production. The detailed stoichiometric combustion calculations are presented in Appendix A.

3.3.4.1 Fuel Feed Rate for Combustion

The fuel feed rate is calculated using stoichiometric combustion of solid fuel in air equation described in Eq. (3.26) [177]. The C, H, N, O and S values are given as weight percentage of each element identified to be present in the biomass by ultimate analysis.

$$\left(\frac{m}{F}\right)_{stoic,mass} = 0.1144C + 0.3433H + 0.098N + 0.0429(S - O) \tag{3.26}$$

where F is the fuel feed rate (kg/s), the amount of biomass required for the combustion process at stoichiometric conditions.

3.3.5 Main Reactor and Free Board

The plenum and main reactor section of the combustor is constructed with high grade austenitic stainless steel 312 pipe (ASTM A-312) 40S (wall thickness of 6.02 mm). This material has a service temperature of up to 1200 °C, and 102 mm nominal I.D size can provide strong resistance against erosions of the reactor section caused by fluidising sand, biomass char particles, and any other solid impurities during the combustion. The freeboard section is constructed by a normal stainless steel 315 pipe (ASTM A-315) 40S 154 mm nominal I.D (wall thickness of 7.11 mm). The different sections of the BFB combustor during manufacturing are shown in Figure 3.2.

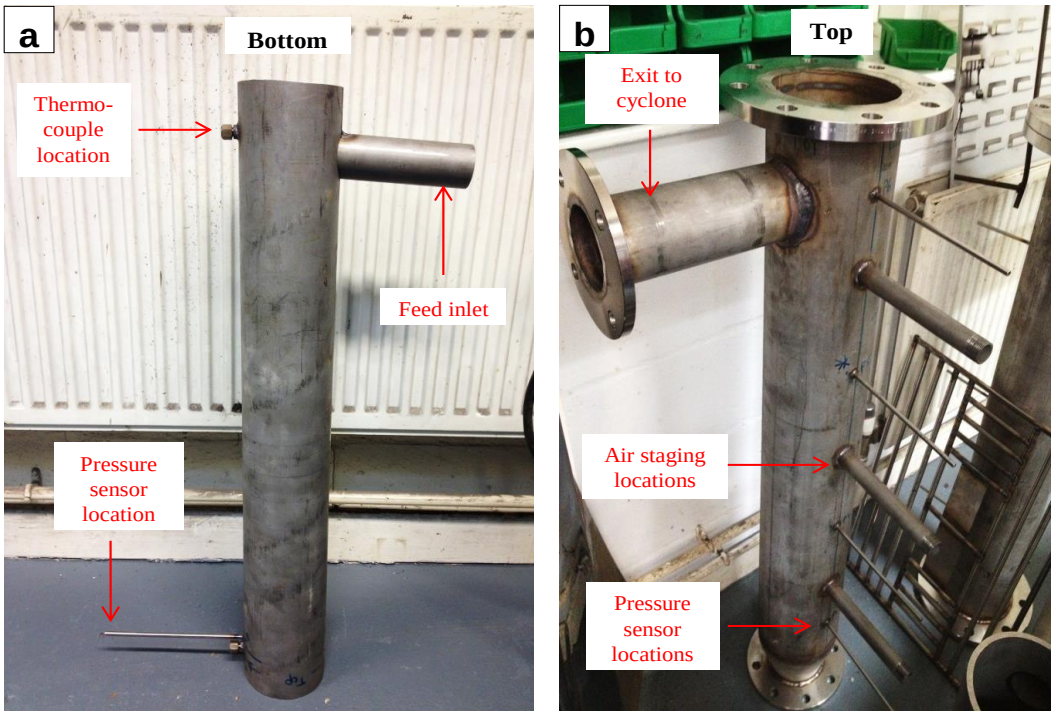


Figure 3.2: BFBC during construction; (a) main reactor section, (b) freeboard section.

The plenum, main reactor and freeboard sections have a height of 300 mm, 780 mm and 1150 mm, respectively, making the combustor with an overall height of 2230 mm. The technical drawings of all these sections are presented in Appendix B. Two semi-cylindrical Watlow ceramic fibre heaters (VS106J18T-B001R), 165 mm ID by 600 mm long with an electrical rating of 120 V–2100 W (total power rating of 4200 W) and a maximum operating temperature of 1000 °C are installed around the main reactor to heat up the bed temperature to the value required for feeding the biomass.

The ceramic fibre heaters are wrapped with 50 mm thick layer of calcium magnesium silicate thermal insulating sheet with a maximum operating temperature of 1150 °C and enclosed in a 3 mm thick aluminium sheet casing. In order to minimise heat loss during operation, the fibre heaters and the outer walls of the main reactor and freeboard are also wrapped with 38 mm of the same insulating calcium magnesium silicate sheet and held together by aluminium tape.

3.3.6 Gas-Solid Separation Cyclone

Cyclone separators provide an efficient way of removing particulate matter from the flue gases leaving the FBs [213]. The gas-solid separation cyclone for the FBC is designed to achieve a high-efficiency standard by using the high-efficiency cyclone, the engineering design principle is shown in Appendix B [214]. However, certain parameters within this standard design principle can be slightly adjusted to adapt individual requirements without having the main effect on the efficiency of the cyclone [215]. These adjustments were made for the ease of fabrication, material sourcing, cost reduction and space restriction within the laboratory.

The altered high-efficiency design used for the construction of biomass BFBC cyclone system is shown in Appendix B, where Dc is given as the diameter of the cylindrical section of the cyclone; in this case, it is 266 mm ID. The cyclone was fabricated using high grade austenitic stainless steel 304. The technical drawing with design specifications of the biomass BFBC cyclone is given in Appendix B, while the actual cyclone is shown in Figure 3.3.

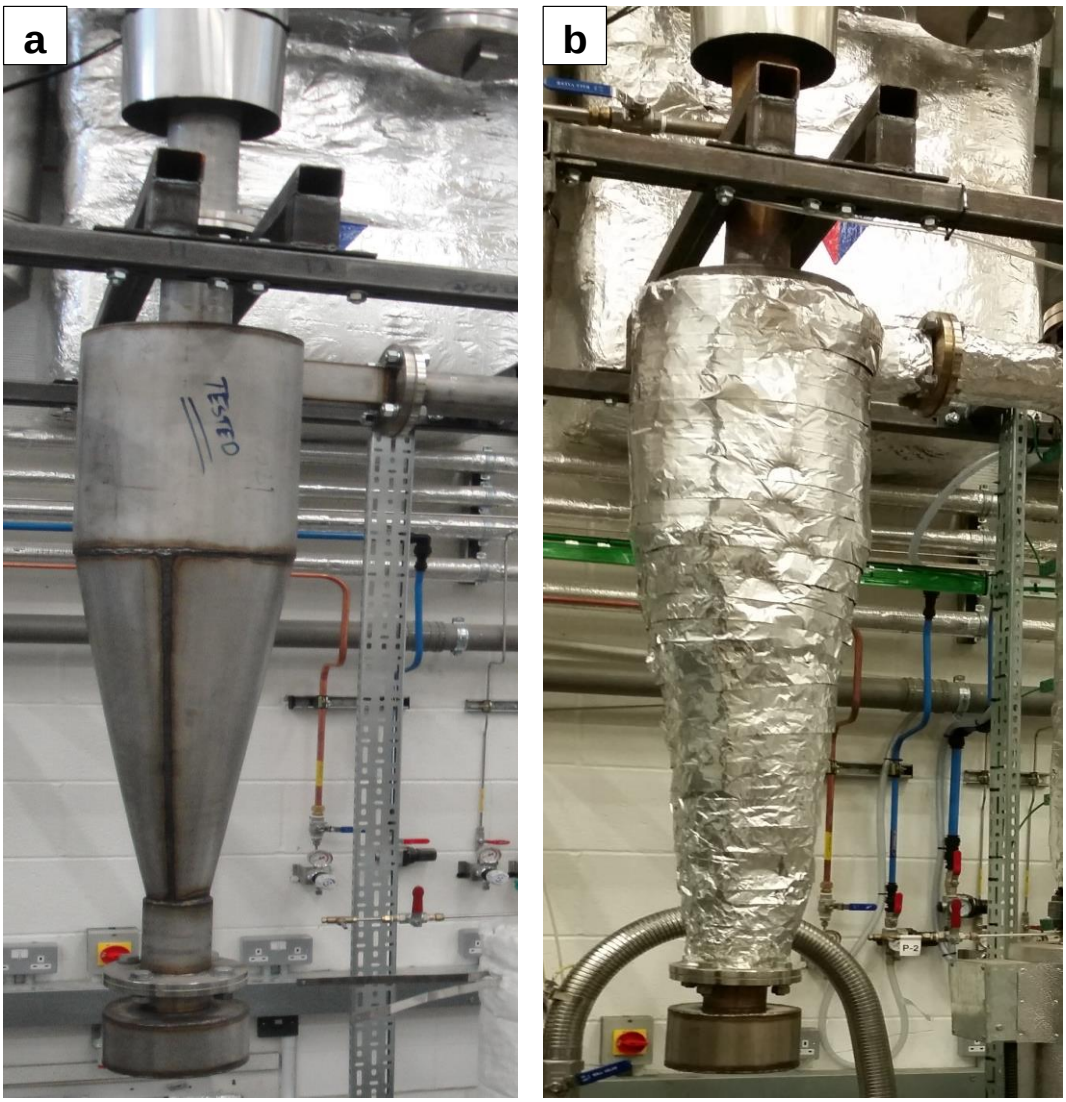


Figure 3.3: Altered high-efficiency cyclone for BFBC; (a) before insulation, (b) after insulation.

3.3.7 Gas Distribution Plate

The vital function of a distributor is to allow the fluidising gas consistently over the cross section of the bed and also to support the weight of the de-fluidised bed. The types of distributor range from a simple porous plate to the ball type and to the special purpose distributors [216]. The distributor plate has a very strong impact on the size and frequency of the bubbles formed in FBs [198]. Many distributor designs have been suggested and are well discussed in the general fluidisation literature [198, 217].

The design criterion set for the distributor is as:

- Sufficient pressure drop across the bed.
- Uniform and stable gas flow.
- Avoid chocking (solids backflow into the air chamber).
- Minimise the dead zones on the distributor.
- Minimise solids attrition.

A sintered distribution plate was chosen to be used in the BFBC, the specification of the distribution plate are given in Table 3.2. The important prerequisite to steady fluidisation process is that the pressure drop across the distributor should be suitably large. In the case of a too low pressure drop the fluidisation is poor [216]. The reason behind is either some parts of the bed receive less gas than as compared with other parts. Therefore, the bed becomes temporarily or permanently de-fluidised during operation, if a part of the bed de-fluidises it may result in blocking that discharge area [216].

Table 3.2: Design specifications of the distribution plate.

Type	Construction material	Plate thickness	Plate diameter	Hole diameter
		mm	mm	mm
Sintered	Stainless steel frits	12	115	0.002

The porous or sintered distribution plates are frequently used on laboratory scale fluidised systems. These types of distributors function more satisfactorily over a wide range of working conditions than other types of distributors. The gas flow rates through sintered materials are proportional to the applied pressure until the beginning of turbulence, at which point they become more preventive to the gas flow [216]. The sintered distribution plate used is shown in Figure 3.4. It is made of stainless steel frits with 115 mm diameter and 12 mm thickness. The plate was engraved inside a 4-inch flange and then fixed between the plenum and main reactor section.

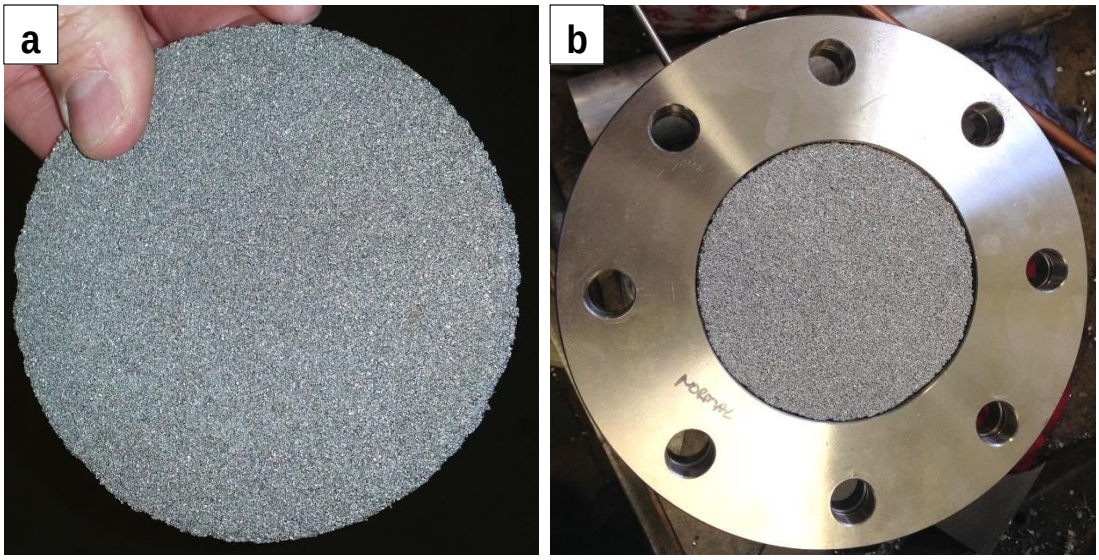


Figure 3.4: Sintered distribution plate; a) before fixing, b) after fixing into the flange.

3.3.8 Biomass Feeding System

The feeding has been the most difficult part of the entire FB combustion system. Feeding becomes challenging by a number of factors; such as biomass particles, whether derived from woody or agricultural sources, vary greatly in moisture content, size, density, shape and compressibility [218]. The parameters such as excessive high moisture content, oversized particles, insufficient or too much high-pressure difference between the feed hopper and reactor can all lead to the failure of the combustion process. If fluidised bed reactor operates at high temperature and/or high-pressure there are some additional challenges in establishing reliable feeding operation [78, 218]. The biomass feeding system used for BDBC is shown in Figure 3.5.

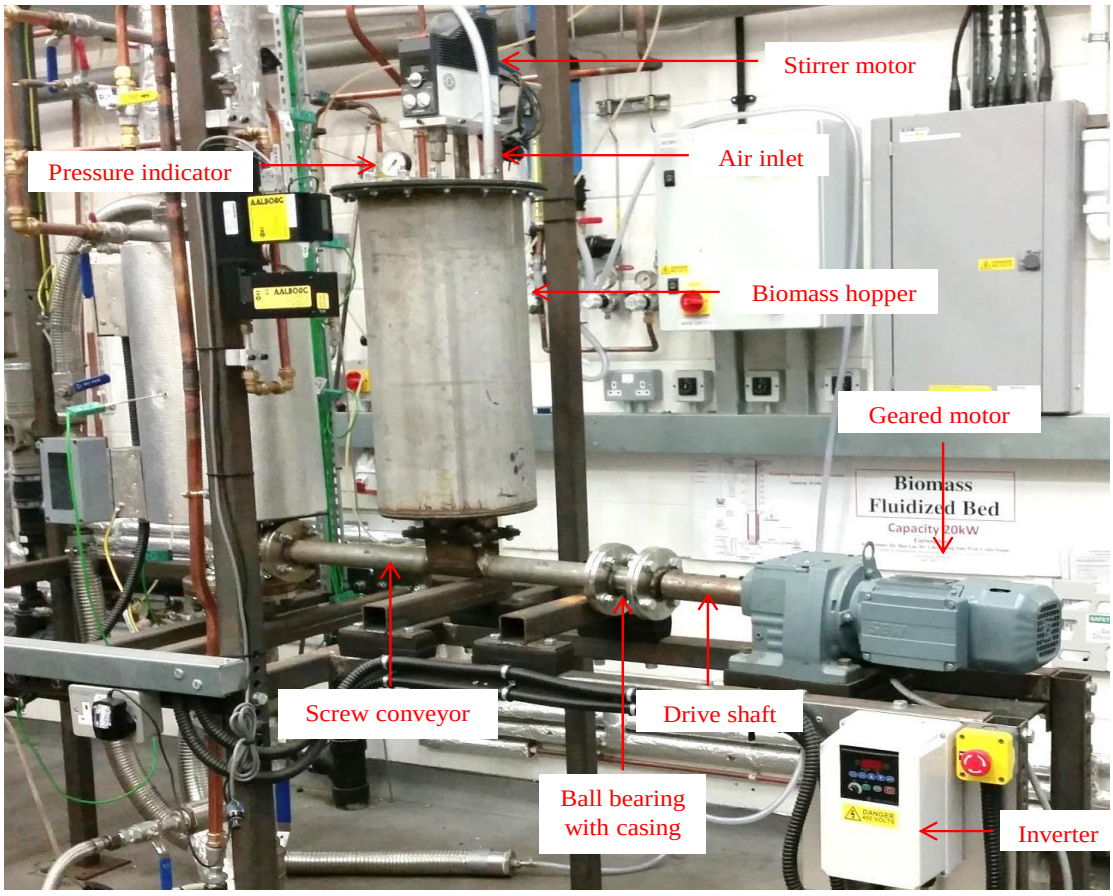


Figure 3.5: Full view of the biomass BFBC feeding system.

The technical engineering drawing of the feeding system with hopper top and the bottom plate is given in Appendix B. It consists of a biomass hopper with a holding capacity of more than 20 kg of biomass pellets which discharges on a screw connected with a Sew-Eurodrive helical geared motor (R67 DRE80M4/TF) which powers the biomass conveyor. The speed of the geared motor is controlled by an Allen–Bradley IP20 variable-frequency drive (Power Flex 4 AC Drive), therefore independent biomass flow rates can be fed from the hopper. The screw auger discharges into a pipe that introduces the biomass fuel into the reactor.

The feeding pipe connector is attached at 90° angle with the combustion chamber and located inside the dense bed 50 mm above the distribution plate, in order to reduce the initial elutriation. The screw auger is made from high grade austenitic stainless steel 316 of 3 mm thickness with service temperature up to 1400 °C. To increase the strength and rigidity of the screw auger for this application, a 16 mm austenitic stainless steel 316 rod is inserted into the ring hole in the screw auger and welded on to serve as a centre shaft.

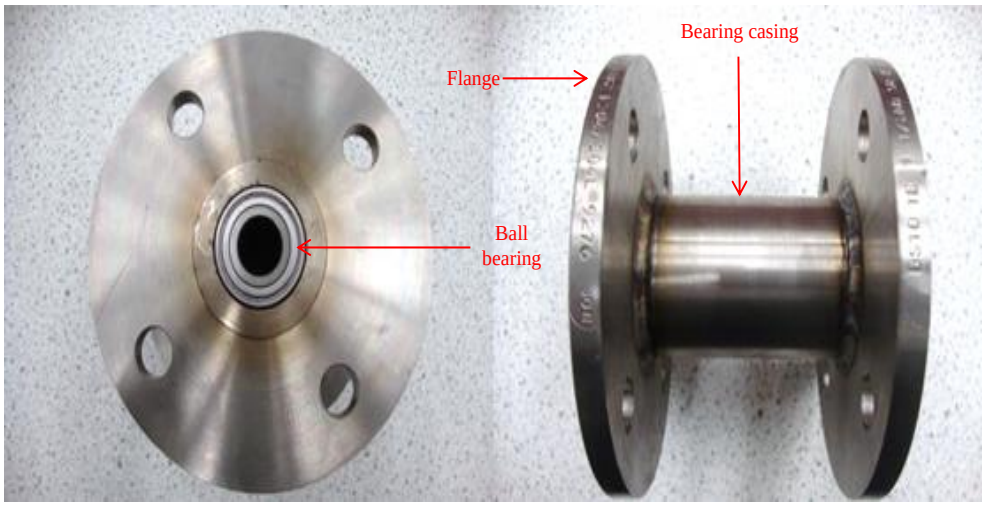


Figure 3.6: Shaft bearing assembly with auger position used in biomass BFBC feeding system.

As part of the conveyor section of the screw feeder, a shaft containing a ball bearing with a gas seal is made from austenitic stainless steel 304 for the ease of rotation of the screw auger and to prevent the air or gas leakage shown in Figure 3.6. The complete assembly of the conveyor section of the screw feeding system for the BFBC is shown in Figure 3.7. The section comprises of the auger, hollow shaft housing the bearing, and a motor driving shaft.

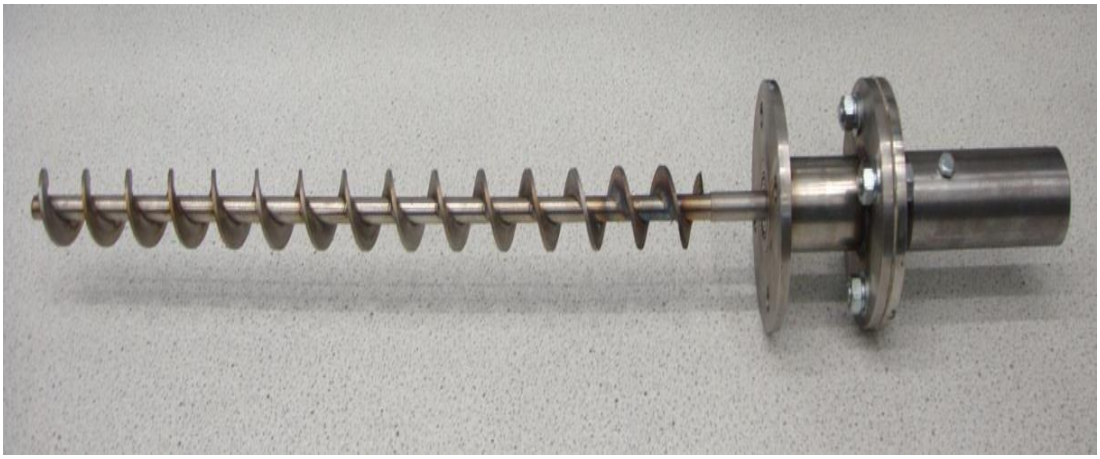


Figure 3.7: Conveyor section of the biomass BFBC feeding system.

The top section of the feeding systems is shown in Figure 3.8. It consists of the biomass fuel inlet port, an internal stirrer with a motor which prevents the formation of bridges in case of problematic fuels. As part of the design with strong emphasis on system safety, the feeding system is designed with two important safety features located on the top of the biomass hopper. The first feature is an air/ CO_2 inlet line, which constantly supplies air during air combustion while air and/or CO_2 during oxy-fuel combustion into the hopper to create slightly positive pressure relative to the working section of the reactor to prevent hot gas flashback which may cause a fire during the operation.

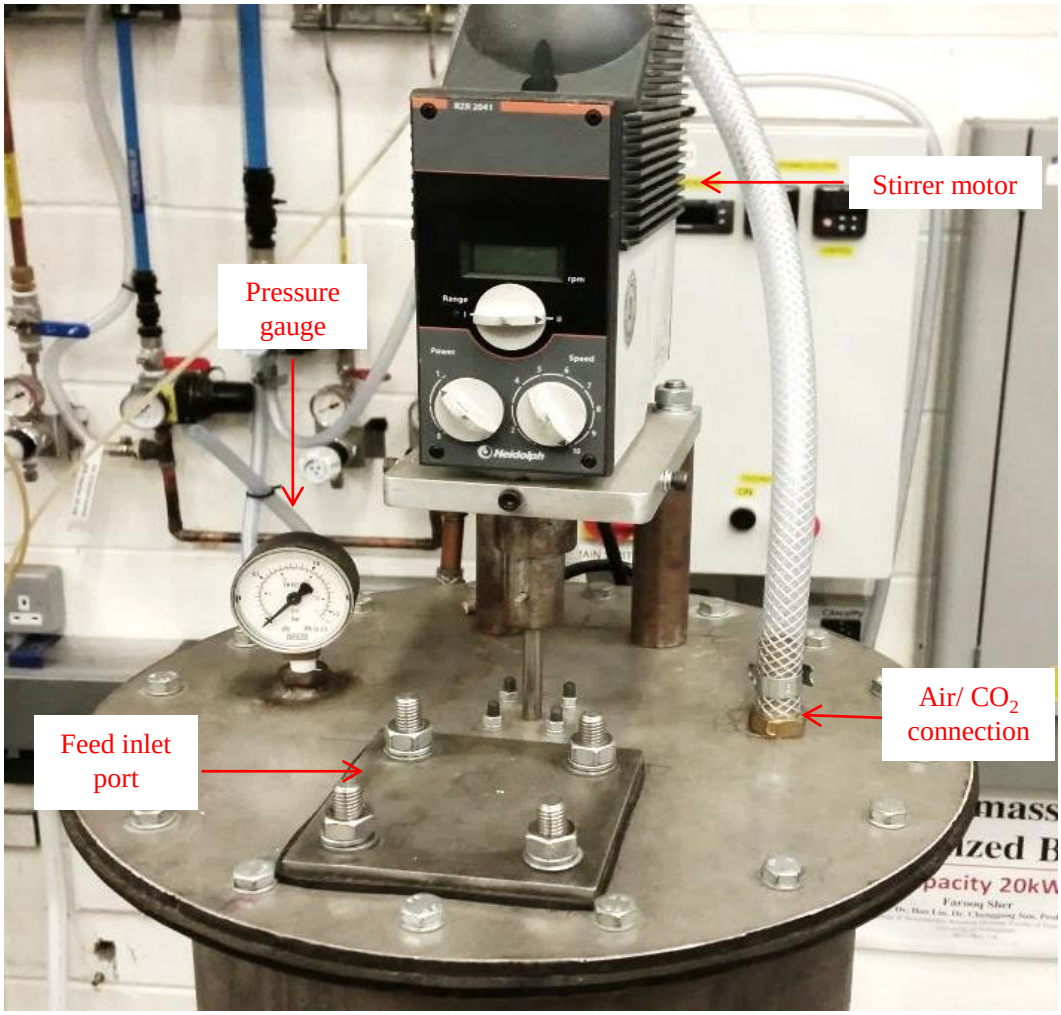


Figure 3.8: Top view of the BFB combustor feeder hopper equipped with safety features.

The second feature is a pressure indicator, which measures the pressure in the hopper. This helps the operator to monitor the pressure and identify pressure build-up which might arise from a blockage of fuel in the conveyor section of the feeding system. The biomass feeding system is calibrated earlier to the combustion tests; by changing different auger speeds over the different biomass fuel feed rates, the calibration results are given in Appendix C.

3.3.9 Water Cooled Heat Extraction Probe

To control the excessive temperatures inside the reactor during operation a water-cooled probe is designed based on the previous water-cooled probe designs. Due to size restrictions and the desire to reduce the maximum overall diameter of the probe, the cooling method is carefully chosen to obtain efficient cooling. The probe consists of two stainless steel 316 concentric tubes (inner tube and outer tube) with fins between them to divide the flow. The total length of the probe is 2.1 m, the inner tube with 6 mm ID and an outer tube with 12 mm ID. The technical drawing of the cooling probe is given in Appendix B. The actual cooling probe during operation of the BFBC is shown in Figure 3.9.

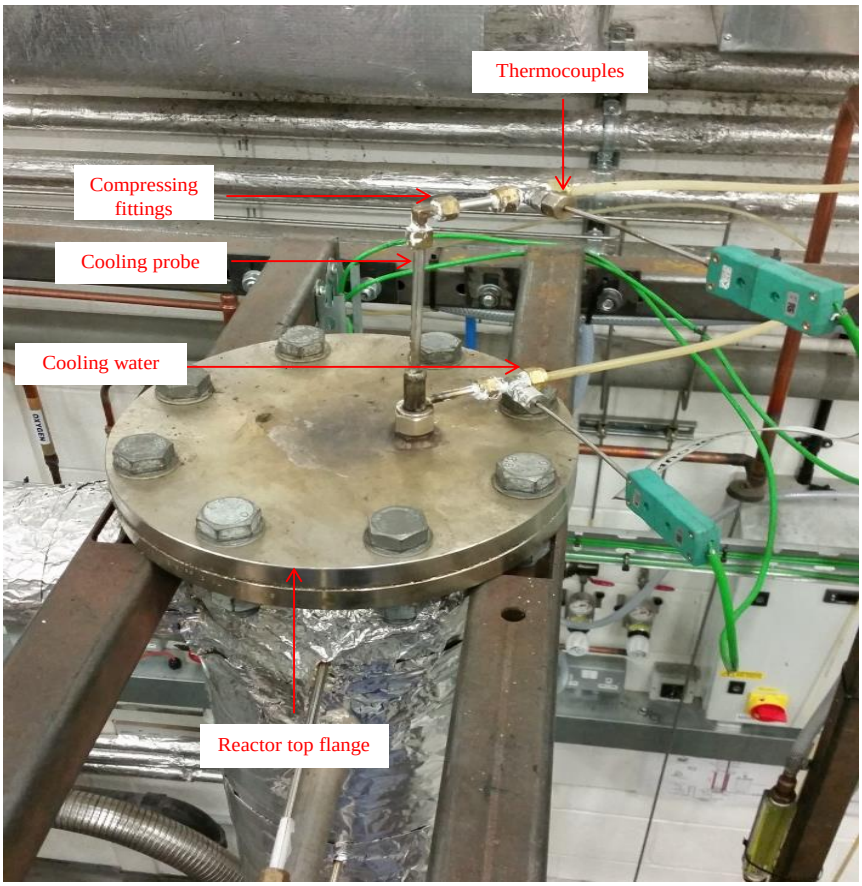


Figure 3.9: Water cooled heat extraction probe arrangements into the BFBC.

The probe tip is capped using a stainless steel disc welded to both the inner tube and the outer tube. A counterbored hole is drilled with fittings on the top flange of the reactor to allow the cooling probe go inside the reactor. Two K-type thermocouples are also installed to measure the cooling water inlet and outlet temperatures, which can be used to calculate the exact amount of the heat extracted from the reactor. A rotameter is installed with a ball valve at the rear of the rig to control the cooling water flow rate into the cooling probe. The high-pressure brass plugs and compression fitting are used for the cooling water inlet and outlet connections which can be seen from Figure 3.9.

3.3.10 Flue Gas Sampling Probe

For the sampling of the flue gas after combustion, a water cooled sampling probe is designed based on practical experience. The design is based on the flow rate of the flue gas to be sampled, which is about 1.0 L/min. The operational modifications in such type of cooling probes can be easily made to improve the cooling effect across the probe for the flow rate of this size by increasing the cooling water flowrate. The water cooled flue gas sampling probe is shown in Figure 3.10.

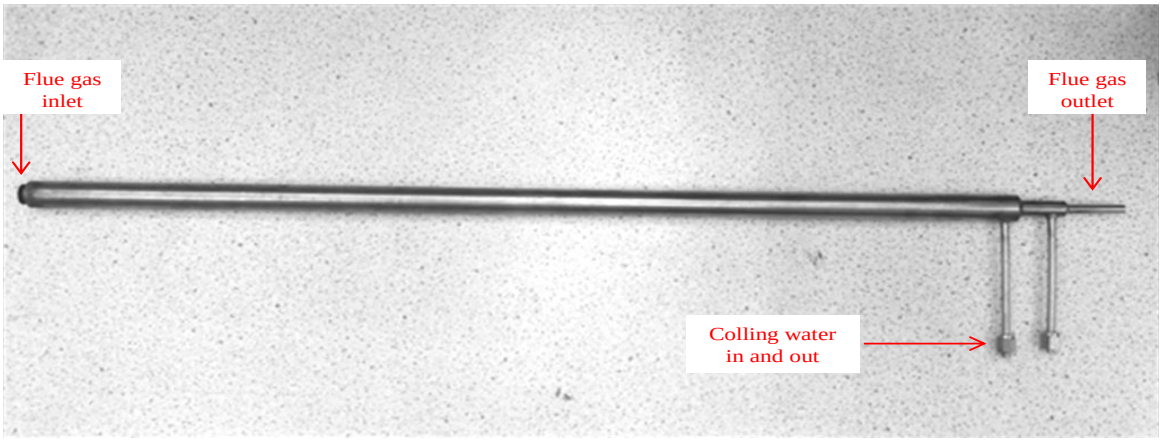


Figure 3.10: Water cooled flue gas sampling probe for BFBC.

The technical diagram of this sampling probe is given in Appendix B. The specific exit temperature of the flue gas from the probe is not very critical as the allowance is made for secondary cooling setup to occur, prior to the gas analyser inlet. The probe consists of three concentric tube layers namely inner, middle and an outer tube with varied I.D of 6 mm, 12 mm, and 18 mm respectively. The material used for the fabrication of the flue gas cooling water probe is stainless steel 316 seamless pipes with a wall thickness of 1.25 mm.

3.3.11 Supporting Frame

The BFBC rig supporting frame is constructed with 50×50 mm mild steel square box section pipes with a wall thickness of 3 mm. A detailed technical drawing of the supporting frame is given in Appendix B. The support frame is divided into three sections as; biomass feeding system fluidised bed and gas-solid cyclone sections with a footprint of 3000 mm (length) by 1000 mm (width) and a height of 3000 mm. The joints are supported and reinforced by cut pieces of 50×50 mm mild steel angle bar to carry the force and stresses during operation.

The frame metal bars are made and produced as single bars for the ease of transportation and were assembled together on the site using a stainless steel M-19 bolt. The use of bolts also makes it easy to take apart when trying to open up the fluidised bed section to check the condition of the bed and to change the bed material after each biomass fuel. The base support of the frame is specified to be located at 2200 mm in order to accommodate the reactor expansion height downwards due to thermal growth which is expected to be about 20–30 mm at 800–900°C operating temperature. The

entire structure is bolted to the floor using 12 pieces of M-12 brass raw bolts 2 on each leg plate of the frame.

3.3.12 Air and Oxy-fuel Gases supply Piping and Sizing

A blower fan was used for the initial cold rig and combustion with air experiments. The sizing of BFBC blower fan was outsourced to Fan and Blowers Ltd, UK, a centrifugal fan designer, and manufacturer. The blower fan was sized based on the fluidising volumetric air flow rates requirements and the pressure drop across the bed section calculated from expressions in section 3.3.1 and 3.3.3. The specified design volumetric flow rate for the blower fan was given as fifteen times the calculated requirement at ambient conditions and the supply pressure requirement was given as three times the calculated pressure drop across the BFBC.

A schematic diagram of the blower fan size as specified by the manufacturer based on the design specification given in Appendix B. The resulting blower fan specified for this application is a 2900 rpm centrifugal fan (model BM 841) which is powered by an 11 kW Brook Crompton IP55 motor controlled by a Weg technology variable speed drive (model CFM-11) and has a total weight of 210 kg. The fan and variable speed drive operations are controlled remotely using Super Drive G2 software supplied by Weg. The blower fan installation diagram is shown in Figure 3.11. For the operation of the fan, air is drawn from laboratory room and the size of the room is sufficiently large that it does not impact the fan or people working in the lab.

The operational safety assessment was done on the fan prior to installation and it was decided that the use of anti-vibrating mounts are required for the safe operation of the blower fan especially at high-speed operation. Six AL40 anti-vibrating mounts with a total weight rating equal to the weight of the fan are installed as shown in Figure 3.11. The anti-vibrating mount casing is made from aluminium with a compressible rubber packing which absorbs vibration during operation.

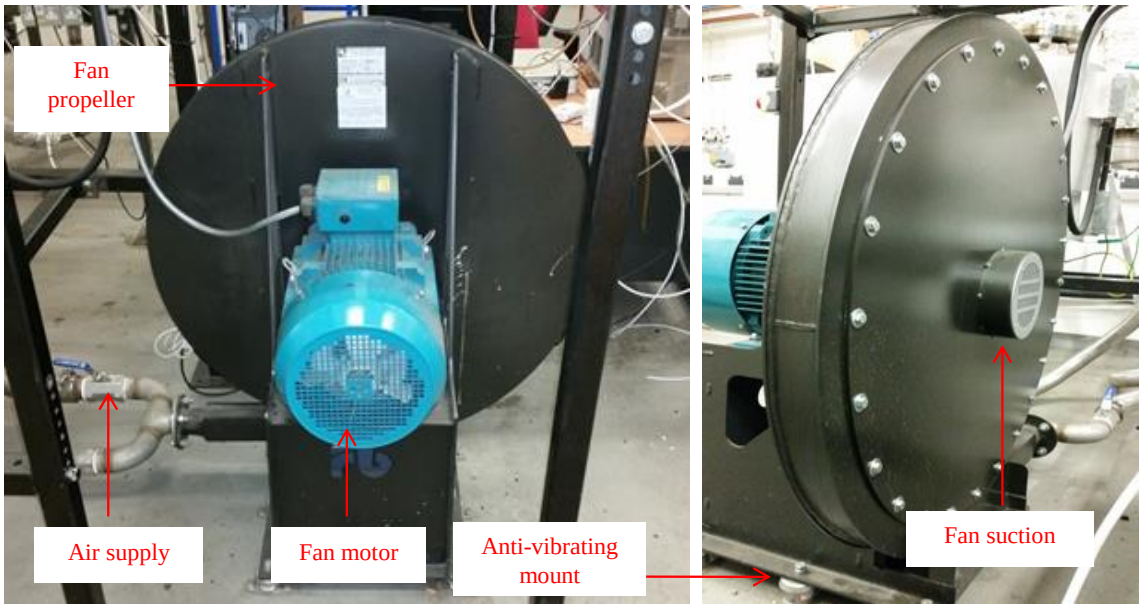


Figure 3.11: The blower fan for BFBC (back and front view the fan sitting on the anti-vibrating mounts).

The volumetric flow rate of the fluidising air supply from the blower fan into the plenum/air chamber of the BFBC is monitored through a low-pressure drop variable area volumetric flowmeter shown in Figure 3.12. The flowmeter was designed by Cache Instrumentation Ltd with a measuring range of between 50–800 L/min (air equivalent) at 1.013 bars and 20 °C. The flow meter has a good repeatability of ±0.5% of flow and a maximum operation temperature of 120 °C. The flowmeter is used as an operational

indicator device to provide the measurements of air flow rate supplied into the BFBC during combustion tests.

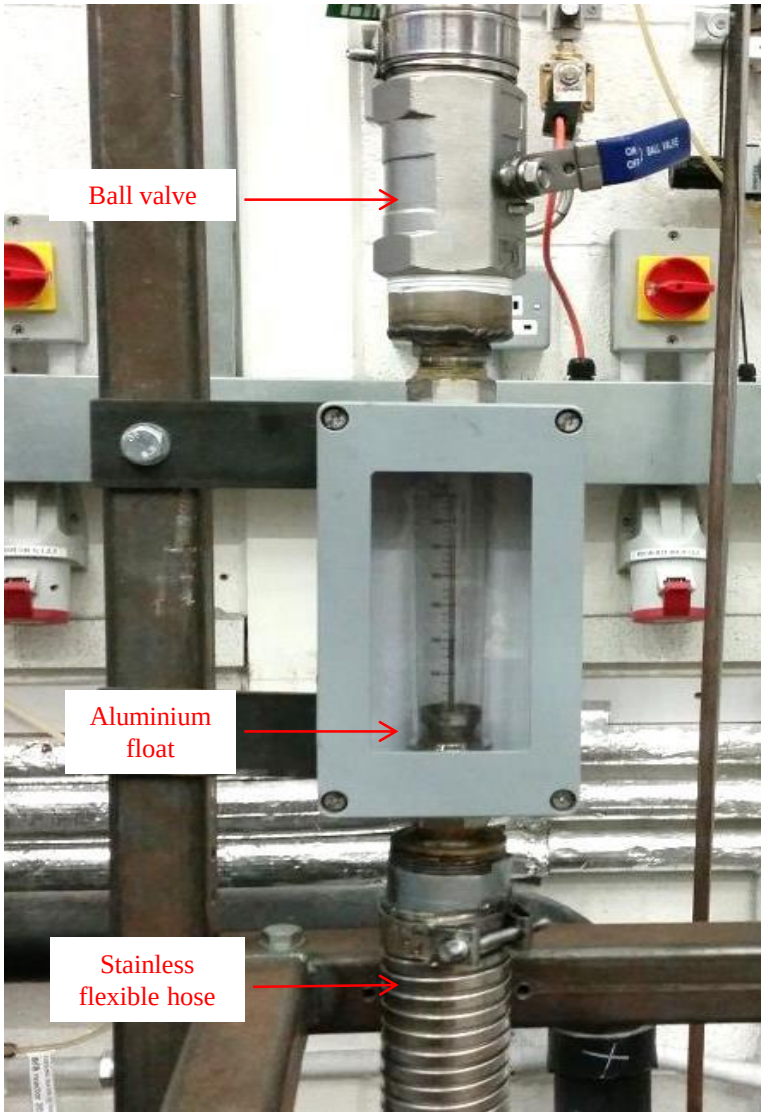


Figure 3.12: The variable area volumetric flowmeter for air supply to the BFBC.

The BFBC is designed to operate under air and oxy-firing conditions. A separate gas system is installed for oxy-fuel combustion conditions as shown in Figure 3.13. Under oxy-fuel initially, the supply of O_2 / CO_2 is separately taken from two blocks of cylinders, two for O_2 and four for CO_2 installed outside the building in a gas cage. The

gas cylinders are connected to each other and are all open at the same time to get enough flow rates for BFBC in the lab. The line pressure is varied between 5–10 bar using an installed online gas regulators inside the gas cage. The estimated maximum CO_2 flow rate required for the experiments is about 250 L/min. Therefore, to achieve this constant high flow rate without freezing the gas due to sudden expansion from the cylinders an additional heater is installed on the CO_2 line next to the gas cylinders inside the gas cage.

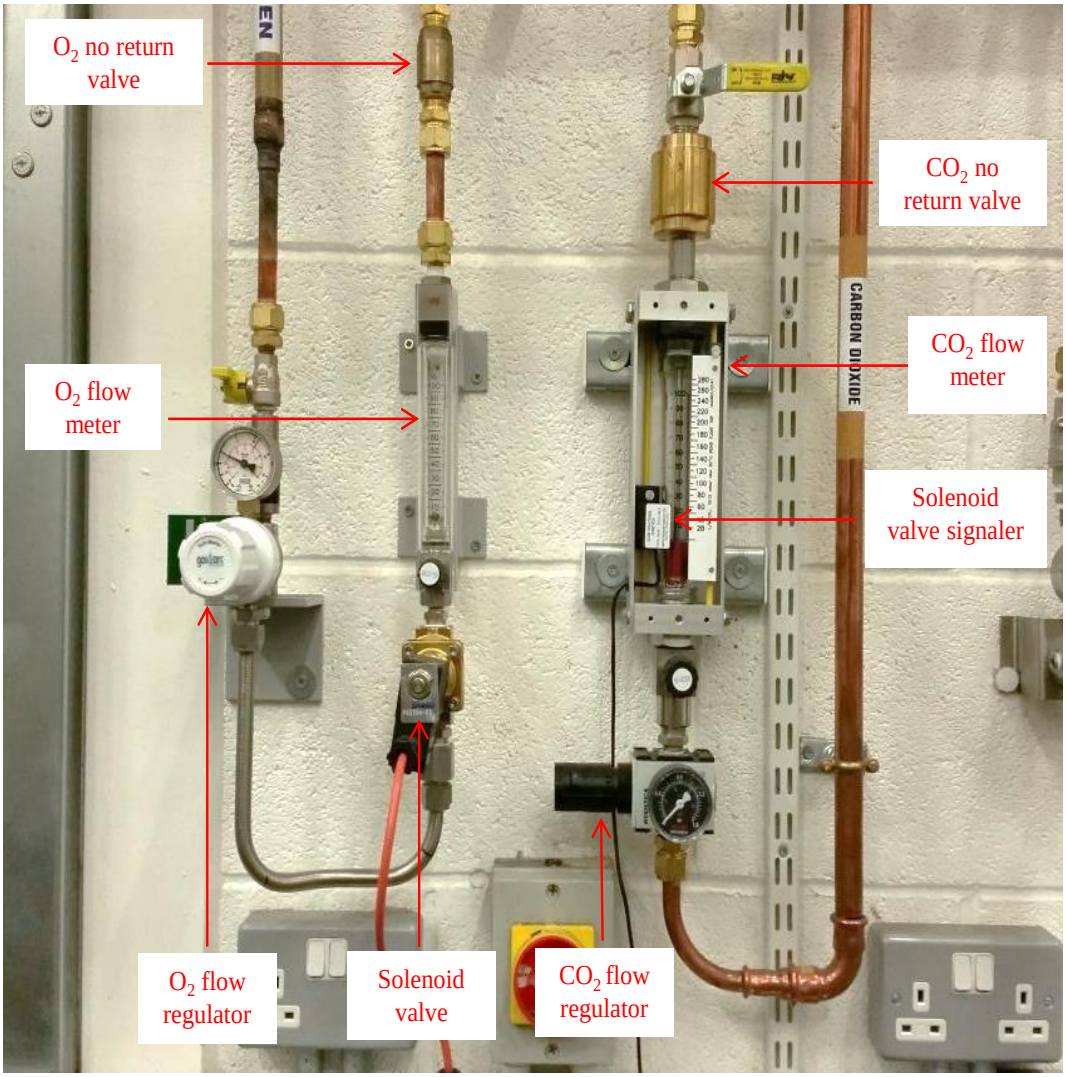


Figure 3.13: Oxy-fuel gas system showing separate gas supplies with solenoid safety valve.

The required flow rate of the O_2/CO_2 mixture is set using separate variable flow meters for O_2 and CO_2 inside the lab as shown in Figure 3.13. This gas system is designed after considering the safety issues of oxy-fuel combustion. A solenoid valve is installed on the O_2 line which gets signals from a signaller inside CO_2 flow meter, in case, CO_2 cylinders are getting empty, it shall give the signal to O_2 solenoid value and it automatically stops O_2 supply to the combustor, which prevents biomass fuel combustion with pure oxygen inside the BFB reactor.

For the supply of air/oxy gases into the plenum /air chamber a high-temperature flexible interlock, stainless metallic tubing made from austenitic stainless steel 304 S16 is used as shown in Figure 3.12. The metallic hose used has a bore size of 2⅜ inches (I.D. 60 mm, thickness 3 mm) and with a maximum working temperature of 650°C. It is connected using a stainless steel bolt hose jubilee clip (size 63–68 mm). The air entering into the combustor is preheated by means of a samox heavy insulated heating tape (model: STH052-120) 940 watt, 12.7 mm wide, 305 mm long, heating capacity up to 750 ^{o}C manufactured by Omega UK which is installed on the flexible stainless metallic hose. The installed heaters are only used to get the required temperatures for start-up combustion inside the combustor; once sufficient biomass combustion is established inside the reactor all of the heaters are switched off.

3.4 Instrumentation and Process Control

The BFBC rig is controlled by a data taker at which most of the instruments (thermocouples, pressure transducer, and gas analysers) are connected. The main

ceramic heaters, flexible air preheater, feeding system motor and blower fan are controlled by their separate controllers installed on the wall next to the rig. All temperature, pressure drop and flue gas composition signals across the BFBC are continuously monitored using dataTaker technology five channel logger (model DT80 series 2). This is connected with twenty-channel expansion module (CEM20). Each dataTaker channel has an accuracy of ±0.01% on a FSS and is logged at a pre-selected time intervals of (10 seconds) for the complete length of the experiment using dEX data logger software supplied by the dataTaker installed on the computer.

3.4.1 Temperature Measurements

K-type, Ni-Cr thermocouples with 250 mm length and 3 mm diameter with temperature measuring a range of 0–1250 °C are used for temperature measurement in the BFBC. The thermocouples are arranged and labelled sequentially from T1 to T7 along the centre line of the BFBC using the welded stainless steel 316 bored through male connector ⅛ inches (O.D) by ⅜ inches male pipe port fitted to the walls of the BFBC. The thermocouples are organised based on the height overhead or underneath the distributor inside the reactor as shown in Table 3.3.

Table 3.3: Positions of thermocouples in the BFBC.

Thermocouple	Positioning from distributor (cm)
T1	-5
T2	5
T3	74
T4	98
T5	123
T6	148
T7	173

Thermocouple 1 is located inside the air chamber, thermocouple 2 is inside the sand bed, whereas thermocouples 4 to 7 are used for the measurements of freeboard temperatures. The thermocouples' tips are inserted into the centre of the BFBC to reduce error due to conducting effect. The exact positions of the thermocouples are shown in the Figure 3.14.

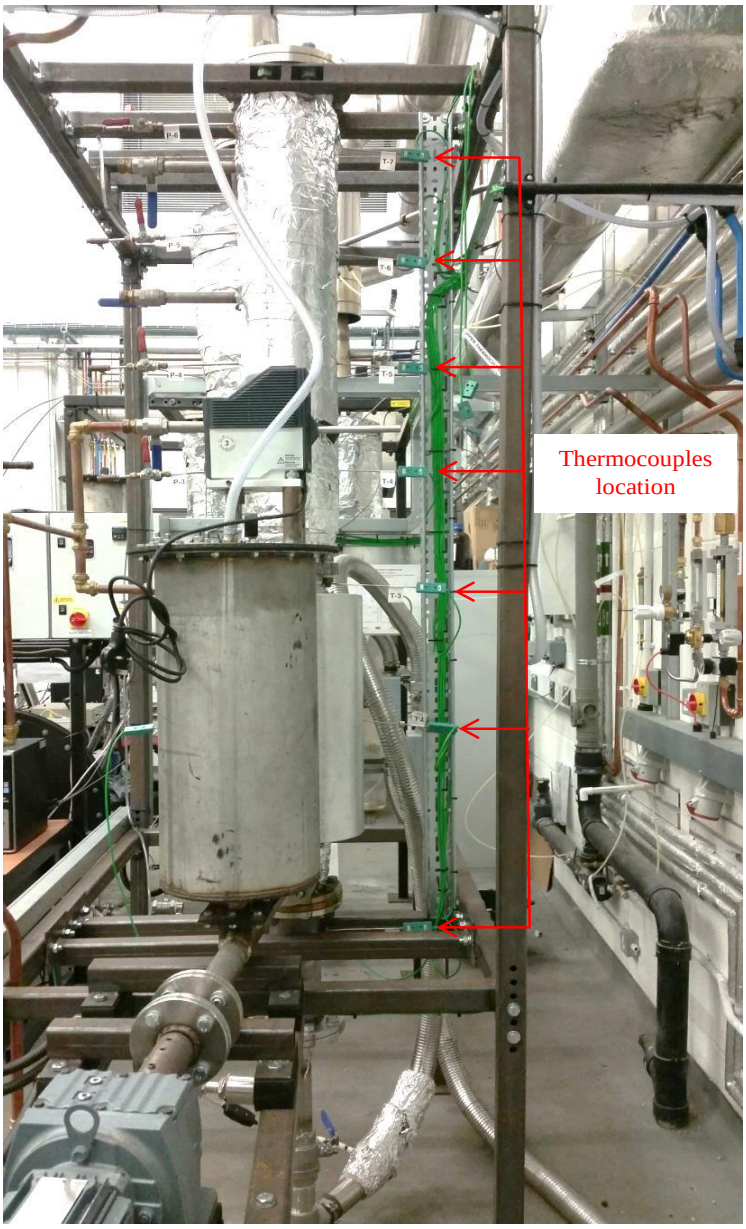


Figure 3.14: Thermocouples locations on the BFBC.

3.4.2 Pressure Measurements

Austenitic stainless steel 304 (¼ inches pipe size) arranged on the opposite side of the thermocouples as shown in Figure 3.2 are used as pressure measuring tapings. The six pressure tapings labelled sequentially from P1 to P6 along the centre line of the BFBC, each connected to a ¼ inches manual ball valve, which is used for selecting the pressure tapping point of choice. The pressure measuring port is connected to an Omega engineering electronic differential pressure transmitter (model PX2300–2DI) with an accuracy of ±0.25% on a FSS and repeatability of 0.05% on a FSS to measure the pressure by providing a 4–20 mA signal calibrated range for pressure measurements 0–140 mbar connected to dataTaker process monitor.

3.4.3 Flue Gas Measurements

The flue gas composition is measured throughout the tests using on-line gas calibrated ABB technology gas analyser (model EL 3020) with a repeatability of ≤0.5% shown in Figure 3.15. The CO_2, O_2, CO and NOx concentrations in the flue gas stream are determined during the tests. The flue gas sampling is carried out using the flue gas sampling probe (see section 3.4.6.), which is connected to a Horiba technology gas sampler (model VS-3000) via an in-house designed gas cooling and cleaning system. The Horiba gas sampler is connected to a regularly calibrated Horiba technology gas analyser (model VA-3000) with a repeatability of ±0.5% on a full-scale range (FSR) to measure NOx concentration in the flue gas.

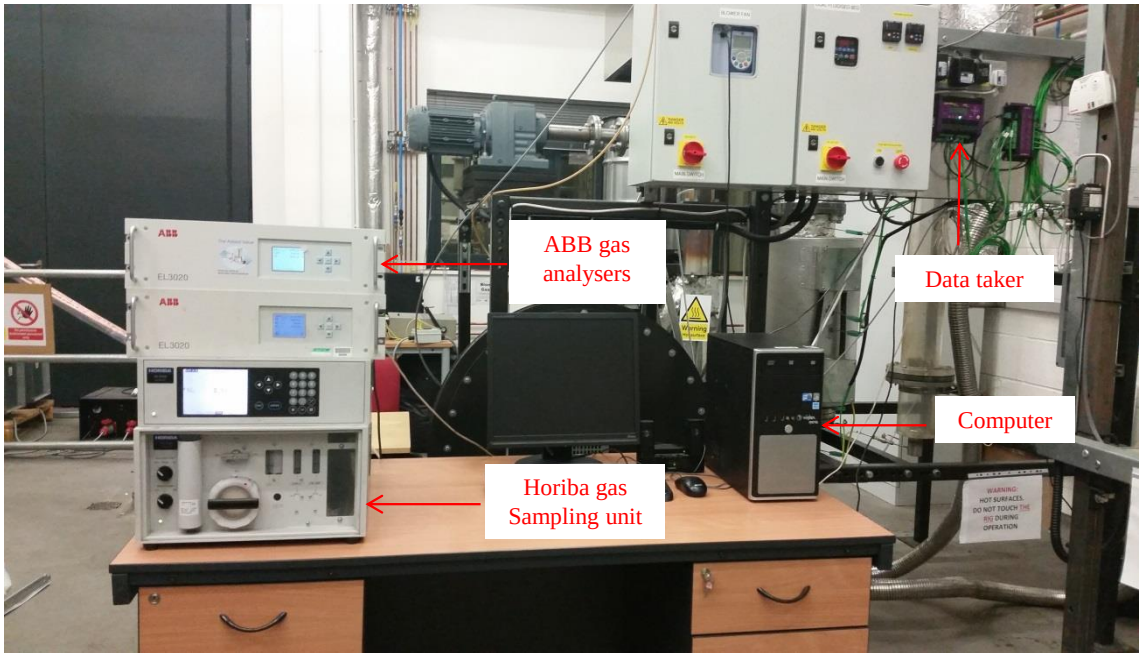


Figure 3.15: Gas sampling unit including analysers and computer with data taker software.

Chapter 4

Materials and Experimental Methods

4.1 Introduction

This chapter provides a detailed explanation of the materials and methods used during the course of this research. The choice of materials used for the purpose of this research is specified to the pre-design requisites criteria mentioned in Chapter 3. The materials specification section covers details of the physical, chemical and thermal degradation properties of the materials used during this study. The first section covers the experimental procedure involved in studying the hydrodynamics of the cold and hot BFBC and the method to calculate fluidisation velocity including visual observations of biomass mixing with bed material. The experimental methods employed for this research have been divided into six phases presented as overall research plan presented in Table 4.1. Phase one covers the materials characterisation of Garside 14/25 sand as

well as thermogravimetric analysis (TGA) and elemental analysis (EA) of eight different biomass fuels. A detailed description of the samples preparation and procedure used for this phase of the investigation is also included in this section. In phase two, the thermal analysis of chosen biomass fuels are performed, which aims to examine the thermal degradation, reactivity, the energy of activation and their relationship with different primary fuel properties under different reactant gas environments. Phase three investigates combustion of two woody and three non-woody biomass fuels in BFBC specifically under air, combustion with the main focus on the combustion behaviour and emission characteristics of these fuels.

Phase four comprises of multi-level air staging combustion with all tests of these biomass fuels in BFBC with the aim to reduce the NOx emissions while maintaining good combustion efficiency. In phase five the oxy-fuel combustion of one woody and two non-woody biomass fuels is studied in BFBC under different O_2/CO_2 mixture ratios to see the effect of O_2/CO_2 ratios on combustion temperatures and gas emissions. The operational procedures of the BFBC biomass combustion tests starting from pre-start up checks to normal operation, shutdown as well as indicating emergency shut down, measurements, samples and data collection are fully outlined in this section.

Phase six investigations focused on the use of SEM-EDX, XRD and XRF characterisation techniques to study the surface morphology and the chemical composition of bed material and ash particles collected after the combustion in BFBC. The results are used to deduce the agglomeration or sintering formation mechanism during biomass combustion in the BFBC system.

Table 4.1: An overview of the complete experimental research plan.

Biomass fuel type	**Phase 1** Materials characterisation	**Phase 2** Thermal analysis in TGA	**Phase 3** Air combustion in BFBC	**Phase 4** Air staging combustion in BFBC	**Phase 5** Oxy-fuel combustion in BFBC	**Phase 6** Bed material and ash analysis using SEM, XRD, XRF
Barley straw	✓	✓	×	×	×	×
Domestic wood	✓	✓	✓	✓	✓	✓
Industrial wood	✓	×	✓	✓	×	✓
Miscanthus	✓	✓	✓	✓	✓	✓
Peanut Shell	✓	×	✓	✓	×	✓
Waste wood	✓	✓	×	×	×	×
Wheat straw	✓	✓	✓	✓	✓	✓
Willow SRC	✓	✓	×	×	×	×

4.2 Material Selection and Characterisation

4.2.1 Bed Material

The Garside 14/25 sand is chosen to be used as the bed material for the operation of BFBC, due to its availability and usage in several UK industrial FBC systems. The physical and chemical analysis of Garside 14/25 sand supplied by the manufacturer is shown in Table 4.2 and Table 4.3 respectively [219]. The particle size distribution of the Garside 14/25 sand bed material was analysed using standard test method for particle size analysis [220].

Table 4.2: Physical analysis of Garside 14/25 sand [219].

Parameters	Description
Grain shape	Subangular to rounded
Colour	Yellowish brown
Size range (mm)	0.6 to 1.18
Specific gravity	2.65
Un-compacted bulk density (t/m^3)	1.56
Nominal effective size (mm)	0.63 – 0.85
Uniformity co-efficient (mm)	<1.4

Two sieving analyses were performed on sand, as received basis and for the size $\leq$1 mm using a different set of sieve arrangement. The sieve pans of 1.70, 1.18, 1.00, 0.85, 0.60, 0.30, 0.21, and 0.15 mm were used for analysis. Each collected size fraction was weighed and recorded using Precisa 165 (BJ 410C) weighing balance, which has a readability and repeatability of 0.01 g. The comparisons between the percentage

retained quantities in each sieve size of the measured particle size fraction distribution are given Appendix C.

The Sauter mean diameter (d_{32}) is also calculated from this analysis for comparison purposes, the method is also given in Appendix C along with calculations [221]. The initial fluidisation tests using sintered distribution plate were carried without and with sand size $\leq$1 mm.

Table 4.3: Chemical analysis of Garside 14/25 sand [219].

Name	Molecular formula	Weight %
Silica	SiO_2	96.67
Alumina	Al_2O_3	0.33
Titania	TiO_2	0.03
Iron	Fe_2O_3	2.4
Magnesium	MgO	<0.01
Calcium	CaO	0.01
Sodium	Na_2O	0.03
Potassium	K_2O	0.01
Phosphate	P_2O_5	<0.01
Manganese	MnO_2	<0.005
Chromium	Cr_2O_3	0.02

4.2.2 Biomass Fuels

Eight different types of biomass fuels; four woody and four non-woody are used during the course of this research work are listed in Table 4.1. All of these fuels were obtained from suppliers, with most of them being harvested and processed within the UK. The biomass fuels were received in pellet forms, within the size ranging from 10–30 mm in length and in a packing of 10–20 kg of polyethene plastic bags except for barley straw.

The bags were kept sealed and stored in a dry place until their further use in the BFBC to avoid a change in the moisture contents. For material characterisation and thermal analysis, about 0.5–1.0 kg of each biomass fuel was ground using a Retsch ultracentrifugal mill ZM 200 to particle sizes less than 212 μm according to the practice of previous research [222].

4.2.3 Proximate and Ultimate Analysis

Thermogravimetric analysis was employed for the proximate analysis of the biomass fuels [223]; which was used to measure the moisture (M), volatile matter (VM), fixed carbon (FC) and ash contents in the TA Instruments TGA Q-500 thermo-gravimetric analyser as shown in Figure 4.1. About 10–20 mg of biomass sample was put into the pan and heated in a flow of N_2 at a rate of 10 ^{o}C/min to 110 ^{o}C then holding at this temperature for 10 min to obtain the moisture content.

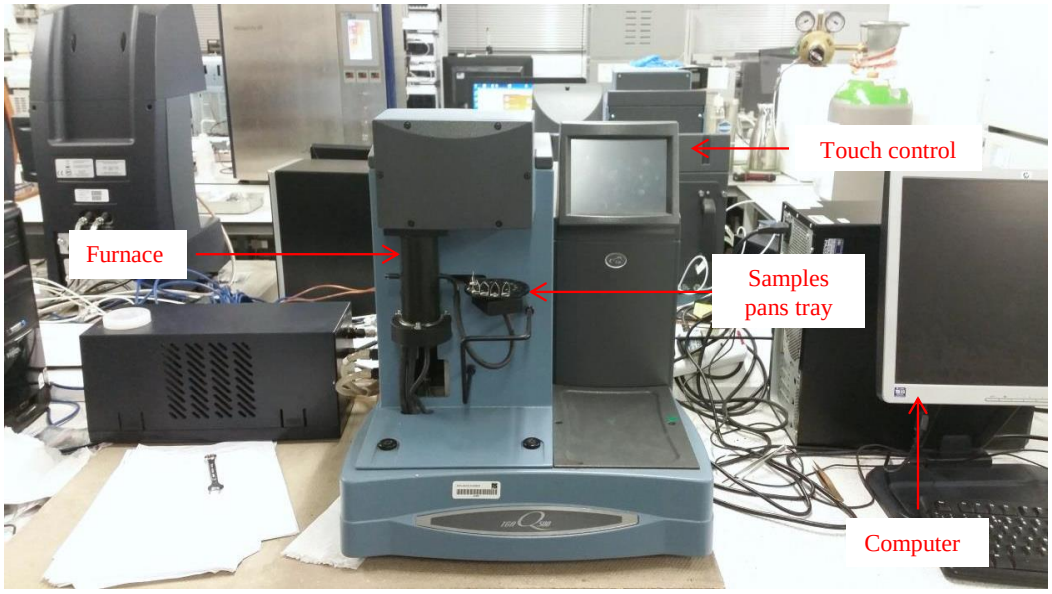


Figure 4.1: TGA Q-500 from TA instruments.

Then temperature was then ramped from 110 ^{o}C at a rate of 20 ^{o}C/min to 700 ^{o}C (same under N_2 flow) and held for 30 min to obtain the weight loss associated with devolatilisation after that temperature was ramped up at the same rate (20 ^{o}C/min) to 900 ^{o}C. Air was then introduced into the furnace and kept it isothermal for 40 min to oxidise the char completely to obtain the fixed carbon and ash content.

The ultimate analysis of biomass fuels; including carbon, hydrogen and nitrogen were determined by using a Leco CHN 628 series, whereas the fuel sulphur content was detected by using Leco 628 S elemental analyser series as shown in Figure 4.2. About 50–75 mg of biomass sample was inserted into the capsule located at the top of the analyser. The analyser combusts the biomass sample in oxygen at 950 °C, converting elemental carbon, hydrogen, and nitrogen into CO_2, H_2O, N_2, and NOx. These gases pass through infrared cells that determine the carbon and hydrogen content, and the thermal conductivity cell that determines N_2.

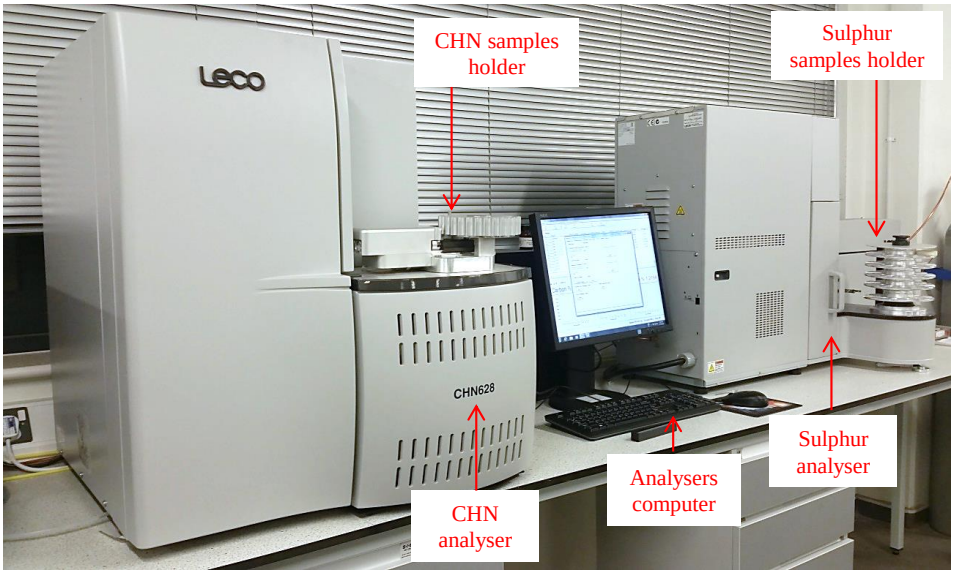


Figure 4.2: Leco CHNS 628 elemental analysers.

The analysis run time is approximately 4–6 minutes. The proximate and ultimate results along with thermos chemical properties of all biomass fuels are summarised in Table 4.4. The higher heating value (HHV) for each selected sample was obtained from using Eq. (4.1) proposed by Channiwala and Parikh (2002), which gives an average absolute error of 1.45% and bias error as 0.00% [224]:

$$HHV = 0.3491C+1.1783H+0.105S–0.1034O–0.0151N–0.0211A \quad (4.1)$$

Where HHV is in MJ/kg, C, H, N, O and A corresponds to hydrogen, sulphur, oxygen, nitrogen and ash contents respectively. All tests were repeated three to five times to get repeatable and reliable data, the average and standard deviations of all these runs are given in Appendix C.

Table 4.4: Ultimate analysis, proximate analysis and calorific values of biomass fuels.

Biomass fuels	Ultimate analysis[a]					Proximate analysis[c]				HHV[e]
	C (%)	H (%)	N (%)	O[b] (%)	S (%)	M[d] (%)	VM (%)	FC (%)	Ash (%)	(MJ/kg)
Barley straw pellets (BS)	40.87	5.78	0.55	52.15	0.65	8.95	78.15	14.70	7.15	15.46
Domestic wood Pellet (DW)	47.18	6.84	0.17	45.64	0.17	3.94	85.11	14.19	0.70	19.81
Industrial wood pellets (IW)	47.57	6.95	0.26	45.01	0.21	5.34	85.00	13.72	1.28	20.13
Miscanthus pellets (MIS)	42.87	6.74	0.38	49.82	0.19	3.34	82.85	15.37	1.80	19.10
Peanut shell pellets (PS)	46.97	6.79	1.34	44.39	0.51	5.96	74.06	22.40	3.55	19.77
Waste wood (WW)	45.78	6.05	0.34	47.75	0.08	5.80	84.48	14.06	1.46	18.12
Wheat straw (WS)	43.80	6.78	0.55	48.29	0.58	5.22	76.31	17.54	9.50	18.21
Willow SRC (SRC)	45.18	5.99	0.32	48.34	0.17	5.97	85.00	13.24	1.77	17.77

M: moisture, VM: volatile matter, FC: fixed carbon, HHV: high heating value.

a. On dry basis except as denoted in the table.
b. Calculated by difference.
c. On dry basis except moisture which is as received basis.
d. As received basis.
e. Calculated based on Channiwala and Parikh (2002) [224].

4.3 Thermogravimetric Analysis

Thermogravimetric analysis (TGA) is the most frequently used thermo-analytical technique for the thermal decomposition studies of solid fuels as it permits the controlled study of global reactions that occur during various thermal or thermochemical conversion processes [225]. In the present research, TGA has been used to identify different fractions present in the biomass materials, and to obtain accurate data on char reactivities under an active environment of interest. The kinetic parameters derived from TGA characterisations are important for the design of pyrolysis reactors, gasifiers and combustors; enabling optimal energy conversion efficiency with the minimised emissions. The TGA analyser used was a vertical and balance analyser as shown in Figure 4.1. It implements differential thermal analysis (DTA) and differential scanning calorimetry (DSC) measurements. The analysis was performed in inert and oxidising atmospheres.

The sample weight was limited to 15–20 mg for each sample in order to limit the potential effect of heat and mass transfer during the process. The temperature was programmed to increase from ambient to 110 ^{o}C at a heating rate of 10 ^{o}C/min and remain isothermally at this temperature for 10 min before it was allowed to be increased at 20 ^{o}C/min to 950 ^{o}C and held isothermally for 40 min. A constant selected gas flow rate of 100 mL/min was used for all test conditions. All of the experiments were repeated two to three times to ensure repeatability. The weight loss profiles and their derivative curves were then obtained as a function of the time and temperature for the

reaction conditions examined. The data obtained from TGA was converted into MS Excel file using TA universal analysis software provided by TA instruments.

TGA and DTG profiles give information about the thermal stability of the biomass feedstock and the overall kinetic progress of the thermal decomposition. They were also used to determine other combustion characteristics, such as average rate of weight loss (R_{avg}), average temperature (T_{avg}), peak temperature (T_{peak}) and the maximum rate of weight loss (R_{max}) for all studied biomass fuels. T_{peak} corresponds to the point at which the reaction is proceeding at its maximum rate, and R_{max} is the associated weight loss rate at T_{peak}. The selection of viable temperature ranges for analysing devolatilisation and combustion reactions can have a significant impact on the calculated values, and there is no general consensus on which approach is best [226]. A method originally devised by Ghetti et al. [227] represented in Eq. (4.2) has been employed to calculate the reactivities of the biomass fuel samples;

$$R_M \times 100 = \frac{R_{M1}}{T_{P1}} + \frac{R_{M2}}{T_{P2}} + \frac{R_{M3}}{T_{P3}} \ldots\ldots\ldots + \frac{R_{Mn}}{T_{Pn}} \quad (4.2)$$

Where R_{M1}, R_{M2} represent the individual reactivates at corresponding temperatures T_{P1}, T_{P2} respectively at different DTG peaks heights. The R_M is the overall mean reactivity at the corresponding peak temperature T_P.

4.4 Cold Rig Testing

4.4.1 Minimum Fluidisation Velocity Measurements

The hydrodynamics and design parameters were calculated according to the methods described in section 3.3, Chapter 3. The initial cold rig tests were carried out for the validation of these parameters and to obtain a visual representation of the fluidisation quality expected in the biomass BFBC at cold conditions. The process flow diagram of the experimental setup is shown in Figure 3.1. The fluidising air was supplied to the rig by a centrifugal fan which is powered by a 5.5 kW Brook Crompton IP55 motor controlled by an in-house built variable speed drive inverter.

Two variables were measured during the cold fluidisation test; fluidising air flow rate and pressure drop across the bed with and without sand. The fluidisation quality was also judged through visual observations from the top of the reactor by removing the top flange. In the first case, the preliminary cold rig testing was carried using sintered distribution plate without a sand bed in the BFBC. The air flow rate was gradually increased, at each increment, the pressure drop readings were recorded after every five-minute interval across the bed using pressure transducer then averaged, the results without sand along with the linear fit correlation from these experiments are presented in Figure 4.3. In the second case, the testing was made using a sand bed of height 25 cm. Initially, the upright bed of sand particles was supported by the distribution plate. The direction of air flow was upward through the sand bed. There is a drag applied on the sand particles by the flowing gas, at low air flow rates the pressure drop resultant from this drag force was small.

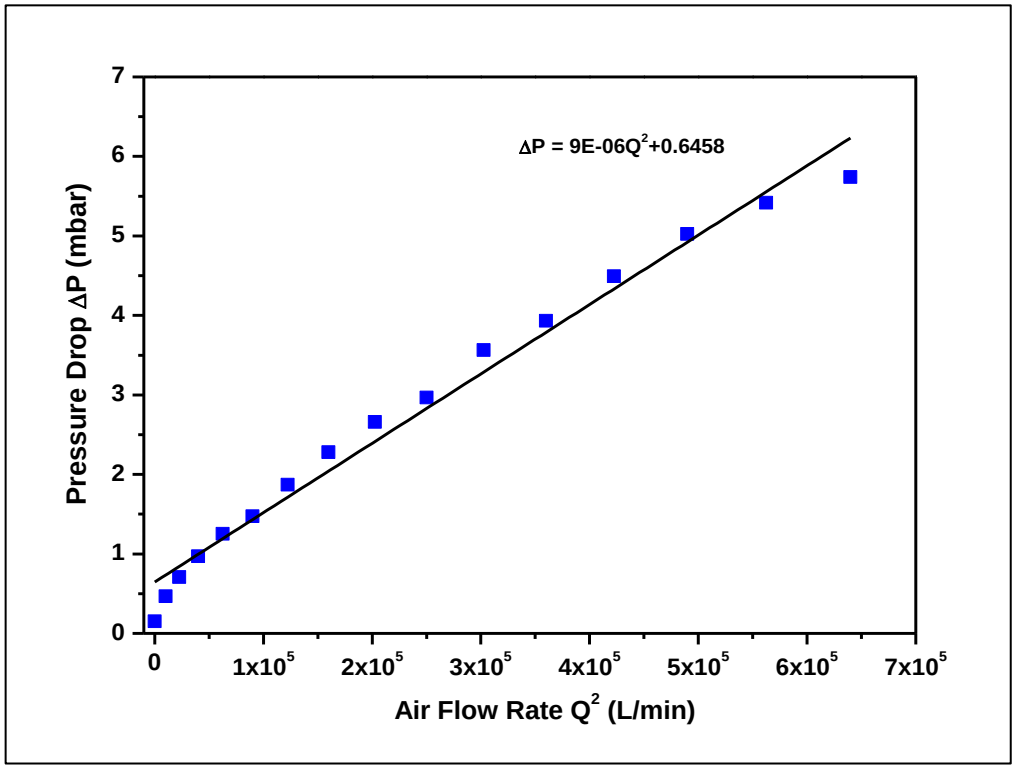


Figure 4.3: Pressure drop measurements using sintered distribution plate without sand.

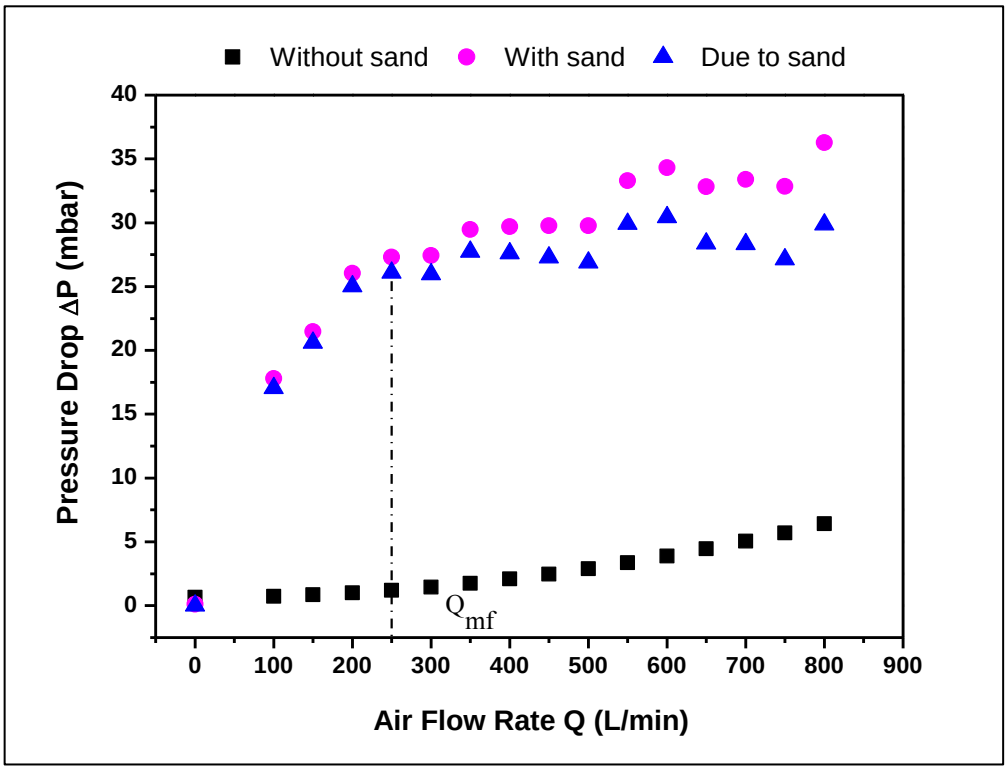


Figure 4.4: Pressure drop measurements using sintered distribution plate without and sand.

The combined fluidisation results are shown in Figure 4.4. It can be seen at air flow rate 100 L/min, the pressure drop was about 18 mbar. The air flow rate was slowly increased in order to break down the internal force to fluidise the bed. It is evident from Figure 4.4, when the air flow rate is increased to a certain value of 250 L/min the pressure drop was 27.5 mbar and the particles start to begin to lift off and just become fluidised in the air. The flow rates of air above the point of minimum fluidisation >250 L/min, the fluidised bed looks much like a dynamically boiling liquid; the gas bubbles rising swiftly and burst on the surface, and the suspension phase is systematically agitated. The bubbles formed near the bottom of the bed, close to the distributor plate [200]. The linear fit correlation from these tests is described in Eq. (4.3).

$$\Delta P_1 = 9 \times 10^{-6} Q^2 + 0.6458 \tag{4.3}$$

The Eq. (4.3) was used to calculated pressure drop without sand (ΔP_1) across the bed. Another correlation which was used for pressure drop with sand (ΔP_2) is described in Eq. (4.4).

$$\Delta P_2 = \frac{W}{A} \tag{4.4}$$

where W is the weight of total solids and A is bed surface area, which can be determined as:

$$A = \pi r^2 \tag{4.5}$$

where r represent the radius of the sand bed respectively. The pressure drop due to total solids on the bed could be calculated by the following relationship.

$$\Delta P_3 = \frac{Wg}{A} \tag{4.6}$$

where g is gravitational drag force on the particles in m/s^2.

Moreover, at higher air flow rates, the bed pressure drop shows a small decrease, which could be attributed to the frictional forces on the walls of the bubbling fluidised bed reactor. The greater air flow rates through the holes when the pitch is larger, giving a higher interstitial gas velocity [177]. The increased gas velocity creates a circulation of particles in the neighbourhood of the holes, thus inducing the condition of fluidisation, and hence lower values of pressure drop. Therefore, the pressure drop is inversely proportional to distributor hole pitch and hole diameter. Other researcher found similar results using different experimental correlations [228].

The experimentally calculated minimum fluidisation velocity was 0.51 m/s, whereas the theoretically calculated value was 0.40 m/s. This slight variation between the theoretically calculated and measured minimum fluidisation velocity can be attributed to the pressure drop across the distribution plate and the lower fluidising air temperature than the assumed ambient conditions used in the theoretical calculation.

4.4.2 Visual Observations during Plexiglas Cold Rig Testing

After the hydrodynamic design and minimum fluidisation velocity parameters calculations; the biomass domestic wood pellet size between 15–30 mm were tested in a fluidising rig made of a clear polycarbonate perplex material. This test enabled the sympathetic validation of the hydrodynamic design parameters calculated in section 3.3, and a visual representation to provide an understanding of the fluidisation quality expected in the biomass BFBC. The experimental rig setup used for the cold visualisation is shown in Figure 4.5. The setup comprises of a BFBR with an I.D. of 154 mm and a total height of 2000 mm, which was divided into the plenum, fluidising section and freeboard section similar to the real BFBC. These sections were connected with each other by flanges, which were glued using adhesive polycarbonate glue.

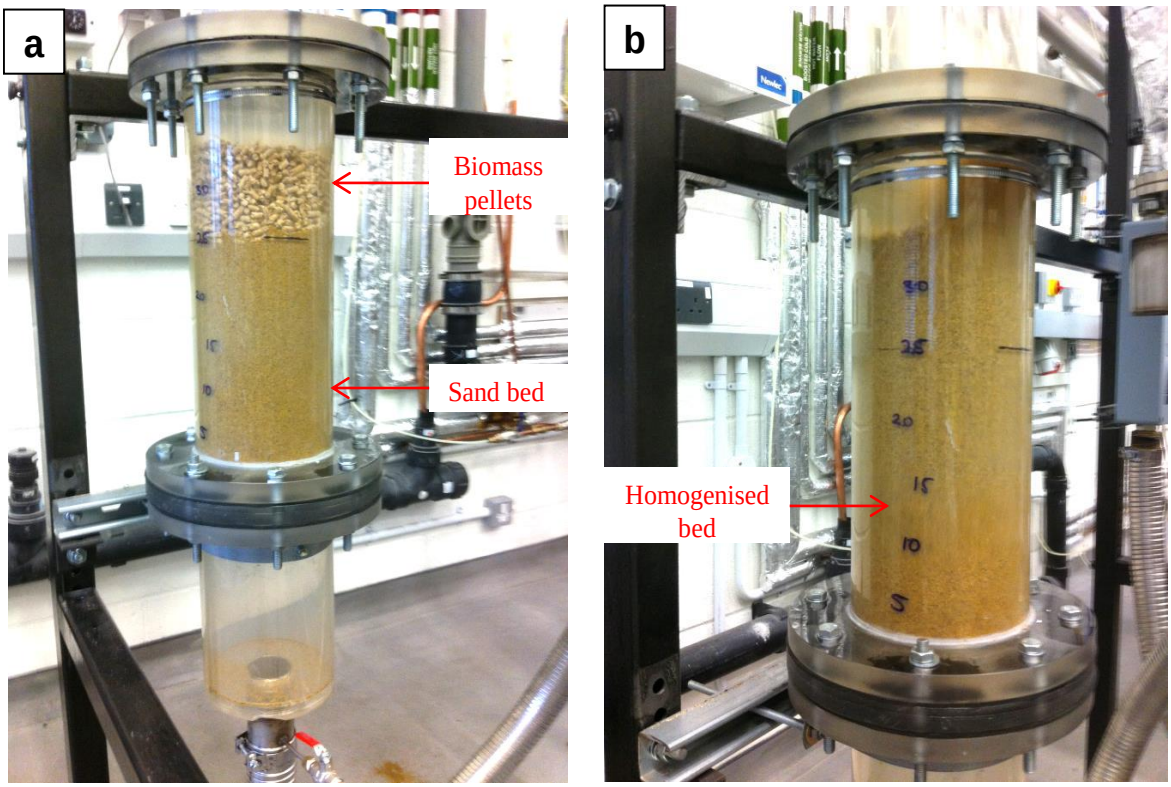


Figure 4.5: The cold rig testing; (a) before fluidisation, (b) after fluidisation.

The rig was filled up to 25 cm of sand of the same Garside 14/25 sand bed material and biomass pellets up to a height 10 cm were added to the top of the bed as can been seen in Figure 4.5. The fluidising air was supplied through air blower and its speed was controlled by an inverter. The fluidisation quality was judged by visual observation of the bed and biomass pellets. From visual observation of the bed during this investigation, it was seen that a slight movement occurred in the bed at a slower speed of 1500 rpm and the bed and biomass pellets mixing became more vigorous as the fan speed was ramped up from 1500 to 2000 rpm.

After a short while, the bed of sand was completely and well mixed with the biomass pellets as can be seen in Figure 4.5, it became difficult to find any separate biomass pellets in the sand bed. This confirms that good quality of fluidisation with the biomass pellets can be expected during in the hot BFBC operation.

4.4.3 Biomass Feeding System Calibration

The calibration of the biomass feeder was carried out by setting different speeds of the feeder screw auger using the inverter connected with the geared motor. A plastic bucket was placed on a weighing scale where conveyed biomass was collected and weighted constantly over a fixed period of time. The full mechanism of feeding system calibration is shown in Appendix B. The biomass size used for calibration was the same as to be used during combustion experiments in BFBC system. The summary of feeding calibration results of five biomass fuels (domestic wood (DW), industrial wood (ID), miscanthus (MIS), peanut shell pellets (PS) and wheat straw (WS)) is presented in Figure 4.6. The calibration results with individual biomass fuel are given in Appendix C

along with the calibration curves and the best linear fit for each type of biomass fuel. It can be seen from Figure 4.6 the feeding rate of each biomass fuel is linearly proportional to the motor frequency set by the inverter.

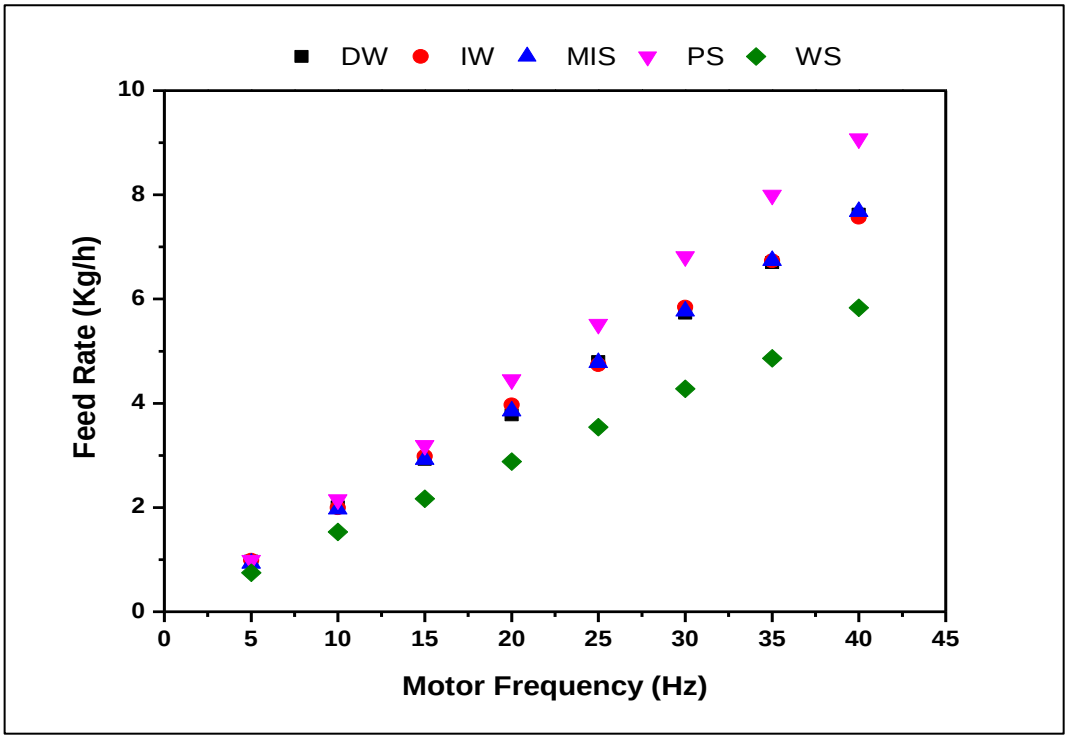


Figure 4.6: Feeding system calibration using five different biomass fuel pellets; domestic wood (DW), industrial wood (ID), miscanthus (MIS), peanut shell pellets (PS) and wheat straw (WS).

4.5 Operational Procedure of BFBC

4.5.1 Pre Start-up Checks

The full experimental setup is shown in Figure 4.7. The sieved sand size <1 mm and measured 3.2 kg of Garside 14/25 sand was poured from the top into the reactor to attain a fixed bed height of about 25 cm. A known amount of the chosen biomass fuel was poured into the hopper which has a holding capacity of up to 25 kg. Pre-start-up

checks with the list given in Appendix C are completed and signed off as part of the pre-start-up checks for each experiment.

4.5.2 Start-up Procedure

After completing the start-up checks the fluidised bed main heaters control system was activated by using the main switch and the heating temperature controllers were set to a temperature ramp rate of 400 °C/h and a set-point of 850 °C. The temperature limit controller was set to 870 °C which is 20°C above the set-point of the heating controller. Black switch on the button for the heaters control system was pressed to start the heating process for the BFBC. Then air pre-heater was turned on and the temperature was set to 450 ^{o}C. After 10 minutes of operation, the blower fan was turned on and was ramped slowly from a speed of 500 rpm to a speed of 2500 rpm using the Super Drive G2 software installed on the connected computer. The fluidising air flow rate was measured using the variable area flowmeter and the system was allowed to operate at these conditions for another 30 minutes after that the fluidising air flow rate was further increased by 50 to 350 L/min at a time interval of 30 minutes from the beginning of the heating process.

This procedure was repeated at 60, 90 and 120 minutes from the beginning of the heating cycle and the fluidising air flow rate was increased by 50 L/min each time to 100, 150, 200, 250 and 300 L/min respectively at each time interval. After two hours of continuous operation from the beginning of the heating process at 350 L/min fluidising air flow rate, the system was further allowed to continue operating at these conditions until a bed temperature of over 500 °C was achieved in the combustor.

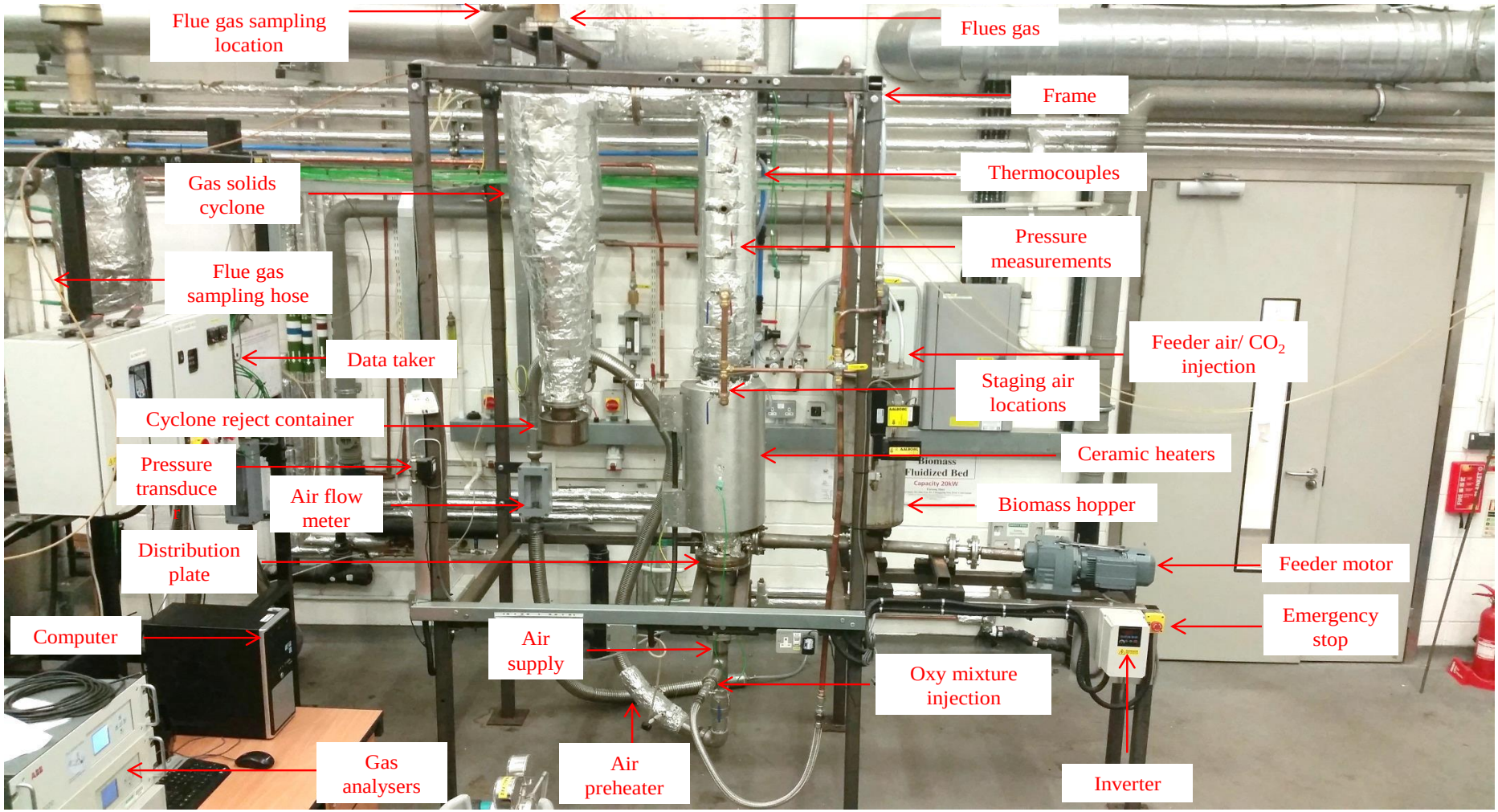


Figure 4.7: Full experimental setup including bubbling fluidised bed combustor (BFBC) with auxiliaries.

This normally takes between 160–180 minutes from the beginning of the heating process. During this period, all the temperatures, pressure and fluidising air flow rate were monitored and recorded.

4.5.3 Unstaged and Staged Air Combustion Procedure

Initially, the bed was heated up with the main ceramic heaters installed along the walls of the reactor. The hot air was also introduced via air pre-heater to stir the bed particles. Once the bed temperature (thermocouple T-2) in the BFBC has reached over 500 °C, biomass feeding was started. The biomass feeder inverter frequency was set at 10 Hz, which equates to a fuel feeding rate of about 2 kg/hour depending on the biomass type.

As soon as the biomass starts combustion the temperature measured across all thermocouples in the reactor rapidly increased, which were observed in the displayed temperature chart on the computer. At this point, the ceramic heaters should have turned off automatically as the wall temperature exceeds the set point of 850 ^{o}C, where the pre-air heater was turned off manually. The bed temperature was left to continue increasing at this condition until a bed temperature of 800 °C was reached after which the heat extraction water-cooled probe was inserted into the fluidised bed to control the bed temperatures and cooling water flow rate was set to about 1 L/min using a manual control valve at the start. As a result of the heat extraction with the cooling probe from the combustor, the measured gas temperatures inside the combustor were seen to be slightly decreasing until reaching steady values. Without air staging (WAS) the tests were carried out with continuous biomass feeding in BFBC and the results were obtained under steady state conditions. The combustor was left to continue operation at

this condition and stabilise to a bed temperature between 750–850 °C. To analyse the effect of the excess of air on the flue gas emissions and combustion efficiency, different excess air ratios including; 15%, 30% and 45% were studied by changing the biomass fuel feed rates and by maintaining a constant total air flow rate at 350 L/min. When the fuel feeding rate was varied, the temperatures along the reactor and freeboard were varied simultaneously as the flow rate of water and position of the cooling probe remained unchanged.

To investigate the effect of the air staging, a part of the total air flow rate (50 L/min) was diverted to one of the two air staging injection pipes, while the total air flow rate was fixed at the constant value of 350 L/min. In order to study how the air staging injection location affects to the gas compositions, the secondary air was injected from two different heights; 70 cm (named AS1) and 110 cm (named AS2) from the distributor plate. For comparison purposes, experiments without air staging (named WAS) were also carried out with all the fuels. At least three to four runs were performed with each biomass for each different condition studied (WAS, AS1 and AS2), in order to verify the results achieved. A matrix showing all the tests performed under WAS, AS1 and AS2 conditions is shown in Table 4.5.

The flue gas sampling was done using the water cooling flue gas sampling probe connected to a gas conditioning and cleaning unit for the condensation and removal of vapour and ash particles before entry to the gas analysers which measure concentrations of O_2, CO_2, CO and NOx present in the flue gas.

Table 4.5: Experimental matrix for the tests performed under without air staging and with air staging combustion.

Batch No.	Biomass fuel type	Combustion environment	Fuel feed rate (kg/hr)	Excess air level (%age)	Temperature range (^{o}C)	Cooling water flow rate (L/min)	Number of runs	Total run time (hrs)
	Domestic wood	WAS	3-5	10-50	750-850	1.2	4	8-12
	Industrial wood	WAS	3-5	10-50	750-850	1.2	4	8-12
1	Miscanthus	WAS	3-5	10-50	750-850	1.0	4	8-12
	Peanut shell	WAS	3-5	10-50	750-850	1.0	4	8-12
	Wheat straw	WAS	3-5	10-50	750-850	1.0	4	8-12
	Domestic wood	AS 1	3-5	10-50	750-850	1.2	4	8-12
	Industrial wood	AS 1	3-5	10-50	750-850	1.2	4	8-12
2	Miscanthus	AS 1	3-5	10-50	750-850	1.0	4	8-12
	Peanut shell	AS 1	3-5	10-50	750-850	1.0	4	8-12
	Wheat straw	AS 1	3-5	10-50	750-850	1.0	4	8-12
	Domestic wood	AS 2	3-5	10-50	750-850	1.2	4	8-12
	Industrial wood	AS 2	3-5	10-50	750-850	1.2	4	8-12
3	Miscanthus	AS 2	3-5	10-50	750-850	1.0	4	8-12
	Peanut shell	AS 2	3-5	10-50	750-850	1.0	4	8-12
	Wheat straw	AS 2	3-5	10-50	750-850	1.0	4	8-12

The temperatures, pressure and flue gas composition ranges were continuously displayed on the computer in the form of charts which were monitored throughout the duration of each experimental run. In addition, the temperature, pressure and flue gas composition including NOx emissions data was continually measured and logged every 10 seconds by the DT80 series data logger.

During one day operation, the BFBC was operated for different conditions while at each condition the system was kept for 1–2 hour at steady state operation. From start up till shutdown the data for all of the parameters were continuously recorded on the computer. The pressure, temperature and flue gas emission data were drawn in the graphical forms as shown in Appendix C for further analysis. A window of about 45 min was maintained for each steady state condition studied and all of the data points for temperatures (T1–T9), pressure (ΔP) and gas emissions (CO_2, CO, O_2 and NOx) were averaged to get one single point on the graphs as explained in Appendix C.

The pressure gauge on the top of the biomass hopper was continuously monitored and the temperature of the feeding pipe was also regularly checked during each test run to get an indication of biomass feed blockage or backfire in the hopper. The stirrer mounted on the biomass hopper has never been used as all biomass pellets have good flowing characteristics and the occasionally occurring bridging at the bottom of the hopper can be easily cleared by tapping the hopper with a rubber mallet. The tapping need was identified by a sudden progressive decrease in bed temperature and the compositions of CO_2 and NOx in the flue gas monitor.

4.5.4 Oxy-fuel Combustion Procedure

The pre-start-up checks, heating and air combustion procedures for this part of the tests are the same as those for the normal combustion procedure detailed in above sections 4.4.5.1, 4.5.2 and 4.5.3 respectively. The only difference is the additional procedure for switching from air to oxy-fuel combustion conditions using the separate gas system installed for oxy-fuel combustion. The air combustion procedures detailed in section 4.5.3 were followed to attain a bed temperature of 500°C or higher, then the biomass air combustion operation was stabilised and maintained for 1 hour. After which, the O_2 and CO_2 gas cylinders were opened and lines pressure was set to 8 bars from the regulator installed inside the gas cylinders' cage. The additional CO_2 line heater was also switched on at least 5 minutes prior to opening the gas cylinders as described in section 3.4.8 in Chapter 3.

To simulate oxy-fuel combustion, which recycles a part of its gas and mixing it with O_2 as the oxidant, O_2 and CO_2 gas mixtures were used to simulate the oxidant for the oxy-fuel combustion. The O_2/CO_2 mixture valve installed at the bottom of the fluidised bed was opened, and then first CO_2 flow rate was set to the required value followed by the adjustment of the O_2 flow rate using separately installed regulators as shown in Figure 3.13. After the BFBC is fully on oxy-fuel oxidants the air supply was shut off and the air ball valve was also turned off. During oxy-fuel combustion, different O_2/CO_2 mixture ratios were adjusted for a time period up to 1 hour. A matrix showing all the tests performed under oxy-fuel combustion is shown in Table 4.6. During these investigations, special attention was paid to the combustion and bed temperatures.

Table 4.6: Experimental matrix of the tests performed under oxy-fuel combustion.

Batch No.	Biomass fuel type	Combustion environment	Fuel Feed rate (kg/hr)	Excess air level (%age)	Temperature range (^{o}C)	Cooling water flow rate (L/min)	Number of runs	Total run time (hrs)
	Domestic wood	21%O_2/79%CO_2	3-5	30	750-850	1.2	3	8-12
	Industrial wood	21%O_2/79%CO_2	3-5	30	750-850	1.2	3	8-12
1	Miscanthus	21%O_2/79%CO_2	3-5	30	750-850	1.0	3	8-12
	Peanut shell	21%O_2/79%CO_2	3-5	30	750-850	1.0	3	8-12
	Wheat straw	21%O_2/79%CO_2	3-5	30	750-850	1.0	3	8-12
	Domestic wood	25%O_2/75%CO_2	3-5	30	750-850	1.2	3	8-12
	Industrial wood	25%O_2/75%CO_2	3-5	30	750-850	1.2	3	8-12
2	Miscanthus	25%O_2/75%CO_2	3-5	30	750-850	1.0	3	8-12
	Peanut shell	25%O_2/75%CO_2	3-5	30	750-850	1.0	3	8-12
	Wheat straw	25%O_2/75%CO_2	3-5	30	750-850	1.0	3	8-12
	Domestic wood	30%O_2/70%CO_2	3-5	30	750-850	1.2	3	8-12
	Industrial wood	30%O_2/70%CO_2	3-5	30	750-850	1.2	3	8-12
3	Miscanthus	30%O_2/70%CO_2	3-5	30	750-850	1.0	3	8-12
	Peanut shell	30%O_2/70%CO_2	3-5	30	750-850	1.0	3	8-12
	Wheat straw	30%O_2/70%CO_2	3-5	30	750-850	1.0	3	8-12

The temperature and pressure profiles across the BFBC, oxy-gases flow rates and composition of flue gas produced were measured and logged every 10 seconds on the dataTaker and saved on the computer as usual. After the oxy-fuel experiments were finished, the whole system was switched back to the air combustion conditions, so that the air combustion tests can be repeated on the same testing day.

4.5.5 Shutdown Procedure

At the end of the combustion experiment, the biomass feeder inverter was turned off and the fluidising fan speed was reduced to 2000 rpm and allowed to continue operating at this condition until the bed temperature drops below 200 °C, after which the heat extraction cooling probe was removed from the reactor. Finally, the shutdown checklist given in Appendix C was completed and signed off as part of the shutdown procedure.

4.6 Bed Material and Ash Characterisation

The solids by the cyclone container were collected after each experiment and stored in plastic sample bags. The bed material and cyclone solids were weighed using Precisa 165 (BJ 410C) weighing scale which has a readability and repeatability of $\pm$0.01 g.

4.6.1 Bed Material Sampling

After completing the combustion experiments with each type of biomass fuel under one set of conditions (air, air staging or oxy-fuel) the bed was opened for visual inspection and samples were collections. The BFBC system was allowed to cool down to room temperature and the fluidising air stainless steel pipe connected to the plenum chamber

shown in Figure 4.7 was removed. This was followed by the removal of the frame supporting bars of the fluidised bed section running through the bottom of the plenum chamber flange. A rectangular plastic sheet of size 1500×1000 mm was laid on the floor to collect the bad material sand. The bolts, nuts and washers attaching the plenum chamber and distribution plate to the fluidising zone were removed and the sand was allowed to flow out and pour onto the plastic sheet.

The collected bed material was visually inspected for signs of any type of agglomeration or sintering and was weighed using Precisa 165 (BJ 410C) weighing scale which has a readability and repeatability of $\pm$0.01 g. A portion of the bed material was stored and packed into labelled sample bags for further processing. The sampled portion of the bed material 100–200 gm was grounded into a powered form of size <50 µm using Ring and puck mill (made by KHD Humboldt Wedag AG) and stored in plastic bags for further analysis using SEM-EDX, XRD and XRF. The above procedure was repeated for the collection of second and third samples to prepare for the next test with a new batch 3.2 kg of fresh Garside 14/25 sand (size <1 mm) added to the reactor as the new bed material.

4.6.2 Cyclone Reject Sampling

During biomass combustion in the BFBC system, the solids including ash, char and/or bed material particles entrained in the up through flue gas from the reactor and carried into the cyclone are collected by the cyclone reject container (see Figure 4.7) and termed as cyclone reject. After each day's run, the cyclone container was opened and the collected material was weighed and stored in labelled plastic sample bags. A portion

of cyclone ash samples were grounded following the same method as described in section 4.6.2 for further analysis under SEM-EDX, XRD and XRF.

4.6.3 SEM-EDX

The scanning electron microscopy (SEM) is a common technique used to study the surface morphology, sintering or agglomeration in various processes such as pyrolysis, gasification and combustion processes. The energy dispersed X-ray (EDX) is an elemental characterisation technique used in combination with SEM. Various researchers have used the SEM-EDX technique to identify and quantify elements present in the particles and to observe a visual explanation of the interaction that occurs between the bed particles and the present binders causing agglomeration or sintering phenomenon during solid fuels combustion including biomass [229-232]. Hence, SEM-EDX can provide a better understanding of the elements and their interactions causing agglomeration and sintering formation in fluidised beds system [233]. The SEM-EDX setup used in the present research is shown in Figure 4.8.

The working principle of SEM-EDX is based on the generation of monochromatic electron beams under vacuum by the electron gun shown in Figure 4.8. The beam of these electrons is collimated by magnetic condenser lenses apertures and then focused onto a selected area of the sample by a final objective lens. When the beam of electrons interacts with the atoms present on the sample surface, serval different signals are generated such as characteristic X-rays, back-scattered electron (BSE), secondary electron (SE), transmitted electrons and specimen current [230]. These signals are collected on the detector on the equipment and then processed. The BSE electrons,

which are formed from the elastic scattering of reflected electrons from the surface of the sample, are often used for SEM imaging.

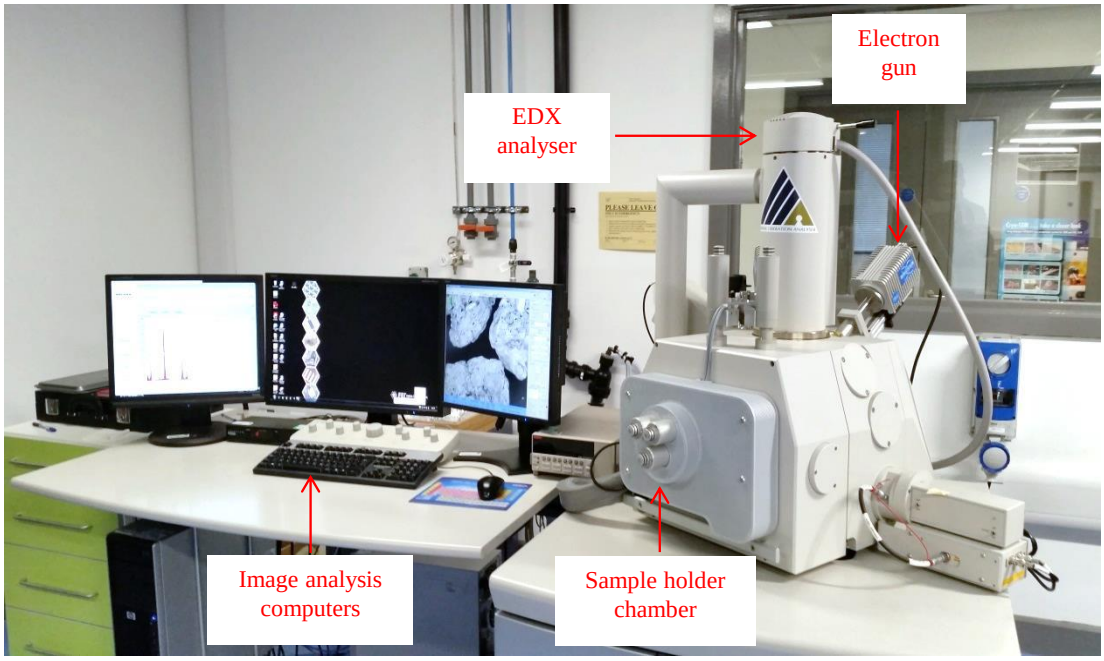


Figure 4.8: FEI Quanta 600 scanning electron microscope.

The characteristic X-ray and continuum X-rays signals are formed when the electron beam removes an inner shell electron, causing a higher energy electron to fill the shell and release energy. This causes an inelastic scattering of the reflected electrons from the surface of the sample [234]. The characterisation abilities of X-ray are due to the unique atomic structure possessed by each element, which allows the formation of distinctive peaks based on the abundance of the element in the specific sample.

Two types of SEM sample preparation techniques were used during these investigations with the first technique a small amount of material was bound on carbon sticky tabs and was then analysed under SEM to investigate the images. With the second technique, the

material was ground into fine powder (size <50 µm) using method described in section 4.6.1.1 then a pellet with the diameter of 5 mm and the thickness of 2 mm was prepared from the ground powder using a hydraulic laboratory press made by Graseby Specac (model 15711), and finally the pellet was analysed under the SEM to get detailed information about the chemical compounds present in the material.

The sample preparation technique takes about two to three hours to complete and can be used for SEM analysis at low vacuum operation. Moreover, the unground sample material provides quality SEM images. The prepared samples were mounted on the sample holder in the SEM sample holder chamber shown in Figure 4.8, which allow automated measurements of up to eighteen samples. The SEM analysis was done using the backscattered electron (BSE) type detector, accelerated voltage 20 kV operated under low vacuum mode for carbon tabs and high vacuum for ground pellets.

The interactive oxides mode method was used for quantification of materials under SEM-EDX. The spectra working distance was 14 mm and the images were captured at different magnifications of 50, 100, 150 and 300 times. The unground analysis shows the surface morphology of the analysed material sample as opposed to the ground material sample pellet analysis which shows the smooth internal structure of the sample being analysed.

4.6.4 XRD

X-ray diffraction (XRD) is a famous and quick analytical technique mainly used for phase identification, crystallographic structure and physical properties of materials.

There are two types of primary XRD analysis; X-ray powder diffraction and single-crystal XRD. The X-ray powder diffraction is usually used in material science, environmental science, geology and engineering [235]. In the present research, the powder X-ray diffractometer D500 system was used as shown in Figure 4.9.

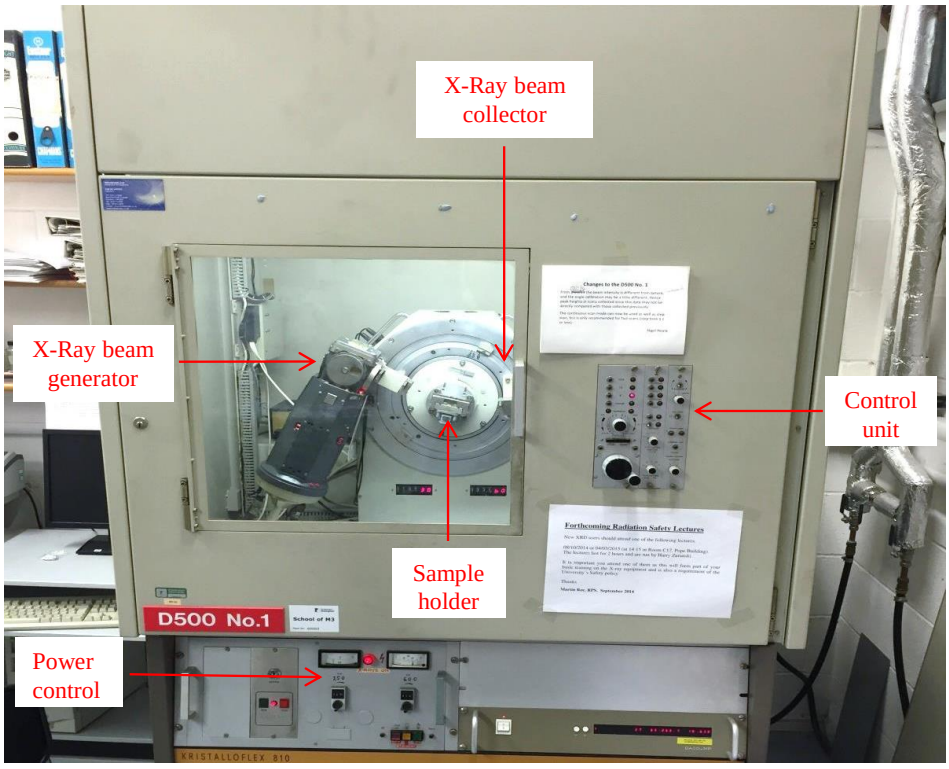


Figure 4.9: Siemens D500 X-ray powder diffraction system.

The working principle of X-ray diffraction is based on constructive interference of monochromatic X-rays and a crystalline sample. These X-rays are generated by a cathode ray tube also called x-ray generator (see Figure 4.9), filtered to produce monochromatic radiation, collimated to concentrate, and directed to the sample material [236]. The contact of the incident rays with the sample produces positive interloping and a diffracted ray when conditions satisfy Bragg's law ($n\lambda=2d \sin \theta$) [237]. These diffracted X-rays are then detected and collected where they are processed and

calculated. By scanning the material through a range of 2θ angles, all possible diffraction directions of the lattice should be attained due to the random orientation of the powdered sample material. Conversion of the diffraction peaks to d-spacings allows the identification of the minerals because each mineral has a set of unique d-spacings. Normally, this is attained by comparison of d-spacings with standard reference patterns [238].

The powdered sample for X-ray diffractometer analysis was prepared using the same method as described in section 4.6.1. The system was equipped with a sample holder for 9 samples that could perform over the night scan (see Figure 4.9). The power diffractometer was operated with parallel beam and very low intensity to estimate the phases with more than 1% presence in the material. The method used in powdered diffractometer was CuKα radiation and scanned from 10 to 80°2 θ angles with 0.05 °2. The θ angle step size and 6 s time per step. As for results evaluation and analysis, TOPAS V5 software was used. The crystallinity (i.e. the amount of crystalline phase vs total) is estimated presuming the same elemental composition of the amorphous phase (s) as the crystalline. The TOPAS V5 is a Rietveld refinement [239] software and uses principles of Hill and Howard [240] for quantities' computation.

4.6.5 XRF

XRF (X-ray fluorescence) is a non-destructive analytical technique used to determine the elemental composition of materials. The XRF spectroscopy is an outstanding technology for qualitative and quantitative analysis of material composition in recent days [241]. It works on wavelength-dispersive spectroscopic principles, XRF analysers

determine the chemical composition of a material by measuring the fluorescent X-ray emitted from a material when it is excited by a primary X-ray source. Each of the elements existing in the material produces a set of characteristic fluorescent X-rays that is unique for that precise element. The comparative ease and little cost of sample preparation, and due to the firmness and comfort of use of x-ray spectrometers make this one of the most broadly used methods for analysis of main and trace elements in rocks, minerals, and sediments [242].

The XRF analyser used in the present research is shown in Figure 4.10. The XRF characterisation was performed using powder samples prepared in the form of 10 mm diameter and 5 mm length pressed pellets. The pressed pellets were prepared by milling the material to be characterised into powder <50 μm using Ring and Puck mill as described in section 4.6.1. The milled powder sample was thoroughly mixed after which 500 mg of the sample was measured and mixed with 100 mg of inert wax binder in the proportion of 5:1 sample to wax binder ratio before been pelletized using a Graseby Specac hydraulic pellet press which is mentioned in section 4.6.2.

The made pressed pellet was placed and tightly secured in an 8 mm aperture size sample holder before being loaded into the sampling chamber of the XRF analyser as shown in Figure 4.10. The door to the sampling chamber was closed and with the use of the XRF sampling sequence digital controller, XRF analysis was initiated. The analysis requires the exactly measured weight of the pellet, type of analysis (element or elemental oxide) and the detection routine of the analysis (duration). For the case of this work, the best detection route was used which has the analysis duration of seven minutes.

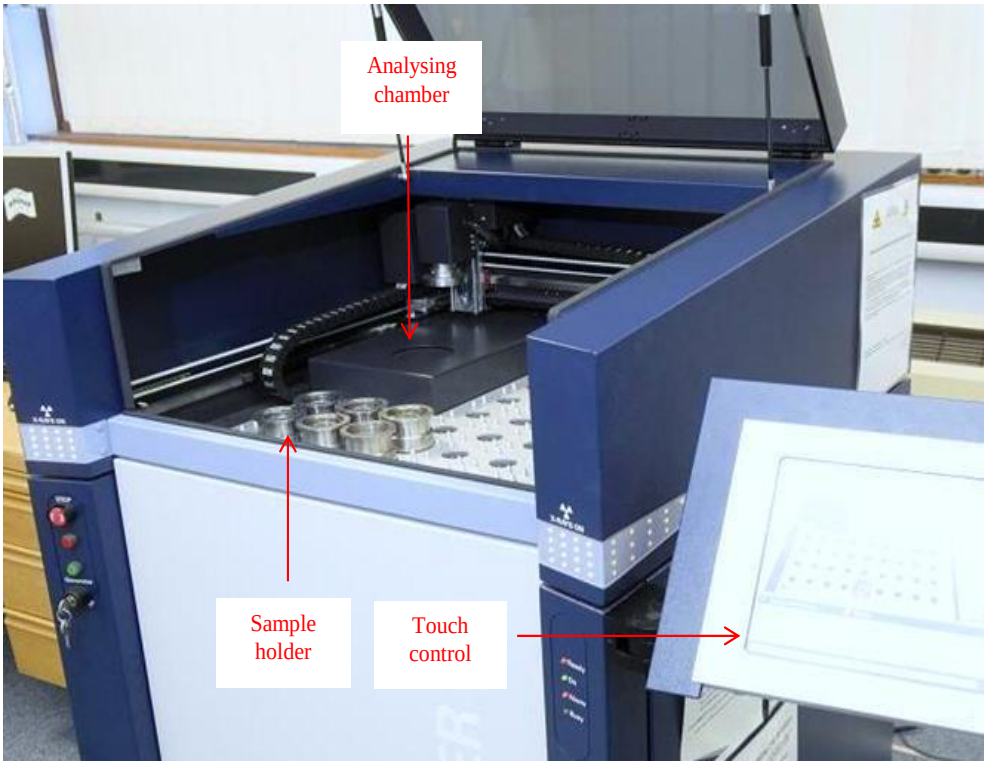


Figure 4.10: Bruker S8 Tiger high-end wavelength dispersive XRF.

Results generated from the XRF analysis were processed using the Spectra plus software version 2.0 and Quant-express software loaded on the XRF computer system [241]. The results were presented in a quantitative format with details of the element or elemental oxides identified to be present in the sample with their respective quantities and the total sum of the total detectable part of the samples.

Chapter 5

Thermal Analysis of Biomass Fuels

5.1 Introduction

Global awareness of climate change and the ever reducing availability of fossil fuels drive the rapid growth in renewable energy sources over recent years [243]. Much attention has been focused on identifying and widening the pool of viable biomass fuels by assessing their ability to replace conventional fossil fuels to provide high-energy outputs. Biomass can be utilised as a source of energy by means of different processes including biochemical or thermal-chemical. The choice of the process is determined by the characteristics of biomass; thus a significant step in the conversion process is the assessment of the biomass obtainability and its thermal, physical and chemical characteristics [244, 245]. Therefore, to use biomass fuels in a clean and extra resourceful way it is important to know their characteristics.

Moreover, biomass is a complex material that contains serval natural polymers, extractable materials, and inorganic compounds also explained in section 2.1.2 in Chapter 2. Analytical techniques can be used to characterise biomass fuels, such as high heating value (HHV), low heating value (LHV), elemental composition (Carbon, Hydrogen, and Nitrogen content) and proximate analysis parameters (Moisture, Ash, and Volatile matter content) [246].

Serval methods are commonly employed depending on the property to investigate. Thermogravimetric analysis (TGA) is the most frequently applied thermoanalytical method for the thermal decomposition studies of biomass as it permits the controlled study of global reactions that occur during various thermal or thermochemical conversion processes. In the case of biomass, TGA has also been used to identify different fractions present in the material, and it can provide accurate data on char reactivities under the active environment of interest [225]. The kinetic parameters derived from TGA characterisations are important for the design of pyrolysis reactors, gasifiers and combustors.

There are a number of studies about pyrolysis and combustion of biomass using thermogravimetric examination in the literature, but the effects of different gas mixtures, especially oxy-fuel combustion gases on the important heating parameters have rarely been investigated. Hence, a comprehensive understanding of the impact of reactant gas mixtures on biomass fuels, especially in terms of reactivity parameters, temperature ranges for devolatilisation and combustion as well as the energy of activation is required. This part of the research aims to examine the thermal

degradation, reactivities, energy of activation of different biomass fuels and their relationship with different primary fuel properties under a range of reactant gas environments and identified reaction zones of interest, in terms of their devolatilisation, gasification and combustion behaviours.

5.2 Biomass Fuels and Sample Preparation

Six different biomass fuels were used; barley straw (BS), miscanthus (MIS), waste wood (WW), wheat straw (WS), willow SRC (SRC) and domestic wood (DW). All biomasses were grown and produced in the UK and were sourced from different suppliers in the UK. The wood pellet was a commercial product "Brites" from Balcas Ltd usually used in domestic boilers. Before analysis, all fuel samples were ground to size $\leq$212 μm using a Retsch ultracentrifugal mill ZM 200. Many analytical standards require the particle size $\leq$212 μm [222, 247].

5.3 Chemical Analysis

Ultimate analysis of the biomass samples was determined using a Flash EA 1112 elemental analyser. Proximate analysis was obtained using a TA Instruments TGA Q-500 thermo-gravimetric analyser by heating the sample in a flow of N_2 at a rate of 10 ^{o}C/min to 110 ^{o}C, then holding at this temperature for 10 min to obtain the moisture content. The temperature was then ramped from 110 ^{o}C at a rate of 20 ^{o}C/min to 700 ^{o}C (also in N_2 flow) and held for 30 min to get the weight loss related with devolatilisation after this temperature was ramped at the same rate 20 ^{o}C/min to 900 ^{o}C. The air was then introduced into the furnace and kept it isothermal for 40 min to oxidise the char

completely to obtain the fixed carbon and ash contents. The high heating value (HHV) for each selected sample was obtained from by Eq. (5.1) proposed by Channiwala and Parikh [224].

$$HHV = 0.3491C+1.1783H+0.105S–0.1034O–0.0151N–0.0211A \quad (5.1)$$

The elemental and proximate analyses along with high heating values (HHV) for these samples are represented in Table 5.1 along with the results reported elsewhere. The overall analysis shows that all biomass samples have high volatiles and oxygen contents. On the other hand, their nitrogen contents are low; it is also noticed these samples have sulphur contents below the detection limit. Wheat straw (WS) contains the highest fixed carbon at 18.22%, whereas SRC has the highest amount of volatile matter at 85%. High heating values (HHV) of the samples ranging from 15.46 to 18.83 MJ/ kg. The higher carbon and hydrogen content and lower oxygen content of wood pellet (DW) result in higher calorific values as compared to the other biomass samples. It is also reported that HHVs increase as an increase in lignin contents in biomass fuels. On the other hand, biomasses with higher cellulose contents have smaller heating values because of its higher degree of oxidation. Comparisons with literature data for these biomasses show that the investigated samples have similar compositions to those reported by other researchers [248-254].

5.4 Experimental Techniques and Kinetic Analysis

The pyrolysis and combustion or gasification kinetics of all biomasses were studied under dynamic conditions in N_2, air ($21\%O_2/79\%N_2$), CO_2 and a typical oxy-fuel

oxidant (30%O_2/70%CO_2), using a non-isothermal thermogravimetric method. The non-isothermal TGA method compromises convinced benefits over the classic isothermal method. Firstly, this analysis reduces the errors caused by the thermal induction period; secondly, it allows a fast scan of the whole range of temperatures. Therefore, many scientists have employed the non-isothermal method to study pyrolysis of many solid fuels [255, 256]. The weight of each sample was limited to 15–20 mg in order to limit the potential effect of heat and mass transfer. For TGA test, the temperature was programmed to increase from ambient to 110 ^{o}C at a heating rate of 10 ^{o}C/ min and remain at this temperature for 10 min before it was allowed to be increased at 20 ^{o}C/ min to 950 ^{o}C and held for 40 min. A constant gas flow rate of 100 mL/min was used for all gas conditions.

All of the experiments were repeated two to three times to assure reproducibility. Weight loss profiles and their derivative curves (Differential Thermogravimetry–DTG) were then obtained as a function of time and temperature for the reaction conditions examined. The biomass pyrolysis and combustion are complex processes due to differences in the chemical compositions of elements within the same fuel. Three to four repeated runs for each biomass fuel were carried out to ensure appropriate repeatability and statistical validity of the results. The average difference between the repeated runs was <2% for all type of fuels. There are several approaches available for determining the kinetics of non-isothermal thermolysis, nevertheless, the method used in the present study to calculate the energy of activation was based on the Arrhenius equation. This has been found to yield acceptable results by a number of researchers [257, 258].

Table 5.1: Ultimate analysis, proximate analysis and calorific values of biomass fuel samples.

Biomass fuels	Ultimate analysis[a]					Proximate analysis[c]				LHV (MJ/kg)	HHV[e] (MJ/kg)	References
	C (%)	H (%)	N (%)	O[b] (%)	S (%)	M[d] (%)	VM (%)	FC (%)	Ash (%)			
Barley straw (BS)	40.87	5.78	0.55	52.15	0.65	8.95	78.15	14.70	7.15	-	15.46	This study
	44.38	5.64	0.78	39.25	0.08	-	70.34	19.79	9.87	16.42	17.65	[248]
	45.00	6.00	0.80	-	0.19	-	-	-	7.20	16.50	-	[259]
	-	-	-	-	-	9.80	77.90	16.0	6.10	-	17.37	[253]
	45.47	5.61	0.39	44.57	0.12	-	81.48	14.30	4.30	17.760	-	[260]
Miscanthus (MIS)	42.87	6.74	0.38	49.82	0.19	3.34	82.85	15.37	1.80	-	19.10	This study
	43.70	5.70	1.10	44.80	0.20	10.0	78.8	9.50	2.70	16.70	-	[249]
	-	-	-	-	-	7.53	79.0	11.4	9.60	-	18.10	[253]
	46.95	5.85	0.92	46.28	-	4.55	75.62	19.92	4.46	17.81	19.06	[252]
Waste wood (WW)	45.78	6.05	0.34	47.75	0.08	5.80	84.48	14.06	1.46	-	18.12	This study
	46.16	5.77	0.80	37.87	-	7.38	72.98	17.64	-	-	-	[250]
Wheat straw (WS)	43.80	6.78	0.55	48.29	0.58	5.22	76.31	17.54	9.50	-	18.21	This study
	46.93	5.71	0.63	48.73	-	4.56	79.92	15.18	4.89	16.00	17.25	[252]
	42.95	5.35	0.00	46.99	-	-	82.12	10.98	6.90	16.80	17.98	[224]
	43.56	6.15	0.71	39.37	0.12	7.20	67.69	15.53	9.58		-	[261]
	45.96	5.92	0.34	44.78	0.28	-	79.85	17.06	3.09	-	-	[260]
	40.78	5.84	0.18	52.92		-	-	-	-	-	16.24	[251]
Willow SRC (SRC)	45.18	5.99	0.32	48.34	0.17	5.97	85.00	13.24	1.77	-	17.77	This study
	48.48	5.74	1.87	43.91	-	5.71	81.19	15.85	2.96	17.81	19.06	[252]
Domestic wood (DW)	47.18	6.84	0.17	45.64	0.17	3.54	85.11	14.19	0.70	-	19.81	This study
	49.80	6.30	0.40	43.50	0.01	7.14	-	-	0.65	17.40	-	[254]
	-	-	-	-	-	7.70	82.0	17.10	1.30		18.22	[253]

M: moisture, VM: volatile matter, FC: fixed carbon, LHV: low heating value, HHV: high heating value.

a. On dry basis except as denoted in the table.
b. Calculated by difference.
c. On dry basis except moisture which is as on received basis.
d. As received basis.
e. Calculated based on Channiwala and Parikh (2002).

The kinetics of decomposition reaction expression has been represented as [257];

$$\frac{dx}{dt} = kf(x) \tag{5.2}$$

where k is the rate constant, x is the conversion rate in time t, and $f(x) = (1-x)^n$, n is the order of reaction. According to the Arrhenius correlation, the rate constant is described as;

$$k = A \exp\left(-\frac{E_a}{RT}\right) \tag{5.3}$$

where A is the pre-exponential factor, E_a is the activation energy, R the universal gas constant and T the reaction temperature. Thus, combining Eq. (5.2) and Eq. (5.3) gives:

$$\frac{dx}{dt} = A \exp\left(-\frac{E_a}{RT}\right)(1-x)^n \tag{5.4}$$

Incorporating the non-isothermal TGA heating rate, β=dT/dt in Eq. (5.4) gives:

$$\frac{dx}{dt} = \left(\frac{A}{\beta}\right) \exp\left(-\frac{E_a}{RT}\right)(1-x)^n \tag{5.5}$$

Taking natural logarithms of both sides of Eq. (5.5) yields:

$$\ln\left[\left(\frac{dx}{dT}\right)(1-x)^n\right] = \ln\left[\frac{A}{\beta}\right] - \frac{E_a}{RT} \tag{5.6}$$

According to Eq. (5.6), a plot of ln $[(dx/dT)\ (1-x)]^n$ versus 1/T should yield a straight line with a slope of $(-E_a/R)$ for different values of n resulting in a regression coefficient near to unity. Eq. (5.6) was used to obtain kinetic parameters for each experiment.

TGA and DTG profiles give information about the thermal stability and overall kinetic progress of thermal decomposition of the biomass fuels. TGA and DTG profiles from the experiments were also used to determine other combustion characteristics, such as average rate of weight loss (R_{avg}), average temperature (T_{avg}), peak temperature (T_{peak}) and the maximum rate of weight loss (R_{max}) for all studied biomasses. T_{peak} corresponds to the point at which the reaction is proceeding at its maximum rate, and R_{max} is the associated weight loss rate at T_{peak}. The selection of viable temperature ranges for analysing devolatilisation and combustion reactions can have a substantial impact on the calculated values, and there is no general consensus on which approach is the best [226]. In this research, a method originally devised by Ghetti et al. [227] represented in section 4.3 in Chapter 4 has been employed to calculate the reactivities of the biomass samples.

5.5 Results and Discussion

5.5.1 Location of Biomass Fuels in Van Krevelen Diagram

The biomass samples are compared with other solid hydrocarbons in Figure 5.1 using the Van Krevelen diagram, a cross plot diagram of H: C as a function of O: C. Devised by Dirk Willem Van Krevelen, the diagram permits a better understanding of the evolution path of organic matter/ rank and is indicative of different regions associated

with solid fuels. As can be seen from Figure 5.1, the biomass samples studied are localised in the region typically associated with biomass, however, they were seen to be relatively uniform in their H/C ratio, but varying bout 30% in their O/C ratios from DW at 0.99, to BS at 1.29. This likely evidences the higher proportion of mineral oxides present in straw and grass species (Family: Poacae), known to be effective gasification catalysts [262], but with a propensity to melt and sinter in the high temperatures of reactors, causing fused deposits [263].

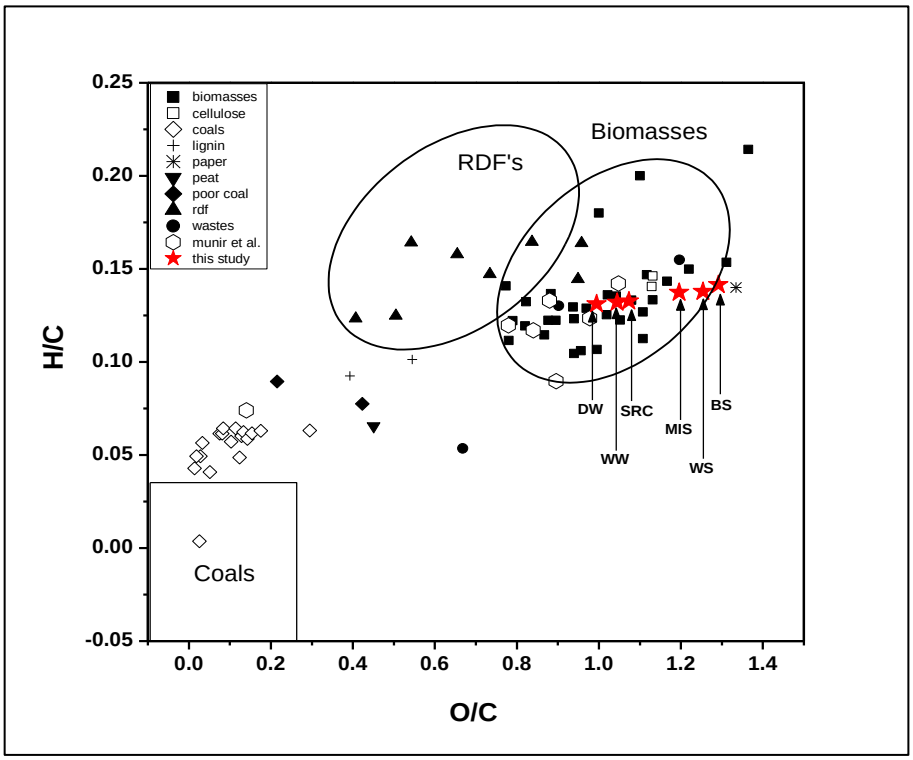


Figure 5.1: Van Krevelen plot for studied biomass fuels; BS, MIS, WW, WS, SRC and DW in comparison with other fuels including biomass (cotton stalk, shea meal, sugar cane bagasse) from Munir et al. [24], RDF = refuse derived fuels.

In general, various types of coal fuels are limited in the range of $0 \leq H/C \leq 0.1$ and $0 \leq O/C \leq 0.3$ whereas biomass fuels having a higher proportion of O/H are categorised in the limits of $0.7 \leq O/C \leq 1.3$ and $0.075 \leq H/C \leq 0.25$.

5.5.2 Thermal Degradation under N_2 Atmosphere

The TGA plots in Figure 5.2a show the weight loss profiles for different biomass fuels. It is well recognised that cellulose, hemicellulose, and lignin are the major natural polymeric components of the biomasses. But different biomasses contain varying types and proportions of cellulose, hemicellulose, lignin and a few other extractives. The thermal decomposition of the main organic components of the biomass generates oxygenated by-products. As the temperature gradually increases, these by-products reach their spontaneous ignition and the released heat contributes to the decomposition of the remaining organic matter [264].

Such behaviour can also be observed through DTG plots in Figure 5.3a by means of a continuous mass loss due to the slight devolatilisation up to the end of the heating programming. The weight loss of 7.0, 6.4, 4.8, 6.0, 5.3 and 5.1% occurred between 25 and 110 °C for BS, MIS, WW, WS, SRC and DW respectively. This initial weight loss (< 110°C) is related with moisture evolution. Devitalisation of BS, MIS, WW, WS, SRC and DW is initiated at different corresponding temperatures of 190, 205, 210, 195, 215 and 220 °C respectively. This variation in devolatilisation temperatures could be related to different elemental and chemical compositions of these biomasses [53].

Pyrolysis of biomass under inert atmosphere can be divided into three stages; first moisture evolution, then devolatilisation and finally continuous slight devolatilisation [258]. The DTG plots in Figure 5.3a show the apparent two-stage release of the first hemicellulose and then cellulose. It is difficult to clearly distinguish between hemicellulose and cellulose devolatilisation regions for WW unlike other fuels (i.e.

SRC, BS, MIS), which is likely due to the inhomogeneous nature of this mixed original sample. At the end of the major peak the slow degradation over wider temperature range continues to produce pyrolysis residue reaching to a constant ratio, sometimes referred as long tailing section [258, 264].

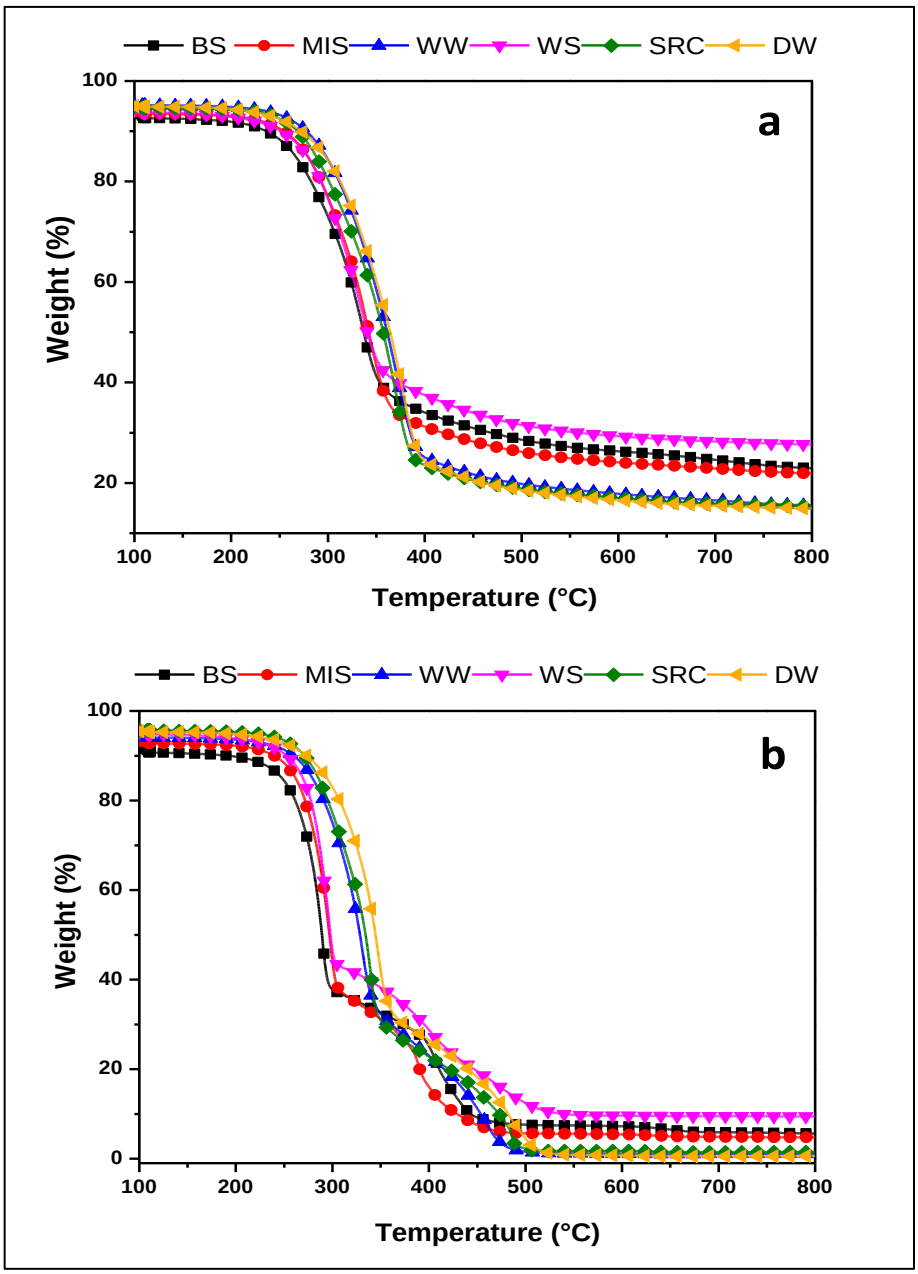


Figure 5.2: TGA profiles of the different biomass fuels under; (a) N_2, (b) air.

The maximum rate of weight loss was 16.0, 17.4, 17.7, 14.9, 19.3 and 19.0% for BS, MIS, WW, WS, SRC, and DW respectively. These rate of weight loss were found to be higher for the fuels with high volatile and lower ash contents [264].

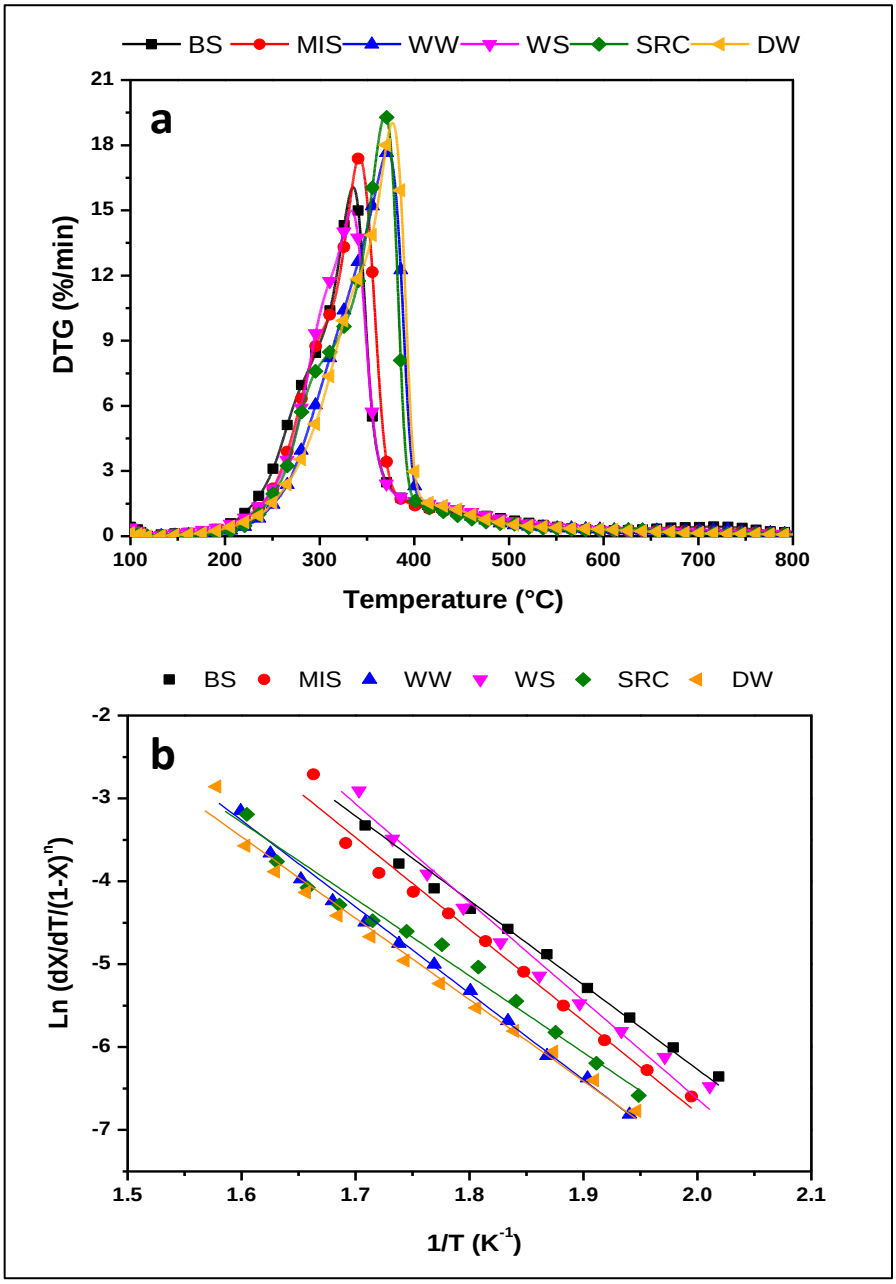


Figure 5.3: (a) DTG profiles of the biomass fuels under N_2, (b) Arrhenius plots for devolatilisation zone.

The thermal degradation results under N_2 are presented in Table 5.3. Biomass species having high cellulose contents are recommendable for bio-thermal conversion processes, whereas those with high lignin content are particularly suitable for combustion and/or gasification utilisations. The devolatilisation rate of the lignocellulosic biomass under nitrogen atmosphere also depends on its major components (cellulose, hemicellulose and lignin), higher the lignin content, the slower the biomass devolatilisation [265]. The temperature range of lignin devolatilisation cannot be discerned from, which often has a broad peak temperature overlapping that of cellulose decomposition [266]. The hemicellulose and cellulose contents of some biomass fuels are calculated from DTG curves using a method shown in Figure 5.4 and presented in Table 5.2, along with those reported elsewhere.

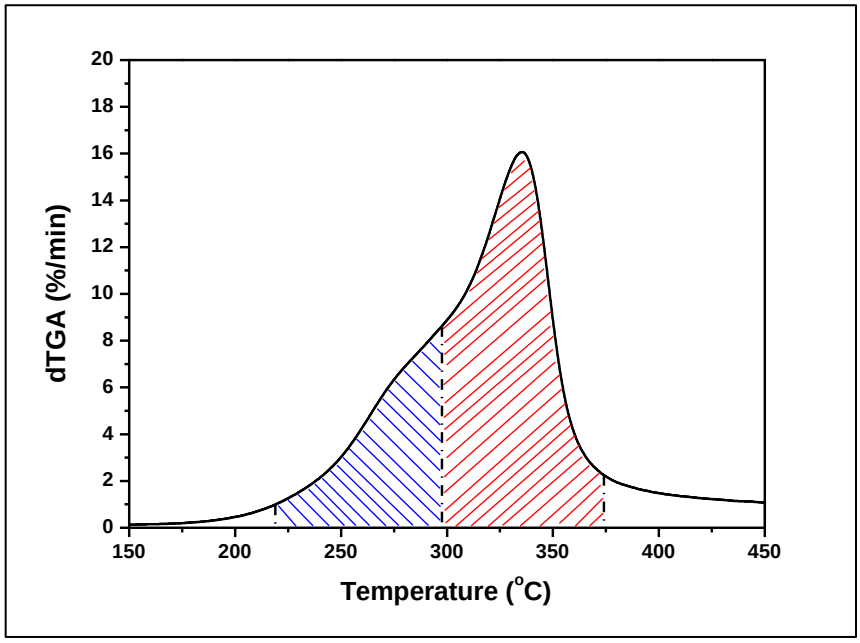


Figure 5.4: Typical DTG profile for biomass, weight loss under the first shoulder (shaded blue) in the first DTG peak corresponds to hemicellulose contents and the weight loss under the main DTG peak (shaded red) corresponds to cellulose contents.

The apparent shoulder in the DTG peak corresponds to hemicellulose whereas the main peak corresponds to the cellulose contents in biomass fuels. Due to not very clear shoulder in the peaks, an error of ± 11% can be attributed as compared with other published results.

Table 5.2: Compositions of the biomass fuels.

Fuels (from this study unless stated)	**Hemicellulose (wt. %)**	**Cellulose (wt. %)**	**Lignin (wt. %)**
BS*	20.00	40.00	-
MIS*	21.00	40.00	-
WS*	20.00	35.00	-
SRC*	12.00	60.00	-
DW*	30.00	38.00	-
Miscanthus [267]	25.70	52.13	12.50
[268]	23.90	54.00	14.94
Wheat straw [269]	28.20	39.90	16.70
[252]	24.70	38.20	23.40
Willow SRC [270]	14.10	49.30	20.00

*Anticipated wt% loss attributed to hemicellulose and cellulose calculated from DTG.

Previous studies on biomass have shown that cellulose comprises 40–50% compared to 20–40% of hemicellulose and 10–40% lignin [52]. The comparative proportions of cellulose and lignin are one of the influential factors in recognising the suitability of biomass fuels since the ratio of cellulose to lignin dictates the rates of thermal decomposition [265]. The final pyrolysis residue for BS, MIS, WW, WS, SRC and DW was 21.7, 21.2, 14.5, 26.8, 14.0 and 14.4% respectively, comprised of unburnt char and ash.

5.5.3 Thermal Degradation under Air Atmosphere

The TGA and DTG profiles obtained under air are presented in Figure 5.2b and Figure 5.5a were different from those under N_2, showing elevated reaction rates in air. Most of the biomass fuels demonstrated three stage weight losses under oxidative environments; the first stage for moisture evaluation, second for oxidative degradation and the third relates to char combustion, which is also evident from Figure 5.2 and Figure 5.5a.

Different peaks and mass loss stages are attributable to moisture evolution and devolatilisation occurred; but with devolatilisation, higher global reaction rates are apparent, evidencing the predominance of different decomposition pathways. The peaks between 215 to 370 ^{o}C are attributed to the devolatilisation zone. In the first zone, BS started to react earliest from 205 ^{o}C with a weight loss of 53%, whereas DW started lastly from 235 ^{o}C with the highest weight loss of 63% (see Figure 5.5a). The thermal degradation results in the first and second reaction zones under air are summarised in Table 5.3. The maximum rate of weight loss (R_{max}) of 39.7% at the peak temperature (T_{peak}) of 288 ^{o}C was observed for BS. The peak temperatures during devolatilisation under air were observed lower than as under N_2.

The average rate of weight loss were 10.3, 11.0, 9.4, 9.4, 10.2 and 9.3% for BS, MIS, WW, WS, SRC, and DW respectively, which are almost twice that under N_2, also supported by previous research [264]. Higher decomposition rates within a narrow temperature range were also observed in this region which is associated with cellulose chemical decomposition [265]. After devolatilisation, char combustion begins but there is an apparent overlapping between these two zones, over a temperature range of 80, 45,

38, 20, 48 and 40 ^{o}C for BS, MIS, WW, WS, SRC, and DW respectively. It had previously been reported [271] that char oxidation could be started during devolatilisation if oxygen reaches the particle's surface.

The mass loss that was seen to occur over a broad range, relatively higher temperature region marked as region 'A' on Figure 5.5a between 385 to 540 ^{o}C showed high variation between samples. This is believed to correspond to the char combustion zone. The anticipated char contents of 22.5, 23.5, 30.0, 19.5 and 24% attributed to temperature regions 360–460 ^{o}C, 390–510 ^{o}C, 340–570 ^{o}C, 410–510 ^{o}C and 410–540 ^{o}C for MIS, WW, WS, SRC and DW respectively. The rate of reaction for all type of biomasses during combustion becomes rapid than that of pyrolysis and devolatilisation. The maximum rates of weight loss during char combustion were found to be 9.47% for SRC.

The SRC rate of weight loss during combustion is the highest among all others fuels with the highest cellulose contents about 60%. It could be concluded from the results that the biomass cellulose contents may enhance the ignition characteristics and decomposition process of lignin subsequently cellulose compounds have a branching chain of polysaccharides rather than aromatic ring, which are easily volatilised. The residue left at the end of the combustion actually comprises of ash. A wide variation in the ash content can be observed within non-woody biomass as and among other types. Irrigation and fertiliser procedure during the growth of herbaceous biomasses leads to high contents of inorganic species compared to that of wood.

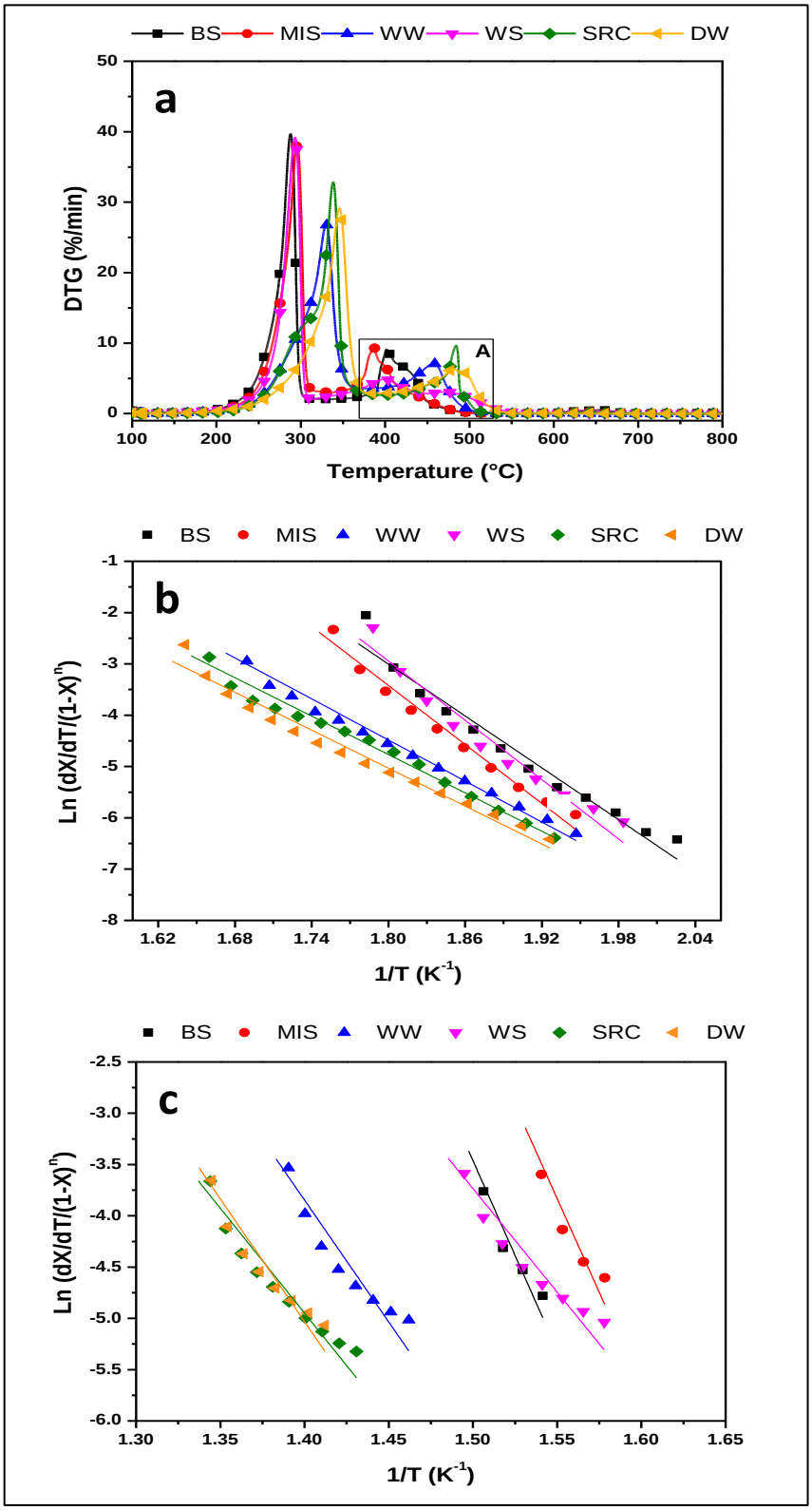


Figure 5.5: (a) DTG profiles of the biomass fuels under air, (b) Arrhenius plots for devolatilisation zone and (c) Arrhenius plots for char combustion zone.

The highest ash content of 9.4% is found with WS. Specifically, the alkali contents are much higher in the non-woody biomass (for example herbaceous materials) compared to the woody biomass. In general Si and K are the two main ash forming species in most of the of the agricultural biomasses [59]. Furthermore, combustion properties of the fuel, as well as the design and operation of combustion systems are affected with these mix inorganic species within each material.

5.5.4 Thermal Degradation under CO_2 Atmosphere

The thermal behaviour of biomass fuels under CO_2 is shown in Figure 5.6a and Figure 5.7. It is evident from Figure 5.2a that when N_2 is used, the end point of devolatilisation cannot be found after the residence time of the second isotherm condition. On the other hand, the use of CO_2 (see Figure 5.6a) highly improves the trend towards reaching a mass loss plateau in the isothermal step and enables the distinction and quantification of volatile material and fixed carbon contents in biomass samples. According to Borrego and Alvarez [272], the use of CO_2 as a carrier gas provides higher resistance to the devolatilisation of bulk components of biomass in relation to N_2.

This resistance may be due to the involvement of CO_2 in the cross-linking reaction on the char surface, which reduces the deformation and clumps its carbonaceous structure. The onset of devolatilisation was seen to occur at higher temperatures in the presence of CO_2 compared to N_2 as shown in Figure 5.7a. The average temperatures for devolatilisation region being higher under CO_2 flow than N_2 (see Table 5.4). The difference in the values of specific heat capacity and thermal conductivity for CO_2 and N_2 influences the degradation/combustion characteristics of the fuels. It has been found

that combustion temperatures are substantially affected by replacement of N_2 with CO_2 with/without the presence of oxygen [137, 273].

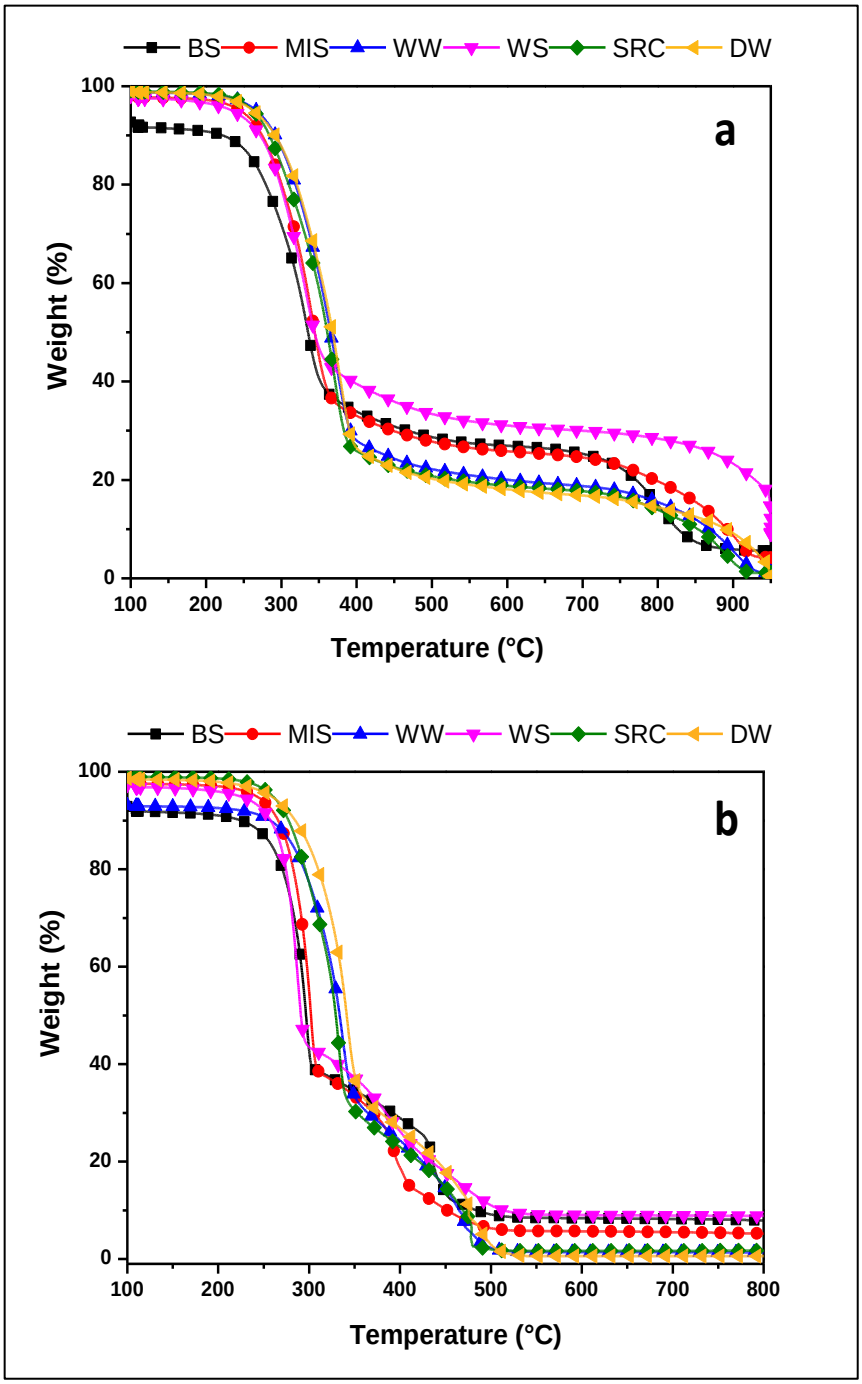


Figure 5.6: TGA profiles of the different biomass fuels under; (a) CO_2, (b) oxy-fuel.

Thus, replacing N_2 with CO_2 would adversely affect the energy input required for biomass combustion applications. The third peak is shown in Figure 5.7a, after devolatilisation at higher temperatures (>700 ^oC signifies the gasification of pyrolysis char via the Bouduard reaction [274]. As illustrated in Eq. (5.7), at lower temperatures (< 700 ^oC), less stable compounds are released and char is formed by the devolatilisation process shown in Eq. (5.7). The char in contact with CO_2 at higher temperatures (> 700 ^oC) and with enough residence time may undergo a Boudouard reaction, which leads to CO formation (reaction part 2) [275].

$$\text{Biomass} \xrightarrow{< 700\ ^oC} \text{Char + Gases} \xrightarrow{> 700\ ^oC} \underbrace{C\ (char) + CO_2 \longrightarrow 2CO}_{\textbf{Boudouard reaction}} + \text{Ash} \qquad (5.7)$$

Higher peak temperatures for char gasification under CO_2 reaction atmosphere are indicative of possible delayed combustion as compared to combustion in air.

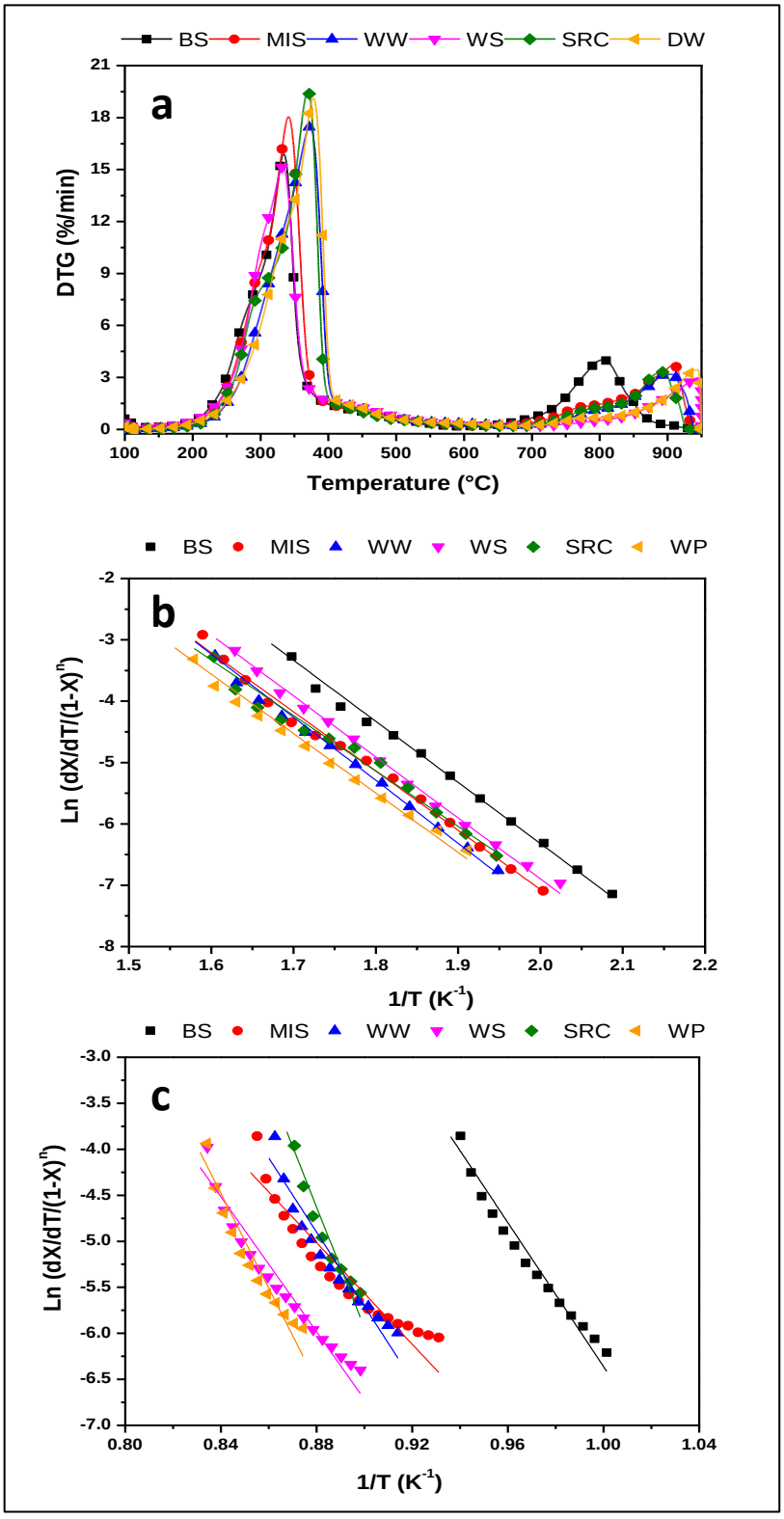


Figure 5.7: (a) DTG profiles of the biomass fuels under CO_2, (b) Arrhenius plots for devolatilisation zone and (c) Arrhenius plots for Char-CO_2 reaction zone.

Table 5.3: Thermogravimetric parameters of biomass fuels under N_2 and air environment.

Biomass fuels (from this study unless stated)	**Under N_2**					**Under Air (21%O_2/79%N_2)**									
	Devolatilisation zone					**Devolatilisation zone**					**Char combustion zone**				
	Temp Range (^oC)	Avg. rate of weight loss R_{avg} (wt% min^{-1})	Avg. Temp T_{avg} (^oC)	Peak Temp T_{peak} (^oC)	Max. rate of weight loss R_{max} (wt% min^{-1})	Temp Range (^oC)	Avg. rate of weight loss R_{avg} (wt% min^{-1})	Avg. Temp T_{avg} (^oC)	Peak Temp T_{peak} (^oC)	Max. rate of weight loss R_{max} (wt% min^{-1})	Temp Range (^oC)	Avg. rate of weight loss R_{avg} (wt% min^{-1})	Avg. Temp T_{avg} (^oC)	Peak Temp T_{peak} (^oC)	Max. rate of weight loss R_{max} (wt% min^{-1})
BS	190–420	5.17	305	335	16.06	205–305	10.32	256	288	39.72	385–465	5.01	425	401	9.14
MIS	205–435	5.56	320	341	17.40	215–315	10.96	266	295	38.18	360–460	4.53	410	387	9.44
WW	210–440	6.30	325	371	17.66	222–352	9.40	288	330	26.82	390–510	3.91	450	456	7.10
WS	195–445	4.70	320	333	14.96	210–320	9.37	266	293	39.22	340–570	2.60	455	403	4.78
SRC	215–425	6.88	320	367	19.26	232–362	10.19	298	338	32.87	410–510	3.93	460	483	9.47
DW	220–460	6.15	340	376	19.00	235–370	9.31	303	346	29.17	410–540	3.71	475	477	6.15
Cotton stalk [33]	200–425	5.46	-	334	10.80	228–327	11.40	-	283	16.80	352–443	4.44	-	-	-
Sugarcane [33]	216–445	5.22	-	355	9.60	226–350	9.6	-	304	11.40	371–480	3.72	-	-	-
Bagasse [33]	214–424	5.04	-	346	10.20	247–357	8.40	-	312	15.60	373–487	3.48	-	-	-
She meal [33]	190–437	3.36	-	325	6.00	232–312	9.00	-	287	12.60	410–500	5.34	-	-	-

5.5.5 Thermal Degradation under Oxy-fuel Atmosphere

Mass loss under oxy-fuel conditions (30% O_2/70%CO_2) is represented in Figure 5.6b and Figure 5.8, the results showed little apparent variation to air combustion. In devolatilisation zone, WS starting earlier at temperature 210°C, but BS was the earliest fuel under air; while DW starting later at temperature 230 °C was similar to that under air at 235 ^{o}C. The DTG profiles in Figure 5.8a show the biomasses high decomposition rates in rather small temperature intervals. The biomasses with high cellulose contents such as BS, MIS, and SRC produce sharp DTG peak with a small amount of char residue. The differences in initial degradation temperatures in the first zone (devolatilisation) were 5 °C for BS, 18 °C for MIS, 12 °C for WW and 8 °C for SRC. The total weight losses during delvolatilisation were in the range of 52–70% for all studied biomasses; 53% for BS, 58% for MIS, 62% for WW, 52% for WS, 70% for SRC and 66% for DW.

Among all the studied fuels, the maximum rate of weight loss; lowest value 27.97% for WW and the highest value 47.41% for MIS were observed in the first reaction zone. These weight losses were slightly higher than under air condition (except BS and WW), e.g. 2.5% for MIS, 0.5% for WS, 3.5% for SRC and 3.0% for DW. This difference in the degradation temperatures and rate of weight loss is because of the difference in cellulose, hemicellulose and lignin contents of biomass fuel samples; this fact is extensively reported in the literature [276] and also presented in Table 5.2. Similar overlapping zone as under air was observed, but with higher temperature ranges.

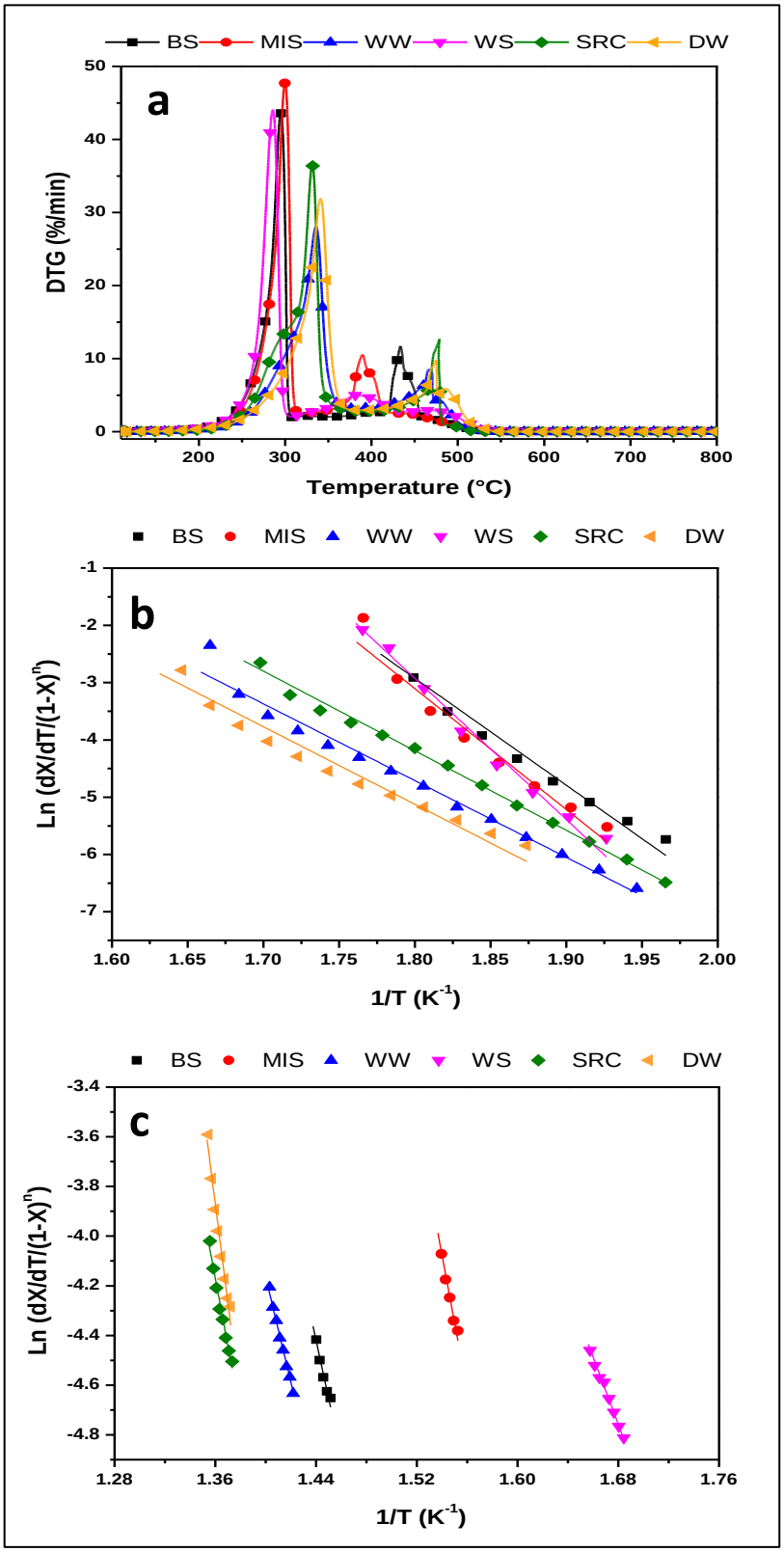


Figure 5.8: (a) DTG profiles of different biomass fuels under oxy-fuel fuel, (b) Arrhenius plots for devolatilisation zone and (c) Arrhenius plots for char combustion zone.

Table 5.4: Thermogravimetric parameters of biomass fuels under CO_2 and oxy-fuel environment.

Biomass fuels (from this study unless stated)	Under CO_2										Under Oxy (30%O_2/70%CO_2)									
	Devolatilisation zone					Char CO_2 reaction zone					Volatile combustion zone					Char combustion zone				
	Temp range (^oC)	Avg. rate of weight loss R_{avg} (wt% min^{-1})	Avg. Temp T_{avg} (^oC)	Peak Temp T_{peak} (^oC)	Max. rate of weight loss R_{max} (wt% min^{-1})	Temp range (^oC)	Avg. rate of weight loss R_{avg} (wt% min^{-1})	Avg. Temp T_{avg} (^oC)	Peak Temp T_{peak} (^oC)	Max. rate of weight loss R_{max} (wt% min^{-1})	Temp range (^oC)	Avg. rate of weight loss R_{avg} (wt% min^{-1})	Avg. Temp T_{avg} (^oC)	Peak Temp T_{peak} (^oC)	Max. rate of weight loss R_{max} (wt% min^{-1})	Temp range (^oC)	Avg. rate of weight loss R_{avg} (wt% min^{-1})	Avg. Temp T_{avg} (^oC)	Peak Temp T_{peak} (^oC)	Max. rate of weight loss R_{max} (wt% min^{-1})
BS	200–380	6.14	290	336	15.83	682–912	1.75	797	809	3.98	215–315	10.35	266	296	43.40	412–484	4.79	448	433	11.59
MIS	210–385	7.19	298	343	17.99	750–940	2.09	850	912	3.65	228–312	13.42	271	299	47.41	368–464	4.53	416	388	10.24
WW	230–410	7.84	320	370	17.33	765–935	1.88	850	909	3.14	222–362	8.79	293	335	27.97	415–515	4.00	465	465	8.37
WS	198–378	6.12	288	331	15.09	790–950	1.62	893	938	2.86	210–300	11.30	256	285	43.83	315–535	2.99	425	378	4.88
SRC	220–400	8.04	310	367	19.24	788–928	1.94	858	889	3.26	218–362	9.69	291	331	36.40	440–505	4.59	472	479	12.65
DW	215–415	7.29	315	379	19.09	845–950	1.65	913	945	3.42	230–370	9.37	301	340	31.84	435–535	4.11	485	474	9.62
Lignite [41]	-	-	-	481	3.2	-	-	-	-	-	-	-	-	317.2	19.00	-	-	-	-	-
Olive Res. [41]	-	-	-	354.9	28.3	-	-	-	-	-	-	-	-	311.2	53.20	-	-	-	413.2	-
Blend Exp.[41]	-	-	-	354.4	15.5	-	-	-	-	-	-	-	-	306.7	29.40	-	-	-	-	-

The anticipated overlapping temperature ranges were found as 95, 55, 50, 25, 80 and 65 °C for BS, MIS, WW, WS, SRC, and DW respectively. This higher degree overlapping may be attributed to higher oxygen contents in oxidising gas as compared to air. It is also supported by the literature that time of char combustion increases relative to the pyrolysis under low oxygen contents and relative time of overlapping reduces as under air [271]. The second weight loss zone is attributed with the combustion of char within the temperature range of 315–535°C.

Similarly, as in first reaction zone WS char combustion is taking place before all the other fuels at 315 °C and DW on the end at 435 °C. The differences in the temperatures of the second reaction zone (char combustion) were 97 °C for BS, 53 °C for MIS, 100 °C for WW and 125 °C for SRC. The total weight losses in the second reaction zone were in the range of 15–33% for all studied fuels; 17% for BS, 22% for MIS, 20% for WW, 33% for WS, 15% for SRC and 20% for DW. The maximum rate of weight loss 12.6% for SRC was observed in the char combustion zone. These weight loss values (except WS in zone two) were lower than under air which is in contrast with zone one, where weight loss values are slightly higher than under air. The thermal degradation results of both reaction zones; CO_2 and oxy-fuel are summarised in Table 5.4.

The comparative analysis of DTG profiles under air and oxy-fuel presented in Figure 5.5a and Figure 5.8a revealed close proximity of peak temperatures for both devolatilisation and char combustion zones. Thermal degradation analysis under air and oxy-fuel also suggests that by replacing N_2 with CO_2 as a diluent; no detrimental effect

on the thermal degradation of biomass fuels was observed provided O_2 concentration was increased from 21–30%. This has also been confirmed by larger scale studies [137, 277] that gas temperature profiles were similar to that of conventional air combustion. The studied biomasses burned at relatively reduced temperatures in oxy-fuel in comparison to with air. The residual left at the end of second reaction zone consists of ash with 6.5, 5.0, 1.0, 9.0, 2.0 and 0.5% for BS, MIS, WW, WS, SRC, and DW respectively. As previously stated, the characteristics of combustion and rate of reaction change by simply replacing N_2 with CO_2 in air. High oxygen concentrations are required to match these characteristics under oxy as compared to air environment although parity can be obtained by increasing concentration of oxygen up to 30% [137].

5.6 Reactivity and Kinetic Analysis

In all DTG profiles except N_2 the two combustion or gasification steps might be observed clearly, the peaks are different in height and position therefore from these positions the information on biomass fuels' reactivities may be obtained. Thus reactivities parameters were calculated for each peak, totalling the share of any secondary peaks or shoulders existing in the burning profile. By this way a value representing the mean reactivity (R_M) was obtained with corresponding peak temperature (T_p) for all biomass fuel samples; the results are presented in Table 5.5.

The reactivity parameters under N_2 focus on the temperature range of 190–460 ^oC, where the maximum value is associated with SRC. Under air, CO_2 and oxy-fuel there

are additional reactions from devolatilisation, char gasification and combustion. Temperature ranges from 205–370 ^{o}C and 315–570 ^{o}C are associated with volatile combustion zones and char combustion zones under air and oxy-fuel respectively. Under oxy-fuel, higher reactivity values were noticed as compared to all other reactive environments. Temperature range from 200–415 ^{o}C and 680–950 ^{o}C are attributed as devolatilisation and char-CO_2 reaction zones respectively. The biomasses such as BS, MIS, and WS with lower lignin content showed higher reactivities.

For comparative analysis based on the values of R_M the fuel samples could be ranked as SRC>MIS>DW>BS>WW>WS under N_2 and CO_2, but under CO_2 the R_M values are slightly higher than those under N_2. Similar these values are greater under oxy-fuel as compared to air and show the trend as WW>DW>SRC>WS except BS and MIS; where BS>MIS under air and MIS>BS under oxy-fuel. The R_M values under oxy-fuel were detected to be higher than those under air, a phenomenon which is also supported by Rathnam, R.K. et al. [278], and one of the reasons for this process to be valued as an alternative to conventional combustion. As would be expected, an increase in char reactivity with increasing concentration of O_2 was also observed for both O_2/N_2 and O_2/CO_2 combustion atmospheres. The kinetic parameters of all type of biomass fuels were determined from TGA profiles using a linear form of the Arrhenius equation. The activation energy (Ea), order of reaction (n) and correlation coefficient (R^2) calculated under different atmospheres of the studied biomasses.

Table 5.5: Reactivity parameters of biomass fuels under N_2, air, CO_2 and oxy-fuel environments.

Biomass fuels (from this study unless stated)	**Under N_2**		**Under Air (21%O_2/79%N_2)**			**Under CO_2**			**Under Oxy-fuel (30%O_2/70%CO_2)**		
	Peak Temp T_p (^oC)	Reactivity $R_M \times 10^3$ (wt% min^{-1} $^oC^{-1}$)	Peak Temp T_{p1} (^oC)	Peak Temp T_{p2} (^oC)	Reactivity $R_M \times 10^3$ (wt% min^{-1} $^oC^{-1}$)	Peak Temp T_{p1} (^oC)	Peak Temp T_{p2} (^oC)	Reactivity $R_M \times 10^3$ (wt% min^{-1} $^oC^{-1}$)	Peak Temp T_{p1} (^oC)	Peak Temp T_{p2} (^oC)	Reactivity $R_M \times 10^3$ (wt% min^{-1} $^oC^{-1}$)
BS	335	0.479	288	401	1.608	336	809	0.521	296	433	1.736
MIS	341	0.510	295	387	1.537	343	912	0.562	299	388	1.849
WW	371	0.476	330	456	0.969	370	909	0.503	335	465	1.015
WS	333	0.450	293	403	1.457	331	938	0.487	285	378	1.668
SRC	367	0.525	338	483	1.168	367	889	0.565	331	479	1.364
DW	376	0.505	346	477	0.972	379	945	0.540	340	474	1.138
Cotton stalk [33]	334	0.54	285	475	1.31	-	-	-	-	-	-
Sugarcane	355	0.45	306	378	0.94	-	-	-	-	-	-
Bagasse [33]	346	0.49	314	461	1.14	-	-	-	-	-	-
She meal [33]	325	0.31	279	442	1.30	-	-	-	-	-	-

The reaction kinetics were modelled at n = 0.5, n =1 and n =2 and it was found that values of Ea increased by as much as twofold between n = 0.5 and n = 2. The best line of fit for the apparent Ea values has been reported for 0.5 order of reaction and is presented in Table 5.6.

There is no consensus in the literature as to reaction order, with some studies supporting these results [33] but others affirming that pyrolysis is best described as a global first order reaction [226]. For comparison of the rate constants, Arrhenius plots of all studied biomasses are plotted in Figure 5.3, Figure 5.5, Figure 5.7 and Figure 5.8. In the devolatilisation zone, there were no substantial changes in the rate constants of the samples. In the initial stages of thermal degradation, the WS had a marginally higher rate constant than those of the other biomasses. The BS retained a high rate constant, whereas the DW retained a low rate constant until the end of the first zone. The rate constant of the BS reached to its maximum value at the end of the first zone under all reaction environments.

The Arrhenius plots slopes also give some indications of the levels of the activation energies of these biomasses. The highest slope corresponds to the WS which had the highest Ea 96.98 kJ/mole (under N_2), 160.20 kJ/mole (under air) and 204.87 kJ/mole (under oxy-fuel), whereas the lowest slopes belong to the SRC and DW, both of which have an activation energy of 76.95 kJ/mole (under N_2), 75.20 kJ/mole (under CO_2) and 102.45 kJ/mole (under air) respectively. The apparent Ea values in devolatilisation zone under N_2 were 98.68> 92.11> 86.72> 84.69> 81.67> 76.95 for WS>MIS>WW>BS>DW>SRC respectively.

Table 5.6: Kinetic parameters of biomass fuels under N_2, air, CO_2 and oxy-fuel environments.

Biomass fuels (from this study unless stated)	Under N_2		Under Air (21%O_2/79%N_2)				Under CO_2				Under Oxy-fuel (30%O_2/70%CO_2)			
	Devolatilisation zone n=0.5		Devolatilisation zone n=0.5		Char combustion zone n=0.5		Devolatilisation zone n=0.5		Char CO_2 reaction zone n=0.5		Devolatilisation zone n=0.5		Char combustion zone n=0.5	
	Ea kJmole^{-1}	R^2	Ea kJmole^{-1}	R^2	Ea kJmole^{-1}	R^2	Ea kJmole^{-1}	R^2	Ea kJmole^{-1}	R^2	Ea kJmole^{-1}	R^2	Ea kJmole^{-1}	R^2
BS	84.69	0.96	140.07	0.95	380.16	0.92	82.82	0.98	325.10	0.92	155.18	0.95	194.48	0.93
MIS	92.11	0.97	159.33	0.96	303.78	0.85	80.30	0.99	229.42	0.85	175.73	0.96	226.80	0.99
WW	86.72	0.97	110.88	0.96	197.58	0.83	85.46	0.97	334.71	0.87	111.40	0.97	339.73	0.83
WS	98.68	0.96	160.20	0.94	167.79	0.85	82.65	0.99	305.00	0.91	204.87	0.99	203.82	0.83
SRC	76.95	0.95	103.63	0.96	170.05	0.85	75.20	0.94	543.99	0.87	115.51	0.98	333.01	0.93
DW	81.67	0.97	102.45	0.95	198.85	0.83	80.57	0.96	428.22	0.88	112.52	0.92	417.21	0.94
Cotton stalk [264]	77.00	0.980	113.00	0.99	-	-	-	-	-	-	-	-	-	-
Sugarcane	58.00	0.980	75.00	0.99	-	-	-	-	-	-	-	-	-	-
Bagasse [264]	71.00	0.975	116.00	0.99	-	-	-	-	-	-	-	-	-	-
She meal [264]	67.00	0.810	108.00	0.83	-	-	-	-	-	-	-	-	-	-

The Ea under CO_2 was observed in the order of WW>BS>WS DW>MIS>SRC and SRC>DW>WW>BS>WS>MIS in devolatilisation zone and char-CO_2 reaction zone respectively. In the char combustion or gasification zone, considerably higher rate constants were detected for the BS under air, SRC under CO_2 and DW under oxy-fuel as related to the others. Even though the rate constant of the MIS under air was higher than that of the BS at the start of the second zone, they had closer rate constants as the end of that zone was approached. Under air BS also had higher slope second zone due to its considerably high Ea (380.16 kJ/mol) as compared to WS (167.79 kJ/mol). Similarly, SRC and DW had the highest slopes under CO_2 (543.99 kJ/mol) and oxy-fuel (417.21 kJ/mol) with the highest Ea.

Among the other biomasses, WS had somewhat higher rate constants at the initial stages of the second reaction zone, which become even less significant towards the end of this zone. The apparent activation energies values 160.20> 159.33> 140.07> 110.88> 103.63> 102.45 for WS>MIS>BS>WW>SRC>DW respectively were observed under air in devolatilisation zone. The calculated apparent activation energy values under oxy-fuel were as 204.87> 175.73> 155.18> 115.51> 112.52> 111.40 for WS> MIS> BS> SRC> DW> WW in devolatilisation zone. It has been reported in the literature [260] that the effect of lignin on biomass degradation strongly depends on the temperature.

The rate of degradation different only a minute with lignin at temperatures below 330 °C. However, above 330 °C could result in a significant increase in the degradation rate and the Ea with declining lignin contents. The reactions above 330 to 350 °C are typically controlled by the decomposition of lignin, which is the case in the char

combustion or gasification reaction zone. Hence, the significantly high rate constants and Ea of BS and SRC are most probably due to their low lignin contents as compared to the other biomasses. With an increase in the concentration of oxygen, the apparent energy barriers decrease resulting in lower values of Ea for both volatile and char combustion zones. On the other hand, in the present case, after replacing N_2 with CO_2 under oxy-fuel the apparent barrier towards the volatile and char combustion reaction zone increases resulting in comparatively higher values of Ea. This could be to some extent due to physical properties of CO_2 in oxy-fuel. The rest of the apparent Ea values found to be nearly synchronised with existing literature [264].

5.7 Summary

The thermal behaviours of six different biomass fuels including barley straw, miscanthus, waste wood, wheat straw, willow SRC and wood pellet were examined in order to evaluate their practicality for energy production, using non-isothermal thermogravimetric analyses (TGA) under N_2, air (21% O_2/79% N_2), CO_2 and selected oxy-fuel (30% O_2/70% CO_2) atmospheres. The rate of thermal decomposition for any type of the biomass in an inert atmosphere was slower than in an oxidising atmosphere.

The results under N_2 (190–460^oC) and CO_2 (198–415^oC) in devolatilisation zones show almost identical weight loss (R), reactivity (R_M) and activation energy (Ea) profiles. However, when devolatilisation occurred in CO_2 conditions at temperatures >700 ^oC, an additional weight loss was observed for all biomass fuels, being indicative of the contribution of CO_2-char gasification reactions. Air and oxy-fuel results show almost

similar profiles for R, R_M and Ea. In oxy-fuel atmospheres, by replacing N_2 with CO_2 a slight rise in the maximum rate of weight loss (R_{Max}) was observed in both reaction zones for all type of the studied fuels. Significantly high rate constants and activation energies were observed for the biomasses which are most likely with low lignin contents (i.e. BS, MIS, WS) as compared to the other fuels.

In terms of reactivity, it appears to be no benefit from running the process in an oxy-fuel environment compared to air, with the similar average rate of weight loss (R_{avg}), average temperature (T_{avg}) and peak (T_p) temperatures observed. Rates of char combustion were also found to be unaffected by changes in oxygen concentration at varying temperatures. Thermal degradation analysis under air and oxy-fuel also suggests that by replacing N_2 with CO_2 as the diluent; no detrimental effect on thermal degradation of biomass fuels was observed provided with the oxygen concentration was increased from 21 to 30%. Reactivity analyses were undertaken in the temperature region $190 \leq °C \leq 460$ under N_2, $205 \leq °C \leq 370$ volatile combustion zones and $315 \leq °C \leq 570$ char reaction zones under air and oxy-fuel respectively, temperature region $200 \leq °C \leq 415$ and $680 \leq °C \leq 950$ devolatilisation and char-CO_2 reaction zones respectively under CO_2. Reactivity (R_M) ranking was found to be SRC>MIS>DW>BS>WW>WS under N_2 and CO_2. Similarly, R_M ranking was found to be BS>MIS>WS>SRC>DW>WW under air and oxy-fuel except for MIS>BS in oxy-fuel case.

Between the different reactant gases, R_M was lowest overall under N_2, and highest under oxy conditions, supporting previous literature. Kinetic analyses were undertaken in the

temperature region $222 \leq °C \leq 365$ under N_2, $220 \leq °C \leq 340$ volatile combustion zones and $320 \leq °C \leq 475$ char reaction zones under air and oxy-fuel respectively, temperature region $205 \leq °C \leq 370$ and $725 \leq °C \leq 930$ devolatilisation and char-CO_2 reaction zones respectively under CO_2. Reaction kinetics were modelled for all conditions at order n = 0.5, n=1, and n=2. Based on linear regression analysis, the closest modelled fit occurred with a reaction order of 0.5 for all samples and conditions. Values of activation energy ranged from $98.68 \geq Ea \geq 76.95$ under N_2, $85.46 \geq Ea \geq 75.20$ for devolatilisation zone $543.99 \geq Ea \geq 229.42$ for Char-CO_2 reaction zones under CO_2, $160.20 \geq Ea \geq 102.45$ for devolatilisation zone and $380.16 \geq Ea \geq 167.79$ for char combustion zone under air and $204.87 \geq Ea \geq 111.40$ for devolatilisation zone and $417.21 \geq Ea \geq 194.48$ for char combustion zone under oxy-fuel.

Chapter 6

Unstaged and staged Air Combustion of Biomass Fuels

6.1 Introduction

The specific properties of biomass materials (e.g. low energy density, low ash melting point, varying moisture content) can pose many operational challenges to biomass combustion boilers. Fluidised bed combustion (FBC) boilers have been developed and used to burn difficult fuels such as biomass waste materials over the past decades. In FBC boiler, the fuels are burned in a turbulent bed of an inert solid bed material, therefore ensuring high heat transfer rates, excellent gas-solid mixing, and good combustion efficiency, at typical combustion temperatures of 800–900 ºC. Although the NOx emissions of FBC boilers are considerably lower than those of the pulverised fuel (PF) combustion boiler, largely due to its combustion temperature of 800–900 ºC is much lower than the typical combustion temperature of PF boilers (1300–1700 ºC),

emissions (NOx, CO and particulates etc.) are still a major issue for biomass combustion systems. Biomass combustion systems emit relatively high levels of NOx and particulates in comparison to the combustion systems of light fuel oil or natural gas. The life cycle assessment (LCA) specifies that almost 40% of the environmental effect of a modern automatic wood combustors is associated with NOx emissions [173].

Among all of the NOx control/ reduction technologies (air staging, fuel staging, selective non-catalytic reduction (SNCR), selective catalytic reduction (SCR) etc.), air staging is the most widely applied due to its low cost and ease of implementation [279-281]. When air staging is applied to a fluidised bed boiler, the combustion air is divided into the primary stream, which establishes the fluidising air supply to the bed, and the secondary stream that is injected higher up in the bed or freeboard. As all of the biomass fuel is fed to the primary combustion region (the bed), the bed is maintained at sub-stoichiometric conditions, hence limiting the oxidation of fuel-nitrogen and reducing the already formed NO by homogeneous reactions with the radical-pool or by the heterogeneous reactions with the char. In addition, the sub-stoichiometric conditions decrease the bed combustion temperature and increase the CO concentration in the bed, both of which contribute to lower NOx emissions [157, 282, 283].

Combustion is completed following the introduction of the secondary air to burn out the carbon monoxide and other unreacted combustible gases. Similar to fixed bed combustion and PF combustion, fluidised bed combustion also needs to be operated with a suitable level of overall excess air to ensure complete combustion can be achieved under both air staging and non-air staging conditions. The suitability of air

staging to control NOx emissions while firing biomass in fluidised beds has been confirmed by a number of researchers [284-288].

As a consequence of its characteristics high volatile matter content, the most part of the solid biomass fuel may be burned in the freeboard region instead of inside the bed. Thus, the strategies for NOx abatement should be adapted considering the decrease in the importance of the dense bed on the NOx chemistry. Further, the success of air staged combustion technique to control NOx emissions from fluidised bed combustion of biomass may strongly depend on, among other variables, the secondary air ratio and the location of the secondary air injection. Saikaew et al. [289] investigated NOx emissions for the co-combustion of sub-bituminous coal with four biomasses (palm shell, coconut shell, sawdust and rice husk) in a circulating fluidised bed combustor with the secondary air injected into the riser at different heights. They found that NOx emissions decreased considerably when the location of the secondary air moved upward from 1 m to 2.4 m. The decrease in NOx emissions was explained by the fact that when the secondary air feeding was near the distributor, the secondary air provided excess oxygen to promote the fuel-nitrogen oxidation in a high-temperature zone. On the other hand, when the secondary air injection was located in the upper zone (2.4 m), the influence of oxygen on the fuel nitrogen oxidation was less since the temperature in the upper region was much lower than the lower region next to the distributor.

Varol et al. [290] studied the effect of air staging on the flue gas emissions in the co-combustion of woodchips and lignite in a 30 kW_{th} CFB combustor. They observed that the position of the secondary air injection had a distinctive effect on the NO emission:

the higher the secondary air injection position, the lower the NO emission. As it can be seen above, several investigations have confirmed the importance of the location of the secondary air injection point to reduce NOx emissions from co-combustion of biomass with coal in fluidised beds. However, few have investigated the effect of air staging with different secondary air injection points on the emissions of fluidised bed combustors/ boilers firing 100% biomass fuels, particularly non-woody biomass fuels.

In order to achieve minimum NOx emissions and improve air quality recognised in EU legislation [22] and at the same time to increase the use of low quality biomass fuels such as agricultural residues for energy generation, further research is still needed so that we can fully understand the combustion behaviour of non-woody biomasses in fluidised bed combustors in terms of NOx and CO emissions and their suitability for combustion in such fluidised bed combustion systems. Most of the previous studies on the fluidised bed combustion of non-woody biomass fuels almost exclusively focused on the agglomeration phenomena, rather than the gas emissions or the effect of air staging on the gas emissions. Regarding the use of peanuts as fuel, only Duan et al. [284] conducted a series of experiments in a vortexing fluidised bed combustor under air staging conditions. However, the influence of the secondary air injection location on the gas emissions was not investigated in this work.

The main focus of this chapter is on the determination of the optimum operating conditions in terms of NOx and CO emissions for the combustion of three different non-woody biomass fuels (straw pellets, peanut shell pellets, and miscanthus pellets) in the newly designed and constructed 20 kW_{th} bubbling fluidised bed combustor (BFBC).

Two woody biomasses were also tested for comparison purposes. The effects of excess air, without staging air and with air staging air on the gas emissions and temperature profiles were thoroughly investigated. The staging air was injected at two different heights in order to study the effects of the secondary air injection location on the gas emissions.

6.2 Biomass Fuels Characteristics

Two woody biomass fuels, domestic wood and industrial wood, and three non-woody biomass fuels miscanthus, straw and peanut shell were selected for the combustion during these experiments. All fuels were used in pellet form with a diameter of 6–10 mm and length of 15–30 mm. The chemical characteristics along with the heating values of these fuels are described in Table 4.4 in Chapter 4.

6.3 Experimental Procedure and Conditions

The detailed description of the experimental setup and procedure is given in section 4.5 in Chapter 4 and full experimental setup is shown in Figure 4.7. The operating conditions for all experiments without and with air staged combustion are summarised in Table 6.1. To analyse the effect of the excess air on temperatures, flue gas emissions and combustion efficiency experiments were carried out by varying the fuel feeding rate and maintaining a constant total air flow rate at 350 L/min. The experiments without air staging (WAS) were also carried out with all type of fuels. When the fuel feeding rate was varied, the temperatures along the reactor and freeboard were varied simultaneously as the cooling water flow rate and position of the cooling probe

remained unchanged. To investigate the effect of the air staging, part of the total air flow rate 50 L/min (secondary air) was diverted to one of the two air staging injection points, while the total air flow rate was fixed at the constant value of 350 L/min.

The secondary air was injected from two different points; air staging point one 70 cm (AS1) and air staging point two 110 cm (AS2) from the distributor. For reliable results at least three runs were performed with each type of fuel under different condition studied (WAS, AS1 and AS2). It was also made sure that the results obtained under steady state conditions.

Table 6.1: Operating conditions for without and with air staging combustion.

Parameters	Values
Main heaters temperature setup (°C)	830
Air preheater temperature setup (°C)	450
Biomass feed rate (kg/h)	3– 5
Bed height (mm)	250
Average bed material diameter (mm)	0.78
Primary air flow rate (L/min)	300
Superficial gas velocity (m/s)	0.72
Feeder air flow rate (L/min)	50
Excess air (%)	10–55
Cooling water flow rate (L/min)	1–1.2

6.3.1 Combustion Efficiency Calculations

The performance of the BFBC for all types of biomass fuels at different operating conditions is measured by calculating combustion efficiency. Two different methods are applied to calculate the combustion efficiency; (1) from the emissions without

considering carbon in fly ash, (2) from the heat losses due to unburnt carbon in fly ash. In the first case the combustion efficiency due to emissions is calculated by a method suggested by Llorente and Cuadrado, (2007) [291] and Burling et. al. (2010) [292], described in Eq. (6.1).

$$\eta = \frac{\%CO_2}{\%CO_2 + \%CO} \times 100 \tag{6.1}$$

where the amounts of CO_2 and CO are volumetric basis measured through the gas analysers in the flue gas during combustion.

In the second case the combustion efficiency is calculated using heat loss method suggested by Ninduangdee and Kuprianov [293], described in Eq. (6.2) and is explained through following steps:

$$\eta = 100 - (q_{uc} + q_{ic}) \tag{6.2}$$

The heat loss due to unburned carbon (%LHV) was estimated using the fuel LHV (kJ/kg), the fuel ash content A (wt%) and the content of unburned carbon in particulate matter, C_{PM} (wt%), as:

$$q_{uc} = \frac{32{,}866}{LHV}\left(\frac{C_{PM}}{100 - C_{PM}}\right)A \tag{6.3}$$

The heat loss due to incomplete combustion (%LHV) was predicted using the concentration of CO in the flue gas at the cyclone gas exit (in vol%, on a dry gas basis and at 6% O_2) and neglecting C_xH_y and H_2 in the flue gas:

$$q_{ic} = (126.4CO)_{@6\%O2}\ V_{dg@6\%O2}\frac{(100-q_{uc})}{LHV} \tag{6.4}$$

where $V_{dg@6\%\ O2}$ is the volume of the dry flue gas (Nm^3/kg, at standard conditions), calculated according to Peng et al. [294], using the ultimate fuel analysis from Table 4.4 given in Chapter 4 and the reference excess air coefficient (α_{ref} = 1.4, corresponding to 6% O_2 in the dry flue gas), as:

$$V_{dg@6\%O2} = 0.01866(C+0.375S)+0.79V^0+0.008N+(\alpha_{ref}-1)V^0 \tag{6.5}$$

The theoretical volume of air (Nm^3/kg, at 0 °C and 1 atm) required for firing 1 kg biomass under stoichiometric conditions was determined based on the ultimate fuel analysis using Eq. (6.6):

$$V^0 = 0.0889(C+0.375S)+0.265H-0.0333O \tag{6.6}$$

where C, H and O are carbon, hydrogen and oxygen contents in the biomass fuels already given Table 4.4 in Chapter 4.

6.4 Results and Discussion

6.4.1 Effect of Unstaged Excess Air on NOx and CO Emissions

The temperature profiles at different heights of the reactor and freeboard, the differential pressure drop in the bed and the gas composition at the outlet of the reactor obtained in a typical experiment with miscanthus pellets fuel are represented in Figure 6.1. The results from other tested biomass fuels are plotted in Appendix D. It shows the effect of the excess air on the temperature profiles, the pressure drop across the bed and the gas composition at the outlet of the reactor burning miscanthus pellets under WAS conditions. As it can be seen from the figure, temperatures along the combustor and the CO_2 concentration at the outlet of the reactor decrease with the excess air level. During these experiments, the total air flow rate was maintained constant, and the stoichiometry or the excess air level was modified by changing the biomass feed rate, and therefore a higher excess air level was achieved with a lower biomass feed rate.

A lower biomass feed rate had led to a less amount of heat released and less amount of CO_2 generated in the combustor. An increase in the excess air also led to a decrease in the CO concentration at the outlet due to the better combustion efficiency achieved. An increase in the excess of air resulted in an increase in the NOx concentration at the outlet as a result of the higher oxygen concentration in the combustor a higher oxygen concentration favours the formation of NOx in the dense bed due to the enhanced combustion of the volatile matter and char and the conversion of fuel-N to NOx in an oxygen rich atmosphere.

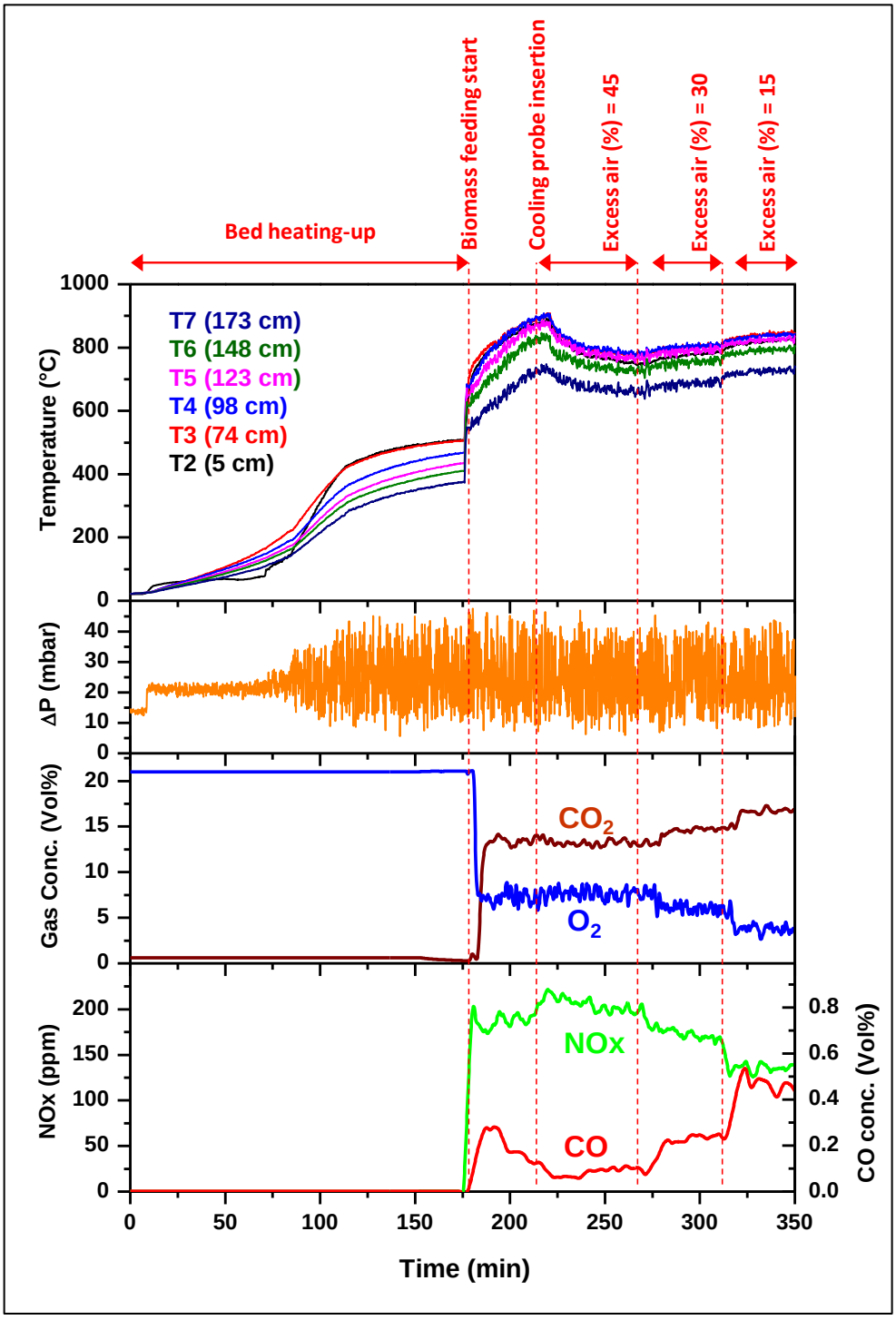


Figure 6.1: Temperature profiles at the different heights of the main reactor and freeboard, the pressure drop across the dense bed and the gas composition (CO_2, O_2, NOx and CO) at the outlet of the BFBC during a typical experiment for miscanthus pellet combustion without air staging (WAS). The NOx and CO are corrected @ 6% O_2 on dry basis.

In addition, a higher oxygen concentration enhances the combustion efficiency which results in lower char and CO concentrations throughout the combustor, reducing the effect of NO reductions by CO and char. These results agree with the findings of other researchers [295, 296]. Similar behaviour was observed in all the experiments performed with the other five type of biomass fuels tested, with and without air staging. The gas composition at the outlet of the combustor and the temperature profiles along the combustor were observed to be uniform during each formal test period under every condition studied and this was the case for all of the biomass fuels studied, with and without air staging.

6.4.2 Effect of Biomass Composition on NOx Emissions

During the combustion process of biomass fuel, NOx (NO and NO_2) can be formed through three different reaction mechanisms, i.e. the prompt-NOx, the thermal-NOx and the fuel-NOx formation mechanisms [281]. Prompt-NOx and thermal-NOx are formed from nitrogen in the air at elevated temperatures but prompt-NOx is formed with the presence of hydrocarbons. Furthermore, fuel-NOx formed from the fuel-N contained in the fuel is likely to be the main part of the overall NOx formed in the combustion process of a solid fuel such as coal and biomass. Figure 6.2a shows the effect of the excess air on the NOx emissions for the five types of fuels used in this study, without using air staging**,** whereas Figure 6.2b shows the fuel-N content of all biomass fuels also listed in Table 4.3 in Chapter 4.

The Figure 6.2 clearly shows that the higher the nitrogen content the higher the NOx emissions at the outlet of the combustor, and this agrees with the expectation that

majority of the NOx originated from the fuel nitrogen. Prompt-NOx and thermal-NOx were not expected to be of importance due to the relatively low combustion temperatures reached in BFBC (seen Figure 6.1**)**. In fact, most fluidised bed systems usually work below 900 °C and hence the formation of thermal-NOx and prompt-NOx are always expected to be of insignificance for coal-fired or biomass fired fluidised bed combustors or boilers [103, 173].

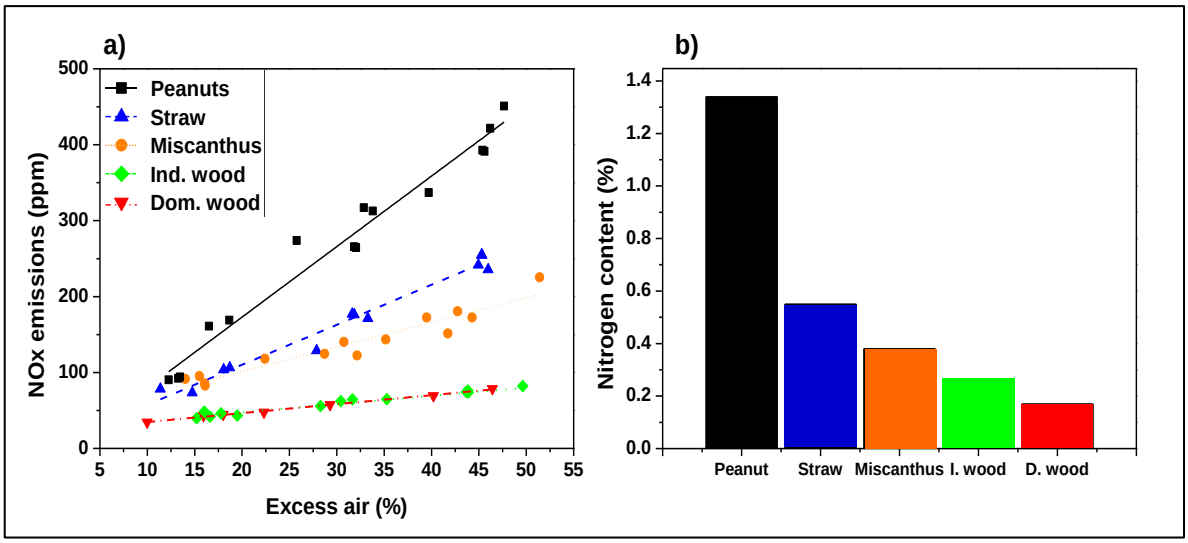


Figure 6.2: (a) Effect of excess air on NOx emissions for different biomass fuels tested without air staging. (b) The nitrogen content of the different biomass fuels. The NOx emissions are corrected @6% O_2 on dry basis.

It can be seen in Figure 6.2b peanut shell pellets have the highest fuel-N content, their combustion in the BFBC without air staging have led to considerable NOx emissions (up to 450 ppm) which are higher than the NOx emitted by the combustion of any other fuels under the same conditions. Duan et al. investigated biomass combustion in circulating fluidised bed combustor and found that during fluidised bed combustion

NOx largely determined by the nitrogen content in the fuel and regardless of the atmosphere, indicating that NO emissions are originated only from fuel-N [297].

This is also a fact that unstaged combustion of biomass in BFBC resulted in high fuel-N conversion due to high volatile matter content in biomass fuels as compared with air staging combustion. In general, agricultural lignocellulosic biomasses have higher fuel-N contents than woody biomasses [298] and hence their combustion will lead to higher NOx emissions if there is no proper NOx abatement strategy incorporated in the combustion system. The two woody biomasses (industrial and domestic wood pellets) are the two fuels with the lowest fuel-N contents and therefore their combustion in the combustor emits the least amounts of NOx, less than 20% of that emitted by the combustion of peanut pellets at high excess air levels.

6.4.3 Effect of Air Staging on Temperature Profiles

Figure 6.3 shows the temperature profiles along the main reactor/ freeboard for all type of tested biomass fuels at two different overall excess air levels (10% and 50%) during operation under WAS, AS1 and AS2 conditions. The heights of the two air staging injection points studied, AS1 and AS2 are indicated in each figure. As expected, working under WAS conditions, the maximum temperature is reached at the splash region and/or beginning of the freeboard. The temperature peak observed in the freeboard (between AS1 and AS2) above the dense bed is attributed to the characteristic high volatile matter content of biomass fuels and to its release and combustion mostly in the splash region and freeboard, instead of inside the dense bed as observed in the case of low volatile matter content coal combustion [299, 300].

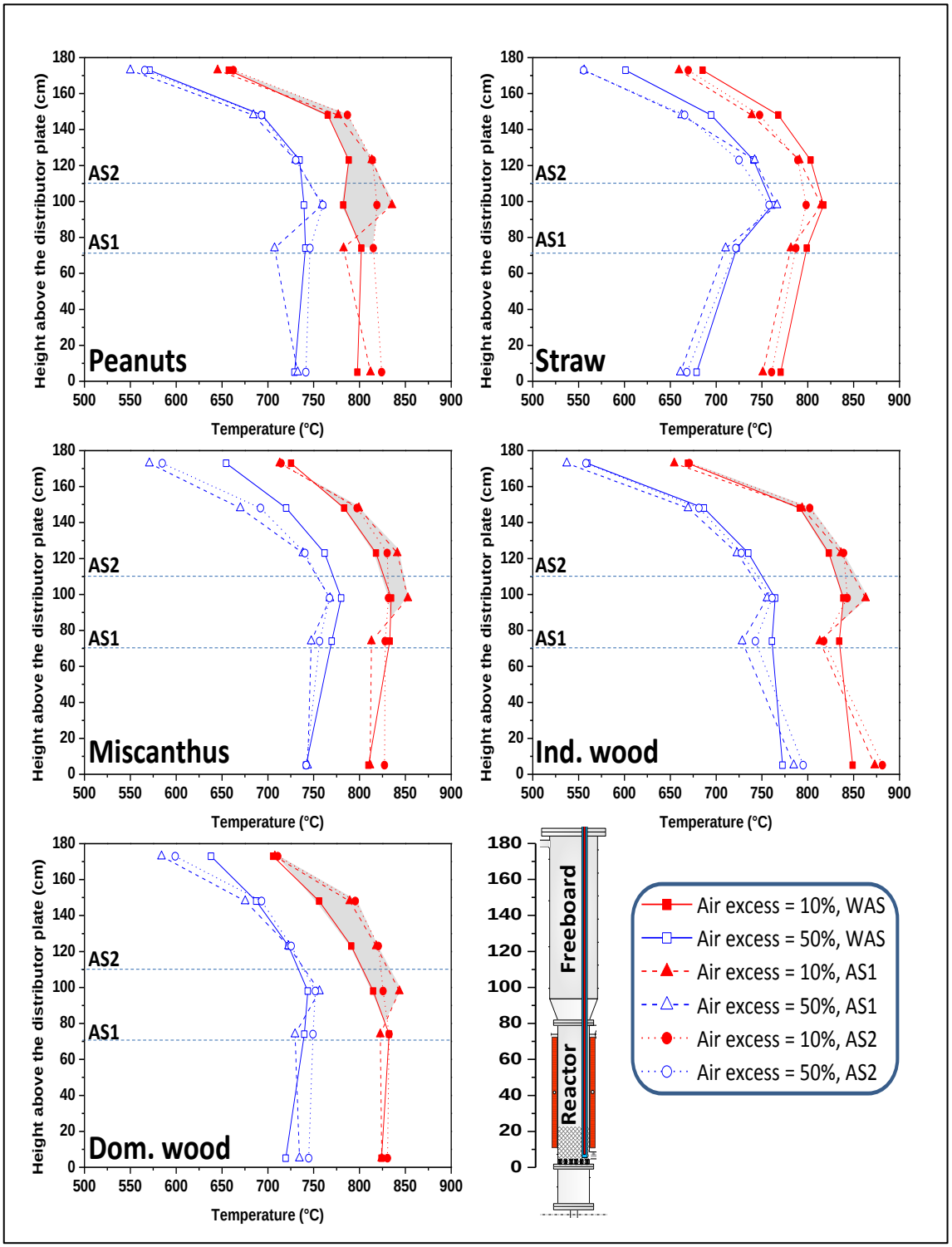


Figure 6.3: Temperature profiles for peanut, straw, miscanthus, industrial wood and domestic wood pellets at different excess air levels without air staging (WAS) and with air staging combustion at injection level one (AS1) and injection level two (AS2).

This behaviour occurs as a result of segregation of fuel particles during devolatilisation at the top of the bed (irrespective of the feeding options including the feeding into the bed option used in this study), and limited in-bed volatile matter combustion [299]. The segregation of biomass fuel particles at the bed surface during devolatilisation has been well documented in the published research [301] and is believed to be related to the lift effect that the volatile bubbles can exert on fuel particles. After the temperature peak, a remarkable temperature decrease in the freeboard above 1 m is observed, due to the fact that the heat extracted by the water cooling probe from the upper part of the freeboard is much higher than the heat released from the combustion of any unburnt fuels within the freeboard region.

It is also observed from the figures that by using air staging (AS1 or AS2) when operating with the overall excess air level at 10%, there was a significant increase in the temperatures in the splashing zone and freeboard region in almost all the cases, see the shaded areas in Figure 6.3 comparing those under WAS conditions. This increase in the temperatures suggests there is a significant amount of unburned gases and volatile matter in the freeboard, as a result of sub-stoichiometric combustion conditions in the dense bed region, and further combustion of the unburned fuels in the freeboard after the injection of the secondary air. On the other hand, when air staging is operated under the condition of 50% overall excess air, similar or lower temperatures than those measured under WAS conditions were observed along the reactor/freeboard for all type of fuels; a higher overall excess air level implies a higher combustion efficiency can be achieved at the lower part of the reactor (in the dense bed region, especially) and therefore almost no unburned gases and volatile matter reach the freeboard.

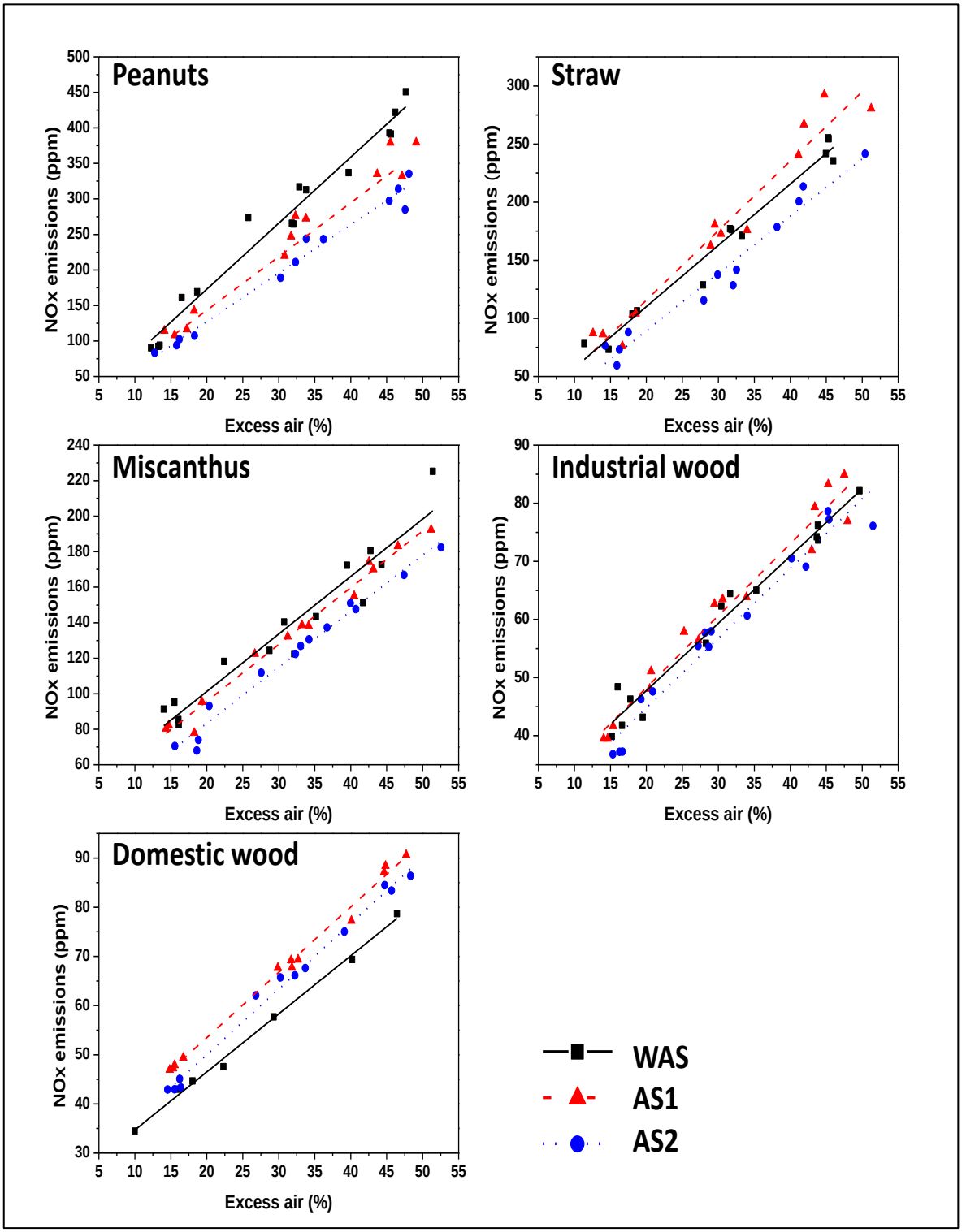


Figure 6.4: Effect of excess air on NOx emissions for peanut, straw, miscatnhus, industrial wood and domestic wood pellets without air staging (WAS) and with staging air combustion at injection level one (AS1) and injection level two (AS2). The NOx are corrected @6% on dry basis.

The results also show that in many cases there is a temporary decrease in the temperature immediately after the injection of the secondary air. This happens because the secondary air is not preheated and hence at a temperature much lower than the primary combustion gas temperature before entering the combustor. The temporary decrease in the temperature is more pronounced when the secondary air is injected at AS1 as there is a thermocouple located next to this injection point.

6.4.4 Effect of Air Staging on NOx Emissions

The effect of excess air levels on NOx emissions for all type of biomass fuels tested in BFBC operating without air staging (WAS) and with air staging at two different injection points is represented in Figure 6.4. Injecting the secondary air at the lower point (AS1) led to a decrease in the NOx emissions when the miscanthus pellets or the peanut shell pellets (see Figure 6.4) were used as the fuel; whereas for other fuels, air staging at AS1 did not lead to a decrease but a small increase in the NOx emissions.

On the contrary, a significant decrease in the NOx emissions was achieved with almost all of the fuels except domestic wood, when the secondary air was injected from the higher point (AS2). As it has been discussed in Section 6.3.3, the temperature profiles obtained with all the fuels suggest that the main combustion reaction (and therefore the formation of NOx) takes place at the splash region and/or beginning of the freeboard due the characteristic high volatile matter content of biomass fuels. Thus, the secondary air with the air staging should be introduced higher up in order to make air staging to be more effective in reducing the NOx emissions.

The lower secondary air injection point (AS1) is located precisely at the splash region/beginning of freeboard, where the main combustion reaction happens and where the maximum temperatures are reached. Therefore, the injection of oxygen (via the secondary air) at this point provides the oxygen needed to promote the fuel-N oxidation in a high temperature zone, and hence favours the formation of NOx as it happens with the cases of straw, industrial and domestic wood (see Figure 6.4). These results agree with those obtained by Saikaew et al. [289] and Varol et al. [290] who also found the lowest NOx emissions under air staging conditions with the secondary air injection at the highest position.

Moreover, the results also confirm that the effect of air staging in reducing NOx emissions is small with the biomasses that have lower fuel-N contents, i.e. woody biomasses: domestic wood pellets and the industrial wood pellets. This is expected as air staging controls NOx emissions by inhibiting the conversion of fuel-N to NOx and to a smaller extent by reducing thermal-NOx formation [302]. With low fuel-N fuels (e.g. the domestic wood pellets and the industrial wood pellets), the NOx emissions are already low and hence the scope for NOx reductions with air staging is limited. Figure 6.5 shows the effect of the overall excess air level on the reduction percentage of NOx emissions in comparison to the NOx emissions under conditions; without air staging (WAS) and with air staging as the secondary air injected at two points (AS1 and AS2) for all type of biomass fuels. As it can be observed, a higher fuel-N content of the fuel implies a higher NOx reduction percentage for almost all cases (except when using straw under AS1 conditions).

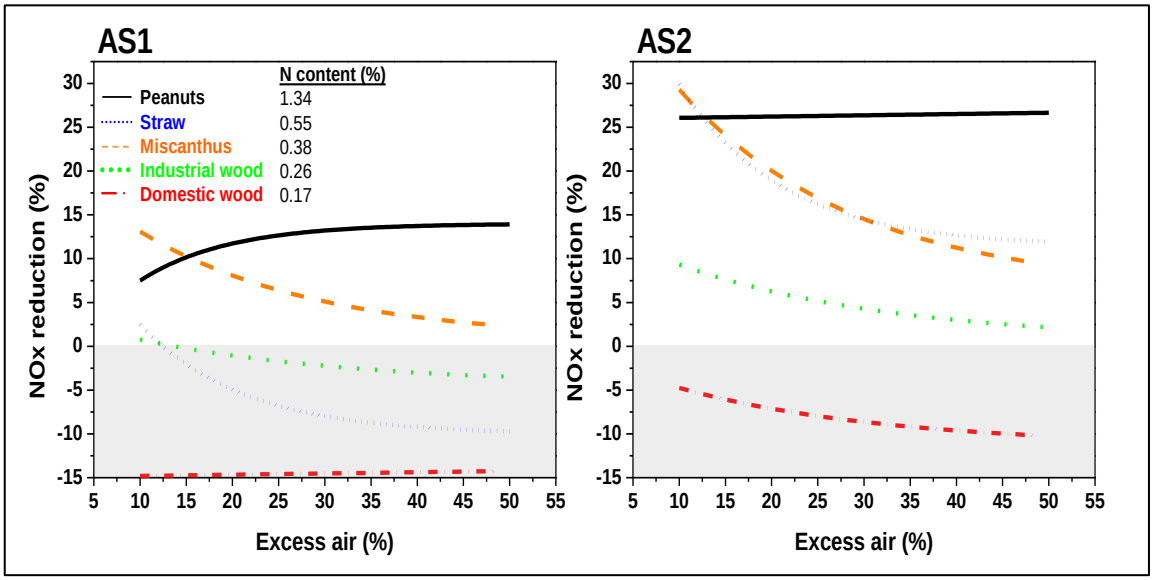


Figure 6.5: Effect of the overall excess air level on the reduction percentage of NOx emissions, in comparison to the NOx emissions under without air staging (WAS) and staging air with the secondary air injected at two locations AS1 and AS2.

The NOx reduction percentage is higher with the non-woody biomasses due to their higher fuel-N contents. The highest NOx reduction at ca. 30% was achieved with the non-woody biomasses under the AS2 conditions when operating with low levels of overall excess air. For woody biomass fuels with low fuel-N contents, a reduction of NOx was only seen under the AS2 conditions with the industrial wood pellets as shown in Figure 6.5. No NOx reduction was achieved in any case with domestic wood pellets, which is the biomass fuel with the lowest fuel-N content as can be seen in Figure 6.2b.

6.4.5 Effect of Air Staging on CO Emissions

Figure 6.6 shows the effect of excess air on the CO emissions for all of the tested biomass fuels under conditions of without air staging (WAS) and air staging at two different injection points (AS1 and AS2).

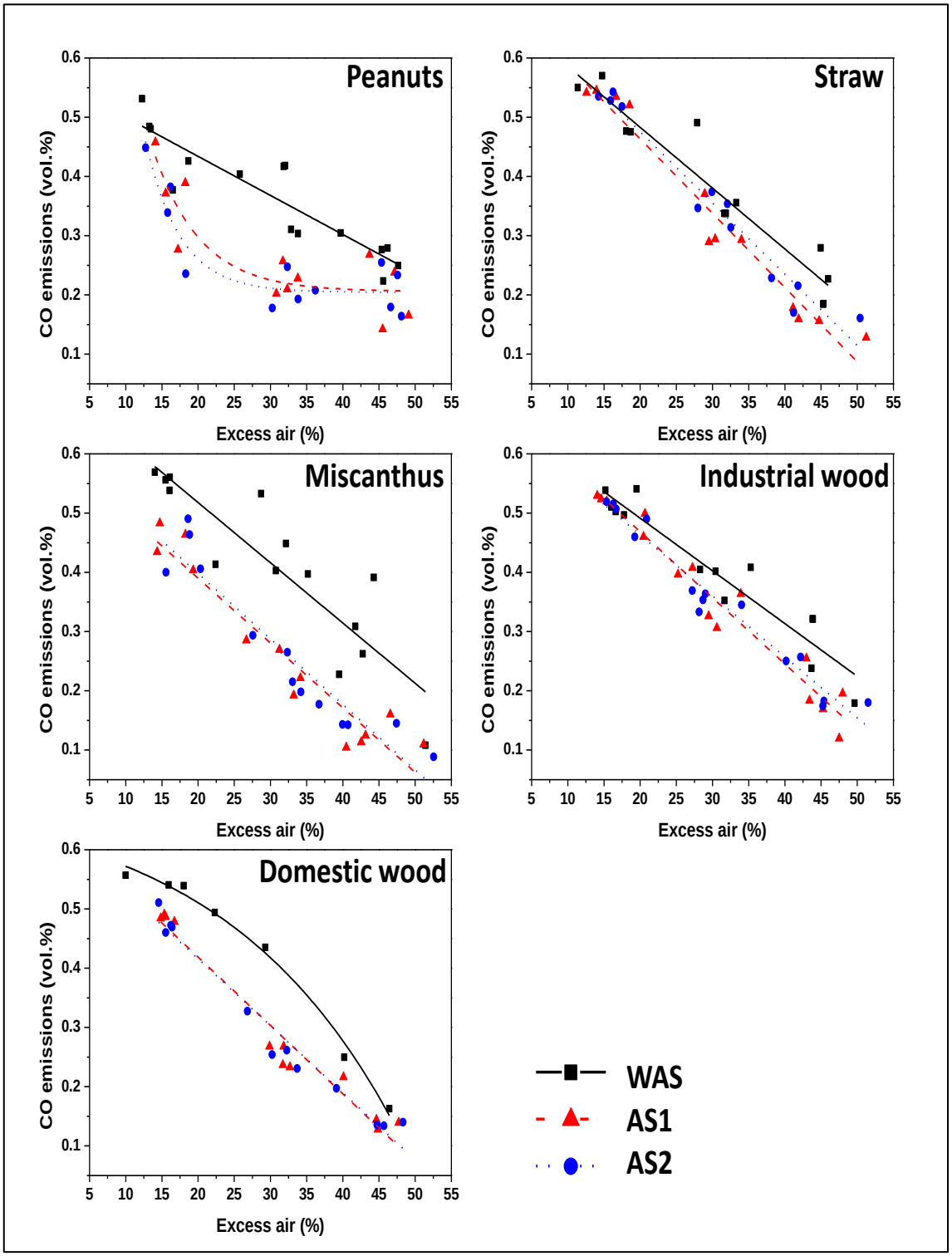


Figure 6.6: Effect of excess air on CO emissions for peanut, straw, miscanthus, industrial wood and domestic wood under conditions of without air staging (WAS) and with air staging combustion at injection level one (AS1) and injection level two (AS2). The CO is corrected @6% on dry basis.

The use of staging air has led to a decrease in CO emissions for almost all cases and the reduction in CO emissions is seen to be quite similar for staging air at AS1 and at AS2. As discussed in section 6.3.3, staging air resulted in an increase in the gas temperatures in the splashing zone and the freeboard, indicating significant conversion of unburned CO in these sections. In addition, the use of staging air resulted in an increase in the fuel residence time in the dense bed region and consequently, this could have contributed to the lowering of the CO emissions [103]. However, the CO emissions achieved with these experiments were quite high, within the range of 0.1–0.6%, and this needs to be addressed in the future.

The observed high CO emissions with all of the tested biomass fuels can be attributed to several factors; firstly, the heat extraction probe crossing the freeboard reduced the gas temperature in the freeboard and therefore inhibited the conversion of CO to CO_2; secondly the freeboard region was not enough high as the original design of the BFBC was restricted by the available ceiling height at the old laboratory. The biomass has a comparatively high volatile content and therefore needs more residence time in the freeboard to completely burn the volatiles; finally, the properties of the biomass pellets, especially the fuel moisture content and amount of the fine particles in the fuels, could also have affected the combustion efficiency and hence the CO emissions.

Some of the non-woody biomass fuels, e.g. miscanthus, peanut shell and straw pellets contain more fines than the woody biomass pellets; the fines can be easily entrained to the freeboard region, resulting in high CO emissions; the high dispersion of the data showed in some cases (see Figure 6.6) are believed to be partly resulted from the variations of the fines in different batches of the tested fuels. The accumulation of the

biomass ash on the surfaces of the burning fuel particles could have weakened the oxygen penetration to the combustible part of the particles [103].

To achieve low CO emissions, a new cooling probe need to be designed and used in the future so that it removes heat mainly from the lower part of the reactor (the dense bed region) rather than from the freeboard and splashing zone which should remain at high temperatures and therefore favour the conversion of CO to CO_2. Test runs without the use of a cooling probe could also be an option if the bed agglomeration and defluidisation can be avoided, for example, by use of alternative bed materials [303].

6.4.6 Combustion Efficiency

The performance of the BFBC for all five types of biomass fuels at different operating conditions is accessed through combustion efficiencies. The combustion efficiency results for different cases considered under without air staging (WAS), with air staging level one (AS1) and air staging level two (AS2) based on the emissions without considering unburnt carbon in the fly ash are shown in Figure 6.7 for tested biomass fuels. The combustion efficiency ranging between 95.5–99.5%, which considered being very good. The combustion efficiency for all tested biomass fuels has improved under air staging conditions. The highest combustion efficiency 99.2% and 99.1% was noticed for miscanthus pellets under air staging AS1 and AS2 conditions respectively, followed by wood pellets with 99% under AS2 using 45% excess air. In general, the combustion efficiency was lower in the case of unstaged air combustion with less excess air. It was observed that all biomass fuels were burned successfully under air staging with a marginal difference in their combustion efficiency.

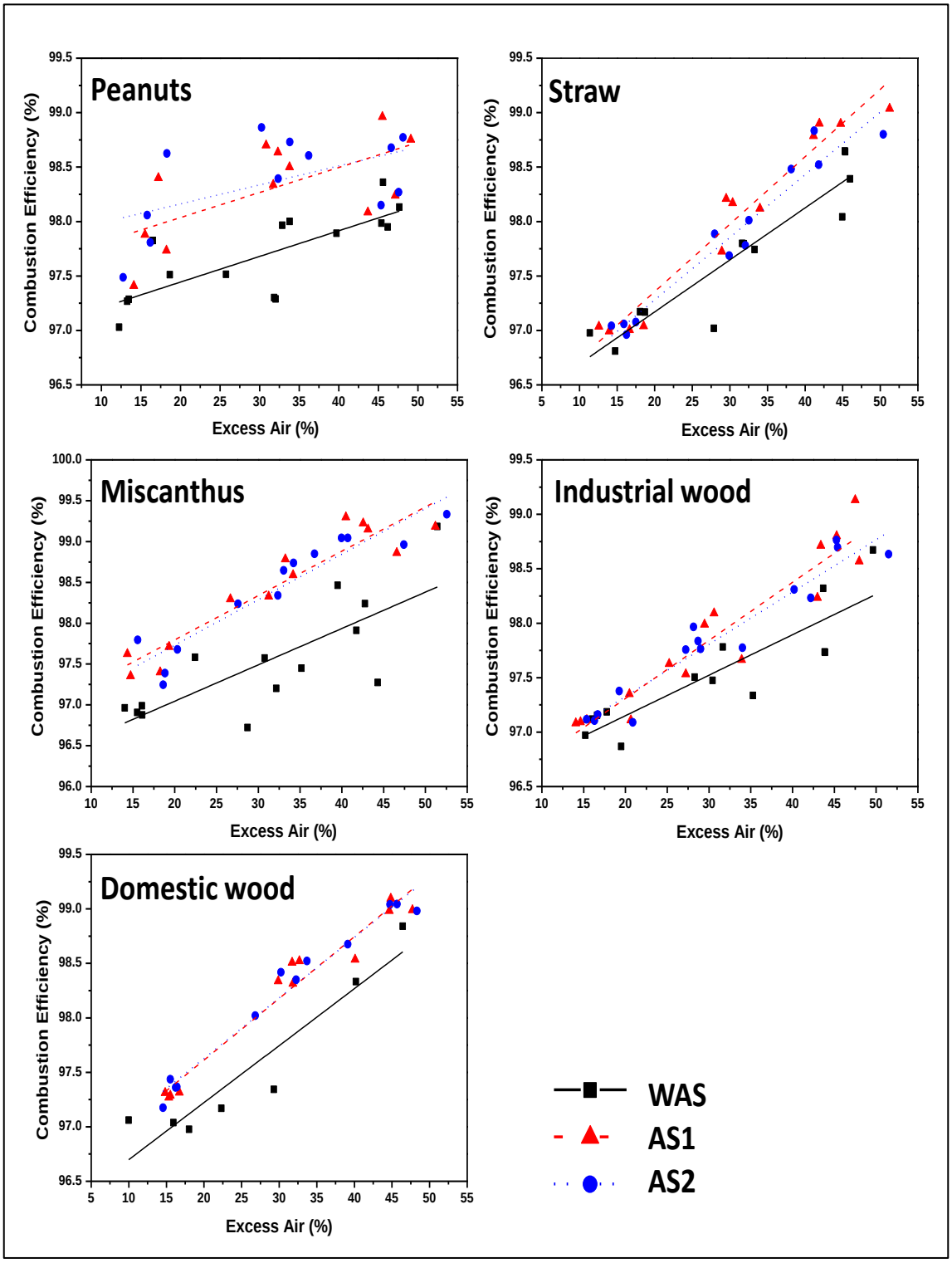


Figure 6.7: Combustion efficiency without considering carbon in fly ash for peanut, straw, miscanthus, industrial wood and domestic wood pellets without air staging (WAS) and with air staging at injection level one (AS1) and injection level two (AS2).

As the level of excess air decreases, there is not enough oxygen in the reactor to complete the combustion, hence combustion efficiency drops. This is understandable since the total air flow to the combustor is limited there is more fuel accumulated (fuel-rich conditions) in the bed region and an increase in bed zone residence time will thus result in a shorter residence time in the freeboard, i.e. a reduced burnout time for the fuel char particles thus resulting in a diminished combustion efficiency.

In another way under fuel rich conditions there is low oxygen concentration in the bed zone, which hindered the combustion, resulted in low efficiency. The drop in combustion efficiency was only marginal for the high volatile content fuels like industrial wood and miscanthus. The maximum drop in efficiency was 3.7% for miscanthus among all tested fuels. The gas temperature is another factor affecting the combustion efficiency. The results also illustrate that combustion efficiency is higher for all tested biomass fuels under air staging conditions this can attribute to the higher gas temperatures during air staging with secondary air injection from different points shown in Figure 6.3. The higher gas temperatures can accelerate the overall combustion process thus resulting in higher combustion efficiency provided other conditions remain the same or similar. Armesto et al. [108] and Rozainee et al. [304] investigated the combustion and fluidisation behaviour of rice husk in a bubbling fluidised bed reactor, they found that the temperature profiles in the reactor had a strong effect on combustion efficiency, the combustion efficiency increase with the temperature. The higher combustion efficiency in terms of emissions reduction was noticed when the staging air was injected from the highest point AS2 in all type of biomass fuels except peanut shell pellets.

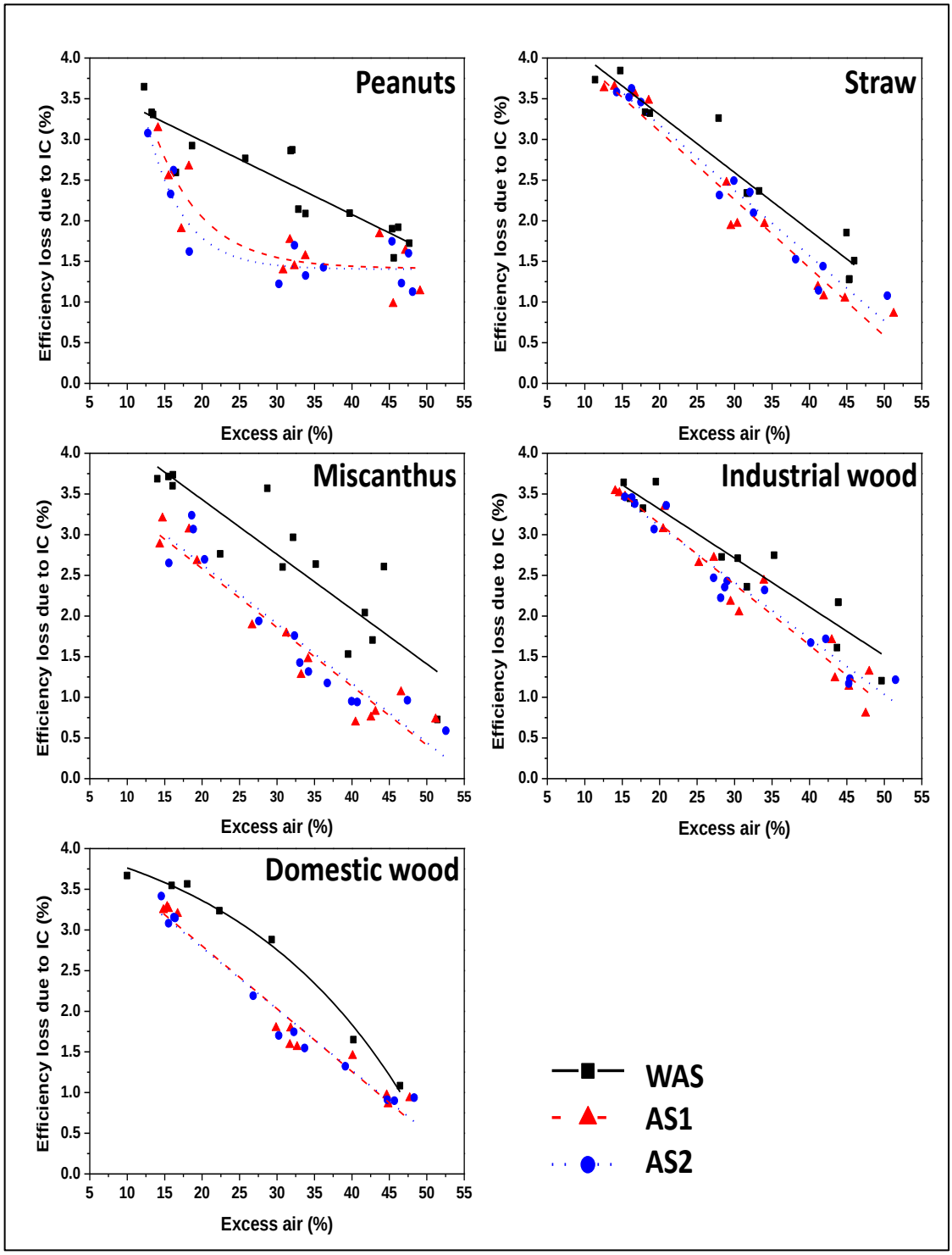


Figure 6.8: Effect of excess air on efficiency loss due to incomplete combustion (IC) for peanut, straw, miscanthus, industrial wood and domestic wood pellets under conditions of without using air staging (WAS) and with air staging at injection level one (AS1) and at injection level two (AS2).

The Figure 6.8 shows the percentage efficiency loss for different types of biomass fuels studied without air staging and with air staging with secondary air injection from two different heights. The efficiency loss is calculated from the heat losses associated with unburned carbon which presents in the fly ash left after each combustion test.

As it has been concluded from the combustion efficiency results established on the level of emissions reduction without considering carbon in fly ash that the combustion efficiency increases under air staging conditions in all cases even though the temperatures were lower at high excess air as a consequence of the low fuel feeding rate, as it could be seen in Figure 6.7. But on the other hand the efficiency losses are higher under air staging conditions when considering unburnt carbon in ash (see Figure 6.9). This can be expected, since the injection of the secondary air implies a decrease in the primary air flow rate, in order to maintain constant the total air flow rate, which affects the local stoichiometry in the bed, so that any gains in combustion efficiency in splash zone and/or beginning of the freeboard may be negated by a drop in efficiency in the bed.

As the CO concentration at the outlet decrease using air staging as it could be observed in Figure 6.6, in this case, the drop in combustion efficiency is mainly attributed to the substantial increase in the heat loss due to unburned carbon when using air staging. Working under air staging conditions implies a high shortage of oxygen in the dense bed of the reactor which decreases the char burning rate, resulting in a greater concentration of char within the bed. Therefore, the rate of char comminution multiplies, yielding a greater amount of elutriable fines and carbon loss. Other authors

found similar trends [305]. The unburnt carbon in fly ash with the non-woody biomasses is higher than the ones obtained with the woody biomasses. In general, due to the specific features of texture, shape, and size of biomass particles, the combustion of some unconventional biomass fuels is accompanied by high CO as well as by elevated unburned carbon content in fly ash which results in deterioration of combustion efficiency [286, 306].

6.4.7 Effect of Air Staging on the Efficiency loss due to Unburned Carbon content in Fly Ash

Figure 6.9 shows the effects of air staging on the unburned carbon (UBC) content in the fly ash for the five biomass fuels tested in BFBC. As the fly ash collected at the end of each testing day resulted from the tests under both air staging conditions (AS1 and AS2), the effect of the secondary air injection location on the UBC content in the fly ash and hence the associated efficiency loss could not be distinguished. For the same reason, the combustion efficiency considering both losses due to incomplete combustion (CO) and the UBC content in the fly ash cannot be calculated for each excess air value. As it can be seen in Figure 6.9, the use of air staging results in a significant increase of the UBC content in the fly ash, and consequently in a higher efficiency loss for all the fuels. This could be expected, since the injection of the secondary air implies a decrease in the primary air flow rate (necessary to maintain constant the total air flow rate) which affects the stoichiometry in the bed, so that any gains in combustion efficiency in splash zone and/or beginning of the freeboard (which results in lower CO concentration at the outlet of the reactor, as shown in Figure 6.6) may be negated by a drop in efficiency in

the main bed zone, which results in a higher UBC content in the fly ash collected in the cyclone.

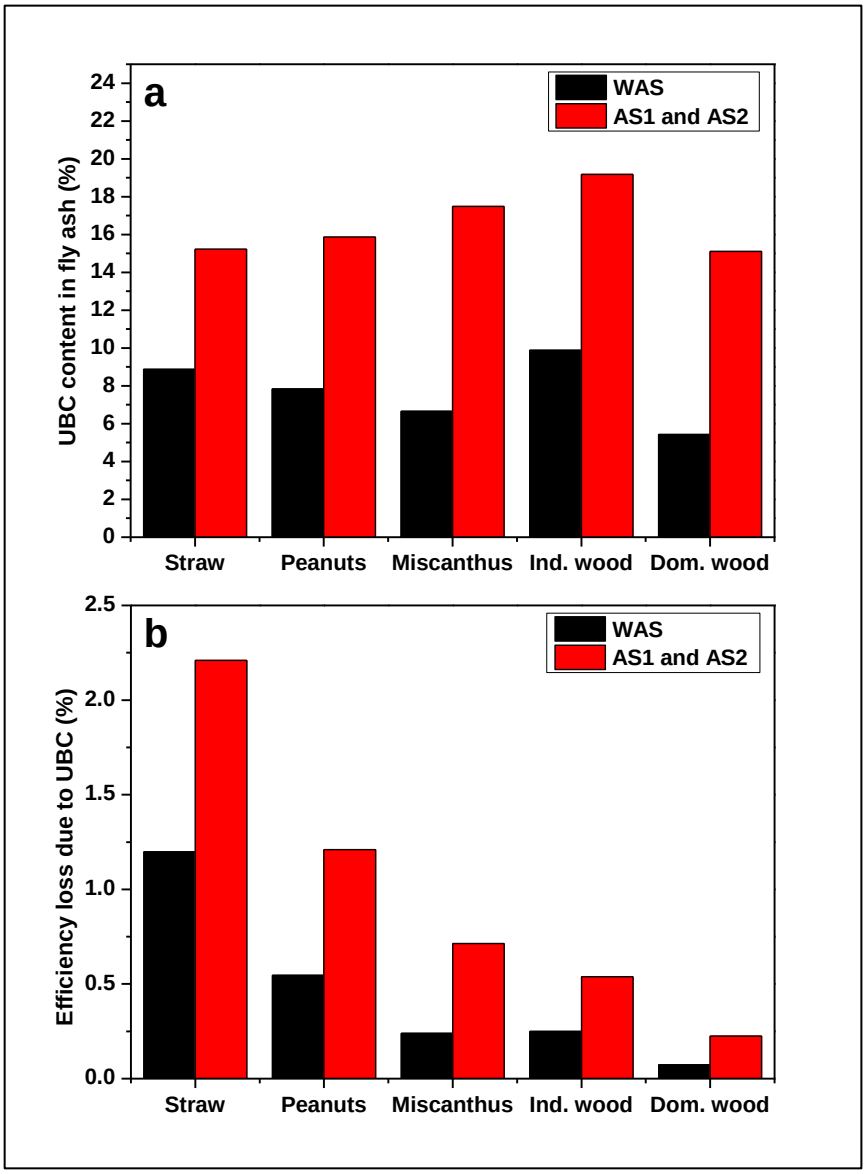


Figure 6.9: (a) Unburnt carbon (UBC) content in the fly ash for different biomass fuels, (b) Efficiency loss due to UBC content in the fly ash.

Further, the higher UBC amount obtained can be explained by the fact that working under air staging conditions implies a high shortage of oxygen in the reactor which decreases the char burning rate, resulting in a greater concentration of char within the

bed. Therefore the char comminution (attrition and fragmentation) rate multiplies, yielding a greater amount of elutriable fines and carbon loss. Other authors find similar trends [305, 307]. It can also be seen in Figure 6.9b that higher ash content of the fuel implies higher efficiency loss due to UBC. The drop in the efficiency due to the higher UBC in the fly ash at air staging conditions is particularly relevant in the case of straw. In this case, the use of air staging leads to a considerable decrease of the combustion efficiency. As straw has much higher ash content than the rest of the fuels has the negative effect of the unburned carbon on the combustion efficiency is more pronounced working with this fuel. In general, the efficiency loss due to UBC will be higher with the non-woody biomasses, given the higher ash content of this kind of fuels comparing with those obtained with woody biomasses.

6.5 Agglomeration and Sintering Effect

Agglomeration is one of the problems that is most frequently occurring during biomass combustion in FBCs [308], usually associated with the large amount of alkali in ash, silicon in quartz sand reacts with the alkali in the ash and forms low melting point materials, causing agglomeration and ultimately leading to defluidisation, which results in unscheduled shutdowns and unnecessary expenses. The wheat straw pellets showed some kind of agglomeration during combustion. However, the quartz sand particles did not show any defluidisation problems during the whole operation period of this study which included the testing of all five different biomass fuels under various operational conditions without air and with air staging with an average total accumulated operational time of over 100 hours. This is mainly due to the successful control of the

bed temperature to be under ca. 850 ^{o}C for all tests with the water cooled heat extraction probe. The bed material and ash characterisation studies are to be detailed in Chapter 8.

6.6 Summary

Five different kinds of biomass pellets (domestic wood, industrial wood miscanthus, peanut shell and wheat straw) were successfully combusted and tested in the newly designed 20 kW_{th} bubbling fluidised bed combustor. The effects of the excess air, without and with air staging at different injection heights on the gas emissions (NOx and CO) were systematically investigated. The main findings can be summarised as follows:

A higher overall excess air always leads to higher NOx emissions for any of the tested biomass fuels as less CO and char are available in the reactor to promote NOx reductions. NOx emissions depend directly on the fuel-N content, whereas the CO emissions are associated with the fuel quality, especially during combustion without air staging. As a consequence of the high volatile matter content of the biomass fuels, the maximum temperatures were reached at the top of the dense bed and/or beginning of the freeboard, which suggests that the main combustion reaction takes place in this part of the combustor. Air staging leads to higher temperatures in the freeboard, especially at low excess air levels, as a result of additional combustion in the freeboard under air staging conditions.

Air staging can be very effective in reducing NOx emissions of non-woody biomass fuels, especially if the secondary air is injected at the higher level of the BFBC and the

combustor is operated with a low overall excess air level. The percentage of NOx reduction that can be achieved with air staging depends directly on the fuel-N content of the biomass fuel and the overall excess air level as well as the position of the secondary air injection point. Up to 30% of NOx reduction has been shown to be achievable with air staging for the non-woody biomass fuels which have higher fuel-N contents than the woody biomass fuels tested.

The combustion efficiency was around 96–99% for all type of biomass fuels; overall combustion efficiency was increased with the overall excess air. The higher gas temperature inside the BFBC improved combustion efficiency, moreover, under fuel rich conditions, the combustion efficiency was hampered by the low oxygen concentration in splashing zone. The use of air staging, with the secondary air injected at any of two positions, also leads to lower CO emissions and higher combustion efficiency this is due to the higher gas temperatures in the splash zone and freeboard as well as the longer residence time of fuel particles in the dense bed region. However, the use of air staging also implies an increase in the UBC content in the fly ash, which results in higher efficiency loss. The quartz sand particles did not show any agglomeration or defluidisation problems during the whole combustion testing period (with the accumulated operational of more than 100 hours) for all the biomasses tested under the conditions of without air staging (WAS) and with air staging at two different heights (AS1 and AS2). The present work helps to better understand the combustion and emissions of biomass fuels in BFBC, in particular, non-woody biomasses which have great potential as cheap alternatives to coal for energy supplies and power generation in the future.

Chapter 7

Oxy-fuel Combustion of Biomass Fuels

7.1 Introduction

As mentioned previously the power generation coal fired plants are the major single point emitters of greenhouse gases to the environment. There is an urgent need for retrofitting existing facilities and the deployment of new technologies for carbon capture and storage (CCS). Recently different initiatives are being taken to promote clean coal technologies for power generation. In the current scenario, the carbon capture costs about 75% of the total cost for carbon capture, transportation and storage from the power plants [182]. The flue gas from the conventional coal power plants under air firing consist of only 10–15% of CO_2 by volume, the rest of the balance is mostly N_2. The capturing process of such low CO_2 volumes results with high capture costs [309].

Over the past decade, oxy-fuel combustion has been known to be a promising technology for capturing CO_2 from coal-fired power plants. However, the majority of the research activities in this area have so far focused on pulverised coal combustion. Several studies have also shown there are such as no economic or technical barriers stopping the construction of pulverised oxy-fuel coal-fired boilers [278, 310-312].

Bubbling fluidised bed combustion (BFBC) is an alternative technology that can be used with the oxy-fuel combustion of solid biomass fuels. BFBC has many advantages over the pulverised coal combustion for oxy-fuel that may make it a better choice for CO_2 capture in some cases. BFBC maintains a fluidised bed of coal/ biomass, ash, sand and sometimes sulphur sorbent. The bed material acts as a heat sink, capturing excess heat in hot spots, and providing the heat needed for drying, devolatilisation and ignition of the fuel within the combustor [313].

Moreover, low fluidisation gas velocities are required for the operation of BFBC in comparison with circulating pulverised coal oxy-fuel combustors, where relatively high gas velocities for the operation must be required at relatively high recycle flue gas rates [314, 315]. BFBCs have the advantage of being able to combust a wide variety of biomass fuels efficiently such as agricultural waste, municipal waste and different types of wood. Combustion of the biomass fuels and sequestering the CO_2 that is produced during the process visa oxy-fuel combustion process can effectively remove CO_2 from the atmosphere. The present chapter presents results of biomass fuels combustion under different oxy-fuel environments in the 20 kW_{th} bubbling fluidised bed combustor (BFBC).

7.2 Biomass Fuels Characteristics

Three types of biomass fuels two non-woody (miscanthus and wheat straw) and one woody (domestic wood) were selected for the oxy-fuel combustion experiments. For comparison purposes, all these fuels were also combusted in air prior to and after each oxy-fuel combustion test schedules. All the fuels used were in pellet form with a diameter of 6–10 mm and length of 15–30 mm. The chemical characteristics along with the heating values of these fuels are described in Table 4.4 in Chapter 4.

7.3 Experimental Procedure and Conditions

The detailed description of the experimental setup and procedure is given in section 4.5 and full experimental setup is shown in Figure 4.7 in Chapter 4. The operating conditions for all experiments with oxy-fuel combustion are summarised in Table 7.1. To analyse the effect of the oxy-gas mixtures on temperatures, flue gas emissions and combustion efficiency, experiments were carried out by varying the O_2/CO_2 ratios and maintaining a constant total excess air level and fuel feed rate. The combustion experiments were also carried out under air with the selected biomass fuels for comparison. The oxy-fuel experiments were conducted using O_2 and CO_2 gases from the gas cylinders without actually using flue gas recirculation.

Each test was always started with conventional biomass air combustion and after stabilisation of the combustion process under air, which took about 2 hours; the combustion environment was changed from air to oxy-fuel with continuous biomass feeding. After finishing the oxy-fuel tests, the combustion oxidant was switched back to

air with continuous biomass feeding operation so that the stability of the biomass feeding and sampling procedures could be checked. The continuous biomass feeding during shifting over from air combustion to O_2/CO_2 combustion minimises any errors resulted from biomass feeding rate differ between the two combustion environments.

Table 7.1: Operating conditions for the oxy-fuel combustion.

Parameters	Air	Oxy-fuel	Oxy-fuel	Oxy-fuel	Air
Excess air (%)	30	30	30	30	30
O_2 in Oxy-fuel mixture (%)	-	21	25	30	-
Feeder air (L/min)	95	95	95	95	95
Primary air (L/min)	250	-	-	-	250
Total O_2 flow (L/min)	72.5	72.5	72.5	72.5	72.5
CO_2 flow (L/min)	-	197.5	157.5	122.5	-
Total gas flow (L/min)	345	345	305	270	345
Biomass feed rate (kg/h)	3–5	3–5	3–5	3–5	3–5
Bed height (mm)	250	250	250	250	250
Aver bed diameter (mm)	0.78	0.78	0.78	0.78	0.78
Cooling water flow rate (L/min)	1–1.2	1–1.2	1–1.2	1–1.2	1–1.2

The O_2/CO_2 mixtures are produced at selected molar ratios by mixing metered O_2 and CO_2 gases before inflowing into the combustor. To investigate the effect of the oxy-fuel firing conditions on the combustion behaviour, similar excess air levels were used in all experiments (30%). To increase the oxygen concentration in the oxy-fuel mixture the CO_2 flow rate was gradually reduced. While the O_2 flow rate was kept constant in all of the experiments to maintain the total excess air/oxygen level at 30%. It was also made sure that the data only obtained under steady state conditions used for further analysis.

7.4 Results and Discussion

7.4.1 Effect on Combustion Fundamentals

One of the priorities in oxy-fuel combustion is to achieve similar heat transfer characteristics in the combustor as that in air combustion. The matching heat transfer characteristics in the oxy-fuel system can also lead to combustion stability, burnout as well as slagging and fouling inclinations [310].

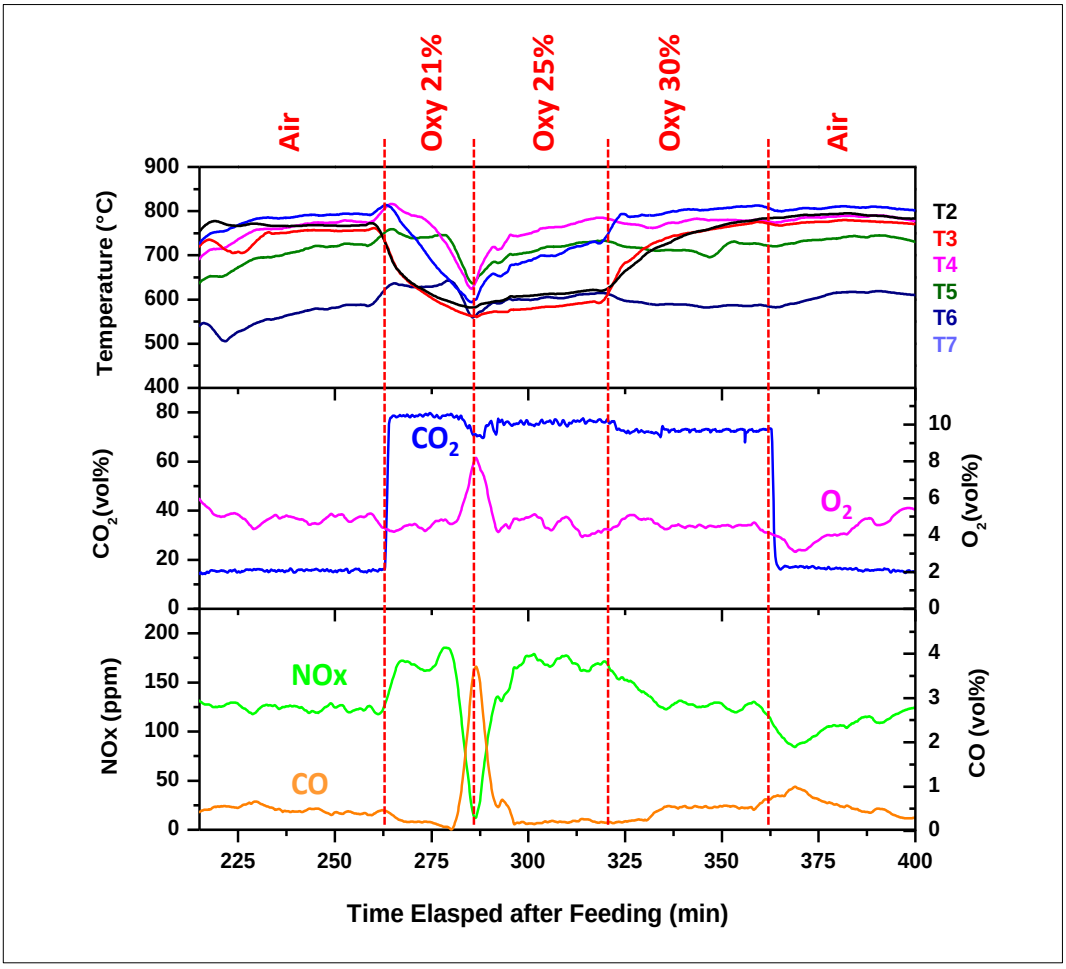


Figure 7.1: The temperature profiles, measured at different heights of the reactor and freeboard with the gas compositions at the outlet of the BFBC during miscanthus pellets combustion under air and oxy-fuel.

Therefore, matching the gas temperature profiles was the starting point in the efforts to maintain similar characteristics of heat transfer in oxy-fuel BFB combustion. The temperature profiles were measured for all types of biomass fuels combusted under air and three different oxy-fuel atmospheres. Figure 7.1 gives a direct comparison of air and different oxy-fuel mixtures during a typical biomass fuel (miscanthus pellets) combustion regarding temperatures and gas emissions profiles. A similar comparison with other biomass fuels under oxy-fuel conditions is given in Appendix E.

7.4.2 Effect of Environment on Fuel Combustion and Temperatures Profiles

The temperature profiles along with the height of the combustor are shown in Figure 7.2 for domestic wood, miscanthus and wheat straw pellets under different combustion environments. Under air, the temperatures increase from the lower bed up to a maximum, located in the first half of the freeboard region. The D-shape temperature profiles (see Figure 7.2) could be described by the increase of heat released due to volatiles combustion, located near the middle of the combustor (start of the freeboard zone). Directly replacing the combustion air with oxy mixture 21% O_2/79% CO_2 causes bed temperatures to be drop significantly (see Figure 7.1).

A continuously decreasing trend among the other temperatures measurements (T3–T7) along the reactor and freeboard was also observed with no steady temperature being reached even after one hour of continuous feeding under the same conditions. Similar decreasing trends in the temperature profiles were also observed during wood and wheat straw pellets combustion under 21% O_2/79% CO_2 conditions.

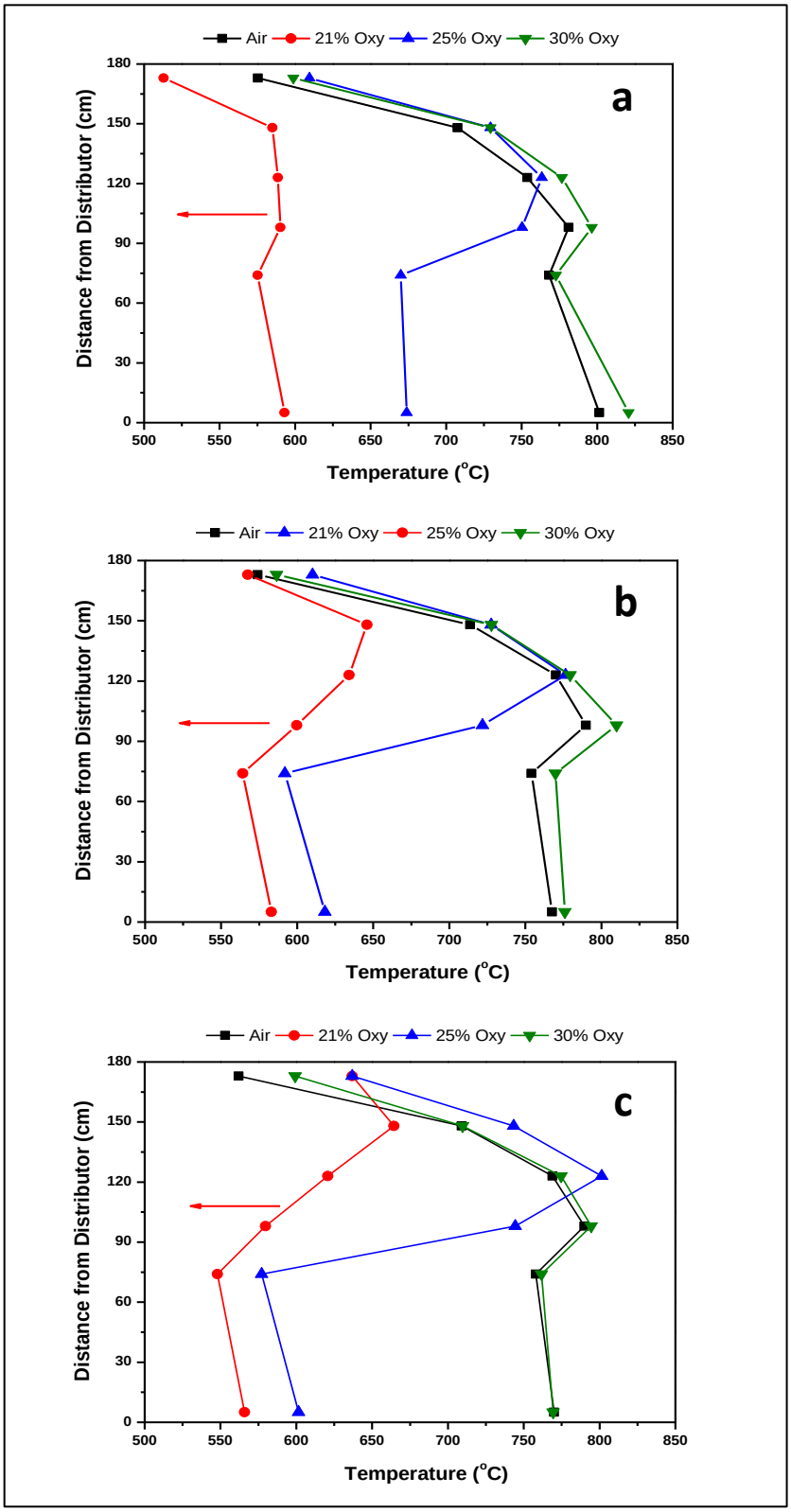


Figure 7.2: Temperature profiles under air and different oxy-fuel environments; (a) domestic wood pellets, (b) miscanthus pellets and (c) straw pellets.

Due to this constant drop in temperatures the steady biomass combustion can no longer be sustained within the combustor. The biomass in 21% O_2/79% CO_2 significantly reduces the combustion temperatures, which is also reported by other researchers [187].

The decrease in temperature could also destabilise the combustion and eventually result in the elimination of the combustion in the combustor. Just replacing N_2 in the air with CO_2; firstly results in a significantly decrease in gas temperatures and secondly decreases the char burnouts due to the higher specific heat of CO_2 compared to N_2. A similar effect was noticed by Kiga et al., (1997) [163]; Molina and Shaddix (2007) [316], they reported that CO_2 distinctly delays the flame propagation speed, ignition of coal particle and reduces overall combustion rate of carbon particles in 21%O_2/79%CO_2 atmosphere as compared with air 21%O_2/79%N_2. The overall gases volumes into the combustor in both atmospheres were kept constant. It is also mentioned in the literature that CO_2 plays a significant role in reducing the fuel burning rates by limiting the concentration of O and H radicals during oxy-fuel combustion [133].

The gas temperatures were observed to increase with increasing O_2 concentration in the O_2/CO_2 mixture. By increasing O_2 concentration from 21% to 25% in O_2/CO_2 mixture a significant increase in the combustion temperatures was noticed. However, the main bed temperature (T2) was still low and the other temperatures were not reached to the temperature profiles equivalent to those of air combustion. The heat capacity of CO_2 is 1.66 times higher on mole basis than that of N_2 due to its larger molecular weight, which leads to lower flame temperatures than for a corresponding concentration of

oxygen in the air combustion atmospheres [317]. A strong increase in temperature associated with an increased oxygen concentration was noticed, especially when the oxygen concentration was raised from 25% to 30% (see Figure 7.2), since the same level of excess oxygen was maintained. The oxy-fuel gas further up in the combustor maintains a higher average temperature. That is most likely due to min combination process in that region and of the higher heat capacity of CO_2. From the analysis of the thermocouples data, significantly higher temperatures are observed at the start of the freeboard region. Moreover, decreases in temperatures at the end of the freeboard region representing the almost end of biomass combustion before exit.

Usually, biomass contains a higher fraction of volatiles in comparison to the other solid fuels such as coal. The volatiles released from the biomass fuels during combustion process are not completely burned in the dense bed of hot solids (mostly sand) but in the freeboard region. Hence, the heat distribution released within the combustor between the bed and the freeboard region is totally different which is also evident from the temperature profiles of all types of studied biomass fuels. The temperatures in the bed and splashing zone are always lower than those of air combustion during combustion under oxy-fuel; 21% O_2/79% CO_2 and 25% O_2/75% CO_2 for all types of combusted biomass fuels.

Liu et al. [137] studied oxy-fuel combustion of coal in a 20 kW down fired furnace and observed unstable combustion when the furnace was operated under 21% O_2/79% CO_2 conditions. The coal particle ignition and peak temperatures were delayed with a dark volatile flame at the downstream of the burner. They concluded that to match the oxy-

fuel gas temperature profiles to those of coal combustion in air, the O_2 concentration in the mixture of O_2/CO_2 must be raised to 30% or higher [137].

Once the oxy-fuel mixture was changed to 30% O_2/70% CO_2 a significant boost in the temperature profiles was noticed. The temperatures in the splashing zone were almost similar to that of air. Furthermore, the elevated temperatures in the lower zone of the combustor during 30% O_2/70% CO_2 oxy-fuel verify that higher O_2 concentration in oxy-mixture enhances volatile oxidation in these lower zones, the findings are in agreement with those of Romeo et al. [318]. Romeo et al. [318] also found that if higher O_2 concentrations are applied at the inlet to the fluidised bed during oxy-fuel combustion without changing fluidisation velocity could result in sudden increase in thermal input which can affect the thermal stressed suffered by the construction material, performance of the installed cooling system and heat transfer distribution in the combustor.

The present results showed that a temperature drop of about 150–200 ^oC for all type of studied biomass fuels in oxy-fuel combustion with 21% concentration oxygen, compared with that of the air combustion, which agrees with the results reported in the literature [317]. Other researchers also found that quick transition from air to oxy-fuel with a higher O_2 concentration in the mixture could cause a sudden increase in the bed temperatures [101, 318]. But during these tests, the shift from air to oxy-fuel was smooth without any type of problems as mentioned by different researchers. Many studies reported a wide range (about 25–35%) of oxygen fraction required to attain the same gas temperatures and heat transfer characteristics similar to those in the air firing

during coal combustion. Croiset et al. [319] and Tan and Croiset [166] performed a number of experiments to investigate the influence of oxygen mole fraction on temperatures and heat transfer in a vertical combustor. A range of oxygen concentrations (21–42%) was tested under O_2/CO_2 mixtures as well as under air combustion modes [277].

In oxy-fuel conditions, the gas temperatures and heat fluxes were found to match with those of air combustion when O_2 mole fraction was between 28–35% for different types of coals. Andersson et al. [320] and Hjartstam et al. [321] used partial flue gas recycle and found they needed about 25% oxygen mole fraction in the feed gas to get the gas temperatures similar to those of air-fired coal combustion. Furthermore, while operating at higher oxygen fraction 27–29%, the combustion temperatures were 50–100 ^{o}C higher than those of air-fired coal combustion. Hence, in order to match the biomass oxy-fuel combustion gas temperatures to that of air combustion, the oxygen concentration in the mixture of O_2/CO_2 has to be increased to 30% or higher, these findings are also verified by other researchers [322].

7.4.3 Effect of Combustion Environment on CO_2 Emissions

In oxy-fuel combustion, the CO_2 concentration is the key point for the consideration on large scale capture plants. During the tests, a high concentration of CO_2 (more than 80%) in the flue gas was achieved with all types of biomass fuels (see Figure 7.1), which is an acceptable ratio when considering oxy-fuel as a carbon capture technology. The O_2 content (moderate to high) in the flue gas during air and oxy-fuel combustion tests was judged as acceptable to ensure good fuel combustion rates. It is possible to

further reduce the O_2 levels in flue gas if the height of the freeboard is increased to get complete combustion. The reduction of oxygen excess and switching the feeder air to oxy-mixture can further increase CO_2 concentration up to 95–99% in the flue gas.

7.4.4 Effect of Combustion Environment on NOx Emissions

In oxy-fuel combustion, the nitrogen gas stream is removed and the flue gas volume is decreased (up to 80%) in comparison with air combustion. The main part of the flue gas (CO_2) is extracted as a part of carbon capture and around 10–20% of the produced flue gas is emitted to the environment [323]. Thus oxy-fuel combustion generates high concentrations of pollutants but these concentration-based emission levels in the flue gas cannot be directly compared with those from air combustion without proper adjustments. The emission standards based on per unit energy produced such as mg/MJ or ng/MJ are commonly used in oxy-fuel combustion to encourage emissions level reduction by improving efficiency.

The efficiency of power generation process (electricity) and associated energy penalties with the separation of O_2 and compression of CO_2 influence the emissions per unit of energy produced. But the emission unit (mg/MJ or ng/MJ) per unit fuel supplied used for oxy-fuel combustion is not affected by the power plant efficiency [324]. The NOx emissions from different types of biomass fuels studied under various combustion environments in the units of ng/MJ are presented in Figure 7.3. The NOx emissions increased when the combustion environment was switched from air to oxy-fuel $21\%O_2/79\%CO_2$ for all types of fuels and the increase was seen to be largest in the case of the wheat straw pellet which has the highest fuel-N contents. The NOx emissions

were slightly decreased when the oxy-fuel mixture was shifted to 25%O_2/75%CO_2 from 21%O_2/79%CO_2 but the values were still higher than those under air combustion. Figure 7.3 also shows that the NOx emissions level is dependent on the type of fuel, or the nitrogen content of the fuel (see Table 4.3).

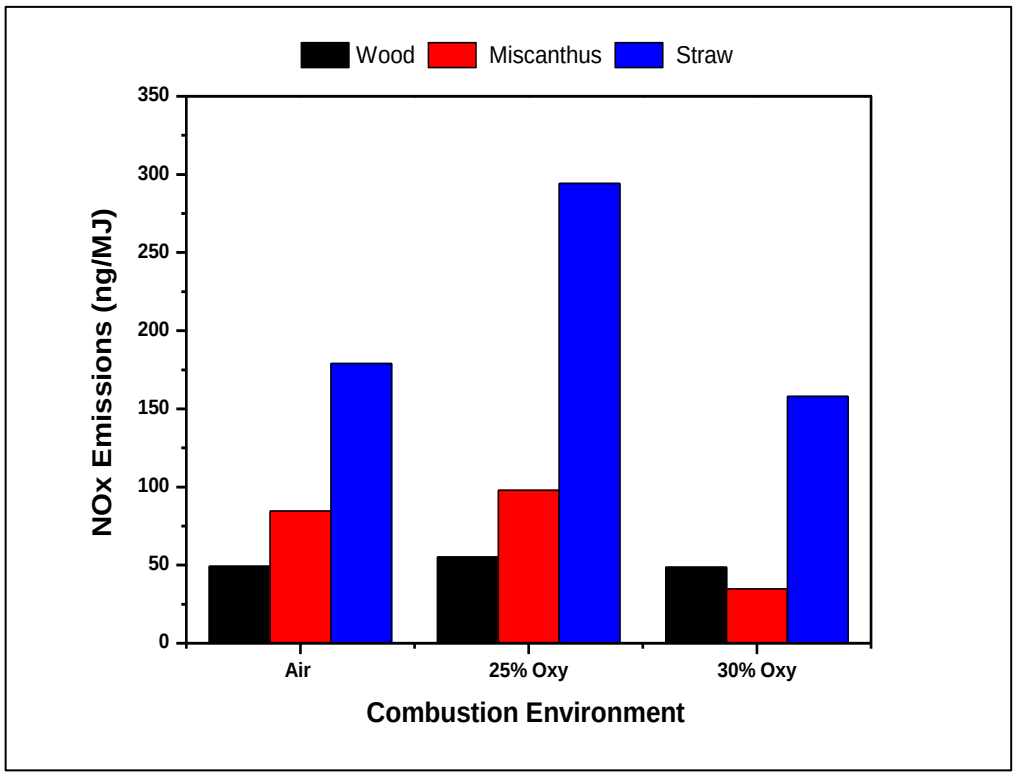


Figure 7.3: NOx emissions from different types of biomass fuels under air and different oxy-fuel combustion environment.

During biomass combustion (750–850 ^oC) fuel-N contents contribute to most of the NO formation. The fuel-N is split into volatile-N and char-N during the initial devolatilisation process. The volatile-N converts into either NO or N_2, while char-N along with oxidation of char reacts through a series of heterogeneous reactions [157]. The split percentage between volatile-N and char-N differs with the type of biomass; depends on the nitrogen content and volatility, but most importantly it is dependent on

combustion conditions (such as heating rates and temperatures). The formed NO can also be converted to N_2, similar to that prompt NOx formation, NO is reduced by hydrocarbons present in the biomass to volatile-N under fuel-rich conditions (most at low temperatures). The formed volatile-N mostly consists of hydrogen cyanide (HCN) and ammonia (NH_3). Finally these species react in a set of reactions and end up as NH and N, while the succeeding reactions to determine the formation of NO or N_2 are highly reliant on O/OH/H radical pool, which is related with the flame conditions, stoichiometry, composition, residence time and temperature [325, 326].

It can be seen in Figure 7.2 that the bed temperatures under oxy-fuel conditions of $21\%O_2/79\%CO_2$ and $25\%O_2/75\%CO_2$ are lower than those of air and oxy-fuel $30\%O_2/70\%CO_2$ for all type of biomass fuels. As a fraction of air was also supplied through the feeder to stop backfire from the main reactor during all tests under air and oxy-fuel combustion, the formation of thermal NOx and prompt NOx is also possible. However, the formation of thermal NOx should be insignificant due to low combustion temperatures while the formation of prompt NOx is also small due to overall oxidising conditions.

When the combustion environment was shifted from air to oxy-fuel the overall temperatures dropped in the combustor. Meanwhile, the oxy-gas mixtures flow rate was reduced to get a higher O_2 percentage in oxy-mixture but at the same time feed rate was keep constant due to which the bed became a fuel rich zone that was an ideal environment for NOx formation. These findings correlate with those from Klas Andersson et al. [170] they investigated NOx emissions in a 100 kW combustor

designed for oxy-fuel combustion of lignite. The effect of bed temperatures on the NOx formation was also studied; the bed temperature measurements against NOx emissions are presented in Figure 7.4. As predicted previously the NOx formations were high under low bed temperatures, especially when O_2 concentration was 21% and 25% in the oxy-fuel gas mixture. The reason for the low temperatures was the high concentration of CO_2 with higher heating capacity as compared with N_2 in air. The most affected biomass fuel because of bed temperatures and in terms of NOx emissions was wheat straw pellets with the highest fuel-N content 0.55% as listed in Table 4.3 in Chapter 4.

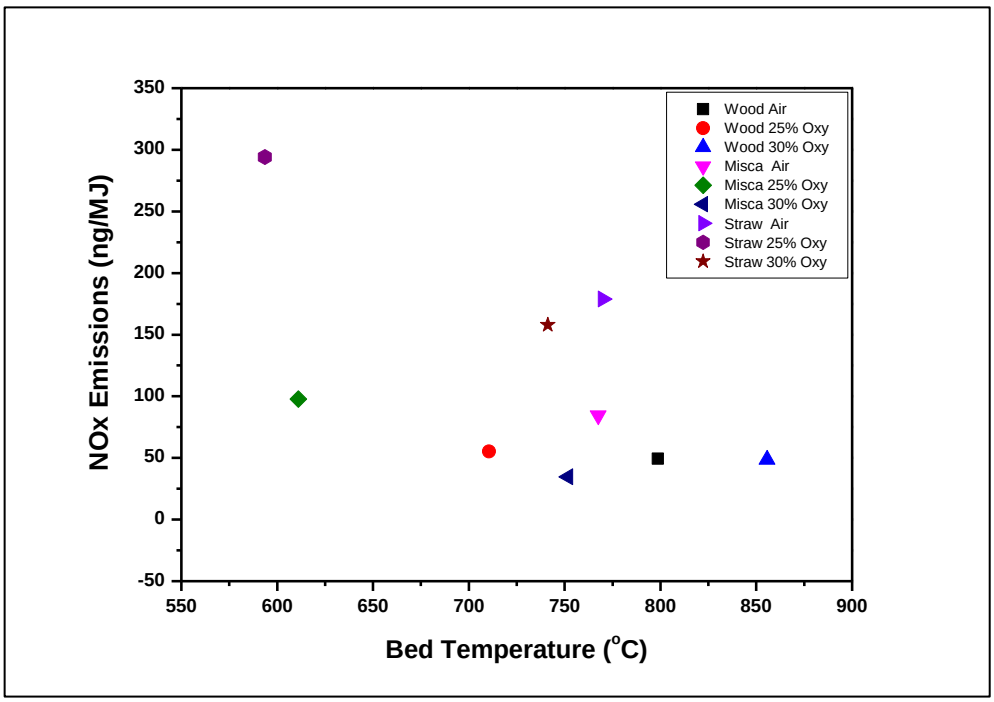


Figure 7.4: Effect of bed temperatures on NOx emissions for all type of biomass fuels under air and different oxy-fuel combustion environments.

Usually, devolatilisation process takes place within the bed zone of the combustor. The biomass fuels are characterised by high O/N ratio as compared with coal. The O/N mass ratio for wheat straw is about 56 which could lead to the formation of NO during

devolatilisation. Lin and Dam Johansen [326] found that 1–4% of the fuel-N directly converted to NO during wheat straw devolatilisation. By changing oxy mixture with $30\%O_2/70\%CO_2$ the temperatures inside the combustor were elevated to an almost same level as that of air and NOx emissions were significantly decreased as compared to oxy-fuel $25\%O_2/75\%CO_2$.

The formation of fuel NOx during oxy-fuel is mainly controlled by the oxygen partial pressure around the burning fuel particle, during this process, the temperature is less significant. This effect is less intense with high oxygen concentrations in the oxy-fuel mixture [327]. Skeen et al. [328] studied Nitric oxide (NO) emissions from sub-bituminous coal under air and oxy-fuel combustion conditions, when they replaced the combustion air with oxy mixture $30\%O_2/70\%CO_2$ no reduction in the NO emissions were noticed even by completely removing N_2 from the system, probably removing the thermal NO potentials. Due to limited studies on biomass oxy-fuel combustion, there are mix agreements between the researchers about the influence of bed temperatures on the level of NOx emissions [188, 327].

Jia et al. studied oxy-fuel combustion of bituminous and sub-bituminous coals in a circulating fluidised bed with global O_2 concentration 28.8%, they found almost similar NOx emissions as with air combustion for sub-bituminous, whereas they found by about only 50% reduction in NOx for bituminous coal [329]. The maximum reductions in NOx emissions were about 60% and 12% for miscanthus and straw pellets respectively, under oxy-fuel $30\%O_2/70\%CO_2$ compared to that under air combustion. Similarly, for domestic wood pellets, the reduction in NOx percentage was about 2% as it was the

biomass fuel with least fuel-N contents as given in Table 4.3 in Chapter 4. Hence, there was a tendency to decrease emissions rate with respect to NOx when changing from air to oxy-fuel combustion with a higher O_2 concentration in the mixture.

7.4.5 Effect of Combustion Environment on CO Emissions

The CO is formed during devolatilisation or from the oxidation of volatile matter present in the biomass fuel near the bed zone in FBC. The char-gasification reaction in splashing or freeboard zone could also cause CO formation. Moreover, during oxy-fuel combustion, the CO concentration is also governed by the reversible exothermic CO_2 dissociation reaction at high temperatures because of the higher partial pressure of CO_2 in the oxy-fuel gas mixture [311]. The results of CO emissions from different types of biomass fuels tested under air and oxy-fuel combustion are plotted in Figure 7.5. The worst situation arose when shifting from air to oxy-fuel 21%O_2/79%CO_2, the CO emissions reached the highest level for all types of biomass fuels. The reason behind it was the incomplete combustion of biomass due to low bed temperatures and unburnt char accumulation in the bed zone.

Similar findings were reported by Kimura et al. [164] during coal combustion on a bench scale 1.5 MW_{th} testing furnace. They observed the amount of unburned carbon was higher and the flame was dark and unstable as compared to air under O_2/CO_2 with oxygen concentration less than 30%. The main cause behind this observation was the specific heat of the main components (CO_2 and water vapours) was higher than that of N_2 which is to be reported the main diluting gas in air combustion. Furthermore, they

concluded that theoretically the oxygen concentration in O_2/CO_2 should be raised to 42% for matching the same adiabatic flame temperature to that of air combustion [164].

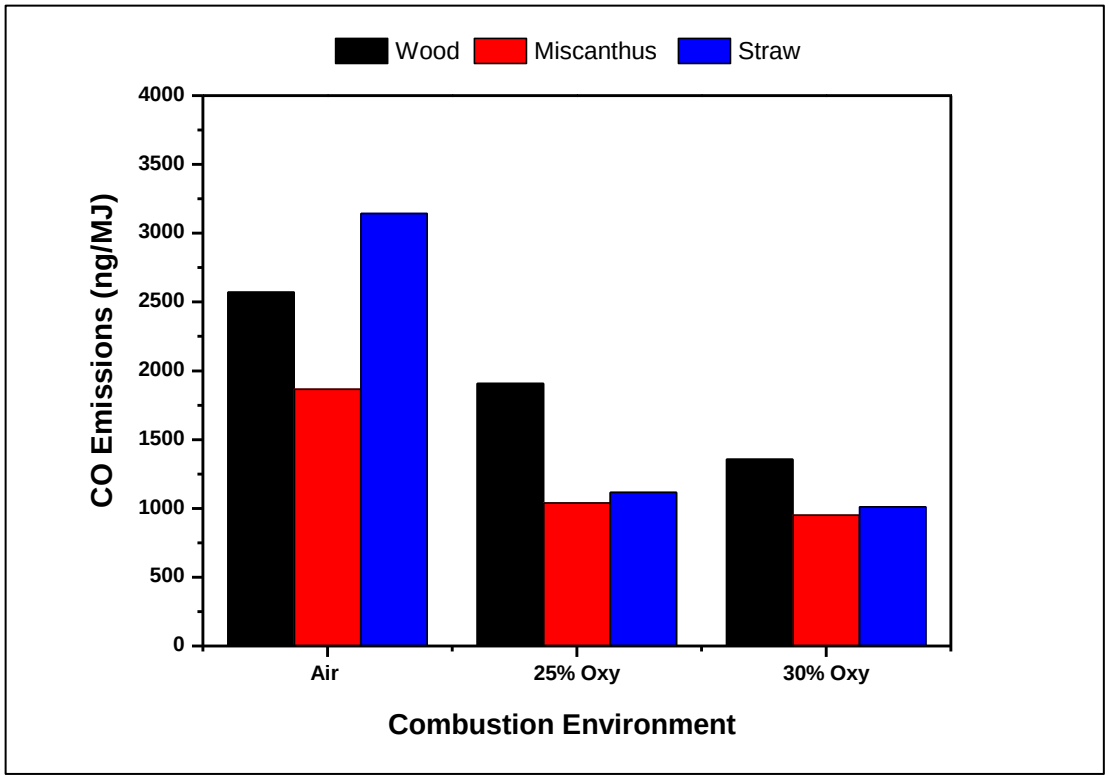


Figure 7.5: CO emissions from different types of biomass fuels under air and different oxy-fuel combustion environment.

The domestic wood pellets show the more elevated level of CO emission. Many factors could have attributed to the observed higher CO emissions for domestic wood pellets, e.g. the reactivity, size of the pellets and percentage of fines in the fuel etc. When the oxy-fuel mixture was changed with $25\%O_2/75\%CO_2$ a decreasing trend in the CO emissions level was observed but still these emission levels were higher than those under air combustion. It is quite clear that the temperatures in the bed and freeboard regions are much lower than air during oxy-fuel $21\%O_2/79\%CO_2$ and $25\%O_2/75\%CO_2$.

It is unlikely to be the Char-CO_2 gasification reaction behind these high CO levels as the temperatures are low. Further observations under oxy-fuel 30%O_2/70%CO_2 have revealed that CO emission at the lowest level for all type of biomass fuels. The oxy-fuel 30%O_2/70%CO_2 efficiently decreased the CO emission to a lower level than that of air (see Figure 7.5). The CO_2 flow rate was decreased to increase the O_2 concentration in the oxy-fuel 30%O_2/70% CO_2 mixture, which resulted in an increase in the fuel residence time in the dense bed region and hence consequently contributed to the lowering of the CO emissions at high temperatures with good combustion efficiency. Figure 7.6 shows the effect of CO emission on NOx level for all types of studied biomass fuels.

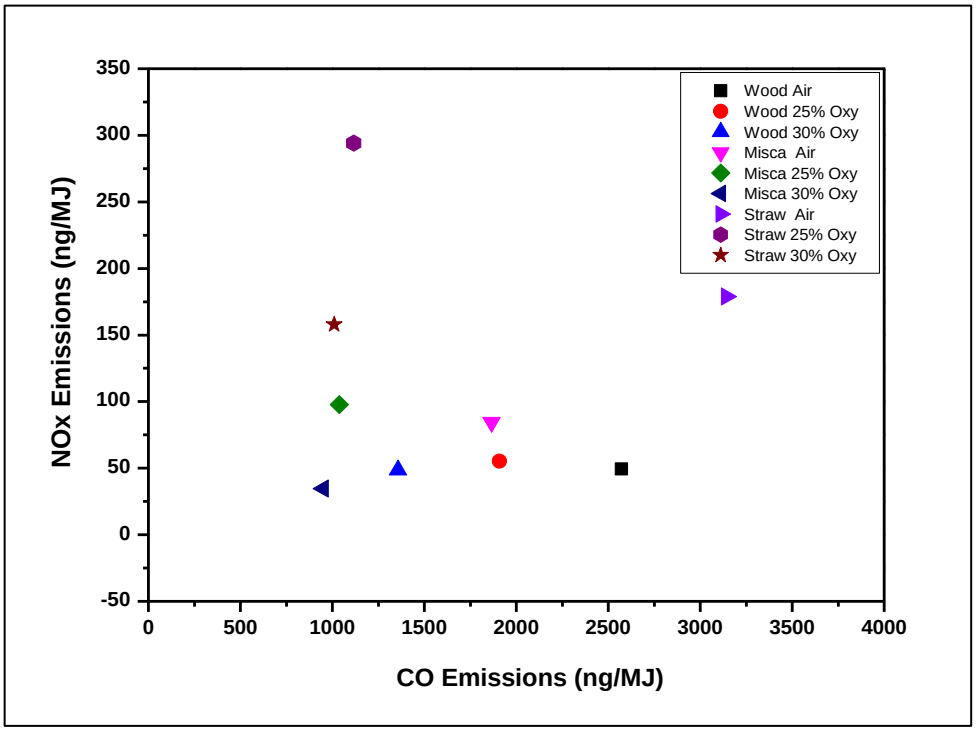


Figure 7.6: Effect of CO on NOx emissions for all types of biomass fuels under air and oxy-fuel combustion environments.

There is no such clear indication that high CO concentration within the combustor controls NOx emission during oxy-fuel, which was observed during air and staging air combustion experiments. These results contradict with the other researchers such as Lupiáñez et al. [327] studied two different types of coals in bubbling fluidised bed combustor under oxy-firing they found that NOx emissions are lower with higher CO. But this is also a fact that higher value of CO emission indicates lower combustion efficiency. The effect of the bed temperature on the CO emissions is presented in Figure 7.7. The influence of bed temperature on CO emission is quite clear for all types of studied biomass fuels especially under oxy 30%O_2/70%CO_2 when the CO values were at the lower levels than air combustion.

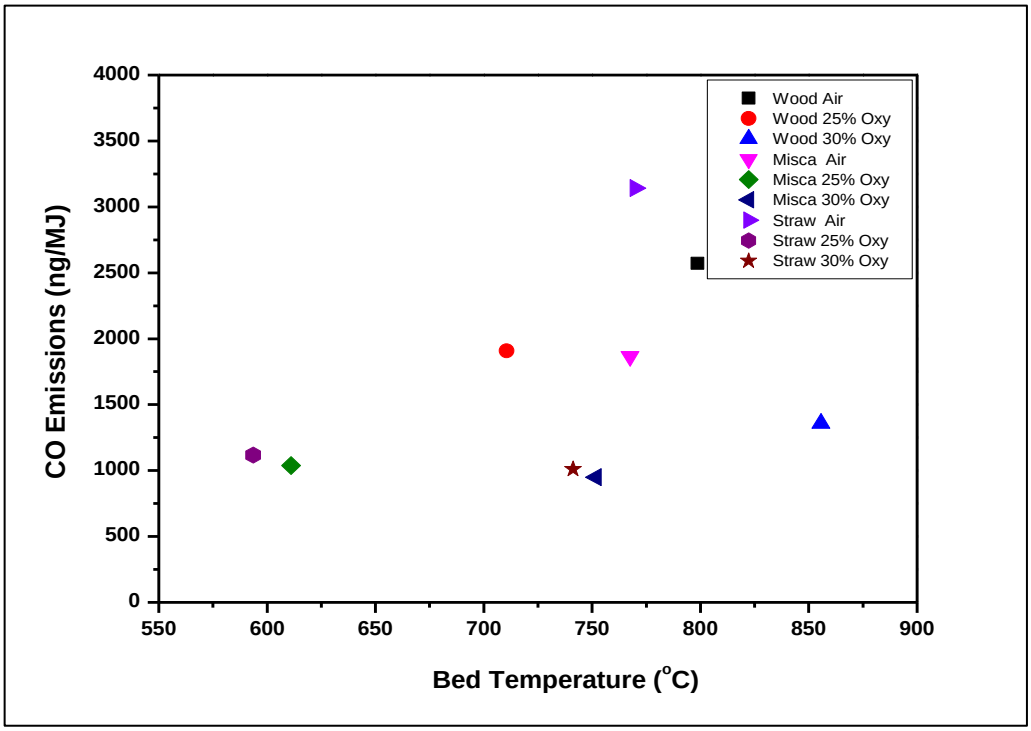


Figure 7.7: Effect of bed temperatures on CO emissions for all type of biomass fuels under air and different oxy-fuel combustion environments.

It's simple the higher bed temperatures the better combustion efficiency. During oxy-fuel, different trends of CO emission from the pilot scale tests are reported in the literature. The experiments conducted by Hjärtstam et al. [321] in Chalmers 100 kW test facility with oxy-fuel combustion reported lower CO emissions, whereas Rehfeldt et al. [330] studied air and oxy-fuel firing of lignite and bituminous coals in 0.5 and 1 MW scale combustion test facilities had stated a higher CO concentration and emissions intensity of flue gas under oxy-fuel compared with air combustion. Hence, overall CO emissions are mainly dependent on the fuel burnout, which is related to the fuel type, stoichiometry, and operating conditions. If the combustion is well controlled, managing CO emission is not a major issue during oxy-fuel combustion of biomass. On the average basis, the CO emissions during oxy-fuel $30\%O_2/70\%CO_2$ combustion conditions were reduced about 50–70% as compared with the air combustion for all types of biomass fuels except instability with $21\%O_2/79\%CO_2$.

7.5 Effect of Combustion Environment on Sintering and Agglomeration Behaviour

With the increasing use of fluidised beds along with operational experience, the agglomeration has more reported than infrequently as a major problem [231, 331, 332]. In the worst case, bed agglomeration may result in total defluidisation of the bed during the combustion process. However, the combustion process under air and oxy-fuel was mostly very smooth without any defluidisation indications for all types of biomass fuels. During the combustion of miscanthus and wheat straw pellets, the bed showed some type of agglomeration as the char was found to be bounded with sand particles but these

agglomerates did not cause any operating problem during the operation of BFBC. Recent studies have also shown that some new types of biomasses such as energy crops (non-woody) are problematic during combustion process [60, 333]. The bed agglomeration mechanism during fluidised bed combustion could be due to silicates melting (viscous flow), sintering, chemical reaction sintering and salt melting (reactive liquid) depending on precise the quantities of elements in the fuel composition and more importantly on the operating conditions during combustion process [334, 335]. To study more closely these characterise of the agglomerated bed particles for non-woody biomasses during oxy-fuel combustion, further analysis using SEM/EDX, XRD and XRF are required.

7.6 Summary

Three types of biomass fuels have been tested under air and various oxy-fuel combustion conditions and valuable operating experience has been obtained. The effect of combustion environment (air or oxy-fuel with different O_2/CO_2 ratios) on temperature profiles and the gas emissions (CO_2, NOx and CO) was systematically investigated. The experimental results showed that oxy-fuel combustion is different from air combustion in several ways, including reduced gas temperatures, delayed flame ignition, increased NOx and CO emissions under oxy-fuel $21\%O_2/79\%CO_2$ and $25\%O_2/75\%CO_2$. Several of these effects can be clarified by differences in gas properties between CO_2 and N_2, the major diluting gases in oxy-fuel and air combustion respectively. CO_2 has different properties from N_2 which influence both heat transfer

and reaction kinetics mechanism. The decrease in the bed temperatures about 150–175 ^{o}C was observed during oxy-fuel 21%O_2/79%CO_2 and 25%O_2/75%CO_2 combustion.

In oxy-fuel combustion, the CO_2 and H_2O levels are high in the combustor both having high emitting power which results in higher gas emissivities. Hence, to attain a similar gas/flame temperature under oxy-fuel the O_2 proportion in the mixture is typically 30%, as compared with that of air (21%). Depending on the acquired stoichiometry of biomass fuel and oxidant at the point of mixing, NOx emission levels showed both increase and decrease trends when changing from air to different oxy-fuel mixtures. Mixing at reducing conditions (less O_2 concentration in oxy-mixture) leads to an increase in the NOx formation, whereas NOx formation was inhibited at both combustion stoichiometry and fuel-lean conditions compared with air combustion. The presence of high CO_2 concentrations acted to increase the presence of OH radicals under fuel-rich conditions thus promoted the formation of NOx. When combustion occurred under higher O_2 excess (30%) conditions, the reduced formation of NOx was caused by a limitation of the O/H radical pool, particularly O, from the increased level of CO_2 in the oxy-mixture. The difference in NOx emission rates between air and oxy-fuel combustion were thus not expected to be caused by high CO formation.

The CO level was increased significantly during oxy-fuel 21%O_2/79%CO_2 and 25%O_2/75%CO_2 combustion compared to that air combustion but this level decreased dramatically under oxy-fuel 30%O_2/70%CO_2 with an average 60–70% decrease in CO emission as compared with air combustion. The volume of flue gas emitting through the combustor is to be reduced by which the extent is dependent on the flow rate of O_2 and

CO_2 in the oxy-fuel gas mixture, which was usually lower in the case of 25% and 30% oxy-fuel combustions condition during the experiments. The oxy-fuels tests with $30\%O_2/70\%CO_2$ have shown higher efficiencies than combustion with air, which remarks oxy-fuel combustion suitability for burning biomass fuels in BFBC.

Chapter 8

Bed Material and Ash Characterisation

8.1 Introduction

Regardless of broader applications of fluidised beds (FBs) for the conversation of solids fuels into energy, the technology is still facing some technical challenges; among others, agglomeration is one of the major operational issues during combustion of solid fuels. Agglomeration and sintering have been widely studied for coal combustion and co-combustion of biomass with coal, while less attention has been paid to the agglomeration problems resulted from biomass combustion and gasification in FBs systems. Agglomeration and sintering issues are more commonly found in biomass and low ranked coals applications. It is a well-established fact that agglomeration and sintering is an ash-related problem, which usually develops between the ash particles and bed materials in FBs [336]. However, the mechanisms responsible for agglomeration and sintering during biomass combustion in FBs suggested by other

researchers need to be further studied in detail in order to know the applicability of these mechanisms. The ash produced during combustion process is considered as one of the major influential constituents for agglomeration and sintering formation even in the absence of the other factors during the FBs combustion process. Moreover, the ability for agglomeration and sintering formation also depends on many other factors such as biomass fuel type, bed material used and localised temperatures during combustion. Many researchers identified that agglomeration and sintering is also associated with the composition of biomass, mainly alkali and alkaline earth metals (including their oxides) as these inorganic metals influence the type of alkaline silicates formed during the firing process [337-339].

Hence, it is vital to identify the particular elements (alkali or/and alkaline earth metals) causing the agglomeration in the biomass fuels. For detailed investigations about the agglomeration and sintering phenomenon, the surface morphology study of the formed agglomerates is also necessary. The surface morphology investigations reveal that agglomeration and sintering is heavily influenced by different combustion stages and temperatures (from the burning of char particle) during combustion of different fuels [339].

In this chapter, main fundamental aspects related to the agglomeration and sintering phenomena were investigated for biomass fuels combusted under air in a bubbling fluidised bed combustor (BFBC). The detailed findings on the characterisation of bed materials and ash samples collected from all experiments during air combustion are reported and discussed. The discussion also covers different types of observations,

which includes surface morphology, weight and colour changes of the bed material particles for different types of biomass fuels tested in BFBC.

8.2 Sample Preparation and Methodology

The Garside 14/25 sand was used as bed material during the combustion of all type of biomass fuels under air combustion. Specifications of the bed material were given in section 4.2.1 and the ash sampling procedure was described in section 4.6.1 in Chapter 4. The experimental analysis methods used for scanning electron microscopy and energy dispersed x-ray (SEM-EDX), X-ray diffraction (XRD) and X-ray fluorescence (XRF) were detailed in section 4.6.2, 4.6.3 and 4.6.4 respectively. During SEM-EDX analysis the spectra working distance was fixed at 13 mm and the high voltage was set at 20 kV. A range of magnifications (500×, 200×, 100× and 50×) with image working distance of 14 mm was used to get clear and magnified images of the samples with the selection of magnification being made according to the area of interest.

For EDX spot analysis, the interactive oxides method was applied to detect the exact composition of elements on a specific point of the agglomerate. For XRD, the powder X-ray diffractometer with parallel beam and very low intensity was used. The Cu$K\alpha$ radiation was applied and scanned from 10 to 80 °2θ with 0.05 °2θ step size and 6 s per step. As for evaluation, TOPAS V5 software was used. The crystallinity (i.e. the amount of crystalline phases vs. total) is estimated presuming the same elemental composition of the amorphous phase(s) as the crystalline. TOPAS V5 is a Rietveld refinement [239] software and uses principles of Hill and Howard [240] for quantities' computation.

8.3 Results and Discussion

Five different types of biomass fuels including domestic wood, industrial wood, miscanthus, wheat straw and peanut shell pellets were tested in the 20 kW_{th} bubbling fluidised bed combustor (BFBC). The process flow diagram of the BFBC is shown in Figure 4.7 in Chapter 4. As mentioned previously Garside 14/25 sand was utilised as a bed material during all combustion experiments. The testing was not a continuous process, each test lasted for 8–12 hours of operation. For repeatability and authenticity of the produced results, each biomass fuel was tested for 3–5 repeated runs with a total of 30–36 hours of operation.

The average temperatures in the BFBC during combustion under air were between 750–850 ^{o}C, as discussed in detail in section 6.3.3 in Chapter 6. The agglomeration or sintering can cause defluidisation, which leads to unscheduled plant shutdowns and extra costs for maintenance. The defluidisation can be indicated by a sudden decrease in the pressure drop across the bed [340]. The temperatures are another indicator during defluidisation. Just before defluidisation the bed temperatures rises rapidly due to poor mixing of fuel in the bed zone [231]. All the temperature and pressure parameters were consistently monitored during the testing, but there was no defluidisation being observed during any type of biomass fuel combusted in the BFBC.

8.3.1 Visual Observations

At the end of each set of experiments with a specific biomass fuel, the bed of sand was opened for observations and samples were collected. Then the bed material replaced

with fresh sand for next fuel's testing. The bed materials collected after the combustion tests of all biomass fuels are shown in Figure 8.1.

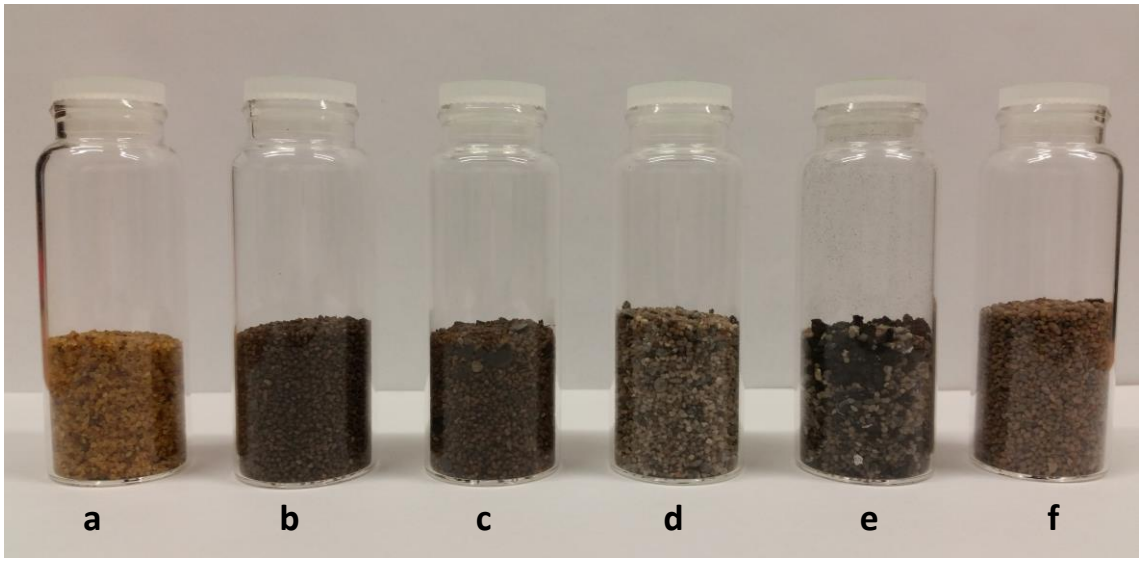


Figure 8.1: The bed samples collected from different biomass fuels; (a) fresh sand, (b) domestic wood, (c) industrial wood, (d) miscanthus, (e) wheat straw and (f) peanut shell.

From visual observations, it was discovered there were big black particles bonded together in the bed material during wheat straw pellets combustion, as shown in Figure 8.1(e). It was also noticed that after each set of combustion tests, the bed materials changed into different colour depending on the biomass fuel used; from yellowish brown (original colour) to brownish black (domestic and industrial wood), grey (Miscanthus), greyish black (wheat straw) and dark brown (peanut shell) colours. The change in the shape of the sand was also noticed in some cases after the combustion tests.

This change in the colour of the sand is probably partly related to the thermal decomposition or oxidation of Fe_2O_3 present in the Garside 14/25 sand (see Table 4.2).

Moreover, the change in the colour of the sand during combustion was found to be dependent on the temperatures and type of biomass fuel combusted with sand [341]. The cyclone container was also emptied after each test run and the cyclone ash samples were collected for further analysis. These bed materials and cyclone ash samples were characterised to establish the mechanism of agglomeration and sintering tendencies during the combustion of different biomass fuels in BFBC.

8.3.2 Agglomeration during Air Combustion

A degree of agglomeration was found during the wheat straw pellets combustion under air as the sand particles were found to be bounded with each other. The real agglomerates can be seen along with bed sand particle in Figure 8.2.

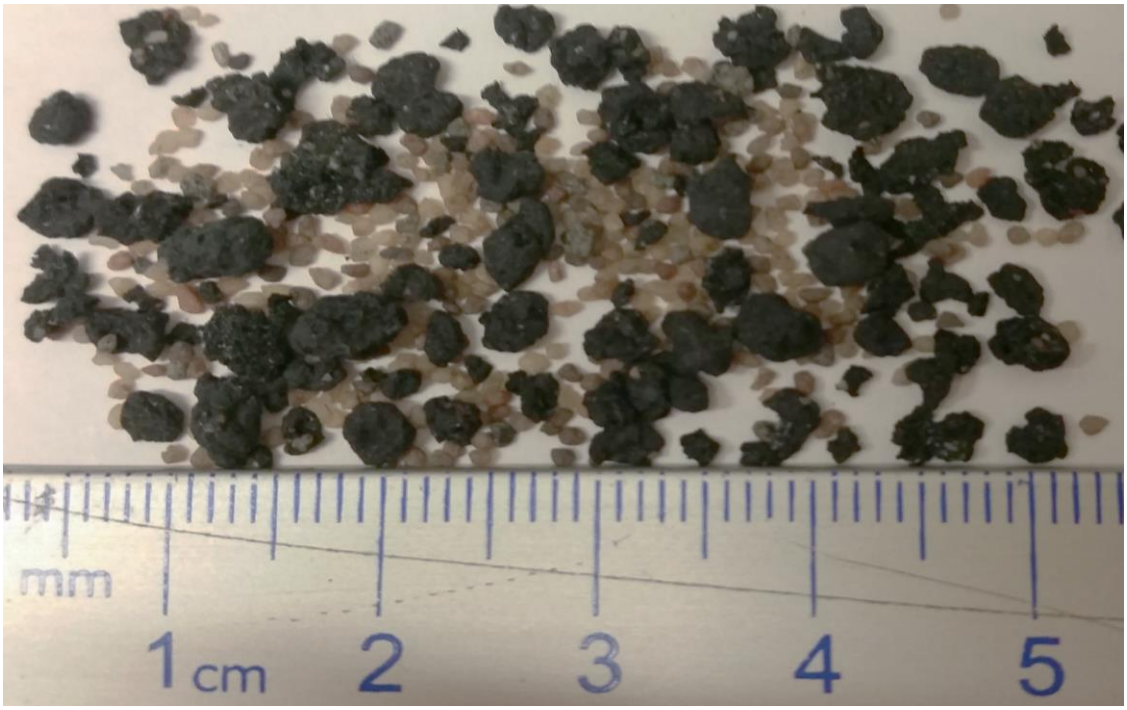


Figure 8.2: The bed material along with agglomerates from wheat straw pellets combustion in BFBC.

The average size of the agglomerates was in the range of 2–4 mm after three testing runs, approximately 30–36 hours of combustion time. The agglomerates were almost round shaped in black colour; it was difficult to distinguish between the sand particles inside of agglomerate. There was no agglomeration observed with any other biomass fuels in the BFBC. The agglomeration observed with wheat straw pellets combusted at 750 ^{o}C could also be due to poor fluidisation, low density and higher porosity as compared with other types of biomass fuels used during combustion. In order to assess the fuel chemical nature and reasons behind these agglomerates, further investigations were performed.

8.3.3 Bed Material Analysis

The results of bed material analysis for all types of tested biomass fuels are presented in Figure 8.3 and Figure 8.4. The detailed composition of all studied bed materials along with their elemental oxides are listed in Appendix E. It is noticed that the bed materials resulted from the combustion of peanut shell and wheat straw contain the highest potassium (K) contents of about 13% and 11% respectively as compared with other fuels' bed materials. Moreover, the industrial wood bed material contains the highest Aluminium (Al) content of ca. 10%. All bed materials also contain a sufficient percentage of Calcium (Ca) except domestic wood pellets. During combustion, the bed material behaves like a sink of the sand with ash from the biomass fuel along with its elements. Usually, less volatile elements such as Al, Si, Mg, P and Ca are present in the bed material but some of other elements with more volatile characteristics like Na and K are less often to be retained in the bed material [342].

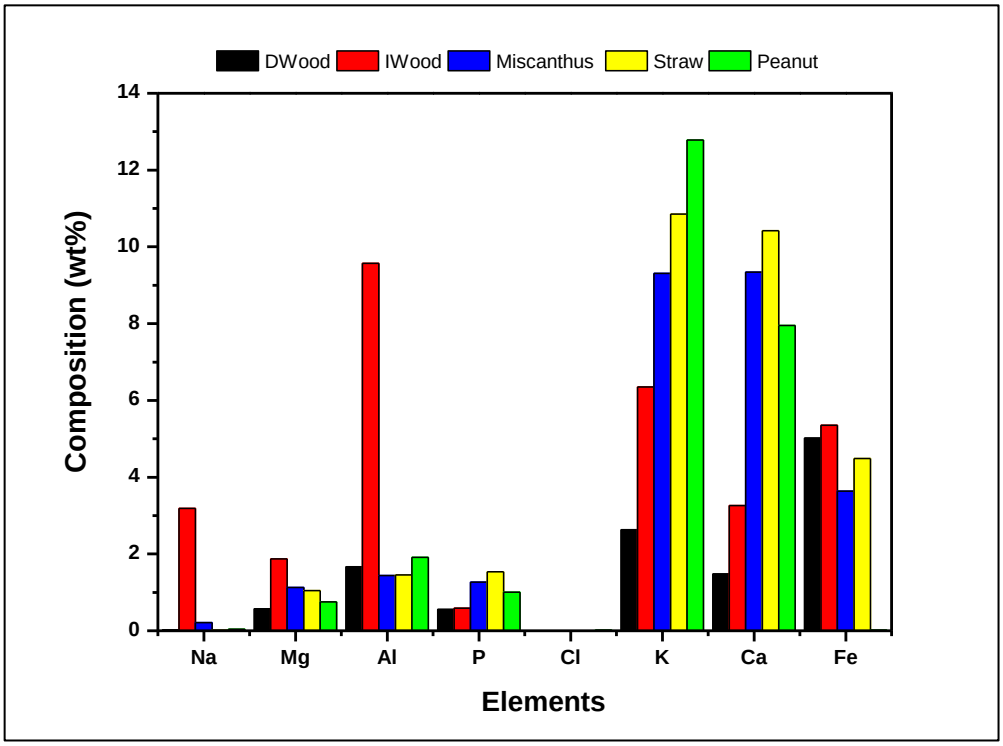


Figure 8.3: The XRF elemental composition in the bed material obtained from different biomass fuels under air combustion. All results are C and O free basis.

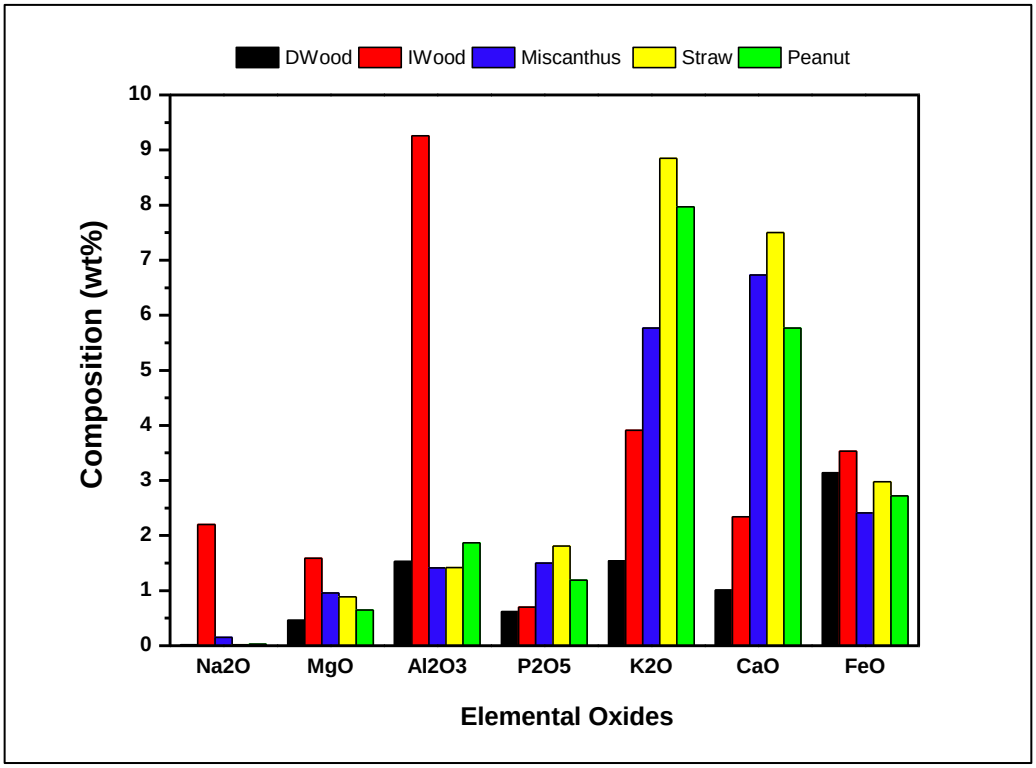


Figure 8.4: The XRF elemental oxides composition in the bed material obtained from different biomass fuels under air combustion.

We already know from the previous observations that wheat straw bed material was affected with agglomeration and this is the biomass fuel left with the second highest K content in the bed material. Moreover, the higher the element retained in the bed, the fewer emissions are associated with that element in the stack. It is also apparent from Figure 8.3 that K is the element mostly retained in the bed material compared with all other elements. When sand (quartz) is used as the bed material in FBC systems, the ash formed during combustion can act as glue or binding medium in the formation of agglomerates.

Hence, it significant to know how the components from ash are transported to the surface of the sand particles. During combustion, the temperature inside the burning particle of char could be significantly higher than that of the bed material. The high temperature can cause the inorganic matter inside the particles to come out to the surfaces. When the bed particles hit the burning particles, they can stick together forming the agglomerates. The burning particles may be molten at bed temperatures as low as 750 ^{o}C, making the particles as a binding medium and catching the sand particles upon collisions.

At temperatures as high as 900 ◦C or above, the burning particles could be completely molten and come in the form of a viscous liquid. When the sand particles collide with these burning particles the liquid could be coated on the surface of the solid bed particles. The condensation of gas evaporated from the burning particles at the surface of bed particles at high temperatures is another possible way of coating formation. Lin et al. [343] studied agglomeration phenomena in fluidised bed combustion of straw and

found that K-rich crystals on the surfaces of the bed material were responsible for the coating formation route. The studied biomass fuels are also enriched with Ca but Ca is unlikely to be considered as the main player in the formation of agglomeration due to high melting points of its compounds [233]. Moreover, some literature reports that K and Na are the two principle elements backing agglomeration during fluidised bed combustion; additionally, Ca decreases agglomeration potential rather than taking a part in this process [344].

Various mechanisms are anticipated on the interactions between ash and bed material particles. Öhman et al. [334] proposed three stages of agglomeration mechanism based on their experimental studies. First of all, ash is being deposited on the bed material surface through a combination of the small particles attachment on the bed particle surface followed by the gaseous alkali condensation and chemical reaction of the bed material surface with these alkali species. Secondly, as the constant deposition on the bed particles continues, the internal coating layer is perhaps homogenised and reinforced by sintering and finally the agglomeration of bed particles, controlled by inter-particle adhesive forces. As temperatures increase during fluidised combustion, the fraction of ash melting increases and the viscosity of this melted substance decreases. As a result of the combination of these factors, the stickiness strength of the bed sand particle coated with ash increases. This finally accelerates the agglomeration process.

The wheat straw behaviour is quite different during combustion in FBs. The wheat straw ash starts melting even at low temperature of 750 ^{o}C and only a small fraction of ash is left to evaporate at higher temperatures. It is already mentioned that the

temperatures during this study were between 750–850 ^{o}C. Most probably during these temperatures the wheat straw ash was already started melting, these observations correlate with those presented by Lin et al. [231]. After this, the K starts accumulating on the bed surface during combustion which increases with time. Therefore, little K was released to the gas phase during wheat straw combustion in BFBC, which is also indicated by Figure 8.3 and Figure 8.6 with the high K content. The XRD spectrum of wheat straw cyclone ash is shown in Figure 8.5, the K element present in the wheat straw pellets was converted into Sylvite (KCl) about 52%.

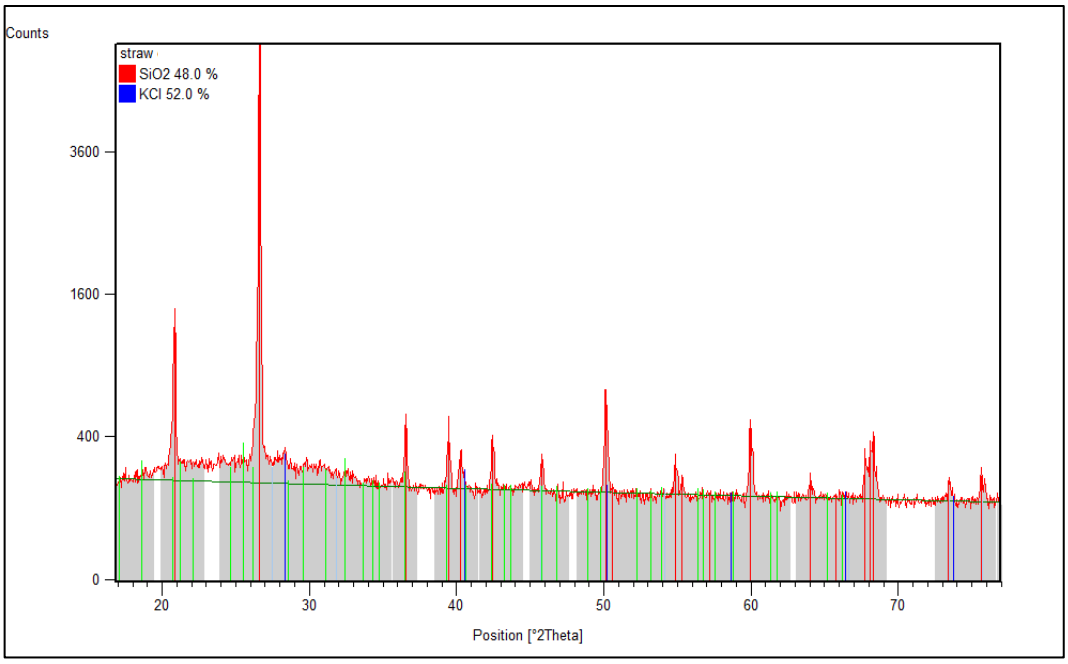


Figure 8.5: The XRD spectrum of wheat straw pellets cyclone ash.

Moreover, the wheat straw bed material's XRD analysis also indicated the presence of Sylvite (KCl). The XRD spectrums of all bed materials along with cycle ash samples are given Appendix E. The results indicate that the coating on the surface of the bed particle may be too thin to be exactly detected by this method. The peanut shell is the biomass fuel with the highest potassium but it did not show any type of agglomeration

during combustion, the possible reason behind it is different volatilisation temperature of potassium in various biomasses [345].

8.3.4 Cyclone Ash Analysis

The biomass ash characteristics are usually different from other fuels such as coal. The composition is dependent on the type of biomass plant and harvesting conditions. The main elemental ash compositions of all tested biomass fuels are presented in Figure 8.6, while the full compositions of these ashes with elemental oxides are listed in Appendix E. Biomass ash is normally dominated by calcium (Ca), silicon (Si), potassium (K) and contains a small amount of aluminium (Al). Si is primarily present in the form of hydrated silica grains, while K is spread in the form of ionic and organometallics [345].

The studied biomass fuels have similar ash elemental compositions as reported by others in the literature [57, 60, 346]. The peanut shell and wheat straw have the highest K content, whereas the industrial wood ash contains the highest Ca as compared with other biomasses. The K is most likely to be volatilised with other organic species during the combustion process. If chlorine (Cl) is present in the fuel then it may be released in the form of KCl, while in the absence of Cl, carbonates, oxides, hydroxides or sulphates could be formed [347]. It is also clear from the XRD spectrum results of wheat straw that most of the K is converted into Sylvite (KCl) which is helping in the formation of agglomerates during combustion. The main elemental oxides present in the ash of studied biomass fuels are presented in Figure 8.7.

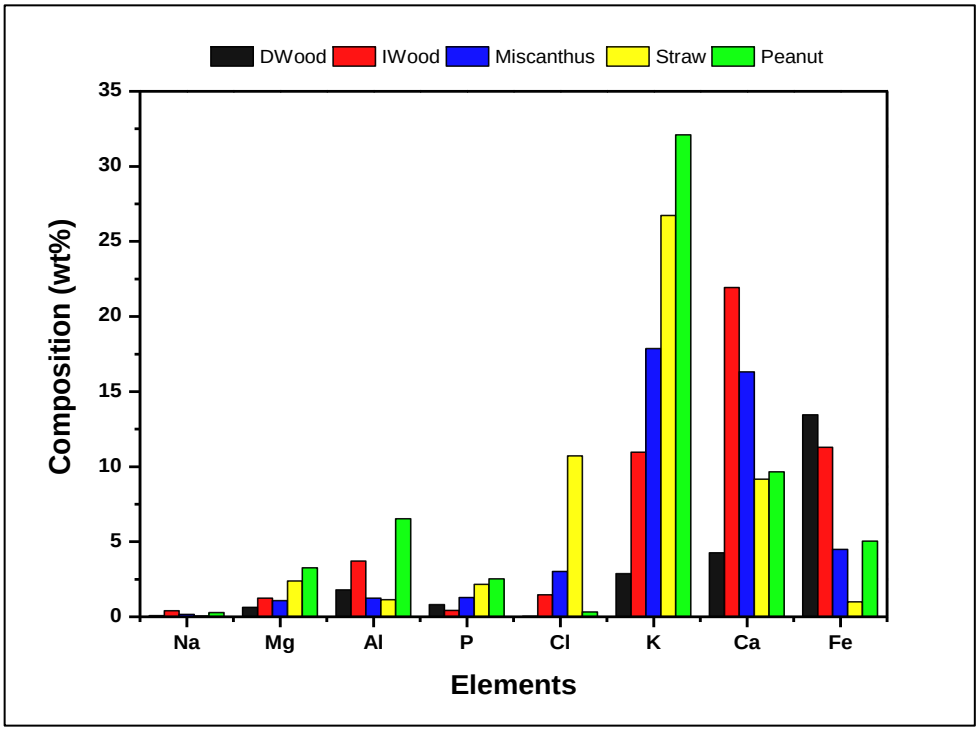


Figure 8.6: The XRF elemental composition in the cyclone ash obtained from different biomass fuels under air combustion, the results presented are without Si.

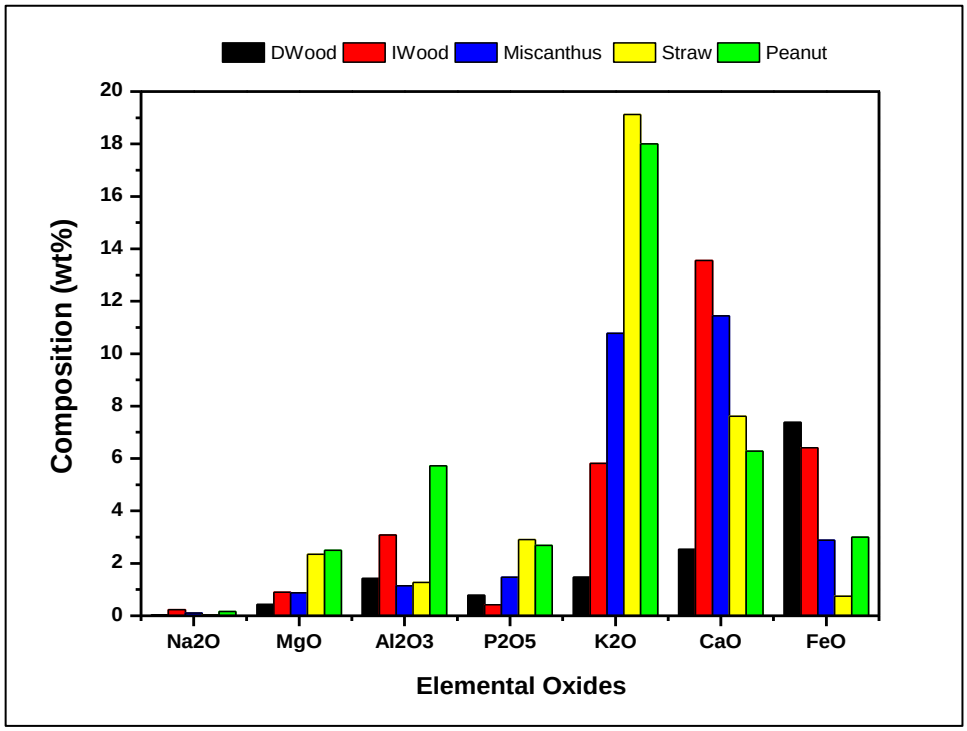


Figure 8.7: The XRF elemental oxides composition in the cyclone ash obtained from different biomass fuels under air combustion, the results presented are without Si.

The results show that wheat straw has the highest K_2O content followed by peanut shell and miscanthus respectively. It has been reported that an ash with less alkali element, higher Al and less Ca is expected to reduce deposition and corrosion problems during combustion of woody biomasses in FBs [348].

Olanders and Steenari [345] studied the characterisation of wood and straw ash, they identified that during ash formation the alkali and alkaline earth metal ions present in biomass were primarily associated with carbonate, sulphate and chloride ions. Skrifvars et al. [349] used different characterisation techniques from various biomass fuels' ash and found that ashing temperatures within the range of 700–900 ^{o}C have not significantly affected the elemental composition of the ash. This indicates that the K compounds may not be released to the gas phase during FB combustion but have a tendency to remain in the ash by recapturing of the vapours by some other mineral compounds present in the ash. Which is also evident from Figure 8.7 that most of the K present in the wheat straw biomass was converted to K_2O (about 19%). This indicates that K_2O-rich ash helps in glueing the particles together and finally creating agglomerates. It has also been observed by the other researchers that the presence of K is seen to be an acute contributor in the formation of agglomeration [65, 103, 350].

Thus biomass fuels containing high K_2O are also more likely to cause agglomeration during combustion [154, 351]. Several researchers have reported agglomeration and de-fluidisation occurrence in fluidised bed biomass combustion and gasification. Ergüdenler and Ghaly [65] studied wheat straw gasification in a fluidised bed using bed material of silica sand. They found that when temperatures reached 800 ^{o}C, the

agglomeration occurred followed by severe defluidisation when temperatures exceeded 800–820 ^{o}C. Their findings disclosed that the main contributor to agglomeration phenomenon was the high content of K in the wheat straw ash. Grubor et al. [352] reported defluidisation problems due to agglomeration in continuously fired BFBC during straw combustion even at temperatures below 700 ^{o}C and as a result, they had to shut down the plant 2–3 times during a month. The possible reason behind this was mentioned was the presence of alkali silicates in straw which melt at low temperatures during combustion.

8.3.5 Surface Morphology and Spot Analysis

A perfect way to identify the constituents that encourage agglomeration is to analyse the coated surface of the particles. For this reason, all types of bed materials along with agglomerates sampled in the course of experiments were physically observed and then examined by SEM/EDX analysis. The agglomerates collected from the bed sand were very hard and were not breakable by fingers. The agglomerates were in a different size up to 4 mm from the fresh sand and some of them were a few sand grains glued together and in black colour. Numerous SEM/EDX analyses were performed on different types of studied bed materials and agglomerates. Some of the most illustrative and explanatory SEMs results are discussed in this section.

The typical images captured for different bed materials from SEM are shown in Figure 8.8. It can be seen that domestic wood and miscanthus pellets' bed materials showed some broken and damaged sand particles. On the other hand, industrial wood bed

material was seen to contain some sharp edge sand particles. This change in the shape of the bed particles could be associated with different fluid dynamic behaviours during biomass combustion at different temperatures in BFBC. The peanut bed particles looked shiny with polished surfaces. In wheat straw agglomerates the ash flakes were linked with bed particles and some particles were attached together by necks.

Most of the grain surfaces were covered with ash but some surfaces were smooth as well. It is also noticeable from SEM images that bounded and/or coated particles have a glossy appearance, which gives an indication of a molten viscous liquid presence during combustion in BFBC. The SEM analysis of typical agglomerates from wheat straw bed material is shown in Figure 8.9. The ash and agglomerate appearances suggest that the wheat straw ash has been melted and the holes on the SEM figure are evident that evaporation from inside has occurred. The bed particles were either glued with ash or necked together by the molten substance on their surfaces.

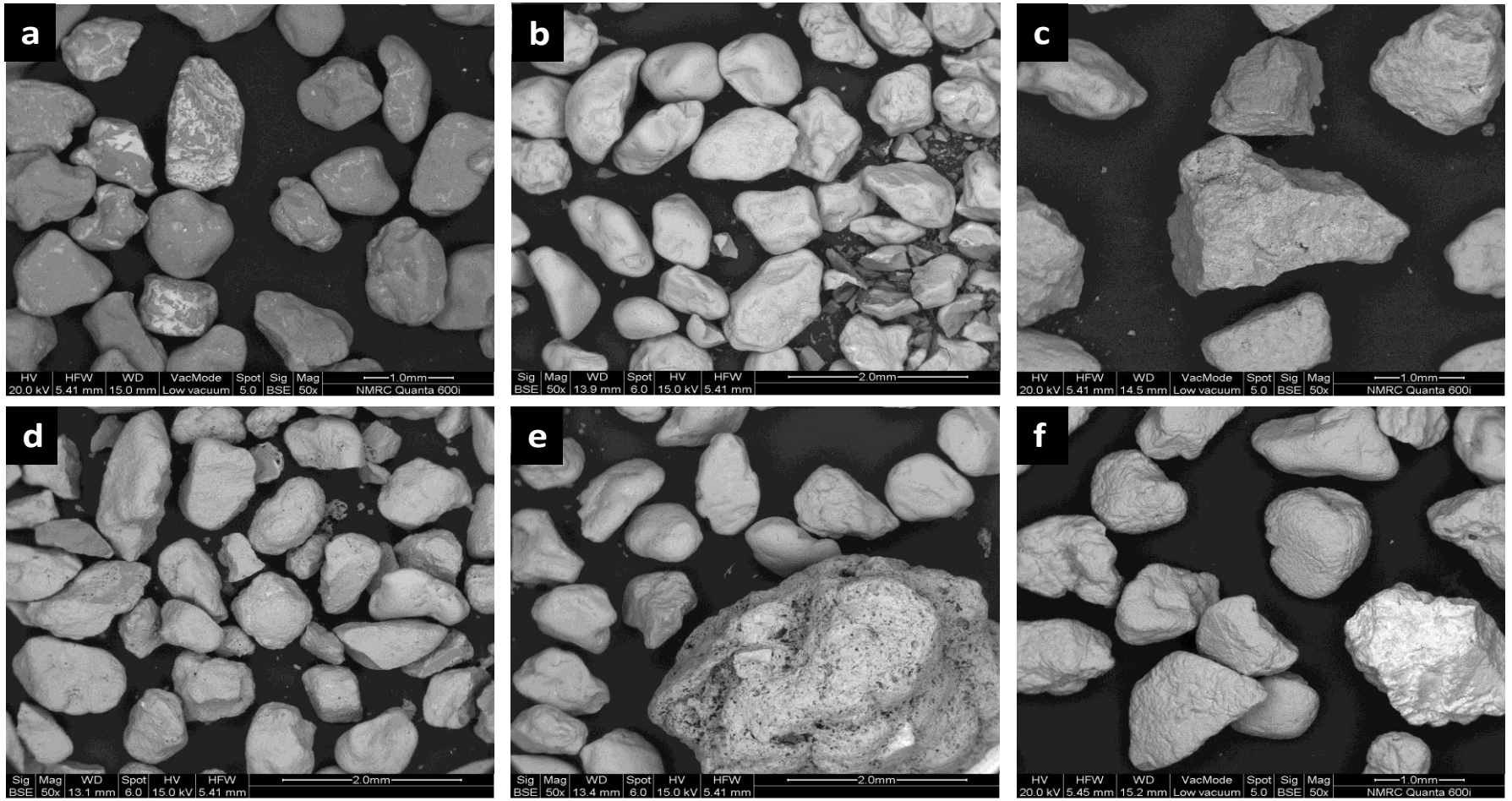


Figure 8.8: SEM micrographs from different bed material at 7.0 ×7.5 cm scale; (a) fresh sand, (b) domestic wood, (c) industrial wood, (d) miscanthus (e) wheat straw and (f) peanut shell.

The SEM micrograms also tell that the coating layer on the bed particle surface was not uniform but with variable thicknesses. Even though the fact that there is no coating on some particles or partially coated surfaces as can be seen in Figure 8.8. These non-uniform coating layers that do occur are enough for the formation of agglomerates and therefore a hindrance to the performance of the BFBC.

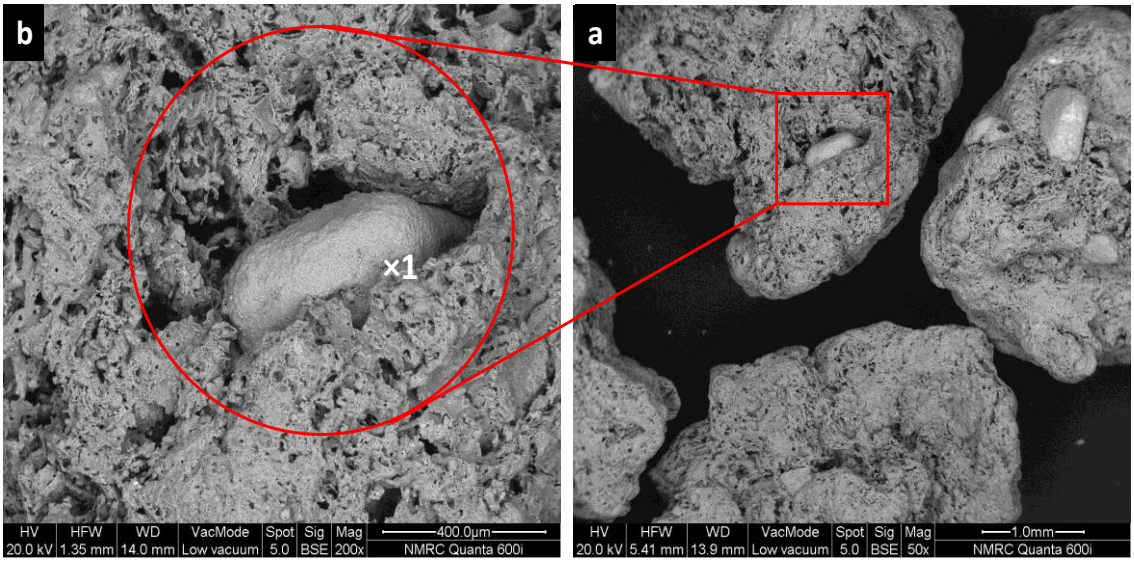


Figure 8.9: SEM micrograph images showing the internal structure of agglomerated bed material at different magnifications; (a) agglomerated bed materials particles, (b) typical agglomerated particle magnified showing the spot analysis point.

Philip et al. [353] reported the similar type of mechanism while controlling agglomeration in a CFB during the combustion of a low-rank coal. They found that the surface tension, thickness and viscosity of the sticky layers were adequate for the formation of agglomerates. This is believed that the agglomerates formed during this study could grow to substantial sizes with increasing quantity in a longer period of operation. For the better understanding and to know the exact chemical composition of the agglomerate formed, an elemental EDX spot analysis with mapping was performed,

the white cross at point 1 marked in Figure 8.9 identifies the precise location of the spot where analysis was performed. The elements from the spot analysis on the agglomerate ash flake are shown in Figure 8.10. The analysis found the major elements Si, K and Ca and traces of Al. These typical elements are also present in the form of SiO_2, K_2O and CaO. The K was found to be the second most abundant element after Ca (Ca-19.06%, K-14.24%). The most abundant elemental oxides are SiO_2 (42.04%), CaO (26.66%) and K_2O (17.15%).

Element	Wt%	Elemental Oxide	Wt%
C	0.00	Na_2O	0.00
O	39.62	MgO	1.80
Na	0.00	Al_2O_3	0.88
Mg	1.09	SiO_2	42.04
Al	0.47	P_2O_5	2.42
Si	19.65	SO_3	5.80
P	1.06	K_2O	17.15
S	2.32	CaO	26.66
Cl	0.00	TiO_2	0.01
K	14.24	Cr_2O_3	0.26
Ca	19.06	FeO	2.91
Ti	0.00	ZnO	0.05
Cr	0.18		
Fe	2.26		
Cu	0.02		
Zn	0.04		

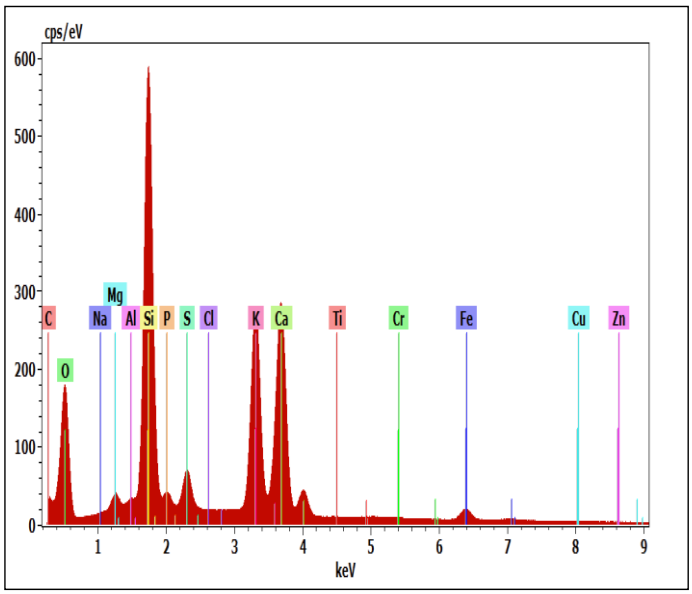


Figure 8.10: EDX elemental spot analysis with elemental spectrum at point 1in agglomerated bed material mentioned in Figure 8.5.

The SEM and elemental EDX spot analysis findings confirm that not only wheat straw ash combine the bed particles together but the rich coating of K on the particle smooth surfaces also contribute towards stickiness in agglomerates. This layer of coating could

be present in the liquid phase during combustion, which was the possible main reason for agglomeration.

8.3.6 Control of Agglomeration

Agglomeration is serious technical issues during FBs combustion which could result in defluidisation but not under all conditions. Defluidisation could occur once the rate of particle agglomeration is greater than the rate of particles separation [354]. As previously concluded from the results of this study one of the main reason of the agglomeration was the formation of low melting point eutectic in the result of the reaction between vaporised alkali (K) and bed material (Si). Therefore, some suggestions to avoid the formation of agglomeration during BFB combustion are; use of greater particle diameter bed material because bigger particles have less overall surface area, use of an alternative bed material which does not cause agglomeration at the specific operating temperatures, use of bed additives which can bind volatilised alkali before it reacts with bed particles and finally try to control operating temperatures in the combustor.

8.4 Summary

The experimental results of bed material and ash generated in a pilot scale BFBC burning five different types of biomass fuels were presented and discussed. All bed materials and cyclone ash from the combustion of various types of biomasses were regularly sampled and then were analysed by SEM-EDX, XRD and XRF analysis. The experimental results show that elemental ash composition of the biomass and the

operating temperature are the important parameters affecting agglomeration. As all of the experiments were conducted under similar combustion conditions with varying levels of stoichiometry.

There was no agglomeration detected except for the combustion of wheat straw and this indicates that the combustion stoichiometry has no or minor effect on the formation of agglomeration. The SEM and EDX analysis results show there are substantial differences in the structures and compositions of the agglomerates from wheat straw and other biomasses materials investigated. The agglomeration formed during combustion is largely due to the high content of potassium in wheat straw ash. The potassium in wheat straw involves a transformation from organic and inorganic forms to various amorphous salts. Most of these compounds have a tendency to remain in the bed at temperatures below 900 ◦C which is the top end of the operation temperatures in FBs combustion.

Based on the experimental results and looking at different agglomeration mechanisms proposed by other researchers, the melting of these compounds is clearly identified as the coating layer on the bed particles which eventually formed agglomerates. There are some alternative methods which can be utilised to avoid agglomeration during BFBC, such as using alternative bed material, reducing combustion temperatures or using bed additives.

Chapter 9

Conclusions and Future Work

The literature review has shown that the biomass is a carbon neutral fuel which could be used as a renewable source of energy. Biomass also has a potential to replace fossil fuels, which are the main contributors to the GHG emissions. Bubbling fluidised bed combustion is an efficient technology primarily for use of low-grade fuels such as biomass with high moisture content. The biomasses containing alkali and alkaline earth metals are problematic during combustion in fluidised beds; these metals are one of the factors causing sintering and agglomeration during combustion. There is more research required about the mechanism for sintering and agglomeration during non-wood biomasses combustion in fluidised bed combustor. Oxy-fuel combustion is found to be a promising technology for carbon capture and storage but still under development.

There are a number of technical uncertainties and challenges which need to be addressed such as; matching gas temperatures, flame stability, oxidant separation cost

optimisation, emissions under CO_2 rich conditions, slagging and fouling as well as the integration of the oxy-fuel system. Moreover, the pure biomass combustion under oxy-fuel environment in fluidised beds is less investigated than coal combustion or co-firing with coal and hence more research is required to clarify the full consequences of biomass combustion in oxy-fuel combustion boilers and their application potentials in the power plants.

A bubbling fluidised bed combustor (BFBC) with a capacity of 20 kW_{th} was designed, manufactured, commissioned and successfully tested for different solid biomass fuels. The BFBC system was operated for more than 350 h (accumulated) at temperatures between 750–850 ^{o}C without any problem or emergency stopovers. The testing and operation of the system proved the feasibility of applying un-staged, air-staged and oxy-fuel combustion technology with five different types of biomass fuels without accounting any technical difficulties. The results presented in this thesis cover four major aspects regarding biomass utilisation for power and energy production both for the convention air and oxy-fuel firing systems: (1) combustion fundamentals in TGA, including devolatilisation and burnout temperatures, (2) combustion tests of five different biomass fuels under air firing conditions, focusing on temperature distribution and air-staging for emissions reduction in the BFBC , (3) combustion tests under oxy-fuel firing conditions, focusing on the gas temperature profiles and emissions of pollutant species in the BFBC, (4) An investigation of agglomeration and sintering mechanism of the studied biomasses under air firing conditions.

9.1 Combustion Fundamentals

The thermal behaviours of six different biomass fuels including barley straw, miscanthus, waste wood, wheat straw, willow SRC and domestic wood have been examined in order to evaluate their practicality for energy production, using non-isothermal thermogravimetric analyses (TGA) under N_2, CO_2, air (21%O_2/79% N_2), CO_2 and selected oxy-fuel (30% O_2/70%CO_2) atmospheres. The results under N_2 (190–460^oC) and CO_2 (198–415^oC) in devolatilisation zones show almost identical weight loss (R), reactivity (R_M) and activation energy (Ea) profiles. However, when devolatilisation occurred under CO_2 conditions at temperatures higher than 700 ^oC, an additional weight loss was observed for all types of biomass fuels, indicating the contribution of CO_2-char gasification reaction. The results of air and oxy-fuel combustion (30% O_2/70%CO_2) show almost similar profiles for R, R_M and Ea. In oxy-fuel atmospheres, a slight increase in the maximum rate of weight loss (R_{Max}) was observed in both reaction zones for all the studied biomass fuels. Significantly high rate constants and activation energies were observed for the biomasses which are most likely with low lignin contents as compared to the other biomass fuels.

9.2 Un-staged and Air-staged Combustion

Five different biomass fuels, three non-woody (miscanthus, wheat straw, peanut) and two woody (domestic and industrial wood) biomasses, were tested in the newly designed 20 kW_{th} BFB combustor. The effects of excess air and air staging at two different heights above the distribution plate (AS1–70 cm and AS2–110 cm) on NOx and CO emissions and temperature profiles were systematically investigated. As

expected, higher excess air always leads to higher NOx emissions. Air staging results in a significant increase in the temperatures in the splashing zone and freeboard as more gases and volatiles are burned in the splashing zone and freeboard. Moreover, air staging under AS2 conditions reduces considerably NOx emissions, up to 30% comparing with the case of without staging air when burning biomass fuels with high fuel-N contents. The use of staging air also reduces CO emissions as fewer biomass fines are carried to and burnt in the freeboard. Air staging changes the temperature profiles in the freeboard, especially at low excess air levels.

The experimental results show that air staging under AS2 conditions can significantly reduce both NOx and CO emissions when the BFB combustor is operated at low excess air levels and burning biomass fuels with high fuel-N contents. In fact, air staging has shown better combustion as compared to without air staging, which is proved from combustion efficiency results. Higher combustion efficiencies values >98% in terms of emissions reduction have been achieved under air staging combustion, comparing without air staging combustion (96–98%). On the other hand, high efficiency losses in terms of heat losses associated with the unburnt carbon in the ash were observed during air staging combustion for all types of studied biomass fuels which is due to the presence of higher carbon content in fly ash.

9.3 Oxy-fuel Combustion

Three biomass fuels including domestic wood (woody), miscanthus and wheat straw (non-woody) were tested in the BFBC under different oxy-fuel mixtures including;

21% O_2/79% CO_2, 25% O_2/75% CO_2 and 30% O_2/70% CO_2. The experimental results indicate that oxy-fuel combustion is different from air combustion in several ways. Replacing air with oxy 21%O_2/79%CO_2 and 25%O_2/75%CO_2 led to reduced gas temperatures, delayed ignition and higher CO and NOx emissions. The main diluting gas CO_2 in oxy-fuel has different properties from N_2 in air, and hence influences both heat transfer and reaction kinetics during biomass combustion in the BFBC. On an average about 150–200 ^oC decrease in the bed temperatures was noticed under oxy-fuel 21%O_2/79%CO_2 and 25%O_2/75%CO_2 combustion for all types of biomass fuels. Both increasing and decreasing trends in the NOx emissions were observed once the combustion environment was changed from air to oxy depending on the biomass fuel type and combustion stoichiometry.

The NOx emissions level was higher with a lower O_2 concentration in the oxy-fuel mixture. In oxy-fuel, the NOx formation was dependent on fuel-N and combustion stoichiometry. The NOx emissions were reduced to its minimum level when O_2 concentration was increased to 30% in oxy-mixture. The CO emission level was increased dramatically during oxy-fuel 21%O_2/79%CO_2 combustion because of very low bed temperatures that were caused by the higher specific heat of CO_2 in the oxy-fuel mixture. Further increase of O_2 concentration in the oxy-fuel mixture results with a reduction in CO emission, on average about 60–70% decrease in CO emissions being achieved under oxy-fuel 30%O_2/70%CO_2 as compared with air combustion. The results also suggested that the bed temperatures are important during oxy-fuel combustion because they strongly affect the combustion kinetics. Moreover, when the oxy-fuel mixture was replaced with 30%O_2/70%CO_2 almost similar gas temperatures as those

under air were attained in the combustor. The biomass fuels tested under oxy 30%O_2/70%CO_2 have shown better efficiencies than air and lower emissions (NOx and CO).

9.4 Agglomeration and Sintering Behaviour

The bed material and cyclone ash were analysed for agglomeration and sintering behaviour for all types of biomass fuels combusted under air in the BFBC. The potassium (K) content present in the biomass fuels showed to be a point of concern during combustion. Wheat straw showed some extent of agglomeration, agglomerates' size was up to 4 mm on an average basis. The results from agglomeration and sintering analysis indicated that K is the major problematic alkali in wheat straw causing agglomeration. Although wheat straw contained a less K content in the bed material but still this collected in the bed and ultimately lead to agglomeration. Peanut shell, on the other hand, contained a significant amount of K in the bed material but and do not led to any type of agglomeration problem.

The K (alkali metal) present in the wheat straw is known for producing low melting point silicate compounds during combustion that helps in agglomeration. The peanut shell contained higher refractory nature of elements like Ca, Mg, Al and P; therefore these could compensate to a certain extent for its high alkali content. The bed temperatures in BFBC were 750–850 ^{o}C, the major part of alkali species is likely to stay in the bed but alkali earth metals such as Ca which are also abundant in some of the non-woody biomasses generally helped in reducing the agglomeration by increasing ash

melting point. None of other biomass fuels studied in BFBC indicated any type of agglomeration or sintering.

9.5 Suggestions for Future Work

This work has shown that it is certainly possible to attain similar combustion conditions with air and an oxy-fuel in BFBC. In order to further investigate the applicability of pure biomass combustion under air and oxy-fuel technology in large scale for CCS the following areas are of interest:

- The improvements in the BFBC are highly recommended for the future work such as making the freeboard region bigger to increase the residence time for better combustion and lower CO emission.
- Due to the continuing efforts to substitute coal power plants with biomass more research into all of the areas investigated in this work should be further enlightened. Especially co-firing of non-woody biomass with coal and woody biomass ashes in boilers is relatively unexplored and the results obtained in this work have shown interesting trends regarding agglomeration and sintering chemistry.
- The staged air combustion has shown promising results in terms of emissions reduction and higher temperatures with better combustion efficiency, it is further recommended to use the higher points for staging air and multi-staged air combustion could be further investigated.
- A potential improvement of the process economics of an oxy-fuel fired power plant by reducing the demand for oxygen which is the only oxy-gas associated

with the highest separation cost, needs investigations, among others on the consequence to the ash deposit formation, boilers heat uptake, flame temperatures, and level of emissions etc.

- It will be beneficial to investigate the impact of the continuous operation of the BFBC for a longer period without stopping as similar operating practices on in the industrial scale FBs system on agglomeration and sintering behaviour for biomass combustion.
- On the basis of agglomeration and sintering results from the air combustion experiments, an investigation on the agglomeration, slagging mechanism during oxy-fuel combustion could be of great importance to the operation of full-scale boilers under oxy-fuel and hence it is recommended for future work.
- Computational Fluid Dynamics (CFD) models of the oxy-fuel combustion in BFBC is highly recommended, which can be used an important tool in the designing and optimisation process for the new plants and retrofits the old ones.

References

1. Root, T.L., et al., Fingerprints of global warming on wild animals and plants. Nature, 2003. 421(6918): p. 57-60.
2. Organization, W.H., Air quality guidelines: global update 2005: particulate matter, ozone, nitrogen dioxide, and sulfur dioxide. 2006: World Health Organization.
3. Sinyak, Y., Global climate and energy systems. Science of The Total Environment, 1994. 143(1): p. 31-51.
4. Birol, F., World energy outlook 2010. International Energy Agency, 2010.
5. Johnson, E., Goodbye to carbon neutral: Getting biomass footprints right. Environmental impact assessment review, 2009. 29(3): p. 165-168.
6. Faaij, A.P., Bio-energy in Europe: changing technology choices. Energy policy, 2006. 34(3): p. 322-342.
7. Khan, A.A., Combustion and co-combustion of biomass in a bubbling fluidized bed boiler. 2007: TU Delft, Delft University of Technology.
8. Sieminski, A., International energy outlook. Energy Information Administration (EIA), 2014.
9. Penner, J., et al., The scientific basis. Contribution of working group I to the third assessment report of the Intergovernmental Panel on Climate Change. Climate Change, 2001.
10. Kiesgen de_Richter, R., T. Ming, and S. Caillol, Fighting global warming by photocatalytic reduction of CO_2 using giant photocatalytic reactors. Renewable and Sustainable Energy Reviews, 2013. 19: p. 82-106.
11. Marland, G., et al., Global, regional, and national fossil fuel CO_2 emissions. Carbon dioxide information analysis center, Oak ridge national laboratory, U.S. Department of Energy, Oak Ridge, Tenn., U.S.A, 2015.
12. Marland, G., et al., Global, regional, and national fossil fuel CO_2 emissions. Trends: A Compendium of Data on Global Change, 2007: p. 37831-6335.
13. Outlook, I.S.A.E., International Energy Agency (IEA). Organisation for Economic Cooperation and Development (OECD): Paris, France, 2013.

14. Sadler, R., et al., An opinion on the distribution and behavior of chemicals in response to climate change, with particular reference to the Asia-Pacific region. Toxicological and Environ Chemistry, 2011. 93(1): p. 3-31.
15. Leadsom , R.H.A., L.o.A. Bourne, and R.H.A. Rudd, Energy Act 2016, D.o.E.a.C. Change, Editor. 2015, UK Government: House of Commons.
16. Pollitt, M.G., UK renewable energy policy since privatisation, in Harnessing renewable energy in electric power systems: Theory, practice, policy. 2010, RFF Press.
17. Roadmap, U.R.E., Department of Energy and Climate Change. UK government, First published, 2011. 12.
18. DECC, U., Renewable energy roadmap. Crown Copyright, Department of Energy & Climate Change, London, 2011.
19. Connor, P.M., UK renewable energy policy: a review. Renewable and Sustainable Energy Reviews, 2003. 7(1): p. 65-82.
20. Association, W.N. Nuclear Power in the United Kingdom. 2016 2 August 2016]; Available from: http://www.world-nuclear.org/information-library/country-profiles/countries-t-z/united-kingdom.aspx.
21. AMRC, N. UK new build plans. 2016 2 August 2016]; Available from: http://namrc.co.uk/intelligence/uk-new-build-plans/.
22. Ares, D.E., The Renewables Obligation. Standard Note: SN/SC/5870, House of Commons Library, London. Available online at: www. parliament. uk/briefing-papers/SN05870. pdf, 2012.
23. Drax. Drax and biomass. 2016 8 August 2016]; Available from: http://www.drax.com/biomass/what-is-biomass/.
24. Association, W.N. Energy Subsidies and External Costs. 2016 2 August 2016]; Available from: http://www.world-nuclear.org/information-library/country-profiles/countries-t-z/united-kingdom.aspx.
25. DECC, U., Renewable Energy Roadmap Update 2012. Crown Copyright, Department of Energy & Climate Change, London, 2012.
26. Klass, D.L., Biomass for renewable energy and fuels. Encyclopedia of energy, 2004. 1(1): p. 193-212.

27. Ladanai, S. and J. Vinterbäck, Global potential of sustainable biomass for energy. 2009.
28. Protocol, K., United Nations framework convention on climate change. Kyoto Protocol, Kyoto, 1997.
29. Lee, C. and T. Schaaf, United Nations Environment Programme (UNEP). 2008.
30. Change, C., Intergovernmental panel on climate change (IPCC). 1995, Cambridge University Press: Cambridge.
31. Hardner, J.J., P.C. Frumhoff, and D.C. Goetze, Prospects for mitigating carbon, conserving biodiversity, and promoting socioeconomic development objectives through the clean development mechanism. Mitigation and Adaptation Strategies for Global Change, 2000. 5(1): p. 61-80.
32. Flato, G., et al., Evaluation of Climate Models. In: Climate Change 2013: The Physical Science Basis. Contribution of Working Group I to the Fifth Assessment Report of the Intergovernmental Panel on Climate Change. Climate Change 2013, 2013. 5: p. 741-866.
33. Wall, T.F., Combustion processes for carbon capture. Proceedings of the Combustion Institute, 2007. 31(1): p. 31-47.
34. Feron, P. and C. Hendriks, CO_2 capture process principles and costs. Oil & Gas Science And Technology, 2005. 60(3): p. 451-459.
35. Markewitz, P. and R. Bongartz, Carbon capture technologies, in Carbon Capture, Storage and Use. 2015, Springer. p. 13-45.
36. Wang, M., et al., Post-combustion CO_2 capture with chemical absorption: a state of the art review. Chemical Engineering Research and Design, 2011. 89(9): p. 1609-1624.
37. Kanniche, M., et al., Pre-combustion, post-combustion and oxy-combustion in thermal power plant for CO_2 capture. Applied Thermal Engineering, 2010. 30(1): p. 53-62.
38. Figueroa, J.D., et al., Advances in CO_2 capture technology-the US Department of Energy's Carbon Sequestration Program. International journal of greenhouse gas control, 2008. 2(1): p. 9-20.

39. Metz, B., et al., IPCC Special Report on Carbon Dioxide Capture and Storage Cambridge University Press. Cambridge, United Kingdom, and New York, NY, USA, 2005.
40. Simmonds, M., I. Miracca, and K. Gerdes. Oxyfuel technologies for CO_2 capture: a techno-economic overview. in 7th international conference on greenhouse gas control technologies. Vancouver, Canada. 2004.
41. Wall, T., R. Stanger, and S. Santos, Demonstrations of coal-fired oxy-fuel technology for carbon capture and storage and issues with commercial deployment. International journal of greenhouse gas control, 2011. 5: p. S5-S15.
42. Figueroa, J.D., et al., Advances in CO_2 capture technology—The US Department of Energy's Carbon Sequestration Program. International Journal of Greenhouse Gas Control, 2008. 2(1): p. 9-20.
43. Abu-Khader, M.M., Recent progress in CO_2 capture/sequestration: a review. Energy Sources, Part A, 2006. 28(14): p. 1261-1279.
44. Eide, L.I., et al., Novel capture processes. Oil & Gas Science And Technology, 2005. 60(3): p. 497-508.
45. Hossain, M.M. and H.I. de Lasa, Chemical-looping combustion (CLC) for inherent CO_2 separations—A review. Chemical Engineering Science, 2008. 63(18): p. 4433-4451.
46. Wall, T., et al., An overview on oxyfuel coal combustion—State of the art research and technology development. Chemical Engineering Research and Design, 2009. 87(8): p. 1003-1016.
47. Brown, R.C., Biorenewable resources. 2003: Iowa State Press.
48. Basu, P., Biomass gasification and pyrolysis: practical design and theory. 2010: Academic press.
49. Van Loo, S. and J. Koppejan, The handbook of biomass combustion and co-firing. 2008: Earthscan.
50. Demirbas, A., Combustion of biomass. Energy Sources, Part A: Recovery, Utilization, and Environmental Effects, 2007. 29(6): p. 549-561.
51. Strathclyde, U.o., Closed carbon cycle, in Biomass Installation Feasibility Tool. 2016.

52. McKendry, P., Energy production from biomass (part 1): overview of biomass. Bioresource technology, 2002. 83(1): p. 37-46.
53. Vassilev, S.V., et al., An overview of the chemical composition of biomass. Fuel, 2010. 89(5): p. 913-933.
54. Kitani, O., Biomass handbook. 1989: Gordon & Breach Science Pub.
55. Yang, H., et al., Characteristics of hemicellulose, cellulose and lignin pyrolysis. Fuel, 2007. 86(12): p. 1781-1788.
56. Wang, T., M.W. Nolte, and B.H. Shanks, Catalytic dehydration of C6 carbohydrates for the production of hydroxymethylfurfural (HMF) as a versatile platform chemical. Green Chemistry, 2014. 16(2): p. 548-572.
57. Demirbas, A., Combustion characteristics of different biomass fuels. Progress in energy and combustion science, 2004. 30(2): p. 219-230.
58. Sutton, D., B. Kelleher, and J.R. Ross, Review of literature on catalysts for biomass gasification. Fuel processing technology, 2001. 73(3): p. 155-173.
59. Dayton, D., et al., Release of inorganic constituents from leached biomass during thermal conversion. Energy & Fuels, 1999. 13(4): p. 860-870.
60. Jenkins, B., et al., Combustion properties of biomass. Fuel processing technology, 1998. 54(1): p. 17-46.
61. Brownell, H., E. Yu, and J. Saddler, Steam-explosion pretreatment of wood: Effect of chip size, acid, moisture content and pressure drop. Biotechnology and bioengineering, 1986. 28(6): p. 792-801.
62. Beenackers, A., Biomass gasification in moving beds, a review of European technologies. Renewable Energy, 1999. 16(1): p. 1180-1186.
63. Mani, S., L.G. Tabil, and S. Sokhansanj, Effects of compressive force, particle size and moisture content on mechanical properties of biomass pellets from grasses. Biomass and Bioenergy, 2006. 30(7): p. 648-654.
64. Jenkins, B., Physical properties of biomass. Biomass handbook, 1989: p. 860-891.
65. Ergudenler, A. and A. Ghaly, Agglomeration of silica sand in a fluidized bed gasifier operating on wheat straw. Biomass and bioenergy, 1993. 4(2): p. 135-147.

66. Meschgbiz, A. and M. Krumbeck. Combined combustion of biomass and brown coal in a pulverized fuel and fluidized bed combustion plant. in 3rd European Conference on Industrial Furnaces and Boilers, Lisbon, Portugal. 1995.
67. Smoot, L.D. and P.J. Smith, Coal combustion and gasification. 2013: Springer Science & Business Media.
68. Sokhansanj, S. and A. Turhollow, Biomass densification–cubing operations and costs for corn stover. Applied engineering in agriculture, 2004. 20(4): p. 495.
69. Bain, R.L., R.P. Overend, and K.R. Craig, Biomass-fired power generation. Fuel Processing Technology, 1998. 54(1): p. 1-16.
70. Demirbas, A., Trace element concentrations in ashes from various types of lichen biomass species. Energy sources, 2004. 26(5): p. 499-506.
71. Demirbas, A., The importance of biomass. Energy sources, 2004. 26(4): p. 361-366.
72. DEMİRBAŞ, A., Fuel and combustion properties of bio-wastes. Energy sources, 2005. 27(5): p. 451-462.
73. Jensen, P.A., B. Sander, and K. Dam-Johansen, Pretreatment of straw for power production by pyrolysis and char wash. Biomass and Bioenergy, 2001. 20(6): p. 431-446.
74. Williams, C., A. Dahiya, and P. Porter, Introduction to bioenergy. 2012.
75. Goldemberg, J., World Energy Assessment: Energy and the challenge of sustainability. 2000: United Nations Pubns.
76. Varma, A.K. and P. Mondal, Physicochemical characterization and kinetic study of pine needle for pyrolysis process. Journal of Thermal Analysis and Calorimetry, 2016. 124(1): p. 487-497.
77. Zhong, W., et al., Fluidization of biomass particles in a gas− solid fluidized bed. Energy & Fuels, 2008. 22(6): p. 4170-4176.
78. Koppejan, J. and S. Van Loo, The handbook of biomass combustion and co-firing. 2012: Routledge.
79. Simoneit, B.R., Biomass burning-a review of organic tracers for smoke from incomplete combustion. Applied Geochemistry, 2002. 17(3): p. 129-162.
80. Oka, S., Fluidized bed combustion. 2003: CRC press.

81. Guenther, C. and M. Syamlal, The effect of numerical diffusion on simulation of isolated bubbles in a gas–solid fluidized bed. Powder Technology, 2001. 116(2): p. 142-154.
82. Howard, J., Fluidized Beds. Combustion and Applications. Applied Science Publishers, Ripple Road, Barking, Essex, England, 1983., 1983.
83. Gupta, R. and S. Gangwal, Enhanced durability of desulfurization sorbents for fluidized-bed applications. 1992, Research Triangle Inst., Research Triangle Park, NC (United States).
84. Johnsen, K., et al., Sorption-enhanced steam reforming of methane in a fluidized bed reactor with dolomite as CO_2-acceptor. Chemical Engineering Science, 2006. 61(4): p. 1195-1202.
85. Grace, J., High-velocity fluidized bed reactors. Chemical Engineering Science, 1990. 45(8): p. 1953-1966.
86. Adris, A., C. Lim, and J. Grace, The fluidized bed membrane reactor system: a pilot scale experimental study. Chemical Engineering Science, 1994. 49(24): p. 5833-5843.
87. Natarajan, E., A. Nordin, and A. Rao, Overview of combustion and gasification of rice husk in fluidized bed reactors. Biomass and Bioenergy, 1998. 14(5-6): p. 533-546.
88. Johnsson, F., Fluidized bed combustion for clean energy. 2007.
89. Anthony, E., Fluidized bed combustion of alternative solid fuels; status, successes and problems of the technology. Progress in energy and combustion science, 1995. 21(3): p. 239-268.
90. Prins, W., Fluidized bed combustion of a single carbon particle. PhD Diss. Twente Univ. of Technology, The Netherlands, 1987.
91. Watson, W.J., Constructing success in the electric power industry: combined cycle gas turbines and fluidised beds. 1997, University of Sussex.
92. Bi, H., et al., Flooding of gas-solids countercurrent flow in fluidized beds. Industrial & engineering chemistry research, 2004. 43(18): p. 5611-5619.
93. Wene, C.-O., Experience curves for energy technology policy. 2000: OECD.
94. Junginger, H.M., Learning in renewable energy technology development. 2005.

95. Colpier, U.C. and D. Cornland, The economics of the combined cycle gas turbine—an experience curve analysis. Energy Policy, 2002. 30(4): p. 309-316.
96. Scherr, F.C. and J.A. Fuller, Costs of atmospheric fluidized-bed combustors for electric power generation. The Energy Journal, 2002: p. 117-132.
97. Johnsson, F., S. Andersson, and B. Leckner, Expansion of a freely bubbling fluidized bed. Powder Technology, 1991. 68(2): p. 117-123.
98. Koornneef, J., M. Junginger, and A. Faaij, Development of fluidized bed combustion-An overview of trends, performance and cost. Progress in energy and combustion science, 2007. 33(1): p. 19-55.
99. dos Santos, F.J. and L. Goldstein Jr, Experimental aspects of biomass fuels in a bubbling fluidized bed combustor. Chemical Engineering and Processing: Process Intensification, 2008. 47(9): p. 1541-1549.
100. Abdullah, M., Z. Husain, and S. Yin Pong, Analysis of cold flow fluidization test results for various biomass fuels. Biomass and Bioenergy, 2003. 24(6): p. 487-494.
101. Czakiert, T., et al. Operating experience with a 0.1 MWth oxyfuel-CFB test rig. in 1st oxyfuel combustion conference, Cottbus, Germany. 2009.
102. Grace, J.R. and H. Bi, Introduction to circulating fluidized beds. 1996: Springer.
103. Khan, A., et al., Biomass combustion in fluidized bed boilers: potential problems and remedies. Fuel processing technology, 2009. 90(1): p. 21-50.
104. Grace, J.R., T. Knowlton, and A. Avidan, Circulating fluidized beds. 2012: Springer Science & Business Media.
105. Minchener, A., Fluidized bed combustion systems for power generation and other industrial applications. Proceedings of the Institution of Mechanical Engineers, Part A: Journal of Power and Energy, 2003. 217(1): p. 9-18.
106. Junginger, M., et al., Technological learning in bioenergy systems. Energy Policy, 2006. 34(18): p. 4024-4041.
107. Basu, P. and S. Fraser, Circulating Fluidized Bed Boiler. 1994: Butterworthh-Heineman.
108. Armesto, L., et al., Combustion behaviour of rice husk in a bubbling fluidised bed. Biomass and Bioenergy, 2002. 23(3): p. 171-179.

109. Basu, P., et al., Fluidized bed boilers: design and application. 1984: Pergamon Press.
110. Oka, S. How to use data about coal combustion in bubbling fluidized beds for design of the circulating fluidized bed boilers. in 41st IEA FBC technical meeting. Salerno: Institute for nuclear Sciences VINA Laboratory for thermal Engineering and Energy Research. 2000.
111. Toupin, K. Modern wood fired boiler designs—history and technology changes. in 2nd Biomass Conference of the Americas, Portland, Oregon. 1995.
112. Boyd, T.J. and D. Mahr, FBC and AFBC Projects and Technology: Presented at the 1993 International Joint Power Generation Conference, Kansas City, Missouri, October 17-22, 1993. Vol. 16. 1993: American Society of Mechanical Engineers.
113. Quaak, P., H. Knoef, and H.E. Stassen, Energy from biomass: a review of combustion and gasification technologies. 1999: World Bank Publications.
114. Khan, A., W. de Jong, and H. Spliethoff, Biomass combustion in fluidized bed boiler. Bioenergy for Wood Industry, Jyväskylä, Finland, 2005: p. 365-370.
115. Llorente, M., et al., Ash behaviour of lignocellulosic biomass in bubbling fluidised bed combustion. Fuel, 2006. 85(9): p. 1157-1165.
116. de Jong, W., A. Khan, and H. Spliethoff, Biomass blend combustion in a 1 MWth bubbling fluidized bed boiler. Clean Air, 2005: p. 1-14.
117. Basu, P., Fluidized bed boilers: design and application. 2013: Elsevier.
118. Coda, B., et al., Behavior of chlorine and enrichment of risky elements in bubbling fluidized bed combustion of biomass and waste assisted by additives. Energy & Fuels, 2001. 15(3): p. 680-690.
119. Oka, S., Fluidized bed combustion. Vol. 162. 2010: CRC Press.
120. Ferrer, E., et al., Fluidized bed combustion of refuse-derived fuel in presence of protective coal ash. Fuel processing technology, 2005. 87(1): p. 33-44.
121. Ding, J. and D. Gidaspow, A bubbling fluidization model using kinetic theory of granular flow. AIChE Journal, 1990. 36(4): p. 523-538.

122. Grass, S.W. and B.M. Jenkins, Biomass fueled fluidized bed combustion: atmospheric emissions, emission control devices and environmental regulations. Biomass and Bioenergy, 1994. 6(4): p. 243-260.
123. Leckner, B., Fluidized bed combustion: mixing and pollutant limitation. Progress in Energy and Combustion Science, 1998. 24(1): p. 31-61.
124. Lackner, M., et al., Carbon conversion of solid fuels in the freeboard of a laboratory-scale fluidized bed combustor—application of in situ laser spectroscopy. Fuel, 2004. 83(10): p. 1289-1298.
125. Gulyurtlu, I., et al. Consideration for mixing different biomass fuels and non-toxic waste during fluidised bed combustion. in 2nd World Conference on Biomass for Energy, Industry and Climate Protection, Rome, Italy. 2004.
126. Toftegaard, M.B., et al., Oxy-fuel combustion of solid fuels. Progress in energy and combustion science, 2010. 36(5): p. 581-625.
127. Change, I.P.O.C., Climate change 2007: the physical science basis. Agenda, 2007. 6(07).
128. Davison, J., Performance and costs of power plants with capture and storage of CO_2. Energy, 2007. 32(7): p. 1163-1176.
129. Bachu, S., CO_2 storage in geological media: role, means, status and barriers to deployment. Progress in Energy and Combustion Science, 2008. 34(2): p. 254-273.
130. Glarborg, P. and L.L. Bentzen, Chemical effects of a high CO_2 concentration in oxy-fuel combustion of methane. Energy & Fuels, 2007. 22(1): p. 291-296.
131. Mackrory, A. and D. Tree. NOx destruction experiments and modeling in oxy-fuel combustion. in The 33rd international technical conference on coal utilization and fuel systems, coal for the future. Clearwater, Florida. 2008.
132. Zheng, L. and E. Furimsky, Assessment of coal combustion in O_2+ CO_2 by equilibrium calculations. Fuel Processing Technology, 2003. 81(1): p. 23-34.
133. Liu, F., H. Guo, and G.J. Smallwood, The chemical effect of CO_2 replacement of N_2 in air on the burning velocity of CH_4 and H_2 premixed flames. Combustion and flame, 2003. 133(4): p. 495-497.

134. Masri, A., R. Dibble, and R. Barlow, Chemical kinetic effects in nonpremixed flames of H_2/CO_2 fuel. Combustion and flame, 1992. 91(3): p. 285-309.
135. Wang, C., et al., Combustion of pulverized coal using waste carbon dioxide and oxygen. Combustion and flame, 1988. 72(3): p. 301-310.
136. Woycenko, D., W. Van de Kamp, and P. Roberts, Combustion of pulverised coal in a mixture of oxygen and recycled flue gas. Summary of the APG research program, IFRF Doc. 1995, F98/Y/4. Ijmuiden, The Netherlands: International Flame Research Foundation (IFRF).
137. Liu, H., R. Zailani, and B.M. Gibbs, Comparisons of pulverized coal combustion in air and in mixtures of O_2/CO_2. Fuel, 2005. 84(7): p. 833-840.
138. Scheffknecht, G. and J. Maier, Firing issues related to the oxyfuel process. VGB Power Tech, 2008. 88(11): p. 91-97.
139. Dhungel, B., J. Maier, and G. Scheffknecht. Emission behaviour during oxy-coal combustion. in AIChE 2007 Annual meeting, Salt Lake City, UT. 2007.
140. Mendiara, T. and P. Glarborg, Reburn chemistry in oxy-fuel combustion of methane. Energy & Fuels, 2009. 23(7): p. 3565-3572.
141. Mendiara, T. and P. Glarborg, Ammonia chemistry in oxy-fuel combustion of methane. Combustion and flame, 2009. 156(10): p. 1937-1949.
142. Khan, A.A., W.D. Jong, and H. Spliethoff, A fluidized bed combustion model with discretized population balance. 2. Experimental studies and model validation. Energy & Fuels, 2007. 21(6): p. 3709-3717.
143. Laursen, K. and J. Grace, Some implications of co-combustion of biomass and coal in a fluidized bed boiler. Fuel Processing Technology, 2002. 76(2): p. 77-89.
144. Winter, F., C. Wartha, and H. Hofbauer, NO and N_2O formation during the combustion of wood, straw, malt waste and peat. Bioresource technology, 1999. 70(1): p. 39-49.
145. Johnsson, J.E., Formation and reduction of nitrogen oxides in fluidized-bed combustion. Fuel, 1994. 73(9): p. 1398-1415.

146. Miller, J.A. and C.T. Bowman, Mechanism and modeling of nitrogen chemistry in combustion. Progress in energy and combustion science, 1989. 15(4): p. 287-338.
147. Obernberger, I., Decentralized biomass combustion: state of the art and future development. Biomass and bioenergy, 1998. 14(1): p. 33-56.
148. Leckner, B. and M. Karlsson, Gaseous emissions from circulating fluidized bed combustion of wood. Biomass and Bioenergy, 1993. 4(5): p. 379-389.
149. Tewksbury, C., Wood combustion and NOx formation control, in Energy from biomass and wastes 15. 1991.
150. Nordin, A., Chemical elemental characteristics of biomass fuels. Biomass and Bioenergy, 1994. 6(5): p. 339-347.
151. Kaynak, B., H. Topal, and A.T. Atimtay, Peach and apricot stone combustion in a bubbling fluidized bed. Fuel Processing Technology, 2005. 86(11): p. 1175-1193.
152. Åmand, L.-E. and B. Leckner, Influence of fuel on the emission of nitrogen oxides (NO and N_2O) from an 8-MW fluidized bed boiler. Combustion and Flame, 1991. 84(1-2): p. 181-196.
153. Lyngfelt, A. and B. Leckner, Combustion of wood-chips in circulating fluidized bed boilers—NO and CO emissions as functions of temperature and air-staging. Fuel, 1999. 78(9): p. 1065-1072.
154. Werther, J., et al., Combustion of agricultural residues. Progress in energy and combustion science, 2000. 26(1): p. 1-27.
155. Löffler, G., V.J. Wargadalam, and F. Winter, Catalytic effect of biomass ash on CO, CH_4 and HCN oxidation under fluidised bed combustor conditions. Fuel, 2002. 81(6): p. 711-717.
156. Lu, Y., I. Hippinen, and A. Jahkola, Control of NOx and N_2O in pressurized fluidized-bed combustion. Fuel, 1995. 74(3): p. 317-322.
157. Glarborg, P., A. Jensen, and J.E. Johnsson, Fuel nitrogen conversion in solid fuel fired systems. Progress in energy and combustion science, 2003. 29(2): p. 89-113.

158. Song, T., et al., Nitrogen transfer of fuel-N in chemical looping combustion. Combustion and Flame, 2012. 159(3): p. 1286-1295.
159. Nussbaumer, T. and J. Hustad, Overview of biomass combustion, in Developments in thermochemical biomass conversion. 1997, Springer. p. 1229-1243.
160. Permchart, W. and V.I. Kouprianov, Emission performance and combustion efficiency of a conical fluidized-bed combustor firing various biomass fuels. Bioresource Technology, 2004. 92(1): p. 83-91.
161. Tillman, D., The combustion of solid fuels and wastes. 2012: Academic Press.
162. McDonald, D.K., et al. 30 MWt Clean Environment Development Oxy-Coal Combustion Test Program. in 33rd International Coal Utilization and Fuel Systems Conference. 2008.
163. Kiga, T., et al., Characteristics of pulverized-coal combustion in the system of oxygen/recycled flue gas combustion. Energy Conversion and Management, 1997. 38: p. S129-S134.
164. Kimura, N., et al., The characteristics of pulverized coal combustion in O_2/CO_2 mixtures for CO_2 recovery. Energy Conversion and Management, 1995. 36(6): p. 805-808.
165. Châtel-Pélage, F., et al., Applications of oxygen for NOx control and CO_2 capture in coal-fired power plants. Thermal Sci, 2006. 10(3): p. 119-42.
166. Tan, Y., et al., Combustion characteristics of coal in a mixture of oxygen and recycled flue gas. Fuel, 2006. 85(4): p. 507-512.
167. Klein, M. and G. Rotzoll, N_2O and NOx formation during coal and char combustion in a fluidized bed. VGB Kraftwerktechnik, 1994. 74(12): p. 1072-1080.
168. Savolainen, K., Co-firing of biomass in coal-fired utility boilers. Applied Energy, 2003. 74(3): p. 369-381.
169. Okazaki, K. and T. Ando, NOx reduction mechanism in coal combustion with recycled CO_2. Energy, 1997. 22(2): p. 207-215.
170. Andersson, K., et al., NO emission during oxy-fuel combustion of lignite. Industrial & engineering chemistry research, 2008. 47(6): p. 1835-1845.

171. Normann, F., et al., High-temperature reduction of nitrogen oxides in oxy-fuel combustion. Fuel, 2008. 87(17): p. 3579-3585.
172. Hu, Y., N. Kobayashi, and M. Hasatani, Effects of coal properties on recycled-NOx reduction in coal combustion with O_2/recycled flue gas. Energy conversion and management, 2003. 44(14): p. 2331-2340.
173. Nussbaumer, T., Combustion and co-combustion of biomass: fundamentals, technologies, and primary measures for emission reduction. Energy & fuels, 2003. 17(6): p. 1510-1521.
174. Myerson, A.L., F.R. Taylor, and B.G. Faunce. Ignition limits and products of the multistage flames of propane-nitrogen dioxide mixtures. in Symposium (International) on Combustion. 1957. Elsevier.
175. Maly, P., et al., Alternative fuel reburning. Fuel, 1999. 78(3): p. 327-334.
176. Harding, N.S. and B.R. Adams, Biomass as a reburning fuel: a specialized cofiring application. Biomass and Bioenergy, 2000. 19(6): p. 429-445.
177. Basu, P., Combustion and gasification in fluidized beds. 2006: CRC press.
178. Jensen, A.D., Nitrogen chemistry in fluidized bed combustion of coal. 1996: Technical University of Denmark (DTU).
179. Keith, D.W. and J.S. Rhodes, Bury, burn or both: a two-for-one deal on biomass carbon and energy. Climatic change, 2002. 54(3): p. 375-377.
180. Obersteiner, M., et al., Managing climate risk. Science, 2001. 294(5543): p. 786-787.
181. Kraxner, F., S. Nilsson, and M. Obersteiner, Negative emissions from BioEnergy use, carbon capture and sequestration (BECS)—the case of biomass production by sustainable forest management from semi-natural temperate forests. Biomass and Bioenergy, 2003. 24(4): p. 285-296.
182. Azar, C., et al., Carbon capture and storage from fossil fuels and biomass–Costs and potential role in stabilizing the atmosphere. Climatic change, 2006. 74(1-3): p. 47-79.
183. Fryda, L., et al., Study on ash deposition under oxyfuel combustion of coal/biomass blends. Fuel, 2010. 89(8): p. 1889-1902.

184. Singh, D., et al., Techno-economic study of CO_2 capture from an existing coal-fired power plant: MEA scrubbing vs. O_2/CO_2 recycle combustion. Energy conversion and Management, 2003. 44(19): p. 3073-3091.
185. Tan, Y., M.A. Douglas, and K.V. Thambimuthu, CO_2 capture using oxygen enhanced combustion strategies for natural gas power plants. Fuel, 2002. 81(8): p. 1007-1016.
186. Tzimas, E., et al., Enhanced oil recovery using carbon dioxide in the European energy system. European Commission Joint Research Centre, Report EUR, 2005. 21895.
187. Arias, B., et al., Effect of biomass blending on coal ignition and burnout during oxy-fuel combustion. Fuel, 2008. 87(12): p. 2753-2759.
188. Jia, L., Y. Tan, and E. Anthony, Emissions of SO_2 and NOx during Oxy− Fuel CFB Combustion Tests in a Mini-Circulating Fluidized Bed Combustion Reactor. Energy & Fuels, 2009. 24(2): p. 910-915.
189. Kim, H.K., et al., Emission characteristics of the 0.2 MW Oxy-fuel combustor. Energy & Fuels, 2009. 23(11): p. 5331-5337.
190. Uddin, S.N. and L. Barreto, Biomass-fired cogeneration systems with CO_2 capture and storage. Renewable Energy, 2007. 32(6): p. 1006-1019.
191. Valero, A., et al. Oxy-Co-firing: a negative CO_2 emission process. in The 8th international conference on greenhouse gas control technologies (GHGT-8). Trondheim, Norway. 2006.
192. Ditaranto, M. and J. Hals, Combustion instabilities in sudden expansion oxy–fuel flames. Combustion and flame, 2006. 146(3): p. 493-512.
193. Chui, E.H., M.A. Douglas, and Y. Tan, Modeling of oxy-fuel combustion for a western Canadian sub-bituminous coal. Fuel, 2003. 82(10): p. 1201-1210.
194. Zheng, L., Oxy-fuel combustion for power generation and carbon dioxide (CO2) capture. 2011: Elsevier.
195. Haykırı-Açma, H., Combustion characteristics of different biomass materials. Energy Conversion and Management, 2003. 44(1): p. 155-162.
196. Khare, S., et al., Factors influencing the ignition of flames from air-fired swirl pf burners retrofitted to oxy-fuel. Fuel, 2008. 87(7): p. 1042-1049.

197. Ochs, T., et al., Results of initial operation of the Jupiter Oxygen Corporation oxy-fuel 15 MWth burner test facility. Energy Procedia, 2009. 1(1): p. 511-518.
198. Kunii, D. and O. Levenspiel, Fluidization engineering. 2013: Elsevier.
199. Punčochář, M., et al., Evaluation of minimum fluidizing velocity in gas fluidized bed from pressure fluctuations. Chemical Engineering Communications, 1985. 35(1-6): p. 81-87.
200. Kunii, D. and O. Levenspiel, Fluidization engineering. Vol. 2. 1991: Butterworth-Heinemann Boston.
201. Wen, C. and Y. Yu, A generalized method for predicting the minimum fluidization velocity. AIChE Journal, 1966. 12(3): p. 610-612.
202. Coulson, J.M., D.G. Peacock, and J.F. Richardson, Chemical Engineering.(vol. 3. Editors: JF Richardson & DG Peacock.). 1971: Pergamon Press.
203. Saxena, S. and G. Vogel, The measurement of incipient fluidization velocities in a bed of coarse dolomite at temperature and pressure. Trans. Inst. Chem. Eng, 1977. 55(3): p. 184-189.
204. Babu, S., B. Shah, and A. Talwalkar. Fluidization correlations for coal gasification materials-minimum fluidization velocity and fluidized bed expansion ratio. in AIChE Symp. Ser. 1978.
205. Chitester, D.C., et al., Characteristics of fluidization at high pressure. Chemical Engineering Science, 1984. 39(2): p. 253-261.
206. Grace, J.R., Contacting modes and behaviour classification of gas-solid and other two-phase suspensions. The Canadian Journal of Chemical Engineering, 1986. 64(3): p. 353-363.
207. Yang, W.-C., Handbook of fluidization and fluid-particle systems. 2003: CRC press.
208. Werther, J., Fluidized-Bed Reactors. 1992: Wiley Online Library.
209. Qureshi, A. and D. Creasy, Fluidised bed gas distributors. Powder Technology, 1979. 22(1): p. 113-119.
210. Basu, P., Design of gas distributors for fluid bed boilers. Fluidised bed boilers: design and application. Nova Scotia, Canada: Pergamon Press Ltd, 1984: p. 45-61.

211. Saberi, S., et al., Comparative study of tuyere designs for fluidized beds. The Chemical Engineering Journal and The Biochemical Engineering Journal, 1995. 60(1): p. 75-79.
212. Fueyo, N. and C. Dopazo, Fluidization fundamentals, in Pressurized Fluidized Bed Combustion. 1995, Springer. p. 38-79.
213. Shanthakumar, S., D. Singh, and R. Phadke, Flue gas conditioning for reducing suspended particulate matter from thermal power stations. Progress in energy and combustion science, 2008. 34(6): p. 685-695.
214. Sinnott, R., Coulson's and Richardson's Chemical Engineering, Volume 6: Chemical Engineering Design. 2005, Elsevier Inc., UK.
215. Hoffmann, A.C. and L.E. Stein, Gas Cyclones and Swirl Tubes: Design and Operation. 2002: Springer.
216. Latif, A., A study of the design of fluidized bed reactors for biomass gasification. 1999, University of London.
217. Geldart, D., Types of gas fluidization. Powder technology, 1973. 7(5): p. 285-292.
218. Dai, J., H. Cui, and J.R. Grace, Biomass feeding for thermochemical reactors. Progress in Energy and Combustion Science, 2012. 38(5): p. 716-736.
219. Aggregae. Garside Sand 14/25. 2013; Available from: http://www.aggregate.com/documents/tds/dried-silica-sand-filler-14-25-tds.pdf.
220. Standard, A., D422–63 (2007) Standard test method for particle-size analysis of soils. ASTM International, West Conshohocken. doi, 2007. 10: p. 1520.
221. Coulson, J. and J. Richardson, Chemical Engineering–Particle Technology and Separation Process, vol. 2. 1991, Pergamon Press, Oxford.
222. Şensöz, S., D. Angın, and S. Yorgun, Influence of particle size on the pyrolysis of rapeseed (Brassica napus L.): fuel properties of bio-oil. Biomass and Bioenergy, 2000. 19(4): p. 271-279.
223. Mayoral, M., et al., Different approaches to proximate analysis by thermogravimetry analysis. Thermochimica Acta, 2001. 370(1): p. 91-97.
224. Channiwala, S. and P. Parikh, A unified correlation for estimating HHV of solid, liquid and gaseous fuels. Fuel, 2002. 81(8): p. 1051-1063.

225. Mészáros, E., et al., Thermogravimetry/mass spectrometry analysis of energy crops. Journal of Thermal Analysis and Calorimetry, 2007. 88(2): p. 477-482.
226. Saddawi, A., et al., Kinetics of the thermal decomposition of biomass. Energy & Fuels, 2009. 24(2): p. 1274-1282.
227. Ghetti, P., L. Ricca, and L. Angelini, Thermal analysis of biomass and corresponding pyrolysis products. Fuel, 1996. 75(5): p. 565-573.
228. Hilal, N., M. Ghannam, and M. Anabtawi, Effect of bed diameter, distributor and inserts on minimum fluidization velocity. Chemical Engineering and Technology, 2001. 24(2): p. 161-166.
229. Brus, E., M. Öhman, and A. Nordin, Mechanisms of bed agglomeration during fluidized-bed combustion of biomass fuels. Energy & Fuels, 2005. 19(3): p. 825-832.
230. Kutchko, B.G. and A.G. Kim, Fly ash characterization by SEM–EDS. Fuel, 2006. 85(17): p. 2537-2544.
231. Lin, W., K. Dam-Johansen, and F. Frandsen, Agglomeration in bio-fuel fired fluidized bed combustors. Chemical Engineering Journal, 2003. 96(1): p. 171-185.
232. Zhong, Y., et al., Prevention of agglomeration/defluidization in fluidized bed reduction of Fe 2 O 3 by CO: the role of magnesium and calcium oxide. Powder technology, 2013. 241: p. 142-148.
233. Scala, F. and R. Chirone, An SEM/EDX study of bed agglomerates formed during fluidized bed combustion of three biomass fuels. Biomass and Bioenergy, 2008. 32(3): p. 252-266.
234. Reed, S.J.B., Electron microprobe analysis and scanning electron microscopy in geology. 2005: Cambridge University Press.
235. Sharma, B., Instrumental methods of chemical analysis. 2000: Krishna Prakashan Media.
236. Skoog, D.A. and D.M. West, Principles of instrumental analysis. Vol. 158. 1980: Saunders College Philadelphia.
237. Klug, H.P. and L.E. Alexander, X-ray diffraction procedures. Vol. 2. 1954: Wiley New York.

238. Cele, N.P., Preparation and characterization of Nafion-based nanocomposite membranes for fuel cell applications. 2010, University of Zululand.
239. Rietveld, H., Line profiles of neutron powder-diffraction peaks for structure refinement. Acta Crystallographica, 1967. 22(1): p. 151-152.
240. Hill, R. and C. Howard, Quantitative phase analysis from neutron powder diffraction data using the Rietveld method. Journal of Applied Crystallography, 1987. 20(6): p. 467-474.
241. Van Grieken, R. and A. Markowicz, Handbook of X-ray Spectrometry. 2001: CRC Press.
242. Tertian, R. and F. Claisse, Principles of quantitative X-ray fluorescence analysis. 1982.
243. Mann, M.K. and P.L. Spath. A comparison of the environmental consequences of power from biomass, coal, and natural gas. in First World Conference and Exhibition on Biomass for Energy and Industry. 2000.
244. Hall, D. and J. Scrase, Will biomass be the environmentally friendly fuel of the future? Biomass and Bioenergy, 1998. 15(4-5): p. 357-367.
245. Fantozzi, F., P. Bartocci, and C. Buratti. Agroforestry biomass availability assessment in Umbria region, preliminary results. in Proceedings of the 16th European Biomass Conference and Exhibition, Spain, Valencia. 2008.
246. Buratti, C., et al. The biomass research centre laboratory for biomass characterization. in Proceedings of 14th European Biomass Conference and Exhibition. Biomass for Energy, Industry and Climate Protection. Paris. 2005.
247. Altun, N.E., C. Hicyilmaz, and M.V. Kök, Effect of particle size and heating rate on the pyrolysis of Silopi asphaltite. Journal of analytical and applied pyrolysis, 2003. 67(2): p. 369-379.
248. Serrano, C., et al., Effect of moisture content, particle size and pine addition on quality parameters of barley straw pellets. Fuel Processing Technology, 2011. 92(3): p. 699-706.
249. Jeguirim, M., et al., Devolatilization kinetics of miscanthus straw from thermogravimetric analysis. International Journal of Green Energy, 2010. 7(2): p. 164-173.

250. Reina, J., E. Velo, and L. Puigjaner, Thermogravimetric study of the pyrolysis of waste wood. Thermochimica Acta, 1998. 320(1): p. 161-167.
251. Mani, T., et al., Pyrolysis of wheat straw in a thermogravimetric analyzer: effect of particle size and heating rate on devolatilization and estimation of global kinetics. Chemical Engineering Research and Design, 2010. 88(8): p. 952-958.
252. Greenhalf, C., et al., A comparative study of straw, perennial grasses and hardwoods in terms of fast pyrolysis products. Fuel, 2013. 108: p. 216-230.
253. García, R., et al., Spanish biofuels heating value estimation. Part I: Ultimate analysis data. Fuel, 2014. 117, Part B(0): p. 1130-1138.
254. Verma, V., et al., Agro-pellets for domestic heating boilers: Standard laboratory and real life performance. Applied Energy, 2012. 90(1): p. 17-23.
255. Xia, Y.-J., et al., Kinetics of isothermal and non-isothermal pyrolysis of oil shale. Oil Shale, 2011. 28(3): p. 415-424.
256. Liu, H., Combustion of coal chars in O_2/CO_2 and O_2/N_2 mixtures: a comparative study with non-isothermal thermogravimetric analyzer (TGA) tests. Energy & Fuels, 2009. 23(9): p. 4278-4285.
257. Williams, P.T. and N. Ahmad, Investigation of oil-shale pyrolysis processing conditions using thermogravimetric analysis. Applied Energy, 2000. 66(2): p. 113-133.
258. Zhang, X., et al., Study on biomass pyrolysis kinetics. Journal of engineering for gas turbines and power, 2006. 128(3): p. 493-496.
259. Várhegyi, G., H. Chen, and S. Godoy, Thermal decomposition of wheat, oat, barley, and Brassica carinata straws. A kinetic study. Energy & Fuels, 2009. 23(2): p. 646-652.
260. Ergüdenler, A. and A. Ghaly, A comparative study on the thermal decomposition of four cereal straws in an oxidizing atmosphere. Bioresource technology, 1994. 50(3): p. 201-208.
261. Chen, D., Y. Zheng, and X. Zhu, In-depth investigation on the pyrolysis kinetics of raw biomass. Part I: Kinetic analysis for the drying and devolatilization stages. Bioresource technology, 2012.

262. Huang, S., et al., The Physicochemical Properties and Catalytic Characteristics of Different Biomass Ashes. Energy Sources, Part A: Recovery, Utilization, and Environmental Effects, 2014. 36(4): p. 402-410.

263. Miles, T.R., et al., Alkali deposits found in biomass power plants: A preliminary investigation of their extent and nature. Volume 1. 1995, National Renewable Energy Lab., Golden, CO (United States); Miles (Thomas R.), Portland, OR (United States); Sandia National Labs., Livermore, CA (United States); Foster Wheeler Development Corp., Livingston, NJ (United States); California Univ., Davis, CA (United States); Bureau of Mines, Albany, OR (United States). Albany Research Center.

264. Munir, S., et al., Thermal analysis and devolatilization kinetics of cotton stalk, sugar cane bagasse and shea meal under nitrogen and air atmospheres. Bioresource technology, 2009. 100(3): p. 1413-1418.

265. Gani, A. and I. Naruse, Effect of cellulose and lignin content on pyrolysis and combustion characteristics for several types of biomass. Renewable Energy, 2007. 32(4): p. 649-661.

266. Biagini, E., F. Barontini, and L. Tognotti, Devolatilization of biomass fuels and biomass components studied by TG/FTIR technique. Industrial & engineering chemistry research, 2006. 45(13): p. 4486-4493.

267. Hodgson, E.M., et al., Variation in Miscanthus chemical composition and implications for conversion by pyrolysis and thermo-chemical bio-refining for fuels and chemicals. Bioresource technology, 2011. 102(3): p. 3411-3418.

268. Hodgson, E., et al., Miscanthus as a feedstock for fast-pyrolysis: Does agronomic treatment affect quality? Bioresource technology, 2010. 101(15): p. 6185-6191.

269. Hague, R.A., Pre-treatment and pyrolysis of biomass for the production of liquids for fuels and speciality chemicals. 1998, Aston University.

270. Bridgeman, T., et al., Torrefaction of reed canary grass, wheat straw and willow to enhance solid fuel qualities and combustion properties. Fuel, 2008. 87(6): p. 844-856.

271. Gurgel Veras, C., et al., Overlapping of the devolatilization and char combustion stages in the burning of coal particles. Combustion and Flame, 1999. 116(4): p. 567-579.
272. Borrego, A.G. and D. Alvarez, Comparison of chars obtained under oxy-fuel and conventional pulverized coal combustion atmospheres. Energy & Fuels, 2007. 21(6): p. 3171-3179.
273. Bejarano, P.A. and Y.A. Levendis, Single-coal-particle combustion in O_2/N_2 and O_2/CO_2 environments. Combustion and flame, 2008. 153(1): p. 270-287.
274. Yuzbasi, N.S. and N. Selçuk, Air and oxy-fuel combustion characteristics of biomass/lignite blends in TGA-FTIR. Fuel Processing Technology, 2011. 92(5): p. 1101-1108.
275. Moon, J., et al., Transient behavior of devolatilization and char reaction during steam gasification of biomass. Bioresource technology, 2013. 133: p. 429-436.
276. Ghaly, A. and A. Al-Taweel, Thermal degradation of cereal straws in air. Energy sources, 1990. 12(4): p. 439-449.
277. Croiset, E., K. Thambimuthu, and A. Palmer, Coal combustion in O2/CO2 mixtures compared with air. The Canadian Journal of Chemical Engineering, 2000. 78(2): p. 402-407.
278. Rathnam, R.K., et al., Differences in reactivity of pulverised coal in air (O2/N2) and oxy-fuel (O2/CO2) conditions. Fuel Processing Technology, 2009. 90(6): p. 797-802.
279. Acero, J.L., et al., Membrane filtration technologies applied to municipal secondary effluents for potential reuse. Journal of Hazardous Materials, 2010. 177(1–3): p. 390-398.
280. Chen, W. and J. Liu, The possibility and applicability of coagulation-MBR hybrid system in reclamation of dairy wastewater. Desalination, 2012. 285(0): p. 226-231.
281. Liu, Z., et al., Energy policy: A low-carbon road map for China. Nature, 2013. 500(7461): p. 143-145.

282. Hayhurst, A. and A. Lawrence, The amounts of NO x and N 2 O formed in a fluidized bed combustor during the burning of coal volatiles and also of char. Combustion and Flame, 1996. 105(3): p. 341-357.
283. Leckner, B., et al., Gaseous emissions from co-combustion of sewage sludge and coal/wood in a fluidized bed. Fuel, 2004. 83(4): p. 477-486.
284. Duan, F., et al., Effect of secondary gas injection on the peanut shell combustion and its pollutant emissions in a vortexing fluidized bed combustor. Bioresource technology, 2014. 154: p. 201-208.
285. Khan, A.A., et al., Scale-up study on combustibility and emission formation with two biomass fuels (B quality wood and pepper plant residue) under BFB conditions. Biomass and Bioenergy, 2008. 32(12): p. 1311-1321.
286. Kuprianov, V.I., R. Kaewklum, and S. Chakritthakul, Effects of operating conditions and fuel properties on emission performance and combustion efficiency of a swirling fluidized-bed combustor fired with a biomass fuel. Energy, 2011. 36(4): p. 2038-2048.
287. Okasha, F., Staged combustion of rice straw in a fluidized bed. Experimental Thermal and Fluid Science, 2007. 32(1): p. 52-59.
288. Qian, F., et al., Combustion and NO emission of high nitrogen content biomass in a pilot-scale vortexing fluidized bed combustor. Bioresource technology, 2011. 102(2): p. 1892-1898.
289. Saikaew, T., et al., Emission of NO x and N_2O from co-combustion of coal and biomasses in CFB combustor. International Journal of Greenhouse Gas Control, 2012. 10: p. 26-32.
290. Varol, M., et al., Emission characteristics of co-combustion of a low calorie and high sulfur–lignite coal and woodchips in a circulating fluidized bed combustor: Part 1. Effect of excess air ratio. Fuel, 2014. 117: p. 792-800.
291. Llorente, M.F. and R.E. Cuadrado, Influence of the amount of bed material on the distribution of biomass inorganic elements in a bubbling fluidised bed combustion pilot plant. Fuel, 2007. 86(5): p. 867-876.

292. Burling, I., et al., Laboratory measurements of trace gas emissions from biomass burning of fuel types from the southeastern and southwestern United States. Atmospheric Chemistry and Physics, 2010. 10(22): p. 11115-11130.
293. Ninduangdee, P. and V.I. Kuprianov, A study on combustion of oil palm empty fruit bunch in a fluidized bed using alternative bed materials: Performance, emissions, and time-domain changes in the bed condition. Applied Energy, 2016. 176: p. 34-48.
294. Peng, Y. and L.T. Fan, Hydrodynamic characteristics of fluidization in liquid-solid tapered beds. Chemical Engineering Science, 1997. 52(14): p. 2277-2290.
295. Liu, H. and B.M. Gibbs, The influence of calcined limestone on NOx and N_2O emissions from char combustion in fluidized bed combustors. Fuel, 2001. 80(9): p. 1211-1215.
296. Liu, H. and B.M. Gibbs, Modelling of NO and N_2O emissions from biomass-fired circulating fluidized bed combustors. Fuel, 2002. 81(3): p. 271-280.
297. Duan, L., et al., NO emission during co-firing coal and biomass in an oxy-fuel circulating fluidized bed combustor. Fuel, 2015. 150: p. 8-13.
298. Villeneuve, J., et al., A critical review of emission standards and regulations regarding biomass combustion in small scale units <3MW. Bioresource technology, 2012. 111: p. 1-11.
299. Tarelho, L.A.d.C., D.S.F. Neves, and M.A.A. Matos, Forest biomass waste combustion in a pilot-scale bubbling fluidised bed combustor. Biomass and bioenergy, 2011. 35(4): p. 1511-1523.
300. Tarelho, L.A.d.C., M.A.A. Matos, and F.J.M.A. Pereira, Axial and radial CO concentration profiles in an atmospheric bubbling FB combustor. Fuel, 2005. 84(9): p. 1128-1135.
301. De Diego, L., et al., Coupled drying and devolatilisation of non-spherical wet pine wood particles in fluidised beds. Journal of Analytical and Applied Pyrolysis, 2002. 65(2): p. 173-184.
302. Liu, H., et al., Control of NOx emissions of a domestic/small-scale biomass pellet boiler by air staging. Fuel, 2013. 103: p. 792-798.

303. Bartels, M., et al., Agglomeration in fluidized beds at high temperatures: Mechanisms, detection and prevention. Progress in Energy and Combustion Science, 2008. 34(5): p. 633-666.
304. Rozainee, M., et al., Effect of fluidising velocity on the combustion of rice husk in a bench-scale fluidised bed combustor for the production of amorphous rice husk ash. Bioresource Technology, 2008. 99(4): p. 703-713.
305. Fan, W.D., et al., Impact of air staging along furnace height on NOx emissions from pulverized coal combustion. Fuel Processing Technology, 2010. 91(6): p. 625-634.
306. Peng, Y. and L. Fan, Hydrodynamic characteristics of fluidization in liquid-solid tapered beds. Chemical Engineering Science, 1997. 52(14): p. 2277-2290.
307. Okasha, F., M. El-Naggar, and E. Zeidan, Enhancing Emissions Reduction and Combustion Processes for Biomass in a Fluidized Bed. Energy & Fuels, 2014. 28(10): p. 6610-6617.
308. Scala, F. and R. Chirone, Characterization and early detection of bed agglomeration during the fluidized bed combustion of olive husk. Energy & fuels, 2006. 20(1): p. 120-132.
309. Metz, B., et al., Carbon dioxide capture and storage. 2005.
310. Buhre, B., et al., Oxy-fuel combustion technology for coal-fired power generation. Progress in energy and combustion science, 2005. 31(4): p. 283-307.
311. Chen, L., S.Z. Yong, and A.F. Ghoniem, Oxy-fuel combustion of pulverized coal: Characterization, fundamentals, stabilization and CFD modeling. Progress in Energy and Combustion Science, 2012. 38(2): p. 156-214.
312. Shaddix, C.R. and A. Molina, Particle imaging of ignition and devolatilization of pulverized coal during oxy-fuel combustion. Proceedings of the Combustion Institute, 2009. 32(2): p. 2091-2098.
313. Yang, W.-C., Bubbling fluidized beds. Chemical Industries New York Marcel Dekker, 2003: p. 53-112.
314. Abanades, J.C., et al., Capture of CO_2 from combustion gases in a fluidized bed of CaO. AIChE Journal, 2004. 50(7): p. 1614-1622.

315. Basu, P., Combustion of coal in circulating fluidized-bed boilers: a review. Chemical Engineering Science, 1999. 54(22): p. 5547-5557.
316. Molina, A. and C.R. Shaddix, Ignition and devolatilization of pulverized bituminous coal particles during oxygen/carbon dioxide coal combustion. Proceedings of the Combustion Institute, 2007. 31(2): p. 1905-1912.
317. Wall, T., et al., An overview on oxyfuel coal combustion—state of the art research and technology development. Chemical Engineering Research and Design, 2009. 87(8): p. 1003-1016.
318. Romeo, L.M., et al., Design and operation assessment of an oxyfuel fluidized bed combustor. Experimental Thermal and Fluid Science, 2011. 35(3): p. 477-484.
319. Croiset, E. and K. Thambimuthu, NOx and SO_2 emissions from O_2/CO_2 recycle coal combustion. Fuel, 2001. 80(14): p. 2117-2121.
320. Andersson, K., et al., Radiation intensity of lignite-fired oxy-fuel flames. Experimental thermal and fluid science, 2008. 33(1): p. 67-76.
321. Hjärtstam, S., et al., Combustion characteristics of lignite-fired oxy-fuel flames. Fuel, 2009. 88(11): p. 2216-2224.
322. Czakiert, T., et al., Oxy-fuel circulating fluidized bed combustion in a small pilot-scale test rig. Fuel Processing Technology, 2010. 91(11): p. 1617-1623.
323. Normann, F., et al., Emission control of nitrogen oxides in the oxy-fuel process. Progress in Energy and Combustion Science, 2009. 35(5): p. 385-397.
324. Sloss, L., Trends in emission standards. IEA Clean Coal Centre Reports, 2003: p. 64.
325. Zeldovich, Y.B., The oxidation of nitrogen in combustion and explosions. Acta Physicochim. URSS, 1946. 21(4): p. 577-628.
326. Zhou, H., et al., Formation and reduction of nitric oxide in fixed-bed combustion of straw. Fuel, 2006. 85(5): p. 705-716.
327. Lupiáñez, C., et al., Experimental study of SO_2 and NOx emissions in fluidized bed oxy-fuel combustion. Fuel processing technology, 2013. 106: p. 587-594.

328. Skeen, S.A., B.M. Kumfer, and R.L. Axelbaum, Nitric oxide emissions during coal and coal/biomass combustion under air-fired and oxy-fuel conditions. Energy & Fuels, 2010. 24(8): p. 4144-4152.
329. Jia, L., et al., Experimental study of oxy-fuel combustion and sulfur capture in a mini-CFBC. Energy & Fuels, 2007. 21(6): p. 3160-3164.
330. Rehfeldt, S., et al. Basic experiments and CFD calculations of air and oxyfuel firing of lignite and bituminous coals in 0.5 and 1 MW scale combustion test facilities. in Proceedings of the 34th International Technical Conference on Clean Coal and Fuel Systems (May 2009). 2009.
331. Skrifvars, B.J., M. Hupa, and M. Hiltunen, Sintering of ash during fluidized bed combustion. Industrial & engineering chemistry research, 1992. 31(4): p. 1026-1030.
332. Dawson, M.R. and R.C. Brown, Bed material cohesion and loss of fluidization during fluidized bed combustion of midwestern coal. Fuel, 1992. 71(5): p. 585-592.
333. Nordin, A., Optimization of sulfur retention in ash when cocombusting high sulfur fuels and biomass fuels in a small pilot scale fluidized bed. Fuel, 1995. 74(4): p. 615-622.
334. Öhman, M., et al., Bed agglomeration characteristics during fluidized bed combustion of biomass fuels. Energy & Fuels, 2000. 14(1): p. 169-178.
335. Yijie, Y., et al., Bed agglomeration characteristics during fluidized-bed combustion of biomass fuels. Kezaisheng Nengyuan/Renewable Energy Resources, 2007. 25(3): p. 50-53.
336. Teixeira, P., et al., Evaluation of slagging and fouling tendency during biomass co-firing with coal in a fluidized bed. biomass and bioenergy, 2012. 39: p. 192-203.
337. Lin, C.-L. and M.-Y. Wey, The effect of mineral compositions of waste and operating conditions on particle agglomeration/defluidization during incineration. Fuel, 2004. 83(17): p. 2335-2343.
338. Datta, S., et al., Agglomeration behaviour of high ash Indian coals in fluidized bed gasification pilot plant. Applied Thermal Engineering, 2015. 86: p. 222-228.

339. Vassilev, S.V., D. Baxter, and C.G. Vassileva, An overview of the behaviour of biomass during combustion: Part I. Phase-mineral transformations of organic and inorganic matter. Fuel, 2013. 112: p. 391-449.
340. Tardos, G. and R. Pfeffer, Chemical reaction induced agglomeration and defluidization of fluidized beds. Powder technology, 1995. 85(1): p. 29-35.
341. Vujtek, M., et al., Ultrafine Particles of Iron (III) Oxides by View of AFM–Novel Route for Study of Polymorphism in Nano-world.
342. Llorente, M.F., et al., Combustion in bubbling fluidised bed with bed material of limestone to reduce the biomass ash agglomeration and sintering. Fuel, 2006. 85(14): p. 2081-2092.
343. Lin, W., et al., Agglomeration phenomena in fluidized bed combustion of straw. 1997, American Society of Mechanical Engineers, New York, NY (United States).
344. Mettanant, V., P. Basu, and J. Butler, Agglomeration of biomass fired fluidized bed gasifier and combustor. The Canadian Journal of Chemical Engineering, 2009. 87(5): p. 656-684.
345. Olanders, B. and B.-M. Steenari, Characterization of ashes from wood and straw. Biomass and Bioenergy, 1995. 8(2): p. 105-115.
346. Obernberger, I. and G. Thek, Physical characterisation and chemical composition of densified biomass fuels with regard to their combustion behaviour. Biomass and bioenergy, 2004. 27(6): p. 653-669.
347. Jenkins, B., et al., Composition of ash deposits in biomass fuelled boilers: results of full-scale experiments and laboratory simulations. Paper-American Society of Agricultural Engineers, 1994(946007).
348. Vamvuka, D. and G. Bandelis, Evaluation of wood residues from Crete as alternative fuels. International Journal of Energy and Environment, 2010. 1(4): p. 667-674.
349. Skrifvars, B.-J., et al., Sintering mechanisms of FBC ashes. Fuel, 1994. 73(2): p. 171-176.

350. Chirone, R., F. Miccio, and F. Scala, Mechanism and prediction of bed agglomeration during fluidized bed combustion of a biomass fuel: effect of the reactor scale. Chemical engineering journal, 2006. 123(3): p. 71-80.
351. Brus, E., et al., Bed agglomeration characteristics of biomass fuels using blast-furnace slag as bed material. Energy & fuels, 2004. 18(4): p. 1187-1193.
352. Grubor, B., et al., Biomass FBC combustion-Bed agglomeration problems. 1995, American Society of Mechanical Engineers, New York, NY (United States).
353. van Eyk, P.J., et al., Control of agglomeration during circulating fluidized bed gasification of a South Australian low-rank coal: pilot scale testing. Energy & Fuels, 2016. 30(3): p. 1771-1782.
354. Yang, W.-C. and D.L. Keairns, Operational analysis of ash-agglomerating fluidized bed gasifiers. Powder technology, 2000. 111(1): p. 168-174.

Appendix A

Biomass Combustion Stoichiometric Calculations

Biomass is usually being represented as (C_hi_os) and the overall general combustion reaction is written as:

$$C_hi_os + (x+0.25y-0.5z)O_x \longrightarrow xCO_2 + (0.5y)H_2O \quad (A.1)$$

For stoichiometric calculation, we can write chemical formula of biomass as $C_6H_{12}O_6$ then the chemical reaction for biomass combustion in oxy-fuel conditions will be.

$$C_6H_{12}O_6 + 6O_2 \longrightarrow 6CO_2 + 6H_2O \quad (A.2)$$

The mass and mole fractions of the components are calculated through following steps. Mass fraction of component *i*, is defined as the ratio of the mass of the component, m_i to the total mass of the mixture, m_{tot}

Yi = m_i/m_{tot}

Total molecular mass of $C_6H_{12}O_6$ is 12×6+1×12+16×6

m_{tot} = 180

Mass fraction of the components:

C: 12×6/180 = 0.40

H: 1×12/180 = 0.07

O: 16×6/180 = 0.53

Mole fraction of component *i*, is defined as the ratio of the number of moles of *i*, N_i to the total number of moles in the mixture, N_{tot}

$Xi = N_i/N_{tot}$

The total numbers of moles in $C_6H_{12}O_6$ are 6+12+6=24

Hence,

N_{tot} = 36

The mole fraction of the each component is as:

C: 6/24 = 0.25

H: 12/24 = 0.50

O: 6/24 = 0.25

The 4 kg/h of biomass fuel is considered for the design basis; as every 4 kg of the biomass fuel consists of C kg carbon, H kg of Hydrogen, O kg of oxygen, Ash kg of Ash and M kg of Moisture. Ash and moisture are assumed to be chemically inert although they absorb heat. Through this basis, the kg of C, H and O were calculated in 4 kg of biomass, by using mass fractions.

C: 4.0 kg × 0.40 = 1.60 kg

H: 4.0 kg × 0.07= 0.28 kg

O: 4.0 kg × 0.53= 2.12 kg

Table A1: The overall mass and mole fractions of components on the basis of 4 kg of biomass fuel.

Component	kg	Wt. fraction	Mol. wt.	kg moles	Mole fraction
C	1.60	1.60/4.0 = 0.4	12	1.60/12 = 0.1	0.1/0.4 = 0.25
H	0.28	0.28/4.0 = 0.1	1	0.28/1 = 0.3	0.2/0.4 = 0.50
O	2.12	2.12/4.0 = 0.5	16	2.12/16 = 0.1	0.1/0.4 = 0.25
Total	4.0	1.0		0.4	1.0

Stoichiometric Air-fuel (Mass) Ratio

Mass fraction of oxygen in the air is 0.233, therefore

$(A/F)_{stoic,\ mass} = (O/F)_{stoic,\ mass} \times 1/0.233$

$(A/F)_{stoic,\ mass} = 1.1 \times 1/0.233$

$(A/F)_{stoic,\ mass} = 4.71$ kg/ kg of biomass

Therefore, total air required for complete combustion of 4 kg biomass fuel = 4.71×4

Total air required = 18.84 kg/hr

Combustion of Biomass under Oxy-fuel

For complete combustion, all carbon will be converted to CO_2, hydrogen converted to H_2O and all the oxygen atoms contained in the fuel are available for combustion, ash and moisture are assumed to be chemically inert.

$$C + O_2 \longrightarrow CO_2 \qquad (A.3)$$

C kg of Carbon requires

32/12×C kg of oxygen

32/12×1.60 = 4.27 kg

$$H + 0.25O_2 \longrightarrow 0.5H_2O \qquad (A.4)$$

H kg of Hydrogen requires 8/1× H kg of oxygen

8/1×0.28 = 28.57 kg

Stoichiometric Oxygen-fuel (Mass) Ratio

As every 100 kg of biomass fuel contains O kg of oxygen which can be used in the combustion process. Therefore, the oxygen needed to be supplied for stoichiometric combustion of 1kg of biomass fuel.

$(O/F)_{stoic, mass}$

$= (32/12 \times C + 8/1 \times H - O)/100$

$= (32/12 \times 40 + 8/1 \times 7 - 53)/100$

$= (106.67 + 56 - 53)/100$

$= 109.67/100$

$(O/F)_{stoic, mass} = 1.1$ kg /kg of biomass

Considering 4 kg/hr of biomass fuel for the design basis.

Therefore, under oxy-fuel conditions, consider oxygen as an oxidant rather than air.

Oxygen required for complete combustion of 4 kg biomass fuel = 1.1×4

Total Oxygen required = 4.4 kg/hr

Density = Mass/Volume and Volume = Mass/Density

The density of oxygen at 20^oC is 1.33 kg/m^3

Total volume oxygen required = 4.4 kg/1.33 kg/m^3

Total volume of oxygen required = 3.31 m^3/hr

Total volume of oxygen required = (3.31×1000)/60 = 55.14 L/min

Hence,

The anticipated volume of Oxygen required

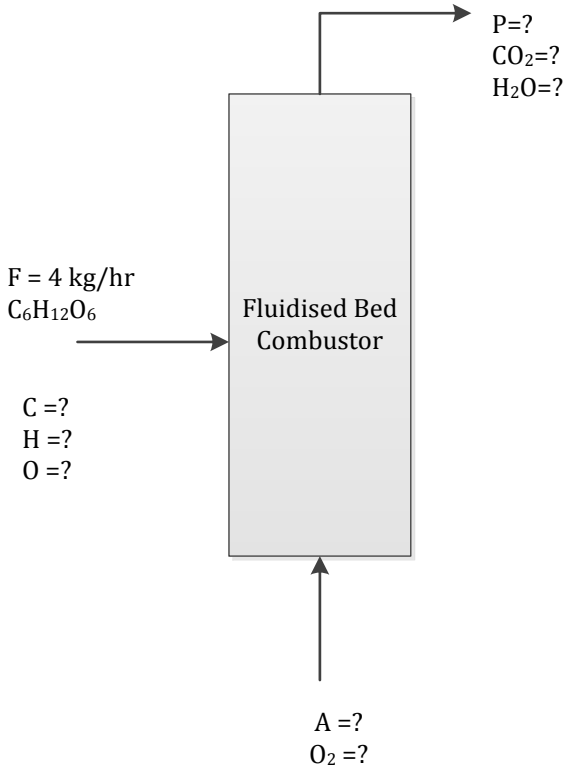
For rig operation = 70 L/min

The anticipated volume of CO_2 required

For rig operation = 210 L/min

Material Balance around Bubbling Fluidised Bed Combustor

The general overview of biomass combustion in BFB combustion under air showing reactants and products.



Basis: 4 kg/hr of Biomass

General chemical reaction for biomass combustion in oxy-fuel conditions.

$$C_6H_{12}O_6 + 6O_2 \longrightarrow 6CO_2 + 6H_2O \quad (A.5)$$

According to law of conservation of mass

Total mass into the system = Total mass out from the system

$$F + A = P \tag{A.6}$$

Mass fraction of the components in the feed.

For carbon

$$C = \frac{4\times12\times6}{12\times6+1\times12+16\times6}$$

C = 1.6 kg/hr

For hydrogen

$$H = \frac{4\times1\times12}{12\times6+1\times12+16\times6}$$

H = 0.3 kg/hr

Similarly for oxygen

$$O = \frac{4\times16\times6}{12\times6+1\times12+16\times6}$$

O = 2.1 kg/hr

Table A2: The mass and mole fractions of components in reactants

Component	kg	Wt. fraction	Mol. wt.	kg moles	Mole fraction
C	1.6	1.6/4.0 = 0.4	12	1.6/12 = 0.1	0.1/0.5 = 0.2
H	0.3	0.3/4.0 = 0.1	1	0.3/1 = 0.3	0.3/0.5 = 0.6
O	2.1	2.1/4.0 = 0.5	16	2.1/16 = 0.1	0.1/0.5 = 0.2
Total	4.0	1.0		0.5	1.0

From the combustion reaction of biomass mass flow rates of reactants and products are calculated.

Mass flow rate of O_2 required to react with 4 kg of $C_6H_{12}O_6$ is

4 kg $C_6H_{12}O_6$	1kg mole $C_6H_{12}O_6$	6kg mole O_2	32 kg O_2
hr	180 kg $C_6H_{12}O_6$	1kg mole $C_6H_{12}O_6$	1kg mole O_2

= 4.27 kg/hr O_2

The mass ratio of O_2 in the air is 0.233.

Hence

Air required (A) = 4.27/0.233

= 18.31 kg Air/hr

Mass flow rate of CO_2

4 kg $C_6H_{12}O_6$	1kg mole $C_6H_{12}O_6$	6 kg mole CO_2	44 kg CO_2
hr	180 kg $C_6H_{12}O_6$	1 kg mole $C_6H_{12}O_6$	1 kg mole CO_2

= 5.87 kg CO_2 /hr

Mass flow rate of H_2O in flue gas

4 kg $C_6H_{12}O_6$	1 kg mole $C_6H_{12}O_6$	6 kg mole H_2O	18 kg H_2O
hr	180 kg $C_6H_{12}O_6$	1 kg mole $C_6H_{12}O_6$	1 kg mole H_2O

= 2.4 kg H_2O /hr

Using Eq (A.6)

P= 4+ 18.31

P = 22.31 kg/hr

Table A3: The mass and mole fractions of the product gas.

Compound	kg	Wt. fraction	Mol. wt.	kg moles	Mole fraction
CO_2	5.87	5.87/8.27 = 0.71	44	5.87/44 = 0.13	0.13/0.26 = 0.5
H_2O	2.40	2.40/8.27= 0.29	18	2.40/18 = 0.13	0.13/0.26 = 0.5
Total	8.27	1.00		0.26	1.0

Fluidisation Velocities for Bubbling Fluidised Bed Combustor

The fluidisation velocities calculations are performed according to the equations explained in section 3.3.1 in Chapter 3.

Table A4: Fluidisation velocity parameters along with calculations.

Parameters	Units	Value
Operating temperature	K	1073
Operating pressure (p)	bar	1
Density of sand particles	kg/m^3	2655
Diameter of sand particles	M	0.00113
Molar weight of gas	g/mol	32
Operating temperature	K	273
Viscosity	kg/ms	0.00001716
Index constant (n)	-	0.67
Reynolds number (Re)	-	4.25
C1	-	33.7
C2	-	0.0408
Gravity	kg/m^2s	9.8
Using above parameters		
Density of gas	kg/m^3	0.36
Dynamic viscosity	kg/ms	4.27×10^{-5}
Archimedes number (Ar)	-	7469.89
Minimum fluidisation velocity (u_{mf})	m/s	0.44
Terminal velocity (u_t)	m/s	10.38
Operating velocity (u_o)	m/s	3.09

Bubbling Fluidised Bed Combustor Area and Diameter

Volumetric flow rate of gas (Q) = $\frac{\text{volume}}{\text{density}}$

The density of gas at 800 ^{o}C = 0.36 kg/m^3

Hence,

Q = 4.4 /0.36

Q = 12.22 m^3//hr

Q = 3.39×10^{-3} m^3/s

For area

A = π/4 D^2

A = 0.78× (0.102)^2

A = 8.17×10^{-3} m^2

Operating velocity (u_o) = $\frac{\text{volume flow rate}}{\text{area}}$

$u_o = \frac{3.39\times10^{-3}}{8.17\times10^{-3}}$

u_o = 0.42 m/s

For diameter

A = π/4 d^2

d = $[(Ax4)/\pi]^{1/2}$

d = $[(0.0081x4)/3.1416]^{1/2}$

d = 0.101 m

d = 4.0 in

Diameter of reactor = 4.0 in

Experimental Determination of Minimum Fluidisation Velocity in Bubbling Fluidised Bed Combustor

Table A5: Pressure drop against the distributor with and without sand at different air flow rates.

Air flow rate (Q) L/min	**Air velocity (U)** m/s	**Without sand (ΔP 1)** mbar	**With sand (ΔP2)** mbar	**Due to sand only (ΔP)** mbar	**Due to sand only (ΔP)** pascal
0	0.00	0.65	0.11	0.00	0.00
100	0.21	0.74	17.79	17.05	1728.03
150	0.31	0.85	21.46	20.61	2088.55
200	0.41	1.01	26.03	25.03	2535.89
250	0.51	1.21	27.31	26.10	2644.30
300	0.62	1.46	27.43	25.97	2631.80
350	0.72	1.75	29.47	27.72	2808.64
400	0.82	2.09	29.69	27.60	2796.65
450	0.93	2.47	29.76	27.29	2764.93
500	1.03	2.90	29.77	26.88	2723.53
550	1.13	3.37	33.29	29.92	3031.43
600	1.23	3.89	34.32	30.43	3083.53
650	1.34	4.45	32.82	28.37	2875.08
700	1.44	5.06	33.39	28.33	2870.71
750	1.54	5.71	32.83	27.13	2748.52
800	1.65	6.41	36.27	29.86	3025.61

Bed diameter = 101.6 mm

Bed height = 250 mm

Bed surface area = πr^2

Bed surface area = 0.00812 m^2

Sand weight = 3.22 kg

Gravity = 9.8 m/s^2

Minimum fluidisation velocity (u_{mf}) = $\frac{250}{60\times0.00811\times1000}$

Hence

u_{mf} = 0.512 m/s

Appendix B

Engineering and Technical Drawings

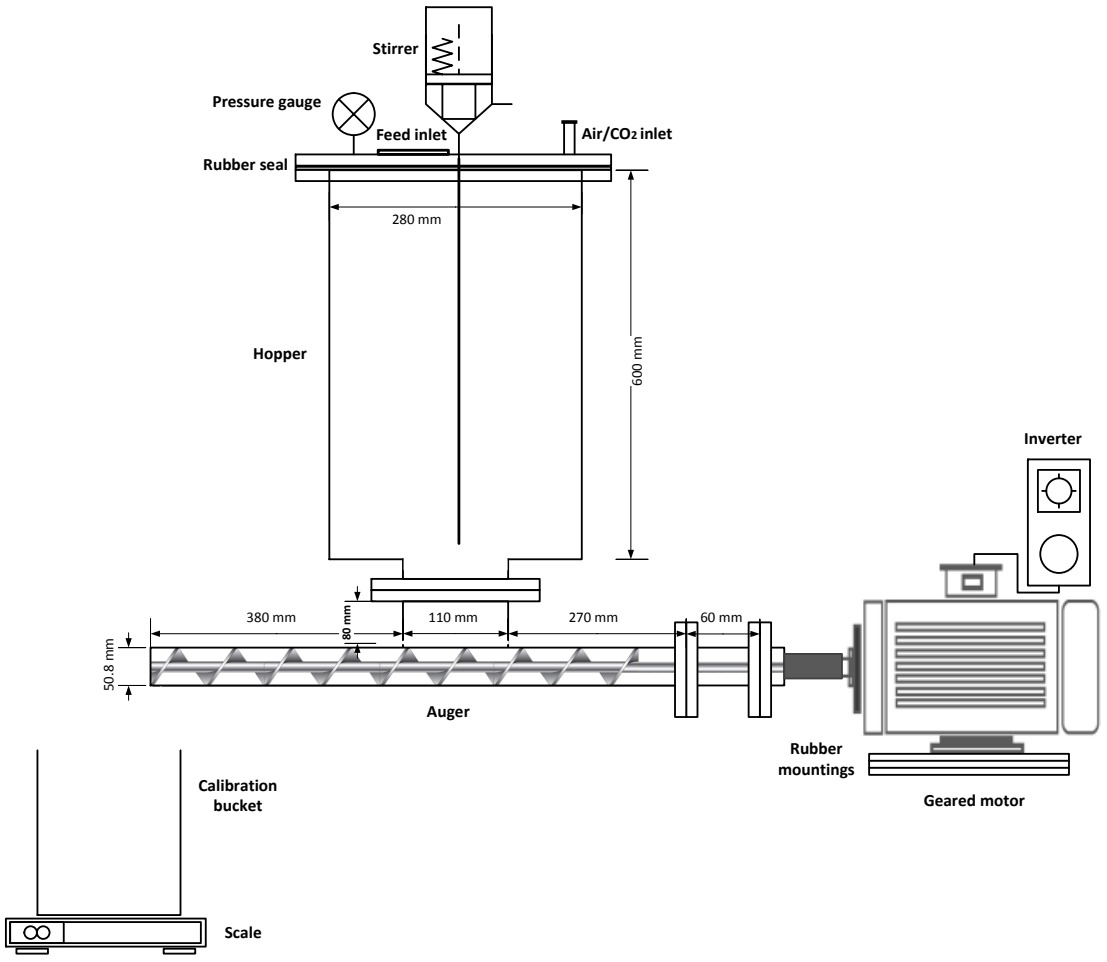


Figure B.1: Biomass feeding system with feed rate calibration auxiliaries.

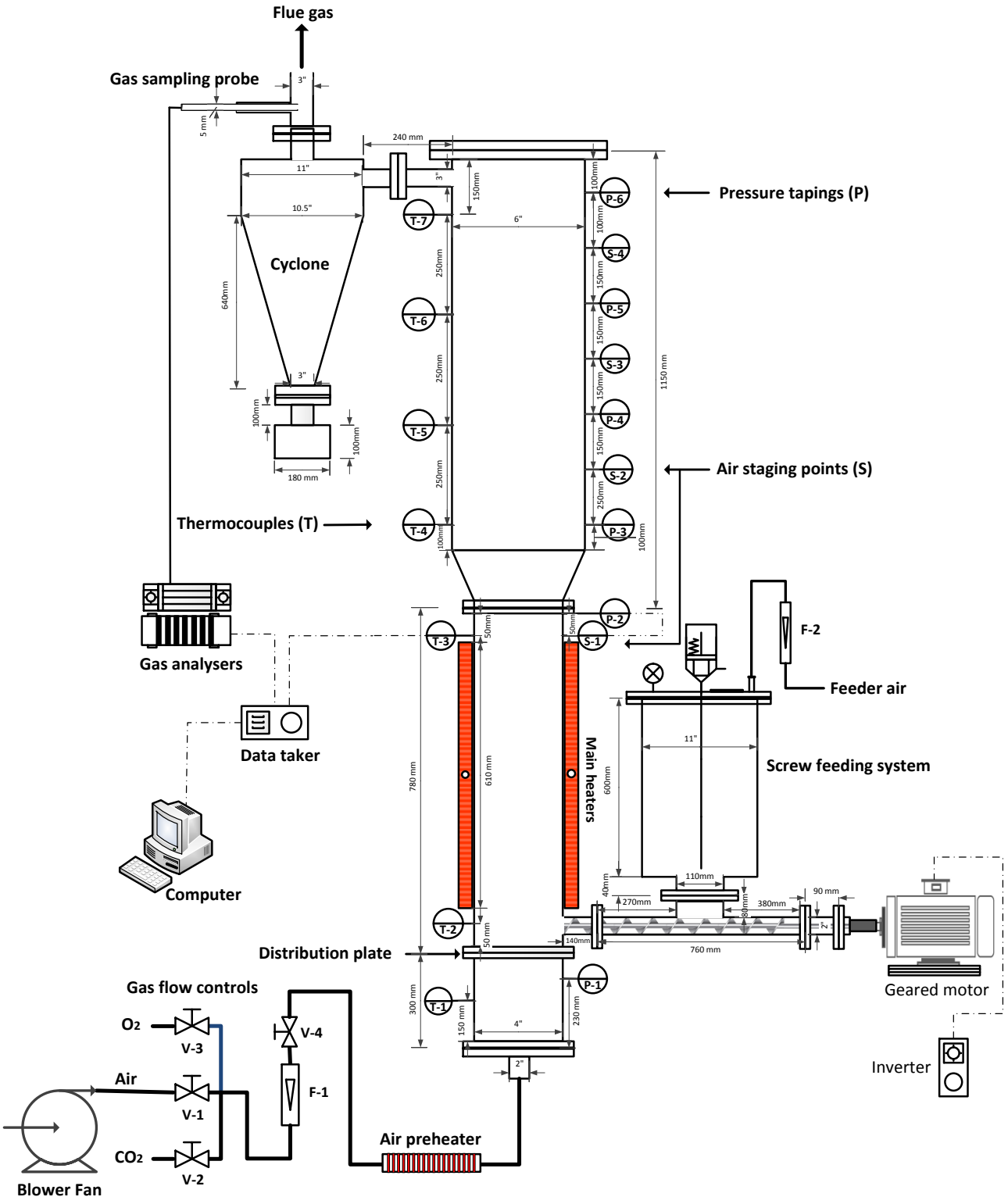


Figure B.2: Biomass BFBC system drawing with auxiliaries.

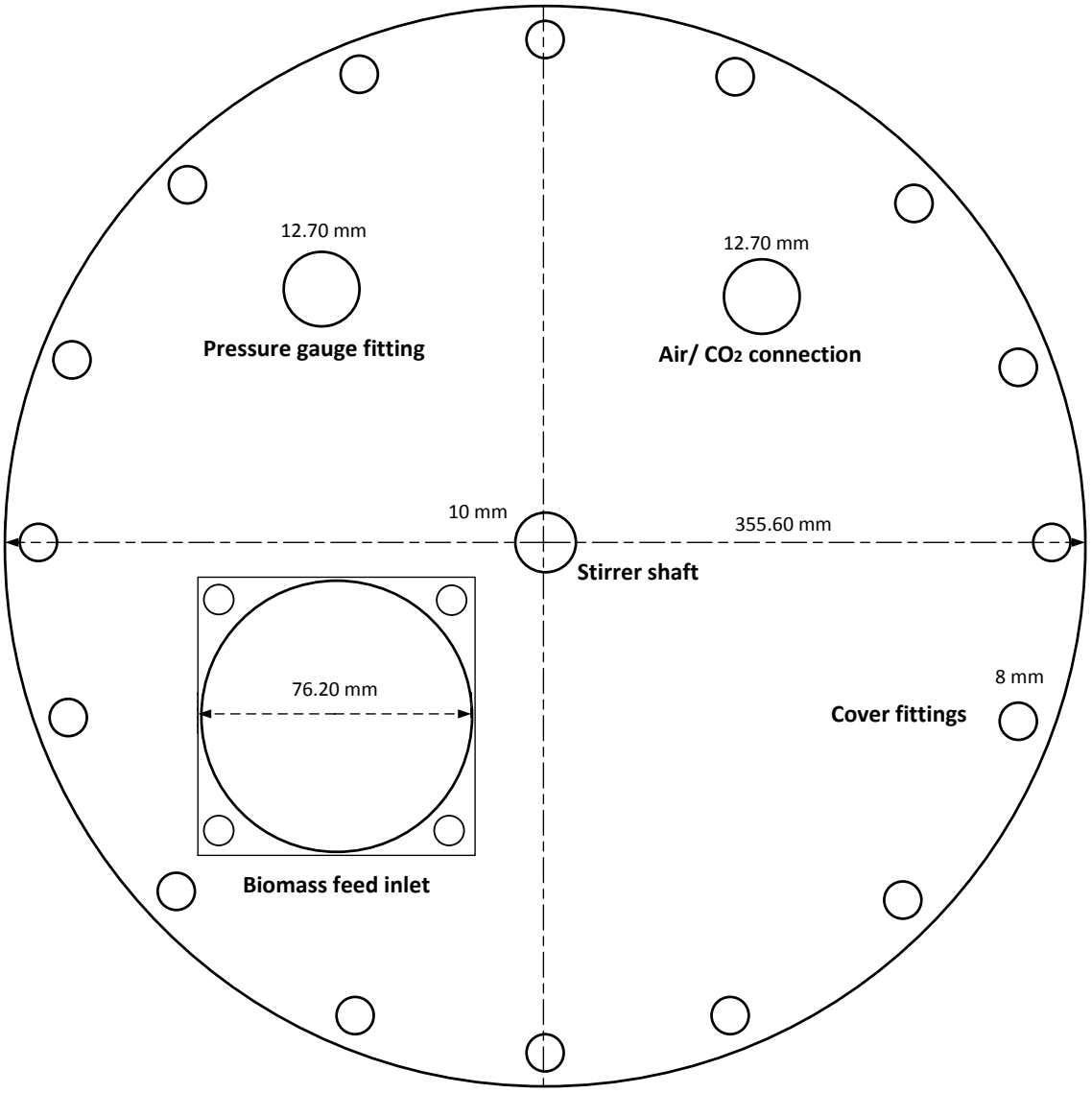


Figure B.3: Biomass hopper top cover plate drawing with fittings.

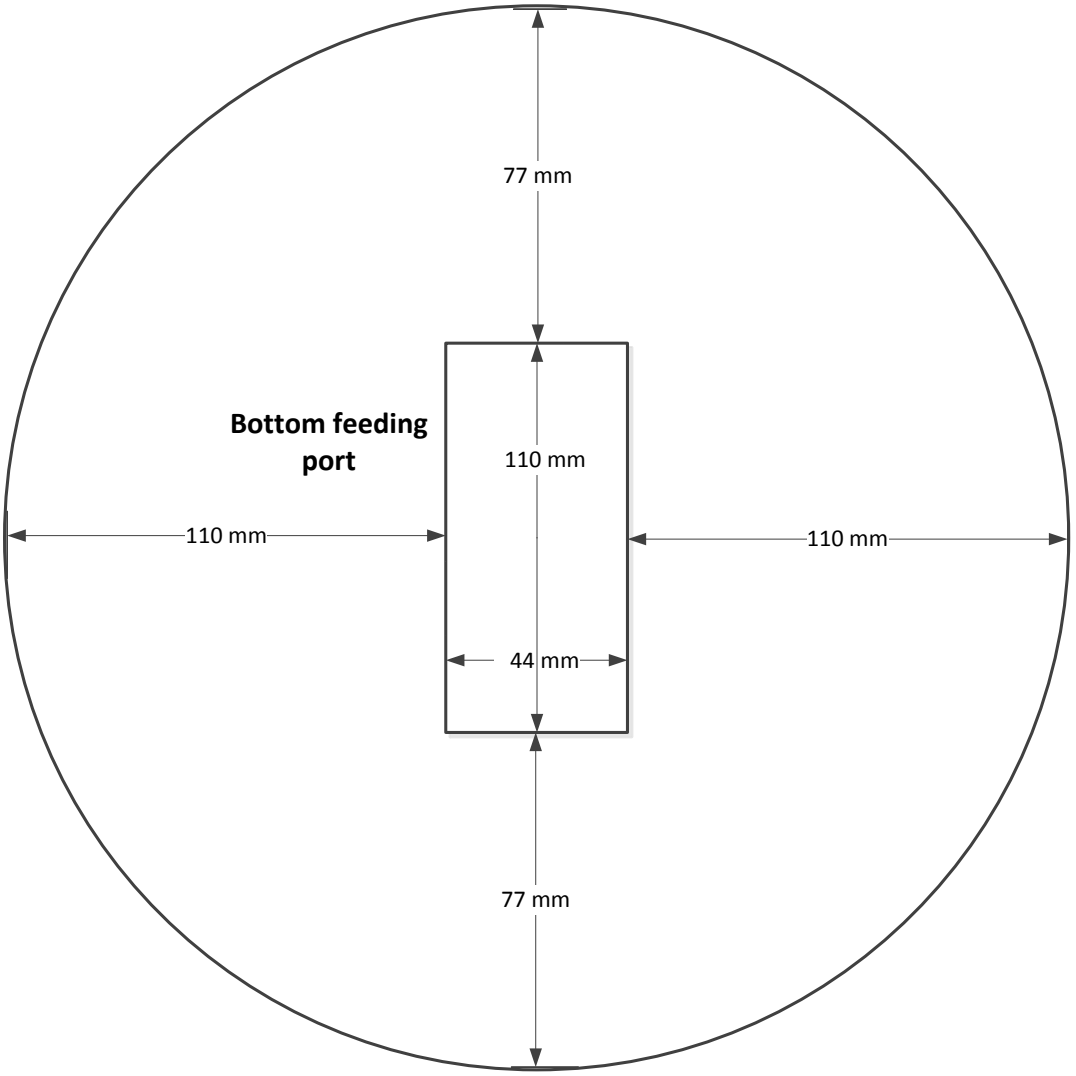


Figure B.4: Biomass hopper bottom plate drawing with feed discharge port.

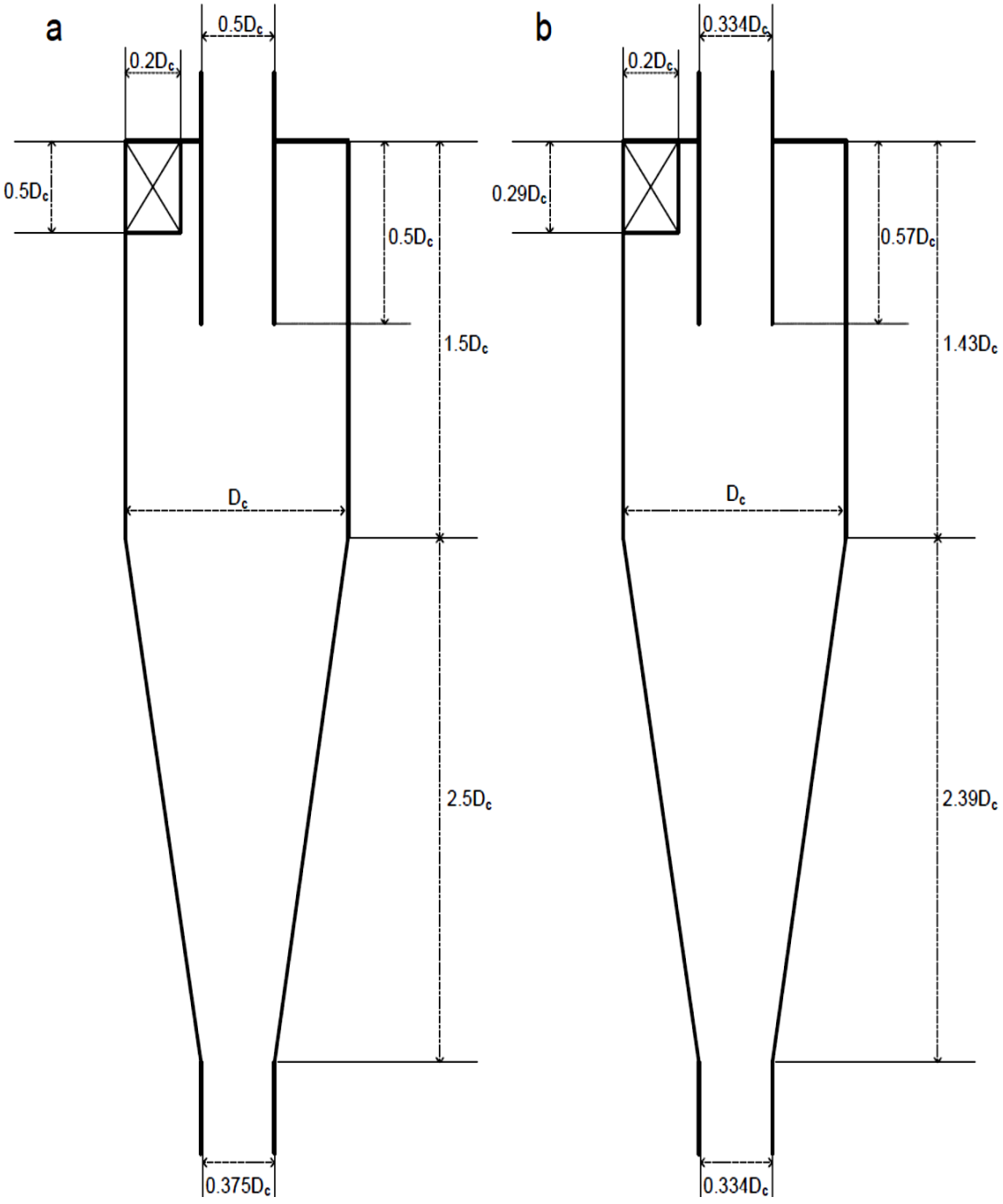


Figure B.5: Cyclone design dimensions; (a) standard high-efficiency, (b) altered high-efficiency.

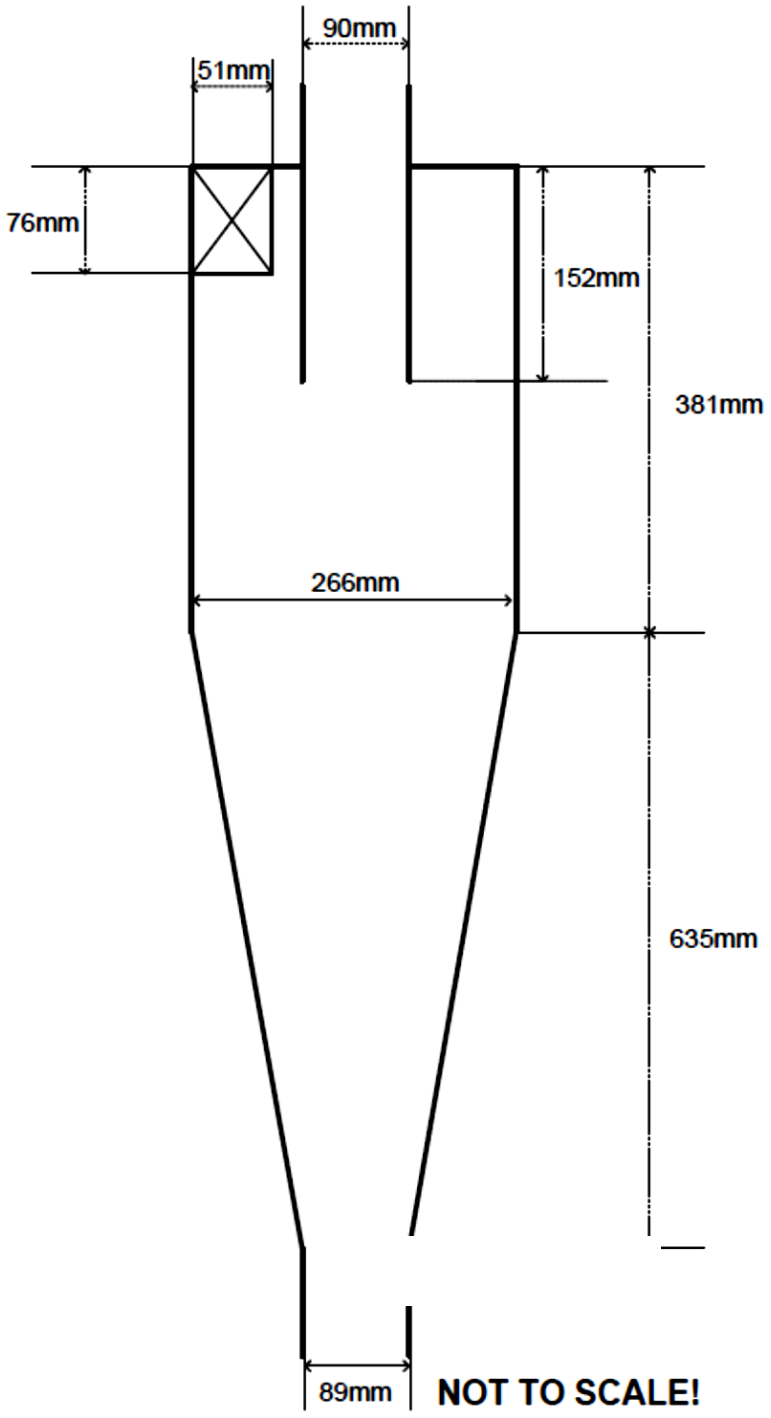


Figure B.6: Biomass BFBC gas-solids cyclone drawing.

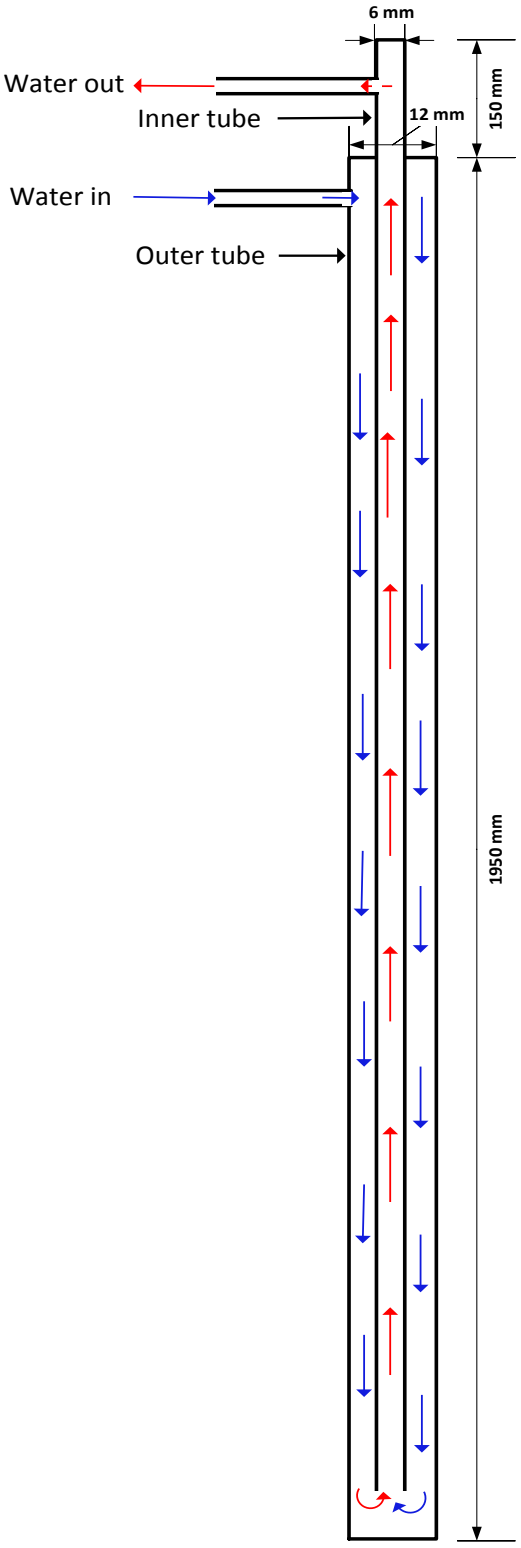


Figure B.7: Water cooled heat extraction cooling problem drawing.

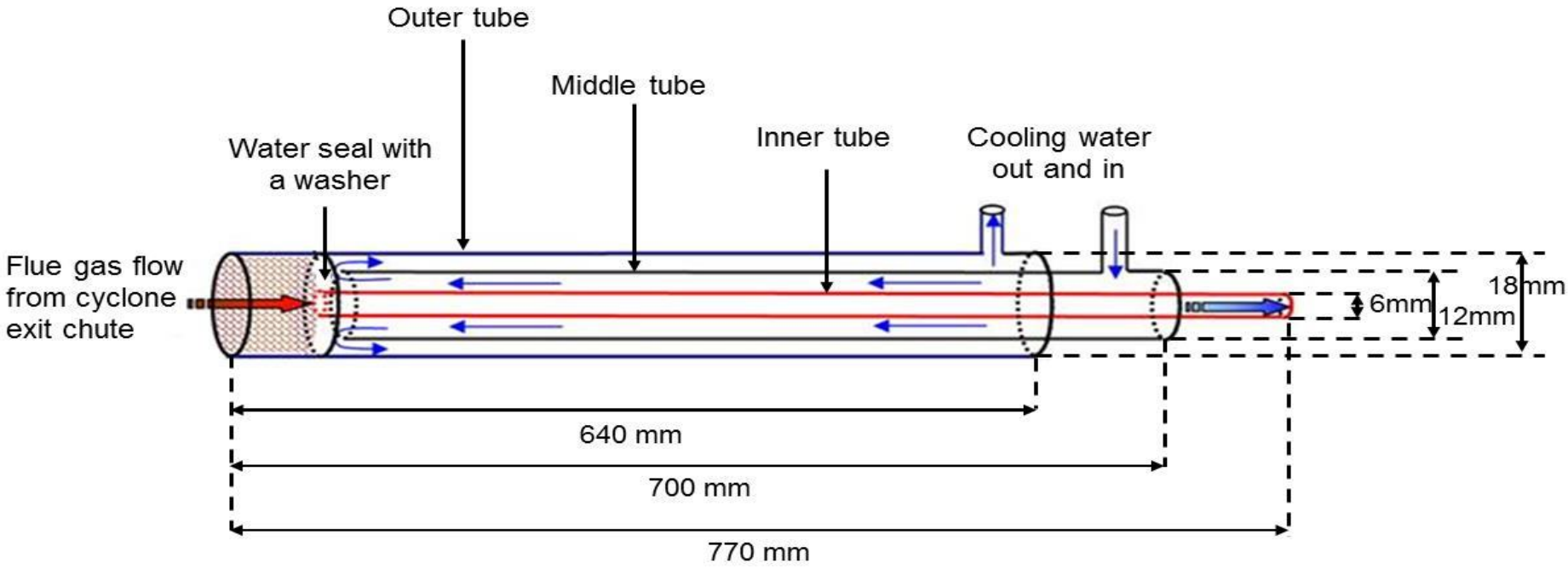


Figure B.8: Water cooled gas sampling probe drawing.

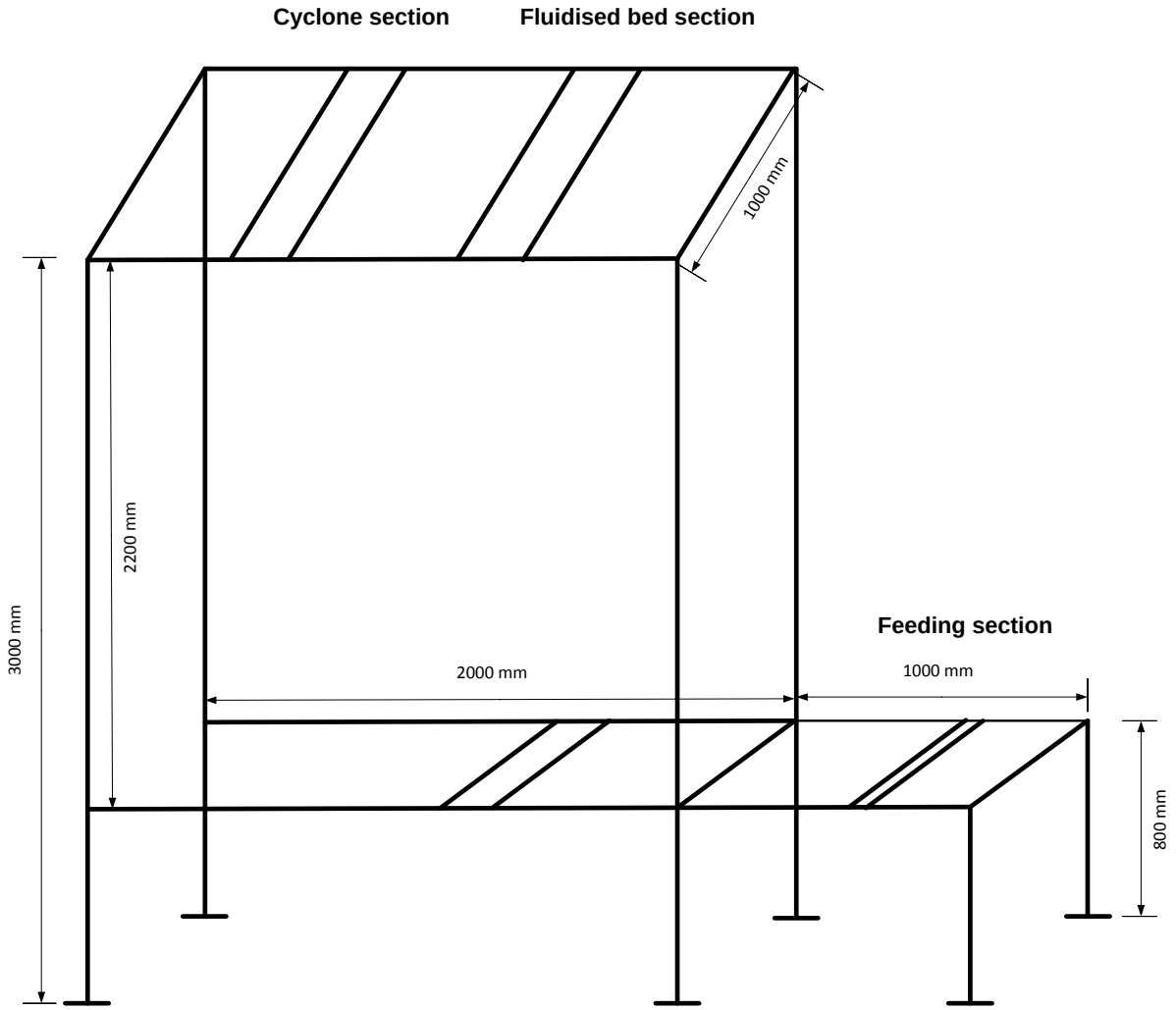


Figure B.9: Biomass FBC supporting frame drawing.

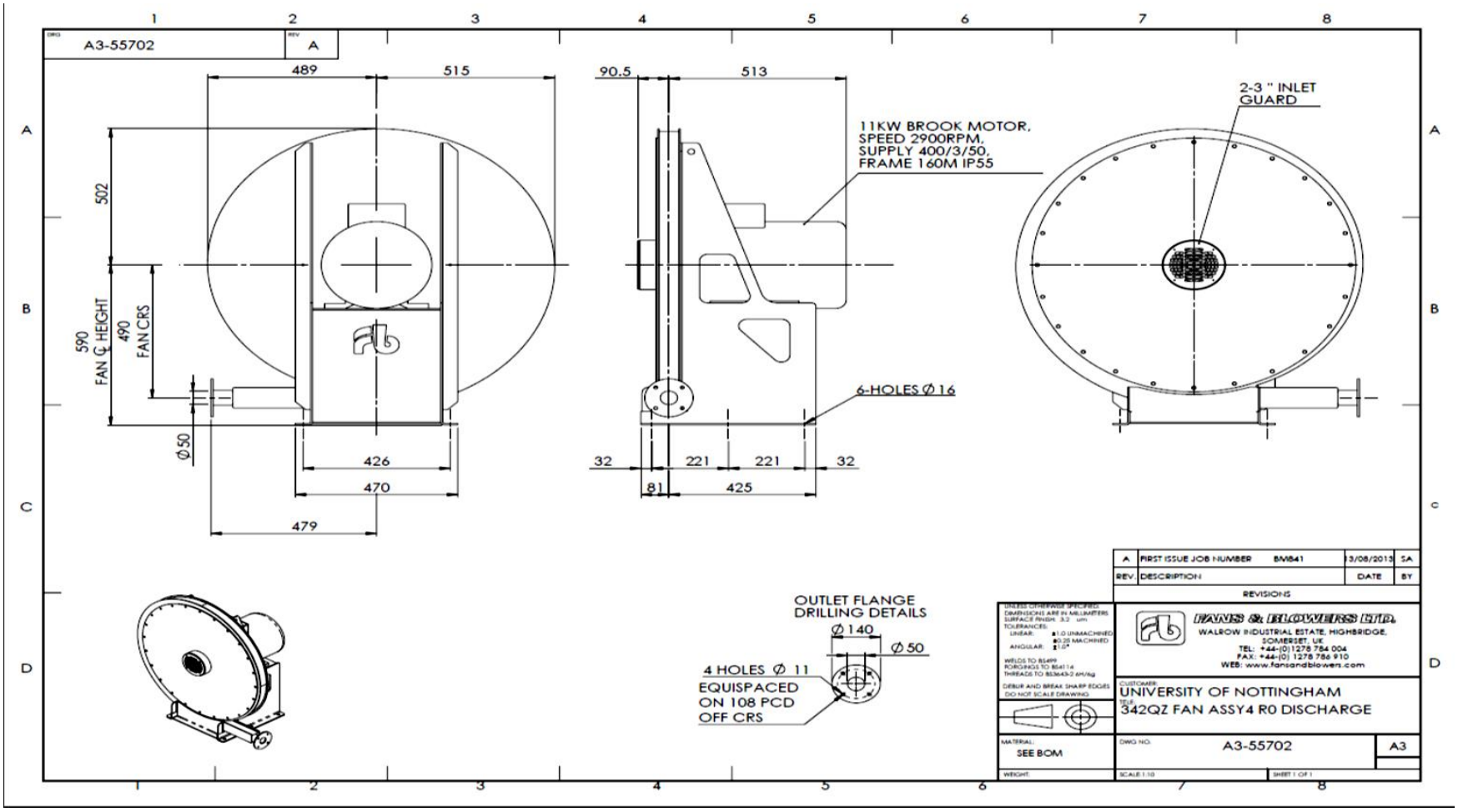


Figure B.10: BFBC blower fan drawing.

Appendix C

Materials and Methods Specifications

Sieve Analysis for Garside 14/25 Sand Bed Material

Table C.1: Sand particles size distribution as received basis.

Particle Size mm	Weight gm	Grading %age	Radius	Vp Kg/m^3	Ap m^2	xi/dpi
1.70	0.55	0.02	0.85	2.57	9.08	0.32
1.18	2.37	0.07	0.72	1.56	6.51	2.01
1.00	458.48	14.18	0.55	0.68	3.73	458.48
0.85	1072.60	33.17	0.46	0.41	2.69	1261.88
0.60	1646.82	50.92	0.36	0.20	1.65	2744.70
0.30	49.92	1.54	0.23	0.05	0.64	166.40
0.21	2.20	0.07	0.13	0.01	0.21	10.38
0.15	0.67	0.02	0.09	0.00	0.10	4.47
0.00	0.23	0.01	0.04	0.00	0.02	0.00

where Vp is Volume of particle and Ap is the particle surface area.

$\sum Vp = 5.49$ and $\sum Ap = 24.63$

$$\boldsymbol{d}32 = 6\frac{\sum Vp}{\sum Ap}$$

$d_{sv} = 0.0019$ mm

d_{32} = 1.34 mm

Sieve Analysis for Garside 14/25 Sand Bed Material

Table C.2: Sand particles size distribution for size ≤ 1 mm.

Particle Size mm	Weight gm	Grading %age	Radius	Vp Kg/m^3	Ap m^2	xi/dpi
0.85	1072.60	38.69	0.43	0.32	2.27	1261.882
0.60	1646.82	59.40	0.36	0.20	1.65	2744.7
0.30	49.92	1.80	0.23	0.05	0.64	166.4
0.21	2.20	0.08	0.13	0.01	0.21	10.37736
0.15	0.67	0.02	0.09	0.00	0.10	4.466667
0.00	0.23	0.01	0.04	0.00	0.02	0.00

where Vp is Volume of particle and Ap is the particle surface area.

$\sum Vp$ =0.58 and $\sum Ap$ = 4.88

$$\boldsymbol{d}32 = 6\frac{\sum Vp}{\sum Ap}$$

d_{sv} = 0.000761784 mm

d_{32} = 0.71 mm

Data Processing and Analysis

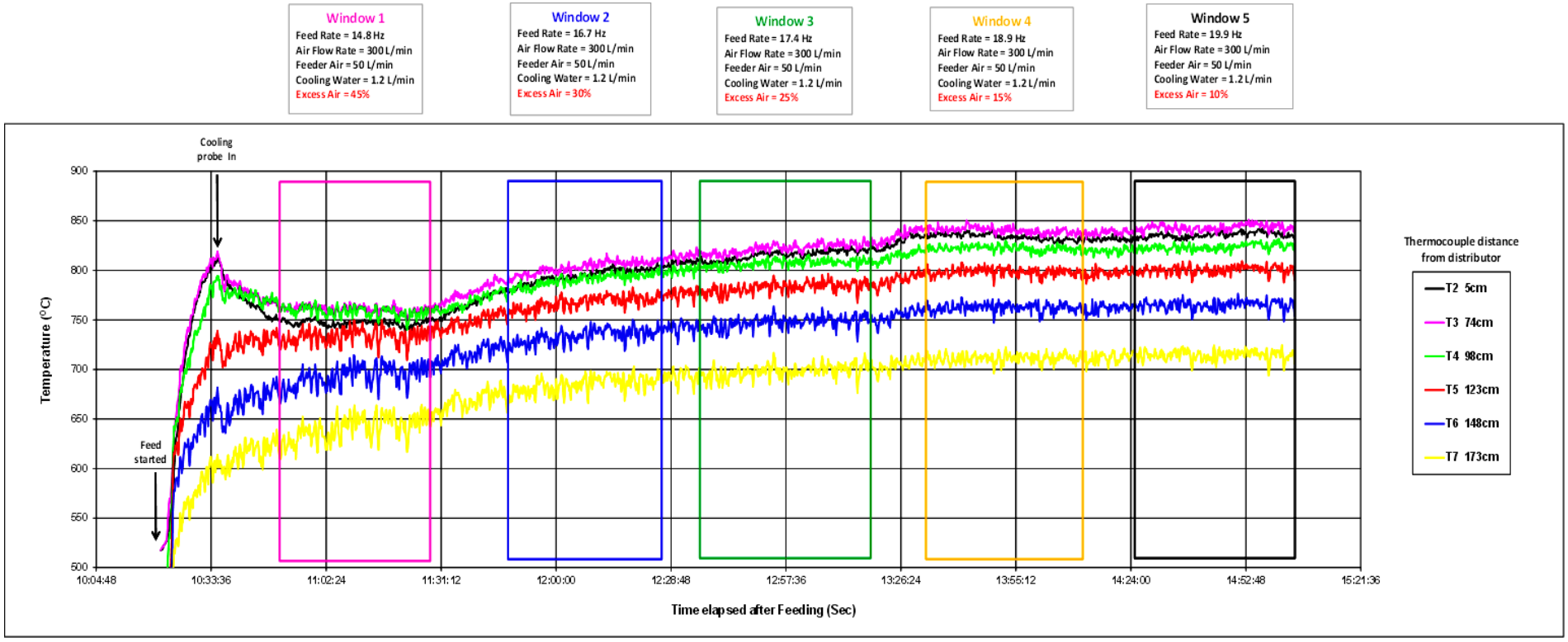


Figure C.1: The temperature data collected for wood pellets combustion under air over a full day run 1, under five various conditions; the different windows representing the selected data under steady state conditions.

Data Processing and Analysis

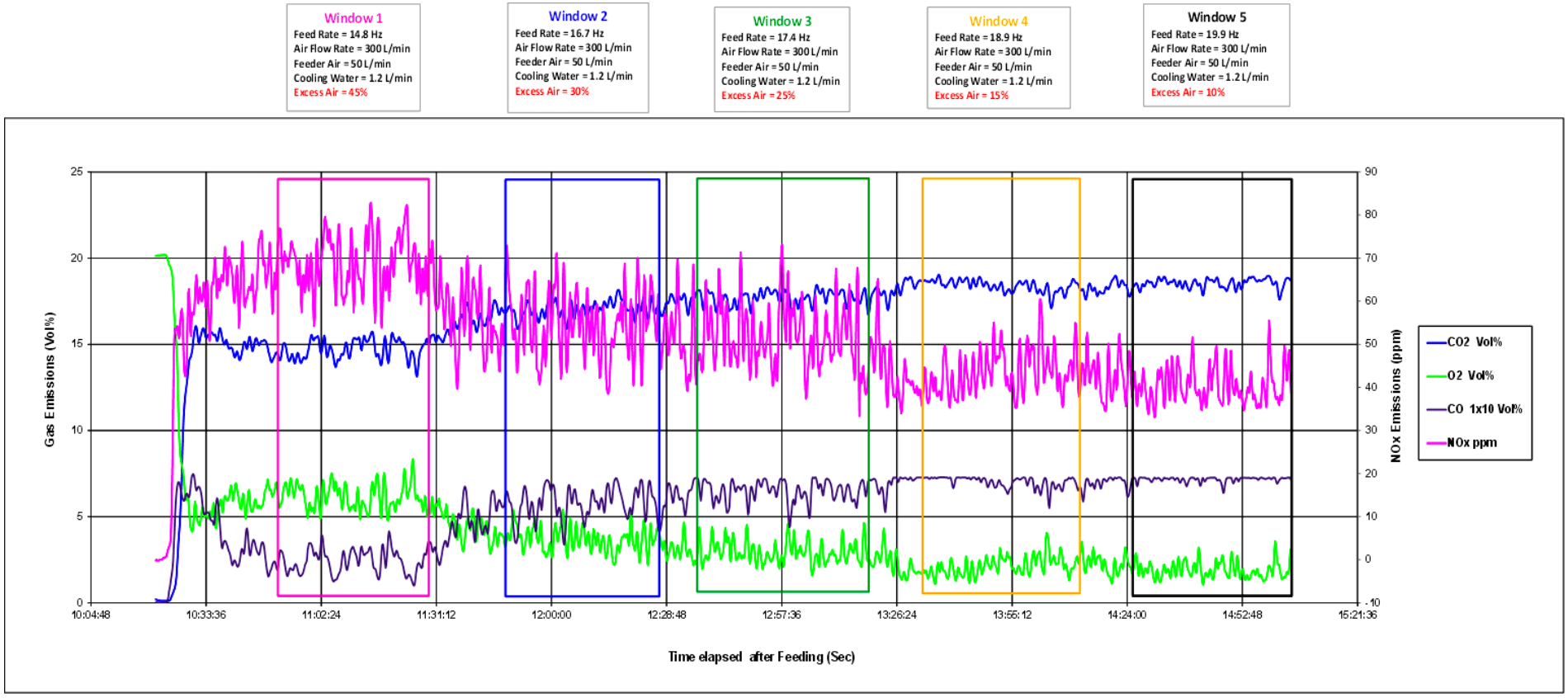


Figure C.2: The flue gas emissions data collected for wood pellets combustion under air over a full day run 1, under five various conditions; the different windows representing the selected data under steady state conditions.

Data Processing and Analysis

Table C.3: The average data from the selected steady state windows form five runs of domestic wood pellets combustion under air with different conditions. The red values are the average of the selected steady state windows mentioned in Figure C.1 and Figure C.2.

Summary	Excess Air	SR	Staging Lavel	Total Time	T1 5cm	T2 5cm	T3 74cm	T4 98cm	T5 123cm	T6 148cm	T7 173cm	T8	T9	ΔP	ΔT	CO_2	CO	O_2	NOx	NO	CO 1x10	Standard O_2	NOx Corrected	CO Corrected	CO Corrected 1x10
	%age		S	hrs	°C	°C	°C	°C	°C	°C	°C	°C	°C	mbar	°C	Vol%	Vol%	Vol%	ppm	ppm	Vol%	Vol%	ppm	%Vol	Vol%
Run 1	45%	1.45	S-0 0cm	0.75	36	748	762	760	733	692	639	7	55	29	48	14.7	0.2	6.2	68.7	0.0	2.5	6.0	69.4	0.2	2.5
	30%	1.30	S-0 0cm	0.75	32	791	800	788	765	731	683	6	62	29	56	17.0	0.6	3.8	54.6	0.0	5.7	6.0	47.5	0.5	4.9
	25%	1.25	S-0 0cm	0.75	31	816	822	807	783	748	698	5	65	27	60	17.7	0.7	2.9	51.8	0.0	6.5	6.0	43.0	0.5	5.4
	15%	1.15	S-0 0cm	0.75	32	834	840	822	798	762	711	5	68	27	63	18.4	0.7	2.1	43.3	0.0	7.0	6.0	34.4	0.6	5.6
	10%	1.10	S-0 0cm	0.67	32	836	843	824	801	765	715	6	69	27	64	18.5	0.7	1.9	40.4	0.0	7.2	6.0	31.8	0.6	5.6
Run 2	45%	1.45	S-0 0cm	0.75	32	736	760	762	745	715	667	6	57	29	51	13.9	0.2	7.0	73.6	0.0	1.5	6.0	78.7	0.2	1.6
	30%	1.30	S-0 0cm	0.75	33	795	812	801	782	754	710	7	66	26	60	16.0	0.3	4.8	71.8	0.0	3.0	6.0	66.5	0.3	2.8
	15%	1.15	S-0 0cm	0.75	33	838	854	837	817	789	746	7	74	25	67	18.0	0.5	2.6	68.0	0.0	5.0	6.0	55.6	0.4	4.1
Run 3	45%	1.45	S-0 0cm	0.75	31	757	772	766	743	707	657	6	58	28	52	15.9	0.5	4.7	62.7	0.0	4.7	6.0	57.7	0.4	4.3
	30%	1.30	S-0 0cm	0.75	30	794	804	793	770	738	690	6	64	27	58	17.3	0.6	3.2	53.0	0.0	6.4	6.0	44.6	0.5	5.4
	15%	1.15	S-0 0cm	0.75	30	824	835	817	794	759	709	6	69	27	63	18.5	0.7	1.7	40.2	0.0	7.2	6.0	31.3	0.6	5.6
	10%	1.10	S-0 0cm	0.75	32	840	849	829	804	768	717	7	73	26	66	18.7	0.7	1.4	39.7	0.0	7.1	6.0	30.4	0.5	5.5
Run 4	45%	1.45	S-0 0cm	0.50	33	741	759	764	737	696	628	9	60	28	51	12.9	0.1	7.5	67.9	75.3	0.9	6.0	75.7	0.1	1.0
	30%	1.30	S-0 0cm	0.50	31	784	797	794	769	736	673	9	68	28	59	14.9	0.2	5.3	65.6	71.8	2.1	6.0	62.8	0.2	2.0
	15%	1.15	S-0 0cm	0.50	32	828	841	835	811	777	716	10	77	27	67	16.9	0.4	3.0	62.8	68.5	4.3	6.0	52.4	0.4	3.6
Run 5	45%	1.45	S-0 0 cm	0.50	32	747	765	770	742	702	638	8	63	30	56	13.7	0.2	6.6	81.9	76.6	1.7	6.0	85.4	0.2	1.7
	30%	1.30	S-0 0cm	0.50	30	797	809	807	781	745	685	8	73	29	65	15.2	0.3	4.9	79.4	74.1	2.6	6.0	74.0	0.2	2.4
	15%	1.15	S-0 0cm	0.50	30	834	847	838	812	776	716	8	80	26	72	16.9	0.5	2.8	72.2	66.8	4.8	6.0	59.5	0.4	3.9

The Proximate Analysis of Different Biomass Fuels as Received Basis

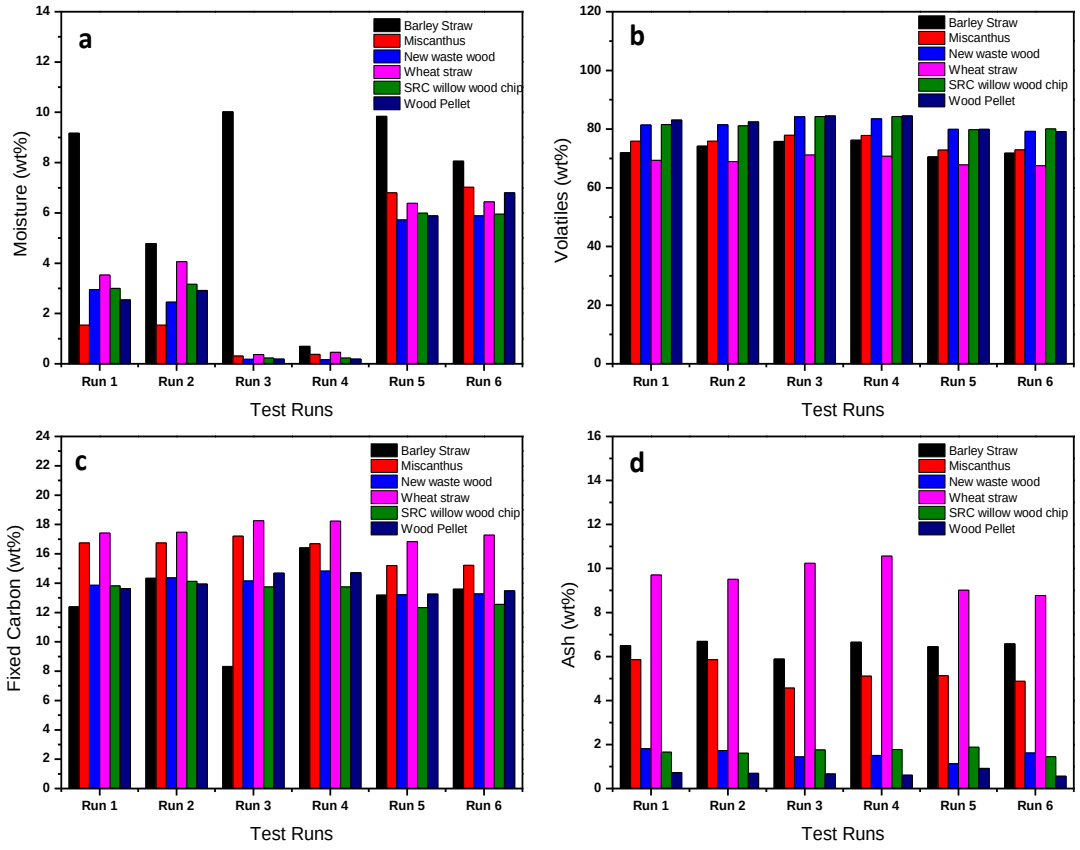


Figure C.3: Repeated experimental runs for proximate analysis of different biomass fuels; (a) moisture content, (b) volatile matter content, (c) fixed carbon content and (d) ash content.

The Ultimate Analysis of Different Biomass Fuels as Received Basis

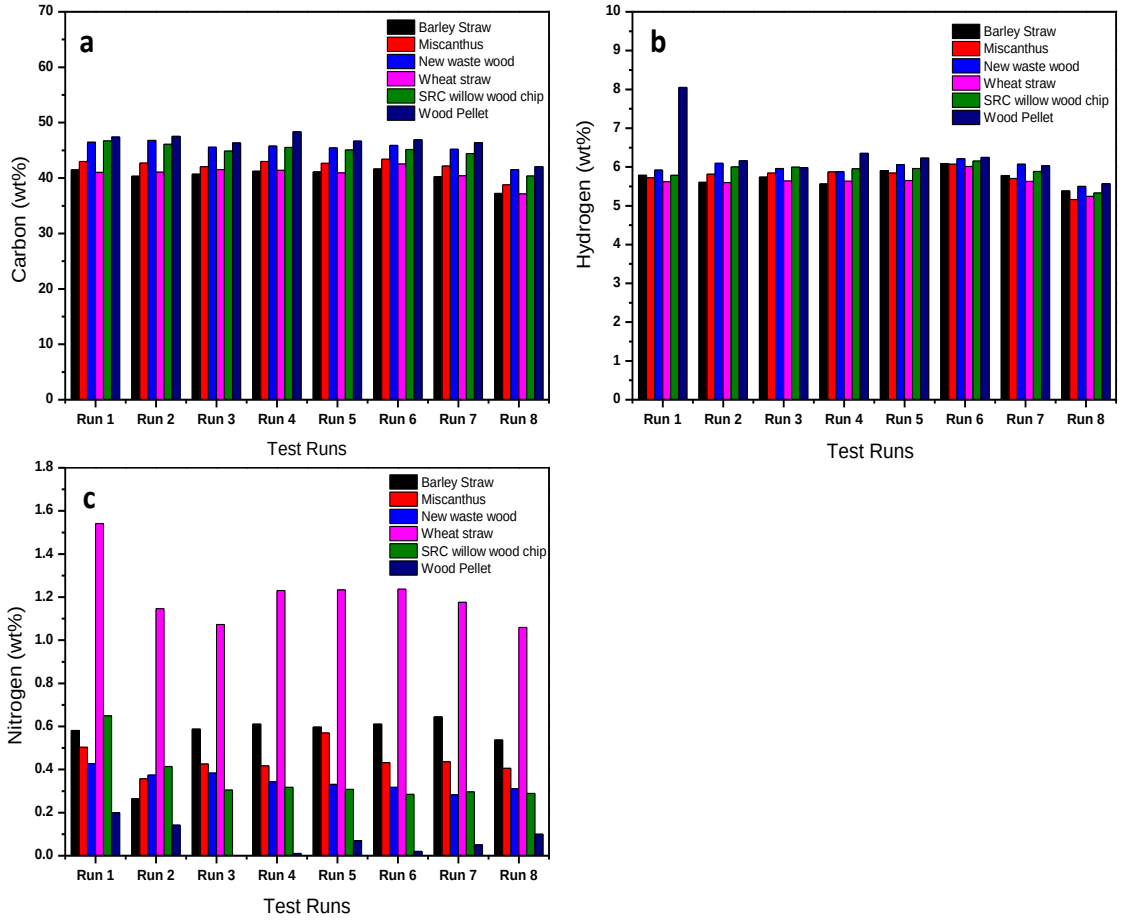


Figure C.4: Repeated experimental runs of ultimate analysis for different biomass fuels; (a) carbon content, (b) hydrogen content and (c) nitrogen content.

Feeding System Calibration with Different Biomass Fuels

Table C.4: Biomass feeder calibration suing different fuels.

Motor frequency (Hz)	**Fuel feed rate (kg/h)**				
	Domestic wood pellets	Industrial wood pellets	Miscanthus pellets	Peanut pellets	Straw pellets
2	0.44	0.25	0.40	0.25	0.34
4	0.82	0.72	0.78	0.72	0.62
6	1.19	1.24	1.16	1.18	0.90
8	1.57	1.65	1.55	1.65	1.19
10	1.95	2.11	1.93	2.11	1.47
12	2.33	2.58	2.32	2.58	1.75
14	2.71	3.04	2.70	3.04	2.03
16	3.09	3.51	3.08	3.51	2.31
18	3.46	3.97	3.47	3.97	2.60
20	3.84	4.44	3.85	4.44	2.88
22	4.22	4.91	4.24	4.91	3.16
24	4.60	5.37	4.62	5.37	3.44
26	4.98	5.84	5.00	5.84	3.72
28	5.36	6.30	5.39	6.30	4.01
30	5.73	6.77	5.77	6.77	4.29
32	6.11	7.23	6.15	7.23	4.57
34	6.49	7.70	6.54	7.70	4.85
36	6.87	8.17	6.92	8.17	5.13
38	7.25	8.63	7.31	8.63	5.42
40	7.63	9.10	7.69	9.10	5.70
42	8.01	9.56	8.07	9.56	5.98
44	8.38	10.03	8.46	10.03	6.26
46	8.76	10.49	8.84	10.49	6.54
48	9.14	10.96	9.22	10.96	6.83
50	9.52	11.42	9.61	11.42	7.11
52	9.90	11.89	9.99	11.89	7.39
54	10.28	12.36	10.38	12.36	7.67
56	10.65	12.82	10.76	12.82	7.95
58	11.03	13.29	11.14	13.29	8.24
60	11.41	13.75	11.53	13.75	8.52

Feeding System Calibration with Different Biomass Fuels with Linear Fittings

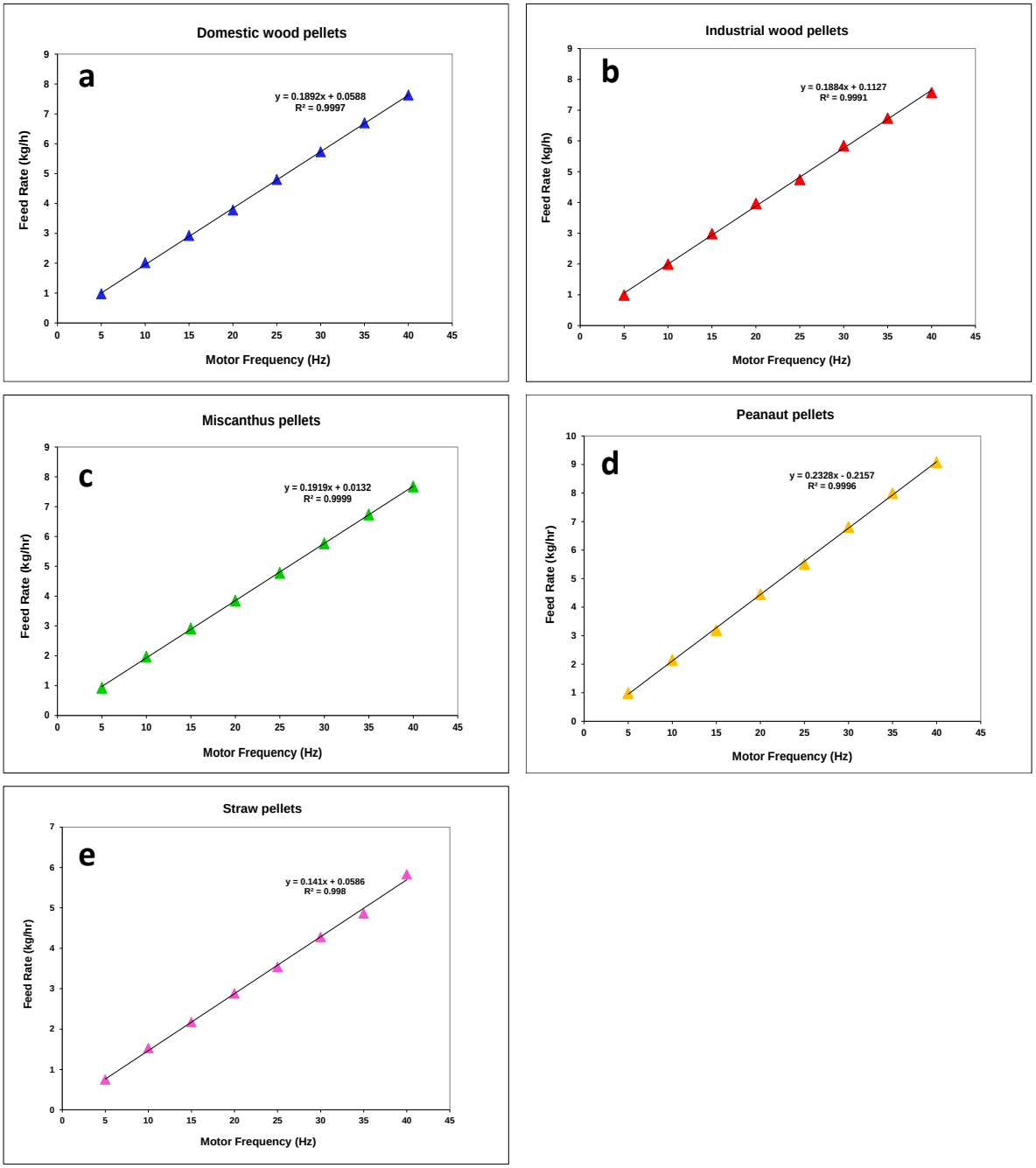


Figure C.5: Feed rate calibration curve for different biomass fuels; (a) domestic wood, (b) industrial wood, (c) miscanthus, (d) peanut and (e) straw pellets.

Operation Check List for Biomass BFBC

Name_____ **Start Time:**_____

Date: _____ **End Time:**_____

Start up

No.	Activity	Checked
1	Switch **ON** extractor fan system	
2	Check the level of biomass in the hopper and fill up if required	
3	Check cyclone container is empty	
4	Connect the sampling gas pipe with gas analyser	
5	Switch **ON** feeder air at a flow rate of 2 L/min mmH_2O. (Approximately 90 L/min Air)	
6	Turn **ON** water valve for sampling probe	
7	Turn **ON** first air valve at the exit of blower fan to full **OPEN** position	
8	Turn **ON** second air valve right after the rota meter at 25% **OPEN** position	
9	Switch **ON** the pressure transducer, blower fan, gas analysers, PC and start softwares	
10	Switch **ON** the main ceramic heaters from main control board	
11	Switch **ON** the air preheater from main control board and set temperature to 450 ^oC	
12	**Start** blower fan at 500 rpm then gradually increase speed to get the required air flow rate	

Shut down

No.	Activity	Checked
1	Turn **OFF** biomass feeder and wait for 15 min to burn any biomass feed inside the reactor	
2	Save data from data logger to the computer	
3	Switch **OFF** main and pre-air heaters and let the temperature cool down to 300°C	
4	Switch **OFF** blower fan when rig temperature is below than 100°C	
5	Turn **OFF** cooling water valve when temperature of air is near room temperature	
6	Turn **OFF** valve for feeder air	
7	Switch **OFF** the pressure transducer, gas analysers, softwares, PC and main switch	

Emergency Shutdown

No.	Activity	Checked
1	In case of backfire in feeder immediately **STOP** feeder motor, feeder air and quickly detach feeder from BFB reactor and **BLOCK** reactor with a blank flange	
2	For any emergency press **RED** emergency **STOP** button installed on the main switch boardd or on the rig near motor	

Appendix D

Biomass Fuels Combustion under Air

Comparison of Combustion Parameter for Different Types of Biomass Fuels under Air Combustion

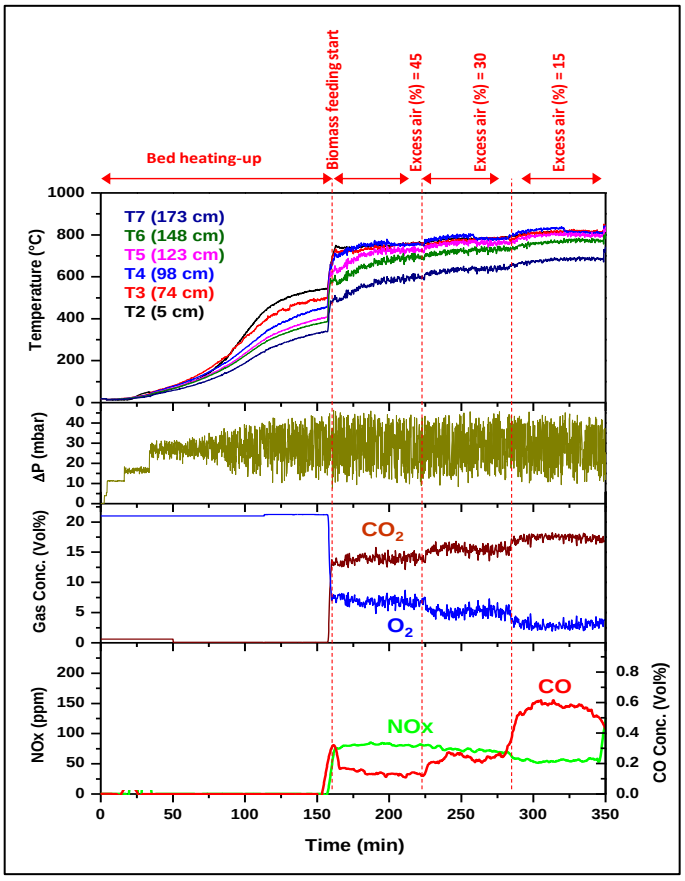


Figure D.1: Temperature profiles at the different heights of the main reactor and freeboard, the pressure drop across the dense bed and the gas composition (CO_2, O_2, NOx and CO) at the outlet of the BFBC during a typical experiment for domestic wood pellets combustion without air staging (WAS).

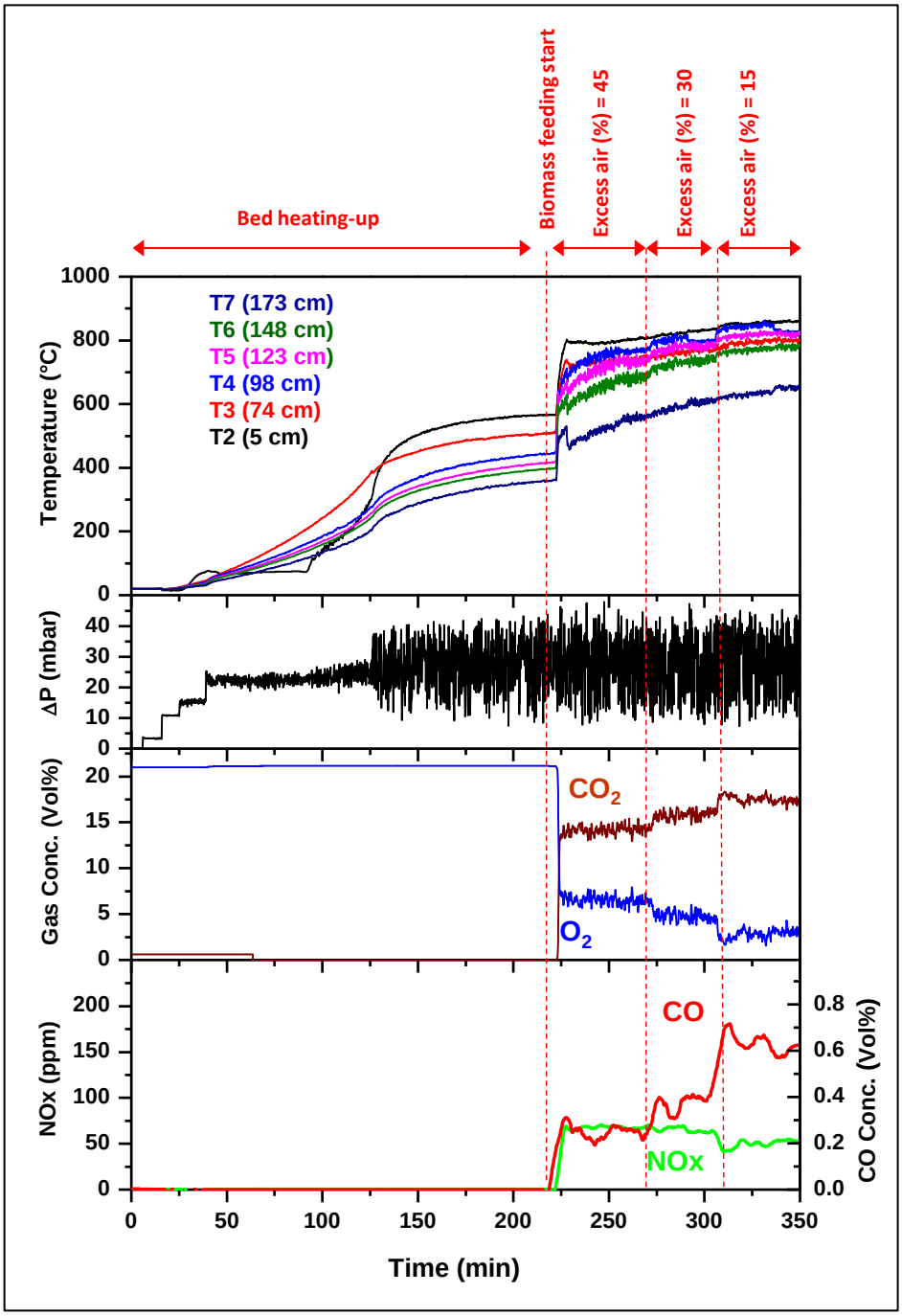


Figure D.2: Temperature profiles at the different heights of the main reactor and freeboard, the pressure drop across the dense bed and the gas composition (CO_2, O_2, NOx and CO) at the outlet of the BFBC during a typical experiment for industrial wood pellets combustion without air staging (WAS).

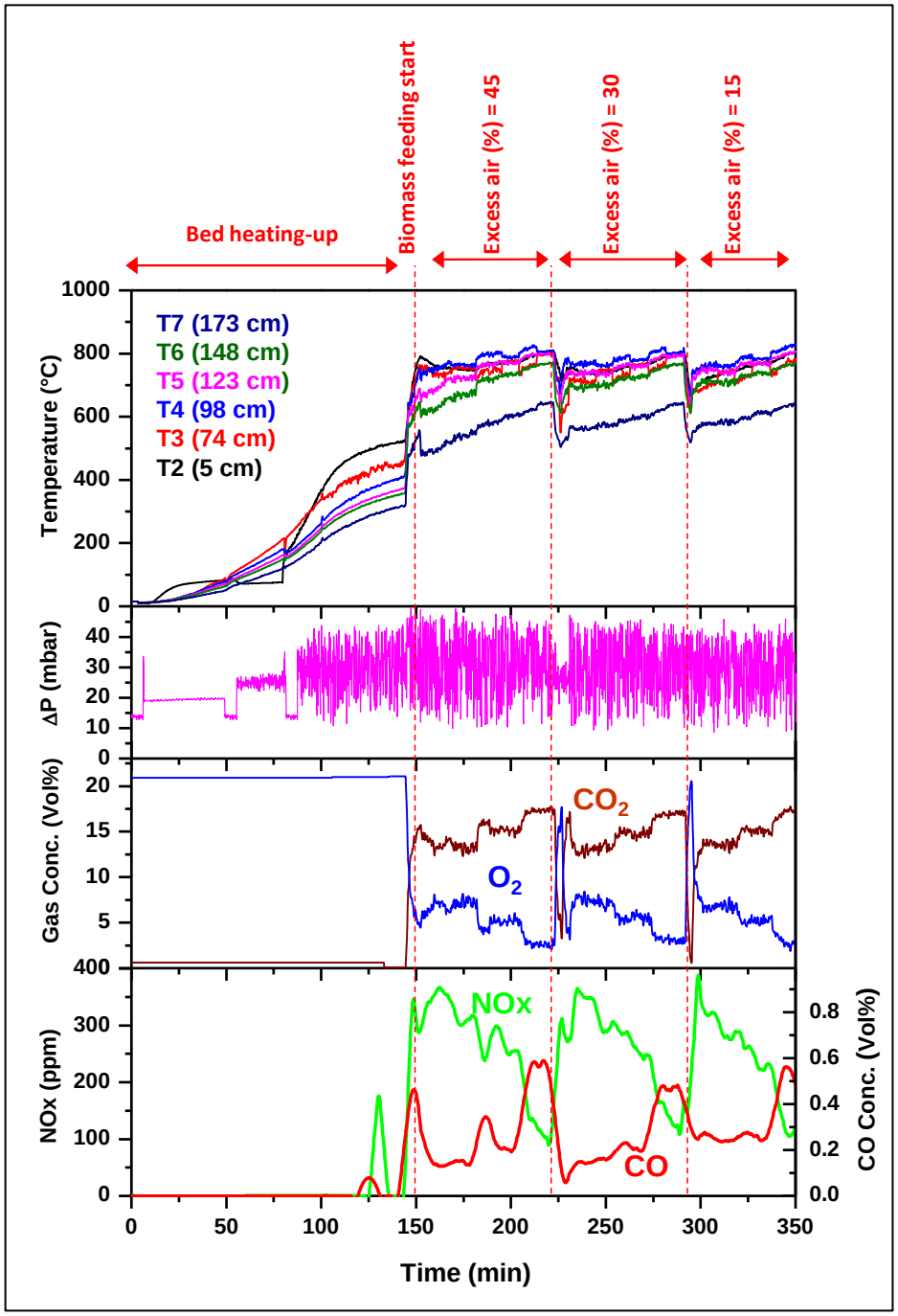


Figure D.3: Temperature profiles at the different heights of the main reactor and freeboard, the pressure drop across the dense bed and the gas composition (CO_2, O_2, NOx and CO) at the outlet of the BFBC during a typical experiment for peanut pellets combustion without air staging (WAS).

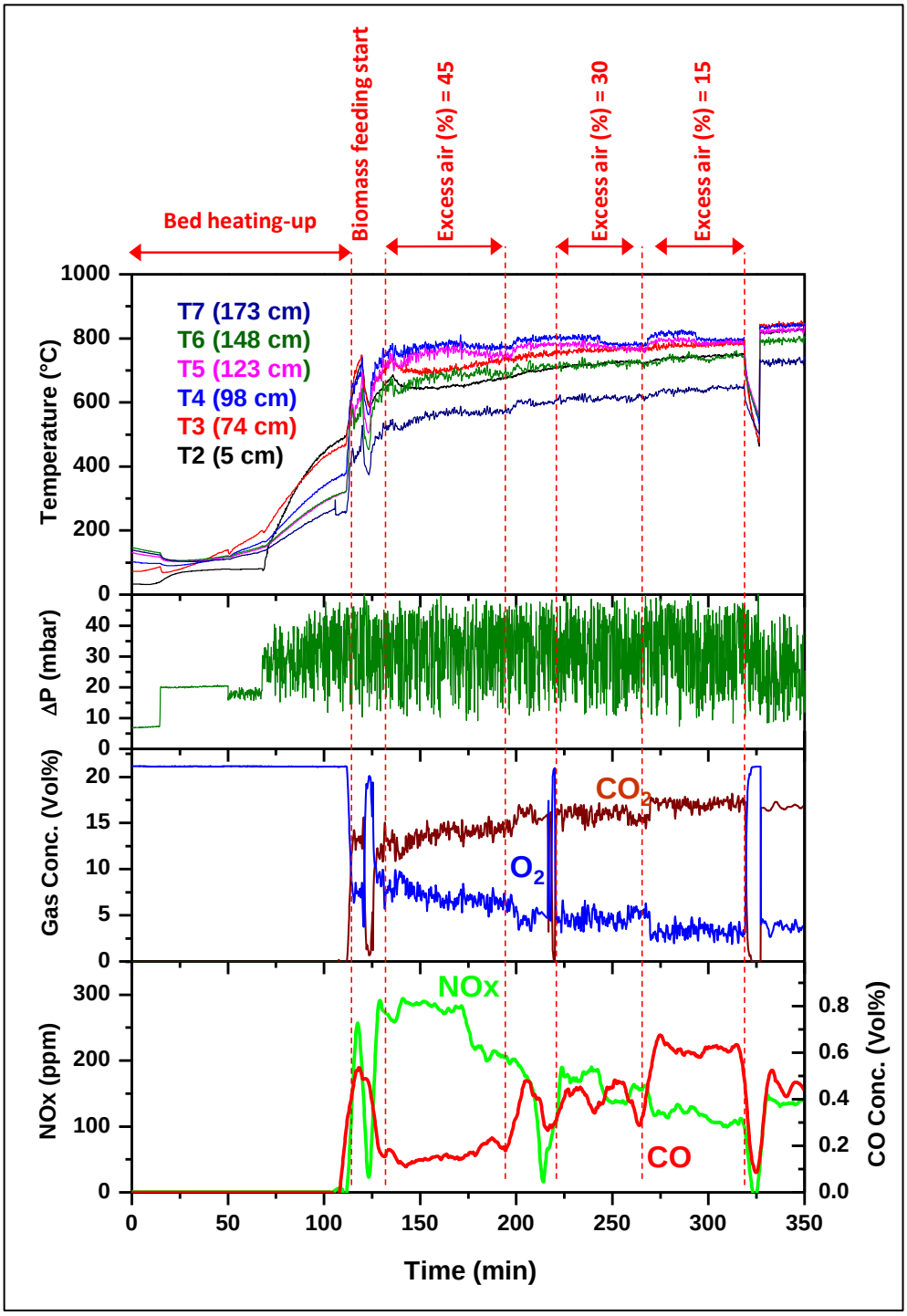


Figure D.4: Temperature profiles at the different heights of the main reactor and freeboard, the pressure drop across the dense bed and the gas composition (CO_2, O_2, NOx and CO) at the outlet of the BFBC during a typical experiment for straw pellets combustion without air staging (WAS).

Comparison of Combustion Efficiencies for Different Biomass Fuels without Air Staging and With Air Staging Experiments

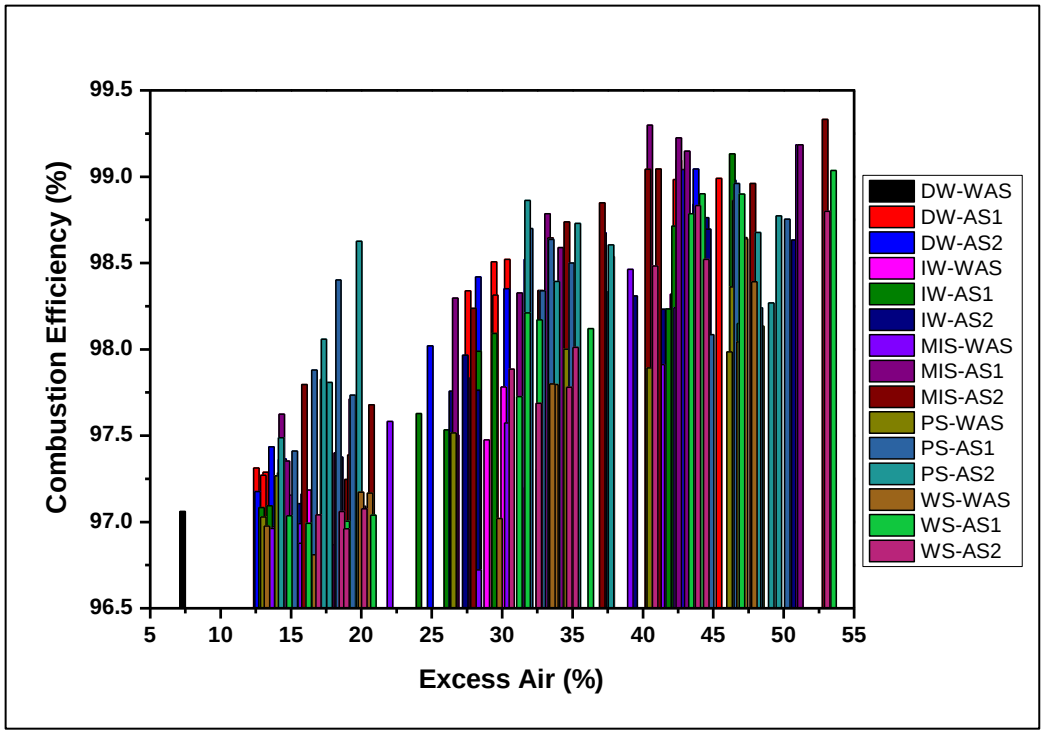


Figure D.5: Comparison of combustion without considering carbon in fly as for all type of studied biomass fuels without air staging (WAS), with air staging at injection level one (AS1) and at level two (AS2), the plotted results are averaged from several test runs.

Appendix E

Biomass Fuels Combustion under Oxy-fuel

Comparison of Combustion Parameter for Different Types of Biomass Fuels under Air Combustion

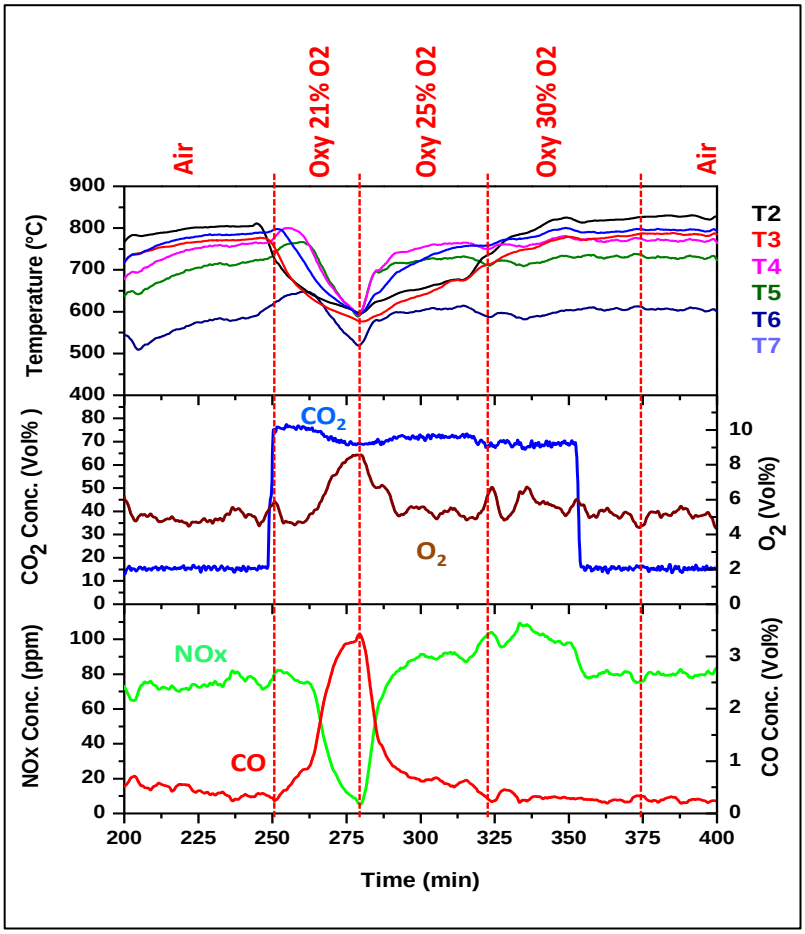


Figure E.1: The temperature profiles, measured at different heights of the reactor and freeboard with the gas compositions at the outlet of the BFBC during miscanthus pellets combustion under air and oxy-fuel.

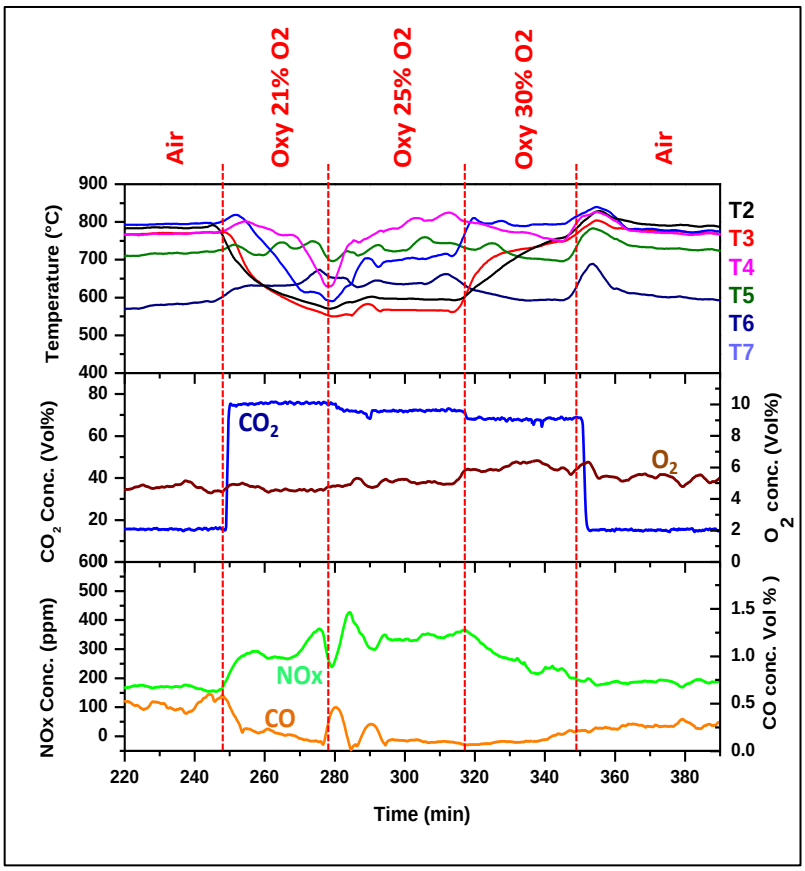


Figure E.2: The temperature profiles, measured at different heights of the reactor and freeboard with the gas compositions at the outlet of the BFBC during straw pellets combustion under air and oxy-fuel.

Appendix F

SEM-EDX, XRF and XRD Results

Elements Analysis Present in Bed Material and Cyclone Ash

Table F.1 The EDX and XRF analysis of bed material and cyclone ash from different biomass fuels studied.

Elements	Bed Material (wt%)						Cyclone reject (wt%)				
	Sand	DW	IW	Mis	Straw	Pnut	DW	IW	Mis	Straw	Pnut
C	0.00	0.00	0.00	0.00	0.00	0.00	16.70	22.77	10.77	0.00	19.75
O	50.99	51.32	48.80	48.51	48.56	48.19	40.69	33.10	39.10	40.62	33.72
Na	0.00	0.01	1.63	0.11	0.01	0.02	0.03	0.17	0.07	0.02	0.12
Mg	0.07	0.28	0.96	0.58	0.54	0.39	0.26	0.54	0.53	1.41	1.51
Al	0.76	0.81	4.90	0.74	0.75	0.99	0.76	1.63	0.61	0.67	3.03
Si	42.18	42.42	35.31	37.51	37.29	35.22	31.90	20.39	25.61	26.99	13.71
P	0.20	0.27	0.30	0.65	0.79	0.52	0.34	0.18	0.64	1.27	1.17
S	0.29	0.28	0.28	0.23	0.26	1.75	0.19	0.98	1.58	0.73	4.77
Cl	0.00	0.00	0.00	0.00	0.00	0.01	0.01	0.64	1.51	6.36	0.14
K	0.94	1.28	3.25	4.79	10.85	6.62	1.22	4.83	8.95	15.87	14.94
Ca	0.00	0.72	1.67	4.81	5.36	4.12	1.81	9.68	8.17	5.44	4.49
Ti	0.01	0.00	0.11	0.00	0.00	0.01	0.01	0.03	0.01	0.00	0.27
Cr	0.24	0.08	0.01	0.13	0.03	0.01	0.24	0.01	0.12	0.01	0.00
Fe	4.18	2.44	2.74	1.87	2.31	2.12	5.73	4.98	0.24	0.58	2.34
Cu	0.11	0.02	0.00	0.01	0.02	0.01	0.01	0.02	0.02	0.01	0.01
Zn	0.03	0.05	0.04	0.04	0.04	0.02	0.08	0.06	0.06	0.01	0.04

Elemental Oxides Analysis Present in Bed Material and Cyclone Ash

Table F.2 The EDX and XRF analysis of bed material and cyclone ash from different biomass fuels studied.

Element	**Bed Material (wt%)**						**Cyclone reject (wt%)**				
Oxides	Sand	DW	IW	Mis	Straw	Pnut	DW	IW	Mis	Straw	Pnut
Na_2O	0.00	0.02	2.20	0.15	0.02	0.03	0.04	0.23	0.10	0.03	0.16
MgO	0.11	0.46	1.59	0.96	0.89	0.65	0.43	0.90	0.88	2.35	2.50
Al_2O_3	1.44	1.53	9.26	1.41	1.42	1.87	1.43	3.08	1.15	1.27	5.72
SiO_2	90.24	90.75	75.53	80.26	79.77	75.35	68.24	43.61	54.78	57.74	29.34
P_2O_5	0.46	0.62	0.70	1.50	1.81	1.19	0.78	0.42	1.47	2.91	2.68
SO_3	0.71	0.71	0.69	0.56	0.64	4.37	0.49	2.44	3.95	1.82	11.92
K_2O	1.14	1.54	3.91	5.77	8.85	7.97	1.47	5.81	10.78	19.12	18.00
CaO	0.00	1.01	2.34	6.73	7.50	5.77	2.53	13.55	11.44	7.61	6.28
TiO_2	0.02	1.01	0.19	0.00	0.01	0.01	0.01	0.04	0.02	0.01	0.044
Cr_2O_3	0.35	0.12	0.01	0.19	0.04	0.02	0.36	0.01	0.17	0.01	0.01
FeO	5.38	3.14	3.53	2.41	2.98	2.72	7.38	6.41	2.88	0.75	3.00
ZnO	0.03	0.06	0.05	0.05	0.05	0.03	0.10	0.08	0.08	0.01	0.05

SEM-EDX Analysis of Different Bed Materials after Combustion

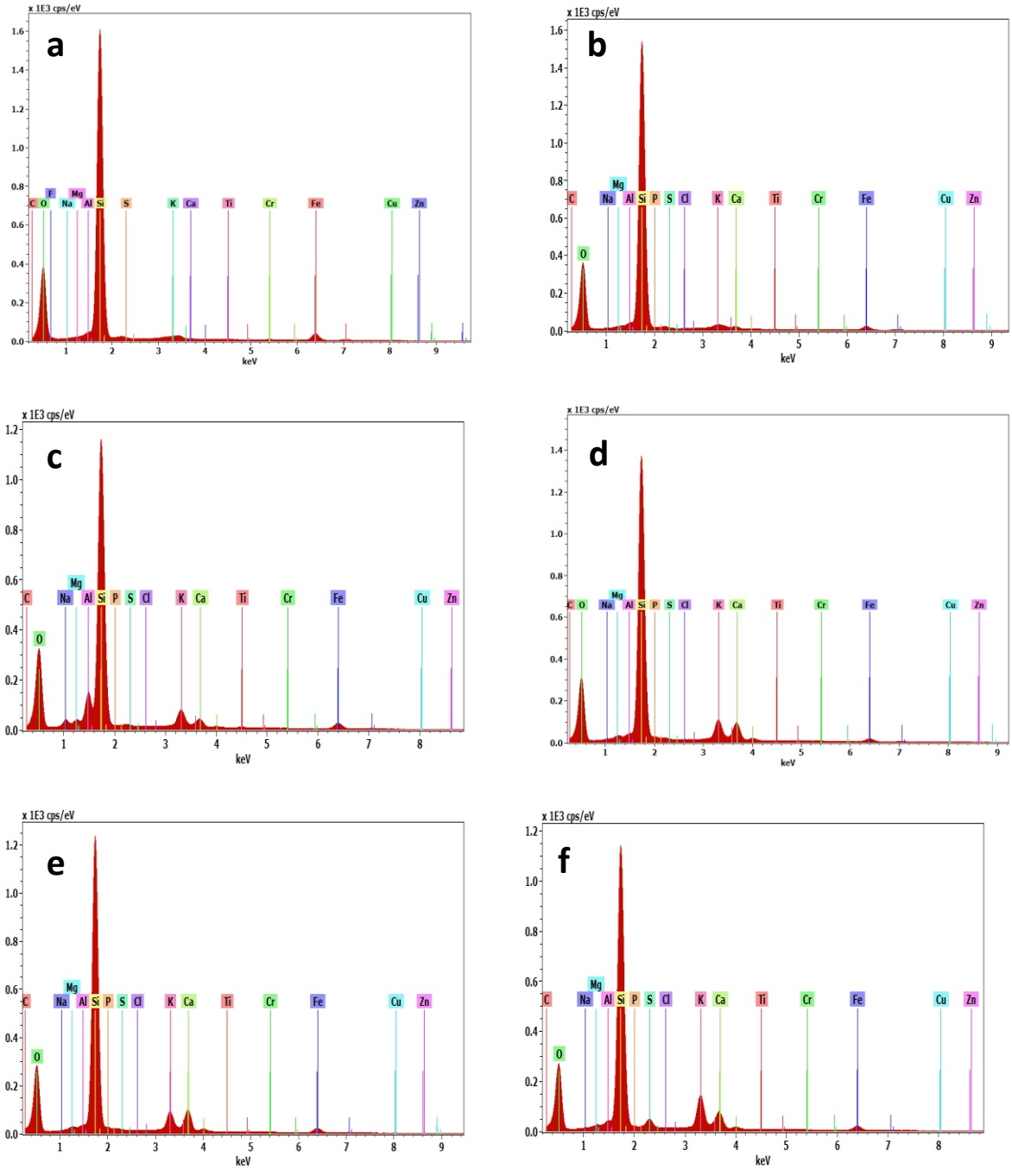


Figure F.1: Elemental spectrum of different fuels bed materials; (a) fresh sand, (b) domestic wood, (c) industrial wood, (d) miscanthus, (e) wheat straw and (f) peanut shell.

SEM-EDX Analysis of Different Cyclone Ash Samples

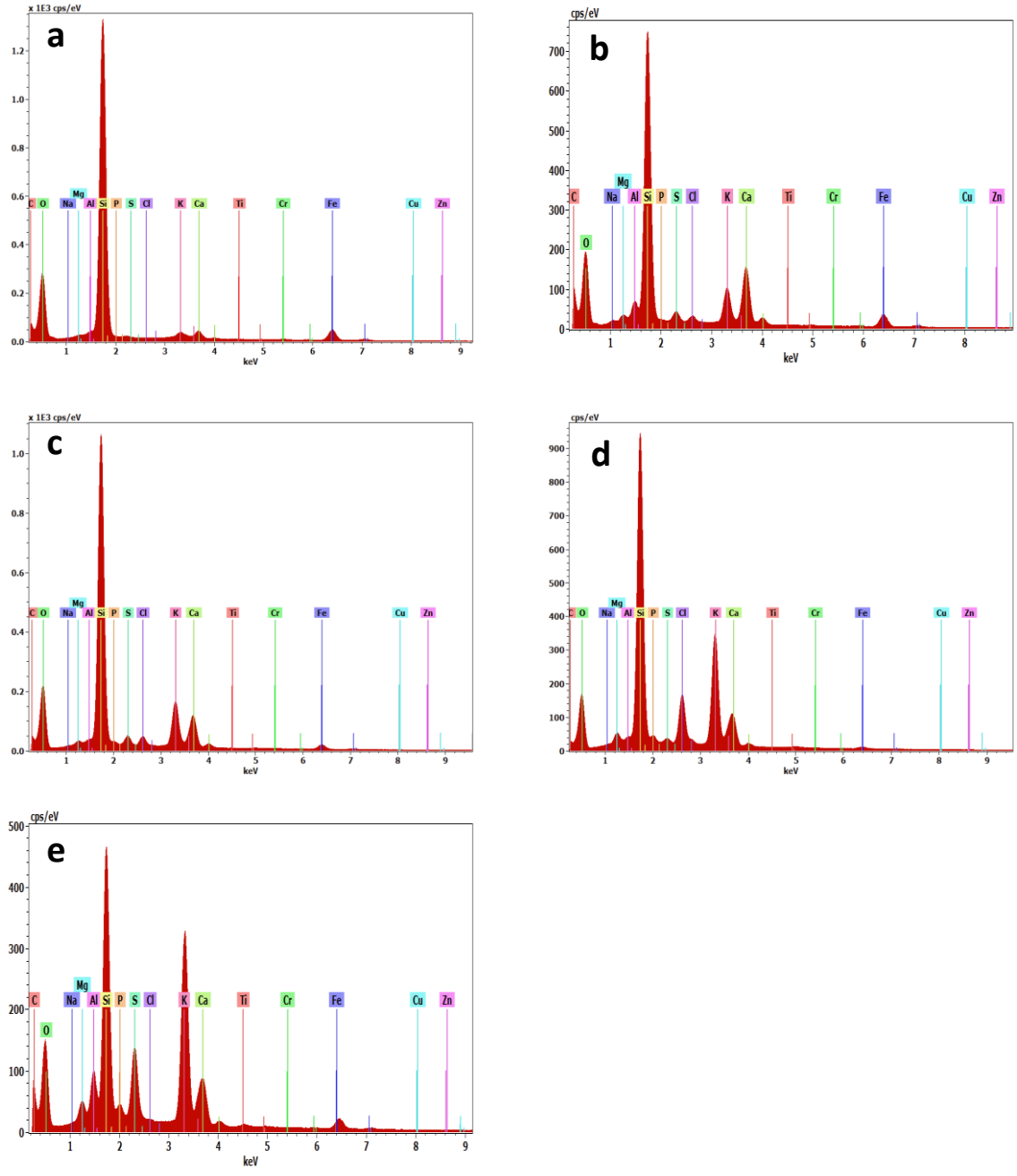


Figure F.2: The elemental spectrum from different fuels cyclone ash; (a) domestic wood, (b) industrial wood, (c) miscanthus, (d) wheat straw and (e) peanut shell.

XRD Spectrum Analysis of Different Bed Materials after Combustion

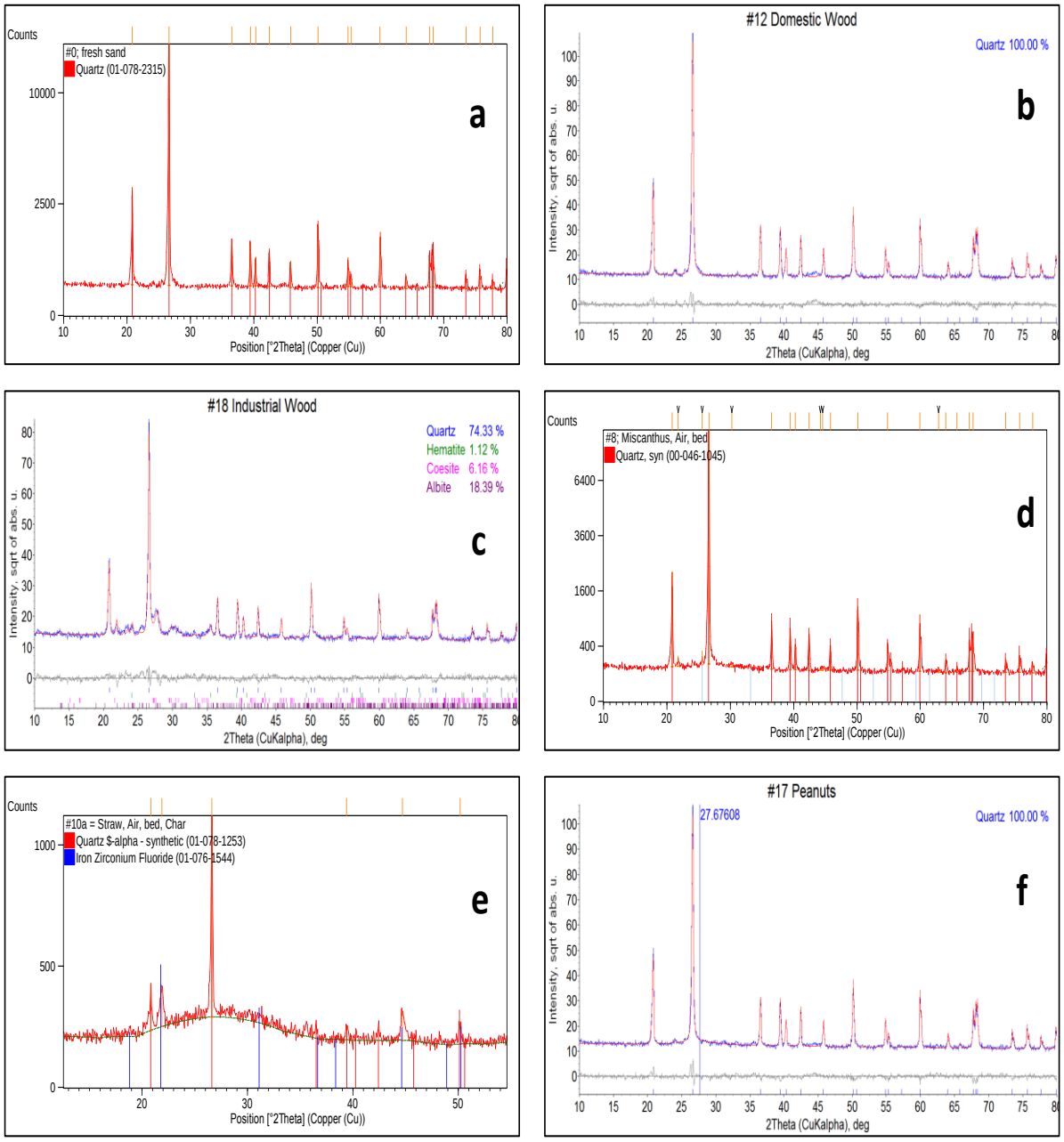


Figure F.3: XRD spectrum of different fuels bed materials; (a) fresh sand, (b) domestic wood, (c) industrial wood, (d) miscanthus, (e) wheat straw and (f) peanut shell.

XRD Spectrum Analysis of Different Cyclone Ash Samples

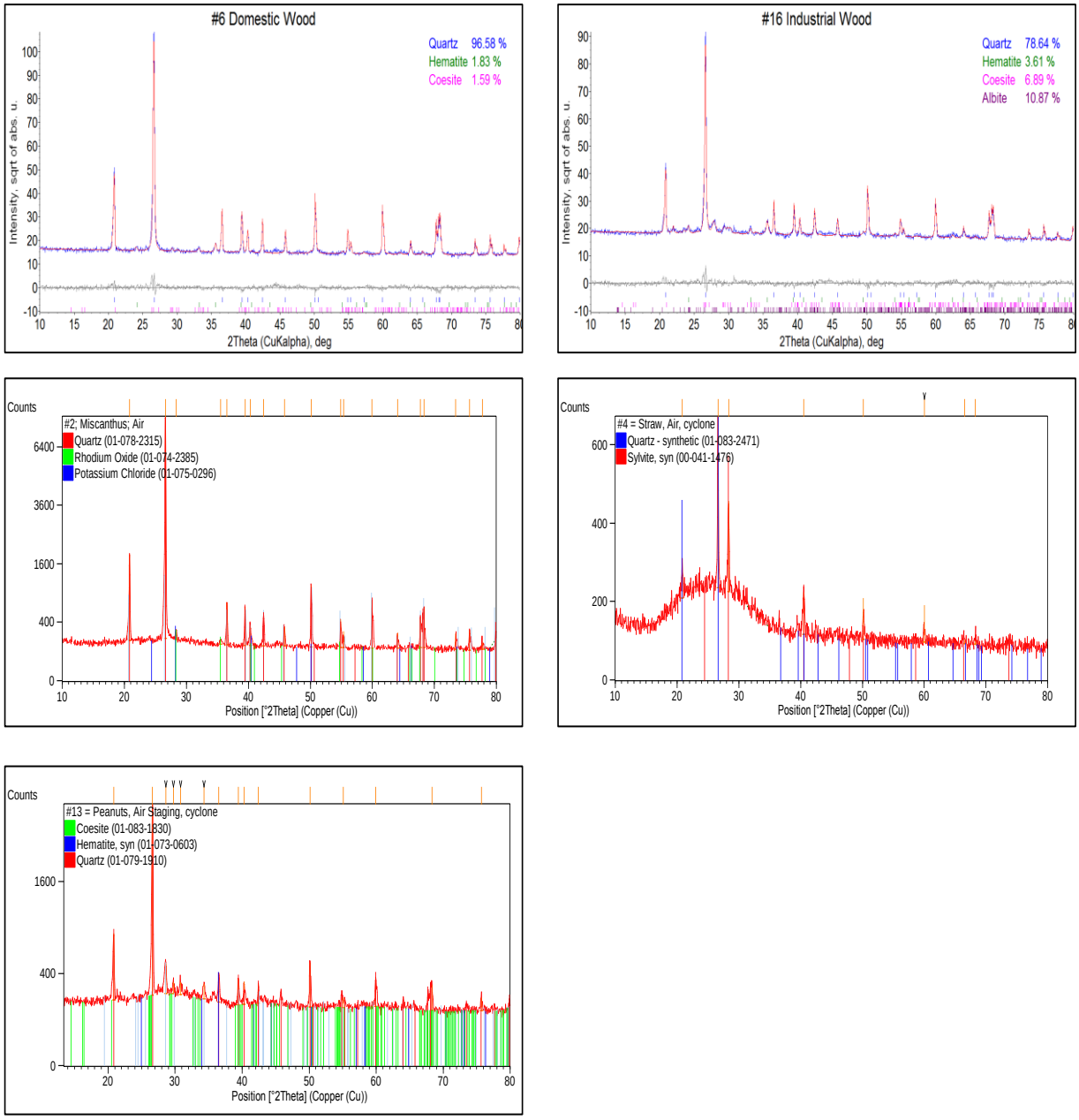


Figure F.4: XRD spectrum from different fuels cyclone ash; (a) domestic wood, (b) industrial wood, (c) miscanthus, (d) wheat straw and (e) peanut shell.